UNIVERSIDADE FEDERAL DO RIO GRANDE DO SUL
INSTITUTO DE GEOCIÊNCIAS
PROGRAMA DE PÓS-GRADUAÇÃO EM GEOCIÊNCIAS

RELAÇÃO DO MAGMATISMO, HIDROTERMALISMO E ALTERAÇÃO SUPERGÊNICA COM A GERAÇÃO DE MINERALIZAÇÕES DE COBRE E AMETISTA NA PROVÍNCIA VULCÂNICA PARANÁ.

SÉRGIO BENJAMIN BAGGIO

Orientador: Prof. Dr. Léo Afraneo Hartmann

Porto Alegre - 2015

UNIVERSIDADE FEDERAL DO RIO GRANDE DO SUL
INSTITUTO DE GEOCIÊNCIAS
PROGRAMA DE PÓS-GRADUAÇÃO EM GEOCIÊNCIAS

RELAÇÃO DO MAGMATISMO, HIDROTERMALISMO E ALTERAÇÃO SUPERGÊNICA COM A GERAÇÃO DE MINERALIZAÇÕES DE COBRE E AMETISTA NA PROVÍNCIA VULCÂNICA PARANÁ

SÉRGIO BENJAMIN BAGGIO

Orientador: Prof. Dr. Léo Afraneo Hartmann

Banca Examinadora:
Prof. Dr. Paulo César Soares, Universidade Federal do Paraná
Prof. Dr. Luiz Henrique Ronchi, Universidade Federal de Pelotas
Prof. Dr. Marcus Vinicius Dorneles Remus, Universidade Federal do Rio Grande do Sul

Tese de Doutorado apresentada como requisito parcial para a obtenção do Título de Doutor em Ciências.

Porto Alegre - 2015

CIP - Catalogação na Publicação

Baggio, Sérgio Benjamin
Relação do magmatismo, hidrotermalismo e alteração supergênica com a geração de mineralizações de cobre e ametista na província vulcânica Paraná / Sérgio Benjamin Baggio. -- 2015.
278 f.

Orientador: Léo Afraneo Hartmann.

Tese (Doutorado) -- Universidade Federal do Rio Grande do Sul, Instituto de Geociências, Programa de Pós-Graduação em Geociências, Porto Alegre, BR-RS, 2015.

1. Província vulcânica Paraná. 2. depósitos hidrotermais. 3. ametista. 4. cobre nativo. 5. sílica gossan. I. Hartmann, Léo Afraneo, orient. II. Título.

Elaborada pelo Sistema de Geração Automática de Ficha Catalográfica da UFRGS com os dados fornecidos pelo(a) autor(a).

Dedicatória

Para
Minha esposa Elaine Burtet e
meu filho Rafael Burtet Baggio

Agradecimentos

Agradeço a Deus pela saúde mental e física que me foi dada em todas as etapas do doutorado e pela pessoa que me tornei ao passar por este processo. À minha esposa Elaine, meu filho Rafael e familiares pelo apoio irrestrito, compreensão e paciência em todas as fases do doutorado.

Agradecimento especial ao meu orientador Prof. Dr. Léo Afraneo Hartmann pela oportunidade, inestimável apoio e presença constante. Aos professores da UFRGS Vítor Paulo Pereira, Ari Roisenberg, Antonio Pedro Viero, Ana Maria Pimentel Mizusaki, Márcio Martins Pimentel, Pedro Luiz Juchem, Marcus Vinicius Dorneles Remus e Ruth Hinrich. Ao Programa de Pós-Graduação em Geociências, especialmente a Roberto Pereira e Letícia Barbosa. Aos meus colegas da UFRGS Lauren Duarte, Víter M. Pinto, Sandro K. Duarte, Juliana Pertille da Silva, Daniel B. Knijnik, Karine R. Arena, Lucas M. Antunes, Denise Stolnik, Thales Petry e Matheus Brückmann.

Agradecimentos aos amigos de Ametista do Sul Valmor Fronza, proprietário da Mina do Museu, pela amizade e por ter disponibilizado sua estrutura para os estudos. Ao Isaldir Sganzerla, presidente da Cooperativa de Garimpeiros do Médio Alto Uruguai Ltda. pelo apoio logístico. Arlindo Norberto Souza e família pela amizade e acompanhamento em campo. Anderson Oliveira, Engenheiro de Minas, pelas discussões técnicas e informações sobre as minas em atividade. Rejane e Gilmar leite, proprietários do Hotel das Pedras pelo apoio e permissão de acesso à mina. Sandro e Osvaldo Pilonetto pelo auxílio no corte das amostras para análises químicas e microssonda.

Ao Sr. David Basso de Taquaruçu do Sul (RS) pelo apoio e permissão para fazer os trabalhos de campo em sua propriedade. Aos amigos de Realeza (PR) Prof. Agostino Munaro pela acolhida e acompanhamento nas áreas de ocorrência de cobre, Claudemir Dalmolin pelo apoio logístico e acompanhamento de campo na área de sua propriedade e à Cristian e Ana Dallagnol pela permissão de acesso à sua propriedade.

Aos amigos de Chiapetta Osmar Kuhn, prefeito municipal, Clarice de Almeida e João Carlos Antenoff que se colocaram à disposição durante o período de campo na região. A Jair Vargas da Silva de Santo Augusto (RS) que permitiu acesso à sua propriedade para coletar amostras de rocha e de cristais de cobre. Agradecimentos a Cito Taper de Dionísio Cerqueira (SC) e à pedreira Rebelatto de Palma Sola (SC).

Agradecimentos aos meus amigos da CPRM/PA Magda Bergmann que foi uma pessoa fundamental para os primeiros passos no doutorado e Wilson Wildner pelas discussões e cessão de análises químicas do sudoeste do Paraná. À amiga Rosa Bello da USP pelo grande esforço e dedicação na execução e discussão das inclusões fluidas.

Aos amigos de Campo Grande (MS), Romualdo H. Paes de Andrade e José Augusto Simões-Neto (DNPM- MS) pelo apoio logístico e empenho durante os estudos em Campo Grande e Serra de Maracaju, a Milton da Hidrosul Ambiental pela cessão dos testemunhos de sondagem da região de Campo Grande. Ao companheiro Gilmar José Rizzotto (CPRM-GO) pelo auxílio no levantamento do sílica gossan Embrapa em Campo Grande e no inesquecível gossan da "dona Zeffa" na Serra de Maracaju. À Gabrielli Gadens-Marcon pela cessão da sondagem no sílica gossan Mina do Museu.

Meu agradecimento a Edgar Bercht (laboratório de difração de Raios-X), Gilberto Santos (laboratório de sedimentologia), Sérgio (geologia isotópica), Marcelo Campos e Juliano Krumel pelo auxílio nos laboratórios. Agradecimentos a Luiz Flávio Lopes pelo auxílio com fotografias em várias etapas do doutorado.

Agradecimentos ao Prof. Dr. Hans-Joachim Massonne e Dr. Thomas Theye pelo apoio do Institut für Mineralogie und Kristalchemie da Universität Stuttgart. Aos doutores Joachim Opitz e Tillmann Viefhaus pelas análises laboratoriais e discussões. Ao amigo Martin Streck pelo apoio em Stuttgart e Hannover. Ao Prof. Dr. Arne Wilnner pelas discussões. Aos colegas Volker Spieth (Tucson, Texas USA), Alexander Schopf, Deborah Lo Pó (Universitá di Bologna), Salvatore Iaccarino (Universitá di Pisa), Li Botão, Cao Wentao, Gelareh e Florian. Aos técnicos Moritz Schmels, Matthias Leiss e Gisela Kwiatkowski. Agradecimento especial a Bettina Wieland pela sua preciosa ajuda em Stuttgart. Agradecimento à Marina Lazarov pelo suporte e apoio durante as análises isotópicas na Universität Hannover.

Os projetos CNPq/VALE (CT MINERAL) e FAPERGS/CNPq garantiram apoio financeiro para a execução de todas as etapas do doutorado. Meu agradecimento ao Conselho Nacional de Desenvolvimento Científico e Tecnológico (CNPq) pela concessão das bolsas DTI-1 (processo 381758/2011-7) durante o período de 05/2011 a 07/2013 e pela bolsa de doutorado sanduíche na Universität Stuttgart, Alemanha (processo 211522/2013-9) durante o período de 01/2014 a 06/2014.

“The ultimate measure of a man is not where he stands in moments of comfort and convenience, but where he stands at times of challenge and controversy.”

Martin Luther King Jr.

RESUMO

A província Paraná é a segunda maior província vulcânica continental do mundo cobrindo áreas do Brasil, Uruguai, Argentina e Paraguai com basalto, andesito basáltico, dacito, riodacito, riolito e localmente rochas piroclásticas. No Cretáceo, o ambiente na Bacia sedimentar do Paraná era desértico com campos de dunas (Formação Botucatu). O evento magmático recobriu expressiva porção deste deserto, gerando um dos maiores aquíferos confinados do mundo, o aquífero Guarani. Além da Formação Botucatu, as demais unidades da Bacia do Paraná também foram afetadas pela alta temperatura dos diques que conduziram a lava para a superfície. O craqueamento do querogênio presente em algumas Formações gerou gás metano (CH_4) que migrou através da bacia. Ao atingir derrames de lava em resfriamento (~1000 ºC) o metano desencadeou a formação de paralavas. Estas rochas apresentam longos e curvos fenocristais de clinopiroxênio (até 10 cm), plagioclásio (~1 cm), magnetita, apatita e matriz vítrea. A maior ocorrência de paralavas está no sudoeste do Paraná. Os teores de cobre nestas rochas são mais elevados (>600 ppm) que a média nos basaltos hospedeiros (~207 ppm). De maneira indireta, o calor residual do vulcanismo também afetou as águas do aquífero Guarani desencadeando eventos hidrotermais com fluidos essencialmente constituídos por água quente e vapor (~150 ºC). Este fluido atravessou os derrames vulcânicos carregando consigo areia inconsolidada (fluidizada) proveniente da Formação Botucatu. Estas areias, deixadas como resíduo ao longo do caminho dos fluidos hidrotermais formaram diques, sills e camadas que foram lentamente silicificadas. Em alguns casos estas estruturas migram lateralmente para agregados de ágata ou quartzo. Brechas hidrotermais, constituídas por fragmentos de basalto amigdaloidal, ocorrem no topo dos derrames e são cimentadas por areia silicificada. A sequência repetida de eventos hidrotermais alterou minerais primários dos basaltos formando argilo-minerais (esmectita e celadonita). Neste processo, o cobre foi liberado da estrutura cristalina dos minerais, principalmente magnetita, remobilizado e depositado em cavidades e na superfície de disjunções colunares. A alteração hidrotermal sobre os derrames vulcânicos culminou na geração dos maiores depósitos de ametista do mundo (e.g., distrito mineiro de Ametista do Sul). Cobre nativo e depósitos de ametista ocorrem associados à assembleia de minerais de baixa

temperatura (até 150 ºC) e a variação $\delta^{65}Cu$ do cobre nativo (-0.59 ‰ a 1.89 ‰) é compatível com razões isotópicas de depósitos hidrotermais e enriquecimento supergênico. Os eventos intempéricos, principalmente do Quaternário, remodelaram os derrames e destacaram na superfície sílica gossans, guias prospectivos de depósitos de ametista e de cobre nativo. Os sílica gossans apresentam formas poligonais, concentração de argilo-minerais e óxidos de ferro, presença de areia silicificada, formação de banhados e mudança abrupta de vegetação, além de anomalias gama-espectrométricas negativas (%K, eU e eTh) que se intensificam sobre áreas com depósitos de ametista. Dentro do sílica gossan as esmectitas apresentam maiores teores de Mg enquanto fora da estrutura, no mesmo derrame, as esmectitas são enriquecidas em K. Estas estruturas ocorrem aos milhares desde o sul até o norte da província e representam uma nova fronteira para depósitos de ametista e cobre nativo na província vulcânica Paraná.

ABSTRACT

The Paraná volcanic province is the second largest continental province in the world covering areas in Brazil, Uruguay, Argentina and Paraguay mainly with basalt, basaltic andesite, dacite, rhyolite and rhyodacite. In the Cretaceous, the environment in the Paraná sedimentary basin was desert with dune fields (Botucatu Formation). A significant portion of this desert was covered with hundreds of horizontal lava flows generating the Guarani aquifer, one of the largest confined aquifer in the world. The Paraná Basin was affected by the high temperature of the dikes that led the lava to the surface. The cracking of kerogen in some formations generated methane (CH_4) that migrated across the basin untill reaching the lava flows that were cooling (~ 1000 °C) and triggered the formation of paralavas. These rocks display native copper mineralization, long and curved clinopyroxene phenocrysts (up to 10 cm), plagioclase (~ 1 cm), magnetite, apatite and glass matrix. The greater occurrence of paralavas is in southwestern of Paraná and has higher copper content (> 600 ppm) than the average host basalts (~ 207 ppm). The residual heat of volcanism affected the Guarani aquifer waters triggering hydrothermal events with fluids consisting essentially of boiling water and vapour (~ 150 °C). The hydrothermal fluid crossed the flows of volcanic pile carrying away large portions of unconsolidated sand from the Botucatu Formation. Along the path of the hydrothermal fluid these sands were left as a residue forming dikes, sills and layers which were slowly silicified. In some cases, they migrate laterally into aggregates of quartz and agate. Hydrothermal breccias, consisting of amigdaloidal basalt fragments occur at the top of the flows and are cemented by silicified sand. The repeated sequence of hydrothermal events altered the primary minerals of basalts forming clay minerals (smectite and celadonite). In this process, copper was released from the crystal structure of minerals (e.g., magnetite), remobilized and deposited in cavities and along the surfaces of columnar joints. This alteration of the volcanic flows resulted in the generation of the world's largest amethyst deposits (e.g., Ametista do Sul mining district). Native copper and amethyst deposits occur associated with low-temperature mineral assembly (up to 150 °C) and the $\delta^{65}Cu$ variation of native copper (-0.59 ‰ to 1.89 ‰) is compatible with isotopic ratios of hydrothermal deposits and supergene enrichment. The weathering events mainly in the Quaternary reshaped the flows and

highlighted silica gossans on the surface, the prospective guides of native copper mineralizations and amethyst deposits. They have polygonal shapes, concentration of clay minerals and iron oxides, presence of silicified sand, formation of altitude ponds and abrupt change in vegetation. Silica gossans have negative gamma-spectrometric anomaly (% K, eU and eTh) that intensify over areas with amethyst deposits. Within the silica gossan the smectites are enriched in Mg while outside silica gossan the smectite is enriched in K. Thousands of silica gossans occur in the province and represent a new frontier for native copper mineralizations and amethyst deposits in the Paraná volcanic province.

Lista de Figuras

Lista de Tabelas

SUMÁRIO

Parte II

Sobre a estrutura desta tese:

Esta tese de Doutorado está estruturada em torno de artigos publicados e submetidos à revisão em periódicos científicos. Conseqüentemente, sua organização compreende as seguintes partes principais:

a) Introdução sobre o tema e descrição do objeto da pesquisa do Doutorado, onde estão sumarizados os objetivos e a filosofia da pesquisa desenvolvida, o estado da arte sobre o tema de pesquisa, seguido de uma discussão integradora com os principais resultados e interpretações.

b) Artigos publicados em periódicos ou submetidos a periódicos com corpo editorial permanente e revisores independentes, escritos pelo autor durante o desenvolvimento de seu Doutorado.

1. Introdução

O magmatismo da província vulcânica Paraná cobriu grande parte do sudeste do Brasil além de áreas do Uruguai, Argentina e Paraguai, totalizando uma área de 917.000 km^2 de lavas. A pilha vulcânica apresenta espessura de até 1.723 m em Cuiabá Paulista (SP), o que corresponde a mais de uma centena de derrames que potencialmente hospedam jazidas de ametista e mineralizações de cobre. A origem dos depósitos minerais e os mecanismos associados à sua formação estão sendo amplamente discutidos na literatura internacional e diversos modelos e hipóteses foram propostos.

O presente estudo, desenvolvido em diversas áreas da província, agrega evidências que reabrem a discussão sob uma nova ótica e analisa a relação do magmatismo, hidrotermalismo e da alteração supergênica com a geração destes depósitos na província Paraná.

1.1. Objetivo e justificativa

O objetivo deste trabalho é o estudo das mineralizações de cobre nativo e dos depósitos de geodos de ametista, com foco nas relações entre o magmatismo, hidrotermalismo e alteração supergênica. Está inserida neste contexto a discussão dos mecanismos de formação e a identificação dos indicadores geológicos de sua presença nos derrames da província vulcânica Paraná. As campanhas de campo com coleta de amostras, geração de dados gama espectrométricos, e as técnicas analíticas aplicadas neste estudo permitiram que estes objetivos pudessem ser alcançados.

A extensão territorial que a província vulcânica Paraná ocupa no Brasil, a distribuição das mineralizações de cobre e a expressão dos depósitos de ametista torna a investigação metalogenética da província um assunto de extrema relevância. O entendimento dos eventos que ocorreram no Cretáceo, suas relações e evolução contribui para o estabelecimento de uma nova perspectiva para os recursos minerais na província Paraná.

1.2. Materiais e métodos

A metodologia aplicada para o desenvolvimento desta tese incluiu extensa avaliação de imagens de satélite, etapas de campo e aplicação de métodos analíticos que objetivaram a resolução dos problemas discutidos nos artigos científicos da tese. Para alcançar os objetivos, foram utilizados laboratórios da Universidade Federal do Rio Grande do Sul (Laboratório de preparação de amostras, petrografia e difração de raios-X), Universidade de São Paulo (Inclusões fluidas), Universidade de Stuttgart (difração de raios-X, Espectrometria Raman, LA–ICPMS, microssonda eletrônica) e Universidade de Hannover (isótopos estáveis de cobre).

1.2.1. Revisão bibliográfica

A revisão bibliográfica permitiu avaliar o estado da arte de cada um dos assuntos discutidos na tese. Para este fim foram utilizadas as estruturas das bibliotecas de Geociências da Universidade Federal do Rio Grande do Sul, da Universidade de São Paulo e do Institut für Mineralogie und Kristalchemie da Universität Stuttgart bem como dos periódicos disponibilizados no portal da Capes.

1.2.2. Trabalhos de campo

Os trabalhos de campo foram realizados em uma ampla área da província. A avaliação das paralavas foi efetuada na região de Francisco Beltrão (PR) e Jardim (MS). Para os trabalhos de campo envolvendo as mineralizações de cobre os trabalhos foram realizados em Taquaruçu do Sul (RS), Dom Pedro de Alcântara (RS), Bom Princípio (RS), Santo Augusto (RS), Chiapetta (RS), Frederico Westphalen (RS), São Lourenço do Oeste (SC), Dionísio Cerqueira (SC), Palma Sola (SC), Francisco Beltrão (PR), Ampére (PR), Realeza (PR), Cascavel (PR), região de Campo Grande (MS) e Serra de Maracaju (MS). Para avaliação dos sílica gossans foram estabelecidas áreas de estudo prioritárias no distrito mineiro de Ametista do Sul (RS), Campo Grande (MS), Serra de Maracaju (MS), Taquaruçu do Sul (RS) e na região de Realeza (PR). Além destas áreas foram eleitas outras áreas para levantamento gama espectrométrico como na região de Torres (RS), Gramado (RS) e Entre Rios (SC). Em todas as áreas o trabalho de campo envolveu levantamento das coordenadas geográficas com GPS

Garmin portátil (Datum WGS84), descrição de afloramentos, coleta de amostras, mapeamento dos derrames vulcânicos e elaboração de seções para estabelecimento da estratigrafia local.

1.2.3. Testemunhos de sondagem

Na região de Campo Grande (MS) foram utilizados dois testemunhos de sondagem que auxiliaram no entendimento da estratigrafia da região (cedidos pela empresa Hidrosul Ambiental). No distrito mineiro de Ametista do Sul foi utilizado o testemunho de sondagem A1T1A executado para fins de estudos palinológicos (Gadens-Marcon *et al*., 2014) no sílica gossan Mina do Museu.

1.2.4. Levantamento gama espectrométrico

Os levantamentos da emissão da radiação gama de derrames da província Paraná foram efetuados com um cintilômetro e um gama espectrômetro em áreas previamente determinadas. O cintilômetro Exploranium GR-110 possui um detector de cristal de NaI com 74 cm^3 e foi utilizado para leituras da contagem total da radiação gama (U+K+Th). O tempo estabelecido para as leituras do GR-110 foram de 10 s e os resultados são expressos em contagem por segundo (cps). O gama-espectrômetro RS-125 dispõe de um detector de cristal de NaI com 103 cm^3 que foi utilizado para avaliar os radionuclídeos em separado. O tempo estabelecido para as leituras do RS-125 foi de 60 s e os resultados apresentam a média percentual de potássio (%K), o urânio equivalente (eU) em partes por milhão (ppm) e o tório equivalente (eTh) em partes por milhão (ppm). Para fins de comparação dos resultados o gama-espectrômetro também foi utilizado para contagem total de radiação (cps). Para cada ponto medido foram efetuadas de cinco a dez leituras, e calculada a média aritmética. Os dados foram utilizados para gerar mapas de contorno espectrométrico com o software Oasis Montaj® (Geosoft Latinoamerica) e também para elaboração de seções com o software Excel® e CorelDraw®.

1.2.5. Petrografia, difração de raios-X e espectrometria Raman

A identificação de minerais foi efetuada a partir da petrografia, difração de raios X e espectrometria Raman. O estudo petrográfico foi conduzido através da descrição de

lâminas delgadas em microscópio ótico de luz transmitida e refletida na UFRGS, USP e Universität Stuttgart. A petrografia, além da identificação de minerais foi importante no entendimento das relações de contato entre os minerais (textura e petrogênese), alterações químicas, mineralizações e reconhecimento de feições para detalhamento na microssonda eletrônica.

Os argilo-minerais dos basaltos foram identificados por difração de raios-X e as técnicas utilizadas incluíram difração de rocha total (pó) e de lâminas orientadas (natural, glicolada e calcinada a 550 ºC) na fração argila (< 4 μm). O difratômetro utilizado na UFRGS foi o SIEMENS – BRUKER-AXS D5000 com goniômetro θ-θ, radiação Kαl, tubo de Cobre, em condições de 40 kV e 25 mA. Para as análises de rocha total o avanço foi de 2 s para degraus de 0.02 de 2 º até 72 º (2θ). Para as amostras orientadas (natural e calcinada) o avanço foi de 2 s para degraus de 0.02 de 2 º até 28 º(2θ) enquanto nas amostras glicoladas foi de 3 s para degraus de 0.02 de 2 º até 28 º(2θ). Na Universidade Stuttgart a difração de raios-X foi efetuada em minerais de cobre com difratômetro Bruker-AXS D8 Advance equipado com tubo monocromado de grafite, radiação Co Kα, 40 kV, 40 nA de 4 º até 72 º(2θ). O software utilizado foi o DIFFRAC^{PLUS} e a interpretação mineralógica baseou-se nos padrões do banco de dados PDF2 e mincryst. O software CorelDraw foi usado para a preparação das figuras.

Para complementar a identificação dos minerais de cobre utilizou-se um microscópio Olympus BX51 acoplado com espectroscópio Raman (Horiba Xplora System). O feixe de laser usado foi de 532 nm ou 638 nm e 0.25 ou 25 mW. O tempo de exposição de cada leitura foi de 10 s. O número de leituras foi entre 5 e 100 dependendo da potência do laser e a composição da amostra. A variação espectral foi entre 70 e 4000 cm^{-1}. Para os cristais de cobre das mounts em epoxi o foco foi ajustado para profundidades com intervalos de 0.5 μm e o software utilizado para avaliação foi o LabSpec5 (Horiba).

1.2.6. Análises químicas de rocha total

As análises químicas foram realizadas no laboratório ACME Analytical laboratories em Vancouver, Canada. Para elementos maiores foi utilizado 0,1 g de amostra fundida por $LiBO_2$ e análise por ICP-ES (Inductively Coupled Plasma Emission Spectrometry). Para elementos menores utilizou-se ICP-MS (Inductively Coupled

Plasma Mass Spectrometry). A perda ao fogo foi obtida a partir da diferença de peso após calcinação a 1000 ºC. Elementos traço e terras raras foram analisados por ICP-MS seguindo o mesmo procedimento para elementos maiores com adição de 0,5g de amostra digerida em água régia. Os dados foram integrados em planilhas excel e interpretados com o auxílio do software Geochemical Data Toolkit freeware (GCDKit).

1.2.7. Inclusões fluidas

O estudo de inclusões fluidas foi desenvolvido no laboratório de inclusões fluidas do Núcleo de Apoio à Pesquisa Geoanalítica do Instituto de Geociências da USP. Quatro lâminas delgadas foram preparadas com polimento em ambos os lados. As inclusões fluidas foram analisadas conforme sua caracterização, distribuição e modo de ocorrência objetivando identificar possível origem (primária, secundária ou pseudo-secundária) e escolha dos melhores campos para as análises microtermométricas. A microtermometria foi efetuada em platina CHAIXMECA MTM 85 calibrada com componentes químicos Merck MSP para temperaturas maiores que 40 °C. Para temperaturas negativas e altas temperaturas a calibração foi efetuada usando padrões sintéticos Syn Flinc (Synthetic Fluid Inclusions). Para -56.6 °C (Padrão 1: composição 75 mol % H_2O e 25 mol % CO_2); -21.2 °C (Padrão 2: Composição eutética do sistema H_2O + NaCl com 23.2 peso % NaCl); -10.7 °C (Padrão 3: Composição eutética do sistema H2O + KCl com 19.65 peso % KCl); 0 °C e 374.1 °C (Padrão 4: Água pura - ponto triplo e ponto crítico, respectivamente) e 573.0 °C (Padrão 5: Transição de quartzo α para quartzo β). A interpretação das salinidades das inclusões fluidas foi efetuada com auxílio do software FLUIDS (Bakker, 2003).

1.2.8. Microssonda eletrônica e LA-ICPMS

A determinação das concentrações dos elementos dos minerais foi efetuada em microssonda eletrônica e também por laser ablation (LA-ICPMS) no Institute für Mineralogie und Kristalchemie da Universität Stuttgart, Alemanha. A microssonda utilizada foi a Cameca SX100 (wavelenght-dispersive X-ray Spectroscopy). A rotina de trabalho utilizada foi de 15 kV de aceleração da corrente, 15 nA de corrente do feixe e diâmetro do spot de 1 μm para silicatos. Para os argilo minerais a corrente foi estabelecida em 10 nA e diâmetro do feixe de 10 μm. Foram também geradas imagens

de elétrons retroespalhados e mapas composicionais de Mg, Al, Fe, Ca e Na das esmectitas. A formula mineral foi calculada com auxílio do aplicativo CalcMin para Excel (Brandelik & Massonne, 2004).

Para determinar a concentração dos elementos nos minerais dos basaltos hospedeiros de mineralizações de cobre foi utilizado LA-ICPMS. Os equipamentos utilizados foram o AGILENT 7700 ICPMS e sistema de laser CETAC LSX-213. O diâmetro do spot de ablação foi de 50 µm, energia do laser 5% (= 4 mJ) e freqüência de disparos 20 Hz. O fluxo de He e Ar foram de 300 ml/min and 800 ml/min, respectivamente. Os padrões utilizados foram DLH7 e DLH20 de P & H (Developments Ltd.) e vidro NIST612. Os isótopos monitorados foram ^{24}Mg, ^{25}Mg, ^{27}Al, ^{29}Si, ^{39}K, ^{55}Mn, ^{56}Fe, ^{57}Fe, ^{60}Ni, ^{63}Cu, ^{65}Cu, ^{66}Zn, ^{68}Zn, ^{89}Y, ^{90}Zr, ^{91}Zr, ^{93}Nb, ^{95}Mo, ^{107}Ag, ^{109}Ag and ^{197}Au. As concentrações de elementos foram calculadas de acordo com o padrão interno do elemento Si (determinada por microssonda eletrônica) assumindo uma distibuição isotópica natural. O software utilizado para calibração e avaliação de dados foi desenvolvido pelo Dr. Joachim Opitz do Institut für Mineralogie und Kristallchemie da Universität Stuttgart.

1.2.9. Análises isotópicas de cobre

As análises isotópicas de cobre foram efetuadas na Universidade Leibniz Hannover em um Finnigan Neptune multicoletor ICP-MS conectado em sistema femtosecond laser ablation (Spectra Physics Solstice, USA). As amostras e o padrão foram analisados em modo “linha” com diâmetro do spot de 35 µm, energia do laser em 16 A e pulsos de 2 - 4.5 Hz. A correção foi efetuada utilizando solução com razões isotópicas ^{62}Ni/^{60}Ni do padrão NIST SRM-986 (National Institute of Standards and Technology, USA) no plasma e monitoramento simultâneo com o laser ablation dos isótopos de cobre (Oeser *et al.*, 2014). O padrão sólido de cobre (NIST SRM976) foi usado alternadamente entre as amostras. A cada três medidas efetuadas na amostra, duas medidas eram efetuadas no padrão. Os resultados da composição isotópica δ^{65}Cu são em per mill (‰) de acordo com a equação: $\delta^{65}Cu = [((^{65}Cu/ ^{63}Cu)_{sample} /(^{65}Cu/ ^{63}Cu)_{NIST\ SRM976})-1]*1000$.

1.3. Contexto geológico

1.3.1. Bacia do Paraná

As rochas sedimentares da Bacia do Paraná não fazem parte do foco central desta tese, porém o envolvimento de algumas unidades sedimentares com o magmatismo Serra Geral as torna muito importantes para o entendimento dos eventos que se sucederam bem como para a metalogenia da província vulcânica Paraná.

A Bacia do Paraná é uma bacia intracratônica (Zalán *et al*., 1987) que ocupa 1.600.000 km^2 do continente sul-americano. Apresenta formato alongado, direcionado a NNE-SSW e no Brasil cobre aproximadamente 1.100.000 Km^2. A depressão que deu origem à Bacia foi gerada no Gondwana, por subsidência termal da crosta após múltiplas colisões durante o ciclo Orogênico Brasiliano-Panafricano. A Bacia tem seus limites nos diversos arcos estruturais soerguidos paralelamente à suas bordas. Os arcos de São Vicente e Canastra delimitam a bacia na sua porção norte. Os arcos de Martim Garcia, Pampeano Ocidental-Oriental e Assunção fazem o limite na porção sul, sudeste e oeste respectivamente. O limite leste projeta-se para a atual plataforma continental por força do tectonismo rúptil do continente Gondwana ocorrido no Mesozóico. O Arco de Ponta Grossa é um elemento tectônico importante; ao norte do Arco, o alinhamento Paranapanema divide zonas com taxas de subsidência diferenciadas e distintos sistemas deposicionais. Mais a sul, o Arco de Rio Grande, e, entre este e o Arco de Ponta Grossa situa-se a Sinclinal de Torres, com blocos rebaixados por falhas escalonadas vinculadas ao alinhamento Torres-Posadas. Os alinhamentos Rio Piquiri e Tietê localizam-se respectivamente a sul e a norte do Arco de Ponta Grossa, e o Arco Campo Grande, no limite noroeste da bacia (Fúlfaro, 1971).

A sedimentação da Bacia iniciou-se provavelmente no Siluriano superior e estendeu-se até o Cretáceo. Foram acumulados mais de 6000 m de espessura com rochas sedimentares e vulcânicas. Diversos estudos (e.g., Soares,1973; Zalán *et al*., 1987, Rostirolla *et al*., 2000) mostram que durante a fase de sedimentação da Bacia, falhas antigas do embasamento foram reativadas por inúmeras vezes e influenciaram na distribuição das formações sedimentares bem como na sua espessura lateral no

registro estratigráfico. Diversas colunas estratigráficas foram propostas para definir a ordem da sedimentação na Bacia do Paraná. Nesta tese, a coluna estratigráfica adotada do Ordoviciano/Siluriano até o Jurássico, representado pela deposição da Formação Botucatu (Fig. 1) segue a proposta de Milani *et al*. (1998). Para o período que engloba o vulcanismo Serra Geral no Cretáceo inferior a divisão estratigráfica está balizada na proposta de Wildner *et al*. (2007) e para o período pós-vulcanismo (Grupo Bauru) a coluna estratigráfica adotada é a de Soares *et al.* (1980).

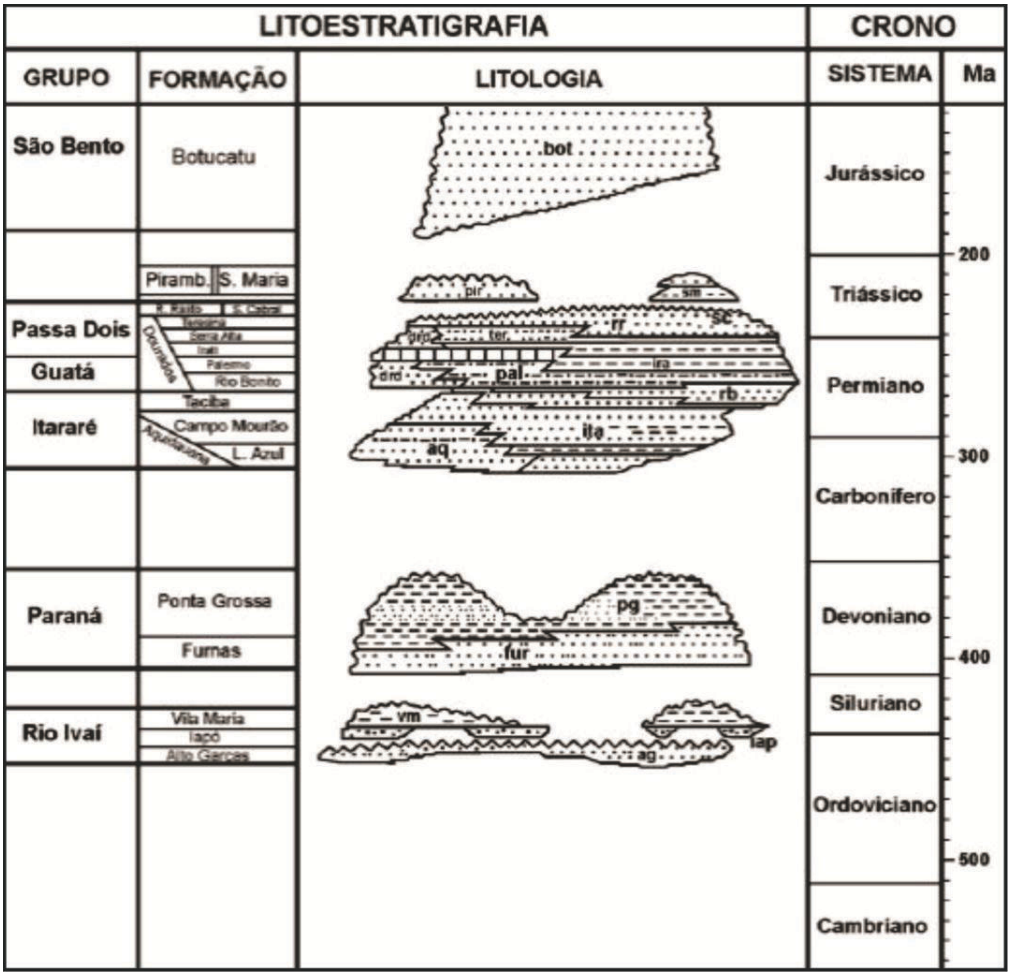

Figura 1. Estratigrafia Bacia do Paraná, Ordoviciano/Jurássico (Milani *et al*., 1998).

O início da sedimentação na Bacia do Paraná foi marcado pelo empilhamento sedimentar do Grupo Rio Ivaí (Assine *et al*., 1994), constituído pelas Formações Alto Garças, Iapó e Vila Maria. Estas Formações apresentam datações para seus registros sedimentares no Ordoviciano / Siluriano. A Formação Alto-Garças constitui o pacote mais antigo da Bacia do Paraná e sua ocorrência é controlada por zonas de fraqueza

do embasamento orientadas a SW-NE (Milani & Ramos, 1998). Esta Formação é composta por arenitos depositados no intervalo Caradociano/Ashgilliano (Assine *et al*., 1998). No meio deste pacote sedimentar está a Formação Iapó que foi proposta por Maack (1947). Apresenta espessura máxima de 20m, é descontínua onde predominam diamictitos com clastos polimíticos de origem glacial (tilitos). No topo da supersequência está a Formação Vila Maria que foi proposta por Faria & Reis Neto (1978) e litologicamente é constituída por arenitos e folhelhos siltosos, depositados em ambiente marinho.

O Devoniano da Bacia do Paraná está representado pelo Grupo Paraná, formalmente definido por Lange & Petri (1967) com a Formação Furnas na base e a Formação Ponta Grossa no topo. A Formação Furnas é litologicamente constituída por arenitos de granulometria média a grossa com estratificação cruzada e horizontal, mas na base da Formação também ocorrem arenitos conglomeráticos. No topo do Grupo Paraná encontra-se a Formação Ponta Grossa que foi inicialmente designada de *"schistos de Ponta Grossa"* (Oliveira, 1912) para identificar as camadas argilosas dos terrenos devonianos próximos à cidade de Ponta Grossa no Paraná. O estudo de Bodziak & Maak (1946) descreve a litologia da unidade como folhelhos limo argilosos depositados em ambiente nerítico, ricos em fósseis marinhos, porém a proposição de Formação Ponta Grossa foi efetuada por Petri (1948). A Formação Ponta Grossa foi posteriormente subdividida da base para o topo pelos membros Jaguariaiva, Tibagi e São Domingos (Lange & Petri, 1967). As litologias da Formação são homogêneas (Schneider *et al*., 1974) e constituidas basicamente por folhelhos, folhelhos síltico-argilosos de cor acinzentada claro ou ainda, esbranquiçado, amarelado, alaranjado, violácea, acastanhada, avermelhada e cinza escuro. Localmente carbonosos ou betuminosos, micáceos, finamente laminados. Subordinadamente ocorrem siltitos e argilitos de coloração cinza-esverdeada a cinza-azulada, com intercalações de arenitos finos a muito finos, micáceos. Quando alterada apresenta cores variegadas, predominando a coloração amarelada, alaranjada, arroxeada e castanha. Apresenta estratificação plano-paralela finamente laminada. Localmente, e em certos níveis, podem ser observadas estratificações cruzadas de pequeno porte, laminação cruzada, marcas ondulares e bioturbações. O ambiente deposicional é essencialmente marinho de águas rasas, sob influência de marés, com grande conteúdo fossilífero (Mineropar,

2001a). Os fósseis encontrados são caracterizados por macrofauna contendo braquiópodes, gastrópodes, trilobitas, crinóides, briozoários, entre outros. Nesta Unidade ocorrem também, fósseis da microfauna tipicamente marinha que permitem datá-la entre o Devoniano Inferior (Emsiano) e o Devoniano Superior (Frasniano), ou seja, entre 408 e 360 Ma. A espessura máxima da Formação Ponta Grossa encontrada até o momento foi de 654 metros em subsuperfície no poço 2-AP-1-PR em Apucarana (PR). O contato com a Formação Campo do Tenente (Grupo Itararé) se dá através de discordância erosiva. A Formação Ponta Grossa é considerada importante rocha fonte de hidrocarbonetos na Bacia. O teor de carbono orgânico total estimado foi de 0.1 – 0.6% (Goulart & Jardim, 1982).

O Permo-Carbonífero está representado pelos Grupos Itararé e Guatá (Super Grupo Tubarão). O termo Itararé foi utilizado primeiramente por Oliveira (1916) para descrever os arenitos, siltitos, ritmitos, folhelhos e diamictitos de ambiente glacial. A formalização como Grupo Itararé foi estabelecida por Gordon Jr. (1947), que propôs o termo Grupo Guatá para descrever os siltitos e arenitos com intercalações de carvão e folhelhos carbonosos que compõem as Formações Rio Bonito e Palermo. A primeira descrição da “camada Rio Bonito” foi efetuada por White (1908) que identificou arenitos associadas a pelitos e camadas de carvão entre as cidades de Lauro Muller, Guatá e São Joaquim (SC). A Formação Rio Bonito, a mais antiga do Grupo Guatá, é constituída por uma sequência sedimentar de arenitos na base passando a essencialmente argilosa na porção média e areno-argilosa no topo. A Formação destaca-se por apresentar as principais camadas de carvão exploradas na Bacia do Paraná e está dividida em três membros denominados Triunfo, Paraguaçu e Siderópolis (Mühlmann *et al*., 1974). O Membro Triunfo é constituído principalmente de arenitos esbranquiçados com granulação fina a média. Em menor proporção ocorrem arenitos finos, siltitos, argilitos, folhelhos carbonosos, camadas de carvão e conglomerados. O Membro Paraguaçu é constituído por siltitos escuros, folhelhos (cinza a esverdeados) com níveis de carbonatos argilosos e camadas de carvão. A sedimentação ocorreu em ambiente marinho transgressivo enquanto as intercalações arenosas do membro Triunfo representam depósitos de barras, barreiras e, possivelmente, acumulações distais de sistemas deltaicos depositados durante o Permiano Médio. O Membro Siderópolis é composto essencialmente por arenitos finos de cor cinza intercalados por

camadas de siltito cinza, siltitos carbonosos e camadas de carvão (camada Bonito). O ambiente de deposição é marinho litorâneo progradante (Medeiros & Thomaz-Filho, 1973). A idade dos sedimentos correspondente ao Permiano Médio-Superior. A variação do carbono orgânico total na camada de carvão denominada Bonito, nas proximidades de Lauro Muller, SC, varia de 2,4 peso % até 44 peso % (Mendonça Filho *et al*., 2013). A observação das sondagens (CPRM) para pesquisa de carvão mostra que a sequência de rochas da Formação Rio Bonito apresenta uma grande quantidade de sills de diabásio alojadas nestas rochas que "queimaram" uma parcela das camadas de carvão e afetaram termicamente os carbonatos e outras litologias da Formação.

A Formação Palermo está sobreposta à Formação Rio Bonito compõe o topo do Grupo Guatá. Constitui-se de siltitos, siltitos arenosos e folhelhos sílticos com intercalações delgadas de arenito muito fino, quartzoso e de coloração cinza a amarelo esverdeada. Em geral estes sedimentos encontram-se bioturbados, comprometendo as estruturas sedimentares. Quando estas estruturas encontram-se preservadas caracterizam laminações cruzadas de muito pequeno porte. De acordo com Bortoluzzi *et al.* (1978) a deposição destes sedimentos deu-se em ambiente subaquoso de águas rasas em condições de baixa energia e fraca a moderada ação de ondas. Ocorrem ainda depósitos de canais de marés. A idade desta Formação é Permiana Média a Superior.

O Grupo Passa Dois, sobreposto ao Grupo Guatá, representa o Permiano Superior da Bacia do Paraná. O termo Passa Dois foi utilizado pela primeira vez por White (1908) e posteriormente Schneider *et al*. (1974) formalizou-o como Grupo definindo o ambiente deposicional destas rochas como marinho, de águas calmas. Fazem parte deste Grupo, da base para o topo, as Formações Irati, Serra Alta e Teresina. A Formação Irati é constituída por folhelhos betuminosos, margas e calcários dolomíticos e foi subdividida nos membros Taquaral e Assistência. A Formação ocupa praticamente 1.000.000 Km^2 incluindo áreas em Goiás, Mato Grosso, Mato Grosso do Sul, São Paulo, Paraná, Santa Catarina e Rio Grande do Sul. No estado de São Paulo a Formação Irati apresenta maior espessura das camadas de carbonatos enquanto que no Paraná e no Rio Grande do Sul as camadas de folhelho pirobetuminoso são mais expressivas (Schneider *et al*., 1974). A espessura média da Formação Irati é de 40 m, com picos de espessura de até 70 m (Holz *et al*., 2010) e apresenta grande

continuidade lateral na Bacia do Paraná. O membro Taquaral foi depositado em ambiente marinho de baixa energia (Schneider *et al*., 1974) e é composto por siltitos argilosos e folhelhos cinza-escuros e cinza-claros com laminação paralela (Barbosa & Almeida, 1949). O membro Assistência também foi depositado em ambiente marinho, mas com pouca oxigenação e circulação de água (Schneider *et al*., 1974) e apresenta folhelhos, siltitos cinza-escuros com laminação paralela, folhelhos pirobetuminosos e calcários dolomíticos. A sedimentação da Formação Irati, de acordo com datações paleontológicas e isótopos radioativos, apresenta aproximadamente 260 Ma (Daemon & Quadros, 1970, Thomaz-Filho *et al.,* 1976). A presença de fósseis do *mesosaurus brasiliensis* (réptil aquático) na Formação Irati, permitiu realizar correlações estratigráficas com as unidades eopermianas do sul da África (Lages, 2004). Este fóssil também é encontrado em São Mateus do Sul (PR) onde a Petrobrás-SIX com interesse em fontes adicionais de hidrocarbonetos explora o folhelho para produção de óleo de xisto, gás liquefeito de xisto, enxofre e nafta. De acordo com a Mineropar (2007) a Formação Irati tem uma reserva de 700 milhões de barris de óleo, 9 milhões de toneladas de gás liquefeito (GLP), 25 bilhões de metros cúbicos de gás de xisto e 18 milhões de toneladas de enxofre. Em São Mateus do Sul há duas camadas desta Formação que são exploradas, a superior com 6,4 m de espessura e 6,4% de teor de óleo, e outra inferior com 3,2 m de espessura e teor de óleo de 9,1% (Mineropar, 2007). O teor de carbono orgânico total (COT) da Formação Irati foi avaliado em vários estudos e os valores indicados para os folhelhos do membro Assistência estão entre 0,62 a 7,9% (Santos Neto, 1993) e 0,30 e 2,48% (Mendonça Filho, 1999). O estudo de Lages (2004) selecionou a sondagem (CPRM) FP-01-PR de Sapopema (PR) motivado pelo fato de que este perfil não apresenta intrusões vulcânicas que poderiam ter alterado as características geoquímicas das rochas e destruído os palinomorfos. Os resultados de carbono orgânico total apresentaram valores médios de 2,10% para o membro Assistência e de 1,61% para o membro Taquaral e amparam a hipótese de que a Formação Irati é um grande potencial gerador de hidrocarbonetos. O exame de 835 testemunhos de sondagem da CPRM para pesquisa de carvão mostra que os sills do magmatismo Serra Geral intrusionaram preferencialmente na Formação Irati (Baggio *et al*., 2014b), seguido pela Formação Rio Bonito e em menor escala nas outras Formações, mostrando que a físsibilidade dos folhelhos deve controlar esta preferência

conforme já interpretado por Araújo *et al*. (2004). Outras formações da Bacia do Paraná também apresentam folhelhos negros associados a intrusões de sills, a exemplo da Formação Serra Alta e Teresina, que recobrem a Formação Irati e também agregam potencial de hidrocarbonetos na Bacia. A Formação Serra Alta, definida por Sanford & Lange (1960), é constituída por folhelhos, argilitos e siltitos cinza-escuros a pretos com concreções calcíferas, e foi depositada em ambiente marinho de águas calmas. A laminação é plano-paralela incipiente, às vezes micácea e a espessura do pacote sedimentar é em média 90m. A Formação Teresina é constituída de argilitos, folhelhos e siltitos esverdeados a cinza-escuros intercalados com arenitos cinza-claros muito finos além de lentes e concreções carbonáticas. A Formação foi depositada em ambiente marinho de água rasa e agitada pela ação da maré. As estruturas sedimentares mais comuns são as laminações flaser, plano-paralela, ondulada e gretas de contração. O pacote sedimentar apresenta em média espessuras de 80 m.

O Triássico da Bacia do Paraná encontra-se representado pelas Formações Pirambóia e Rosário do Sul que, associadas a outras unidades perfazem o Sistema Aquífero Guarani. O termo Pirambóia foi utilizado por Pacheco (1927) e por Sanford & Lange (1960) e formalizado como unidade litoestratigráfica por Soares (1975). A Formação Pirambóia é constituída por arenitos médios a muito finos, formando intercalação de arenitos de deposição eólica, fluvial e lacustre e a Formação Rosário do Sul, proposta por Gamermann (1973), é constituída essencialmente de arenitos, apresentando no topo uma fácies pelítica. O estudo de Soares *et al*. (2008) no Sistema Aquífero Guarani, mostra que a variação na espessura da Formação Pirambóia é em média 250 m na compartimentação Noroeste e Oeste do SAG, enquanto que na compartimentação Sudeste a média é de 80m com variação entre 30 m a 200 m (Fig. 2) e, de acordo com os autores, a variação de espessura para Oeste é indicativo de controle tectônico.

O Juro-Cretáceo da Bacia do Paraná, representado pelo Grupo São Bento, foi definido por Schneider *et al*. (1974) e incluía a Formação Botucatu e os derrames de lavas do magmatismo Serra Geral. O estudo de Wildner *et al*. (2007) retira as rochas vulcânicas deste Grupo e propõe a elas o status de Grupo Serra Geral. A Formação Botucatu foi redefinida formalmente por Soares (1973, 1975). Na base da Formação ocorrem arenitos com fácies torrencial conglomerática e no topo, arenitos avermelhados

de fácies eólica, depositados em ambiente desértico. A Formação, que também faz parte do Sistema Aqüífero Guarani apresenta morfologia de campos de dunas e de interdunas, constituída por arenitos finos com pouca argila na matriz e bem selecionados (Petri & Fúlfaro, 1983). A predominância é de quartzo arenitos finos a médios (IPT, 1981), mas subordinadamente ocorrem subarcóseos (Wu & Caetano-Chang, 1992). A bimodalidade também ocorre com granulometria grossa e fina (Soares *et al*., 2008) e os grãos são bem arredondados, foscos e com maturidade textural variando de maturo e supermaturo. A estratificação dos arenitos é cruzada acanalada de grande porte, devido à migração lateral das dunas, com sets de até 20 m (Soares *et al*., 2008), mas também ocorre estratificação cruzada tabular tangencial na base e estratificação plano-paralela (Wu & Caetano-Chang, 1992). A Formação Botucatu está presente em praticamente toda a Bacia do Paraná com espessura variável. Na região de São Jerônimo da Serra (PR) apresenta espessura de 50 m (Strugale *et al*., 2004) e na região de Ribeirão Preto (SP) a espessura é de 80 m (Sinelli, 1980). O estudo de Soares *et al*. (2008) mostra que a variação na espessura do arenito Botucatu (Fig. 2) ocorre desde 0,00 m até 70,00 m na compartimentação Noroeste e Oeste do Sistema Aquífero Guarani e entre 80,00 m até 120,00 m na compartimentação Nordeste e Centro Leste, sendo que nas demais compartimentações apresenta espessuras entre 50,00 m e 80,00 m. Esta variação é atribuída à distribuição dos campos de dunas e seu recobrimento pelos derrames basálticos (Assine *et al*., 2004) que ocorreu em diferentes níveis, ora em superfícies erosivas, ora em superfície deposicional (Soares *et al*., 2008) com preservação da morfologia da duna.

O contato entre a Formação Botucatu e os derrames vulcânicos é concordante e marcado na base do primeiro derrame (Carneiro, 2007). A efusão dos primeiros derrames foi contemporânea à deposição das areias eólicas da Formação Botucatu e está marcada pela intercalação de areia e rochas vulcânicas. Por outro lado, a presença de areia nos derrames posicionados na porção superior da pilha vulcânica é aqui atribuída aos eventos hidrotermais. Os mecanismos de transporte e deposição serão descritos nesta tese.

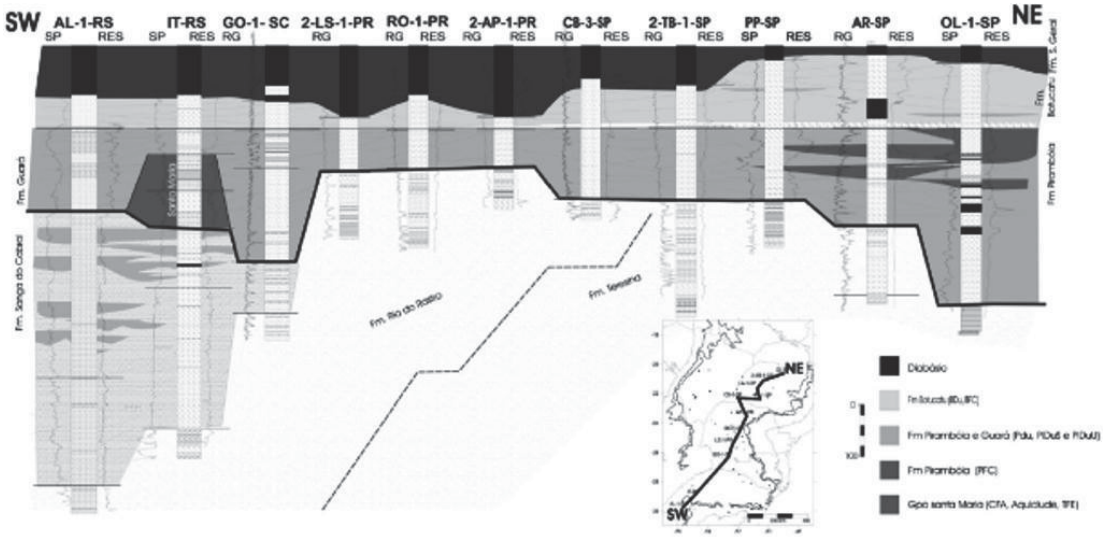

Figura 2. Seção estratigráfica longitudinal nivelada na base da Formação Botucatu. Observar a variação de espessura das Formações que compõem o Sistema Aquífero Guarani e da pilha vulcânica da província Paraná (Soares *et al*., 2008).

Sotopostas aos arenitos da Formação Botucatu, as rochas do Grupo Serra Geral representam o período de cisão do supercontinente Gondwana. O evento magmático deu origem a segunda maior província vulcânica do mundo, causou subsidências na Bacia do Paraná e a inflexão do Arco de Ponta Grossa. A elevação deste arco causou intenso fraturamento NW-SE e permitiu a passagem do magma através da estratigrafia da Bacia do Paraná até a superfície com geração de um enxame de diques de diabásio com granulação fina a média e inúmeros sills nas formações sedimentares. As rochas associadas ao vulcanismo do Grupo Serra Geral serão descritas no item 1.3.2.

Os sedimentos do Grupo Bauru depositados sobre os derrames vulcânicos da província Paraná completaram o preenchimento da Bacia do Paraná no Cretáceo Superior. O Grupo Bauru é constituído por sedimentos siliciclásticos continentais, depositados em ambiente aluvial fluvial além de conglomerados, arenitos e argilitos. Da base para o topo, o Grupo Bauru é constituído pelas Formações Caiuá, Santo Anastácio, Adamantina e Marília (Soares *et al*., 1980). A espessura máxima do Grupo Bauru em locais onde está preservado é de 300 m, a exemplo da região de Marília, SP (Paula e Silva *et al*., 2003), mas a média é de 100 m de espessura.

1.3.2. Derrames basálticos da província vulcânica Paraná

A origem da lava das províncias vulcânicas é assunto de amplo debate científico. O estudo de Coltice *et al.* (2007) sugere para a província vulcânica Paraná uma origem relacionada a um super aquecimento do manto abaixo do Gondwana, sem participação de pluma mantélica. O modelo envolve a geração de zonas aquecidas no manto devido ao isolamento térmico provocado pelo supercontinente Gondwana. Porém, o modelo mais defendido invoca a hipótese de plumas mantélicas e suas variações (White & Mackenzie, 1989, 1995; Richards *et al.,* 1989; Campbell & Griffiths, 1990; O'Connor *et al.,* 1990; Hill, 1991; Hill *et al.,* 1992; Renne *et al.,* 1992). Segundo este modelo, a anomalia térmica gerada pela pluma mantélica de Tristão da Cunha (Fig. 3) foi a responsável pelo magmatismo Paraná-Etendeka, ruptura e separação do Gondwana.

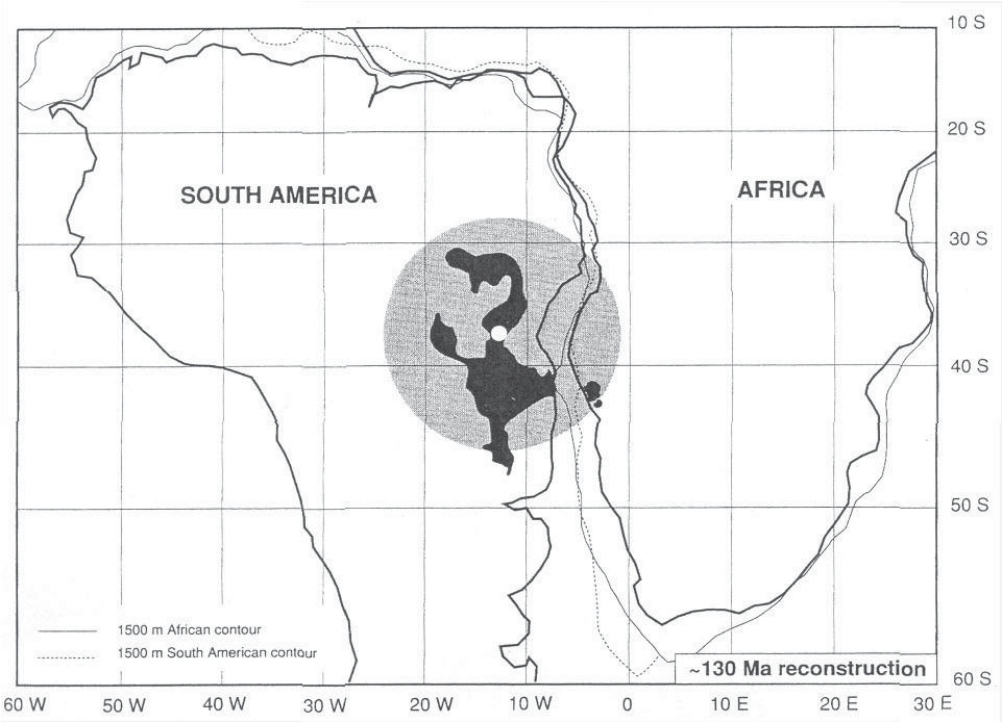

Figura 3. Área de influência da pluma mantélica Tristão da Cunha. Província vulcânica Paraná-Etendeka (O'Connor *et al.,* 1990).

A partir do evento magmático do Cretáceo, derrames de lava toleiítica começaram a recobrir as dunas de areia da Formação Botucatu no Brasil, Formação Misiones (Argentina e Paraguai) e Formação Taquarembó no Uruguai, estabelecendo o

fim do ambiente desértico e o início da atividade vulcânica na Bacia do Paraná. Este evento gerou a província vulcânica Paraná (Fig. 4) uma das maiores do mundo.

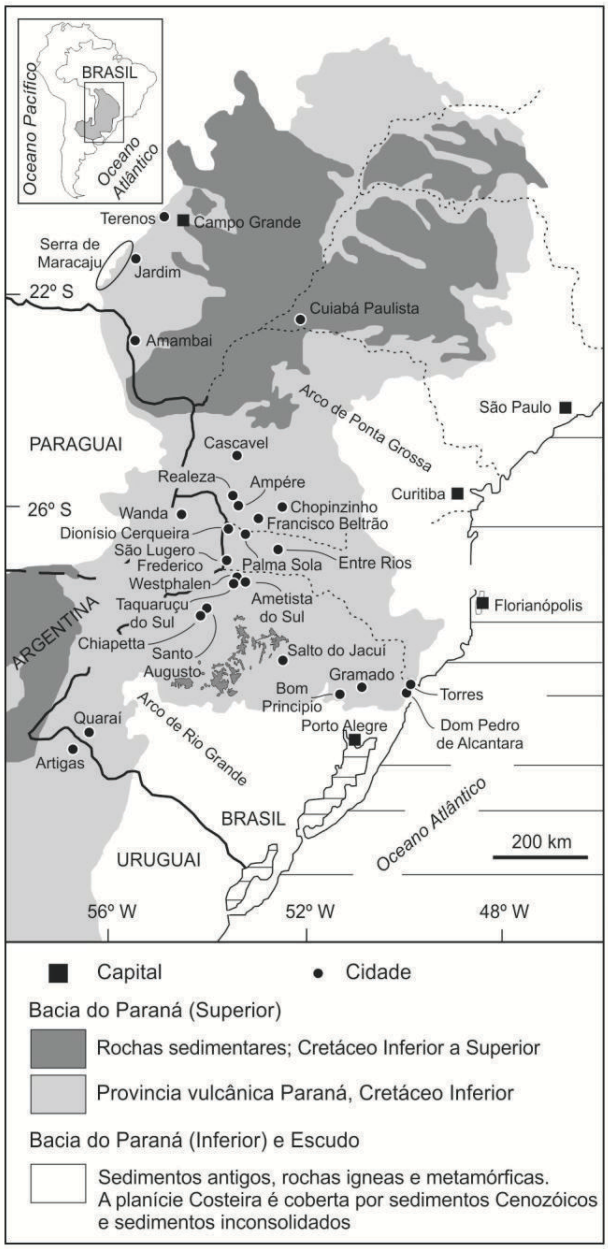

Figura 4. Província vulcânica Paraná. Localidades com mineralizações de cobre, depósitos de ametista e/ou citadas na tese. Modificado de Peate *et al.* (1992)

Os derrames de lava da província vulcânica Paraná são compostos basicamente por basaltos e andesitos basálticos. Subordinadamente ocorrem riodacitos, dacitos, quartzo latitos e riolitos (SiO_2>62%) que geralmente afloram na porção sul da província (Melfi *et al.,* 1988), na parcela superior da pilha vulcânica. Há ainda a ocorrência restrita

de rochas intrusivas. Os derrames da província Paraná segundo Renne *et al.* (1992) recobrem 1.2 x 10^6 km^2, aproximadamente 70% da área da Bacia do Paraná (Bellieni *et al.,* 1986). Nos Estados de Minas Gerais e Goiás as rochas da província vulcânica Paraná estão em contato direto com o embasamento cristalino Pré Cambriano (Petri & Fúlfaro, 1983). Por outro lado Frank *et al.* (2009) recalcularam a área das lavas para 917.000 km^2 com volume de 450.000 km^3 de lavas expelidas, além de 112.000 km^3 de lava que permaneceu em subsuperfície (diques e sills). A espessura total da pilha vulcânica atinge 1.723 m (poço de Cuiabá Paulista). Para Sul o pacote torna-se progressivamente mais delgado até atingir valores próximos a 50 m na região da fronteira do Brasil com a Argentina (Almeida, 1986). Já a espessura individual de cada derrame segundo Peate *et al.* (1999) é de 5 a 80 m, sendo em média 20 m. A estrutura interna dos derrames foi descrita inicialmente por Leinz (1949) em afloramentos de Três Forquilhas (RS). Ele descreve uma zona com diáclase horizontal, seguida por uma zona amigdaloidal, por vezes preenchida por zeolitas, com 5 a 10 m de espessura. Na região de Frederico Westphalen (RS), Gomes (1996) caracterizou doze derrames de rochas basálticas que compõem a coluna estratigráfica. As características estruturais e petrográficas destas rochas levaram a autora a descrever dois tipos de derrames. O derrame tipo I apresenta espessuras entre 15-30 m, com estruturação interna determinada por delgado nível vesicular no topo e abaixo uma zona intensamente fraturada. A sequência apresenta uma zona macrovesicular interna, que por vezes apresenta geodos mineralizados com ametista e uma zona central maciça. Na base, pode ocorrer um delgado nível vesicular. O Derrame Tipo II apresenta espessuras entre 30 e 50 m. É caracterizado pela presença de nível vesicular de topo e na base, e uma zona central intensamente fraturada, em alguns casos com a formação de três níveis diferenciados pelo padrão de fraturamento como colunado superior, entablamento e colunado inferior. Na porção oeste do Paraná, estudos conduzidos por Waichel (2006) e Waichel *et al.* (2006) descrevem os aspectos vulcanológicos e morfológicos dos derrames do tipo *´a´a e* tipo pahoehoe. Os derrames *´a´a* são caracterizados por topo e base escoriáceos e vesículas alongadas. Os derrames tipo pahoehoe apresentam superfície lisa, ondulada ou em corda, e ocorrem como fluxos simples e também como fluxos compostos formados por múltiplos lobos. Os derrames pahoehoe foram estruturados em três zonas: crosta inferior, núcleo e crosta superior. É destacada a

presença de micro vesículas entre os cristais de plagioclásio e piroxênio que foi definido como textura diktaxítica, indicativa de alto conteúdo de voláteis no magma gerador destes derrames.

A idade e duração do magmatismo Serra Geral têm sido debatida desde o início dos anos 60. Através do método Rb-Sr Mantovani *et al*. (1985) apontaram uma isócrona de idade de 135.5±3.2 Ma a partir de amostras de riolito (magma-tipo Chapecó). Três anos mais tarde Rocha-Campos *et al.* (1988) elaboraram um estudo das idades dos derrames basálticos disponíveis na literatura. Os autores avaliaram 206 dados obtidos pelo método K-Ar e 22 obtidos pelo método Rb-Sr. O estudo indicou que a principal fase da atividade vulcânica ocorreu entre 130-135 Ma. Mincato (2000) apresentou informações radiométricas (Ar-Ar) de 18 amostras de rochas da província vulcânica Paraná (basaltos e riolitos). A avaliação do autor mostrou que o evento magmático teve uma duração de 3,5 Ma, entre 133,90 e 130,36 Ma. Os estudos desenvolvidos a partir de 2005 utilizaram a datação pelo método U/Pb. Lustrino *et al*. (2005) dataram zircão de rocha sienítica do sudeste do Uruguai e indicaram idade de 128.1±1.6 Ma. Wildner *et al.* (2006) utilizaram SHRIMP (*Sensitive High Resolution Microprobe*) em rochas vulcânicas riodacíticas do tipo Chapecó e apresentaram idades entre 134 e 139 Ma. O estudo de Pinto *et al*. (2011a) determinou pela primeira vez datação U/Pb (SHRIMP) de zircões magmáticos de basaltos da província vulcânica Paraná com idades de 133.7 Ma ± 1.2 Ma. Esta idade (133 - 135 Ma) foi confirmada por Janasi *et al*. (2011) como o pico do vulcanismo em datação de badeleíta. Recentemente, Brückmann *et al.* (2014) demonstrou a partir de zircões magmáticos que a atividade vulcânica se prolongou até 119 Ma, idade que estende a duração do vulcanismo na província Paraná para 16 Ma.

A partir dos estudos desenvolvidos por Bellieni *et al.* (1984) e Mantovani *et al.* (1985), as rochas basálticas da província vulcânica Paraná foram divididas nos grupos Alto Ti (ATi = TiO2 >2%) e Baixo Ti (BTi = TiO2<2%). Com base nestes grupos, o estudo de Piccirillo *et al*. (1988) compartimentou a província vulcânica Paraná em três regiões delimitadas por lineamentos tectônicos e diferentes afinidades químicas. A primeira região denominada sul do lineamento do Rio Uruguai apresenta rochas basálticas de baixo Ti e riodacíticas do tipo Palmas. A segunda região denominada parte norte é caracterizada por rochas basálticas alto-Ti e raros derrames ácidos do tipo Chapecó. A região central, entre os lineamentos Uruguai e Piquiri é caracterizada por

rochas basálticas de alto e baixo-Ti e rochas riodacíticas tanto do tipo Palmas como do tipo Chapecó. No entanto, para Peate *et al.*(1992), esta divisão geográfica baseada nos lineamentos é arbitrária, está enraizada na literatura, e efetivamente não tem nenhum controle óbvio sobre a natureza e a distribuição dos tipos de magma na superfície.

A divisão proposta por Peate *et al.* (1992), com base em teores de elementos maiores, elementos traço e razões entre elementos-traço, indicou 6 magmas tipo, sendo três na porção norte da província: Pitanga, Paranapanema e Ribeira e três na porção sul da Província: Gramado, Esmeralda e Urubici (Tabela 1). O estudo de Nakamura *et al*. (2003) propôs a inclusão do grupo Ti intermediário com os magma tipo Ribeira e Paranapanema. Nesta proposição o grupo Baixo Ti mantém os magma-tipo Gramado e Esmeralda e o grupo Alto Ti os magma-tipo Pitanga e Urubici. As rochas riodacíticas foram quimicamente divididas em dois principais magma-tipo (Bellieni *et al*., 1986). O tipo Chapecó possui alto Ti, P (La, Ce, Zr) enquanto que o tipo Palmas tem baixo Ti e P. O magma-tipo Chapecó foi subdividido (Nardy *et al*., 2008) com base em geoquímica nos subtipos Guarapuava, Tamarana e Ourinhos e o magma-tipo Palmas em cinco subtipos denominados Anita Garibaldi, Jacuí, Caxias do Sul, Clevelândia e Santa Maria. Estudos recentes, estabelecidos por Licht & Arioli (2012) reavaliaram a divisão geoquímica e sugerem para a comunidade científica uma nova divisão com pelo menos 12-16 tipos químicos.

Grupo		Alto-Ti			Baixo-Ti	
Magmas-tipo	Urubici	Pitanga	Paranapanema	Ribeira	Esmeralda	Gramado
Subprovíncia	Sul	Norte	Norte	Norte	Sul	Sul
SiO_2 (%)	>49	>47	48-53	49-52	48-55	49-60
TiO_2 (%)	>3,3	>2,8	1,7-3,2	1,5-2,3	1,1-2,3	0,7-2,0
P_2O_5 (%)	>0,45	>0,35	0,2-0,8	0,15-0,50	0,1-0,35	0,05-0,40
Fe_2O_3 (t)(%)	<14,5	12,5-18	12,5-17	12-16	12-17	9-16
Sr (µg/g)	>550	>350	200-450	200-375	<250	140-400
Ba (µg/g)	>500	>200	200-650	200-600	90-400	100-700
Zr (µg/g)	>250	>200	120-250	100-200	65-210	65-275
Ti/Zr	>57	>60	>65	>65	>60	<70
Ti/Y	>500	>350	>350	>300	<330	<330
Zr/Y	>6,5	>5,5	4,0-7,0	3,5-7,0	2,0-5,0	3,5-6,5
Sr/Y	>14	>8	4,5-15	5-17	<9	<13
Ba/Y	>14	>9	5-19	6-19	<12	<19

Tabela 1. Critérios de Classificação dos magmas tipo da província vulcânica Paraná (Peate *et al*., 1992).

A estratigrafia dos derrames vulcânicos da província foi avaliada nos estudos de Wildner *et al.* (2007) com base em seções geológicas, pesquisas de campo e investigações geoquímicas. O estudo propôs a modificação do status de Formação Serra Geral para Grupo Serra Geral que engloba nesta proposta 16 novas Formações (Tabela 2, Fig. 5) agrupadas de acordo com os magmas tipo (Peate, 1997). O Grupo Serra Geral continua associado à Supersequência Gondwana III estabelecida por Milani *et al*. (2007).

FORMAÇÃO	MAGMA-TIPO	CARACTERÍSTICAS
Esmeralda	Esmeralda	Basalto – Baixo Ti/Y
Várzea do Cedro	Palmas	Riolito – Baixo Ti
Palmas	Palmas	Riolito – Baixo Ti
Ourinhos	Chapecó	Riolito – Alto Ti-Zr
Chapecó	Chapecó	Riolito – Alto Ti-Zr
Paranapanema	Paranapanema	Basalto–Intermediário Ti/Y
Campo Erê	Paranapanema	Basalto–Intermediário Ti/Y
Cordilheira Alta	Paranapanema	Basalto–Intermediário Ti/Y
Capanema	Paranapanema	Basalto–Intermediário Ti/Y
Campos Novos	Esmeralda	Basalto – Baixo Ti/Y
Alegrete	Gramado	Basalto – Baixo Ti/Y
Gramado	Gramado	Basalto – Baixo Ti/Y
Nova Laranjeiras	Pitanga	Basalto – Alto Ti/Y
Pitanga	Pitanga	Basalto – Alto Ti/Y
Urubici	Urubici	Basalto – Alto Ti/Y
Ribeira	Ribeira	Basalto – Alto Ti/Y
Complexo Morungava	Morungava	Sills Picrítico Máfico-Ultramáfico

Tabela 2. Nomenclatura estratigráfica das Formações do Grupo Serra Geral e conexões químicas com os magmas-tipo propostos por Peate (1997). (Wildner *et al.,* 2007).

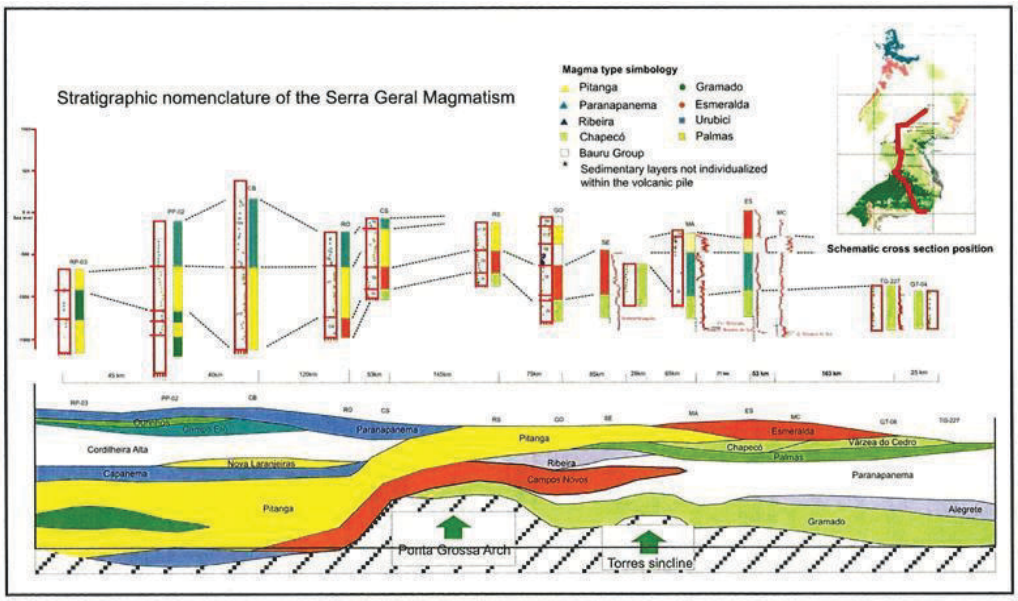

Figura 5. Estratigrafia e secção transversal esquemática Grupo Serra Geral (Wildner *et al.,* 2007).

Um grupo especial de rochas, denominado na literatura como “pegmatitos”, ocorre restritamente em algumas áreas da pilha vulcânica, principalmente no noroeste do Paraná. Estas rochas apresentam mineralização de cobre nativo e por este motivo foram incluídas nas avaliações da tese. Entretanto durante as discussões sobre a origem destas rochas, as evidências de campo estabelecidas na pedreira Dalba em Francisco Beltrão (PR) e os resultados obtidos, derivaram para uma interpretação diferente daquela proposta na literatura internacional. A partir disso, a denominação “paralavas” foi entendida como coerente para estas rochas, conforme detalhado no artigo *“Paralavas in the Paraná volcanic province, Brazil – An interpretation of the basaltic rocks containing phenocrysts and glass”*.

As paralavas apresentam dimensões entre 0,1-2,0 m de espessura e 1-10 m e máximo de 100 m de comprimento. São camadas verticais, horizontais ou inclinadas com contato gradacional nítido com a rocha hospedeira. Ocorrem geralmente em derrames espessos (> 70 m) compostos por basalto, andesito basáltico e andesito com disjunção colunar. O rápido resfriamento dos derrames mais finos parece impedir a formação de paralavas e não foram observadas paralavas injetadas em disjunções colunares, o que indica que as paralavas são mais antigas que as disjunções.

O processo de formação das paralavas está associado à intrusão de diques e sills de lava que afetaram termicamente a bacia do Paraná, principalmente ao longo do arco de Ponta Grossa onde a densidade deles é maior. As unidades estratigráficas portadoras de carbono orgânico total que tiveram contato direto com a lava, sofreram craqueamento do querogênio e geração de gás metano. A avaliação de 835 testemunhos de sondagem da bacia carbonífera executadas pela CPRM (Tabela 3) mostra que os sills estão intrusionados em muitas unidades da Bacia, mas ocorrem preferencialmente na Formação Irati, que apresenta até 7,9% de carbono orgânico total.

Formação Bacia do Paraná	Número de sills	Espessura média (m)
Serra Alta	42	22
Irati	377	23
Palermo	31	12
Rio Bonito	109	18
Itararé	13	27

Tabela 3. Correlação da quantidade de sills intrudidos nas formações sedimentares portadoras de carbono orgânico da região sudeste da Bacia do Paraná.

A interpretação do mecanismo de formação destas rochas prevê que o gás metano formado pelo craqueamento do querogênio, em ascensão à superfície, ao atingir a base do derrame mais jovem, ainda em resfriamento, com temperaturas da ordem de 1000 ºC entrou em combustão, elevando a temperatura local para 1600 °C promovendo refusão parcial do basalto. O líquido neo-formado apresenta uma proporção maior de elementos leves, por isso é mais "diferenciado" e ascende por gravidade para a porção central e superior do núcleo do derrame onde sofre *quenching* e forma as paralavas. O modelo do processo (Fig. 6) prevê um derrame de 70 m de espessura onde diques, sills e *stockworks* de paralava são formadas no seu núcleo. Ao resfriar são formadas as disjunções colunares do derrame que muitas vezes segmentam as paralavas.

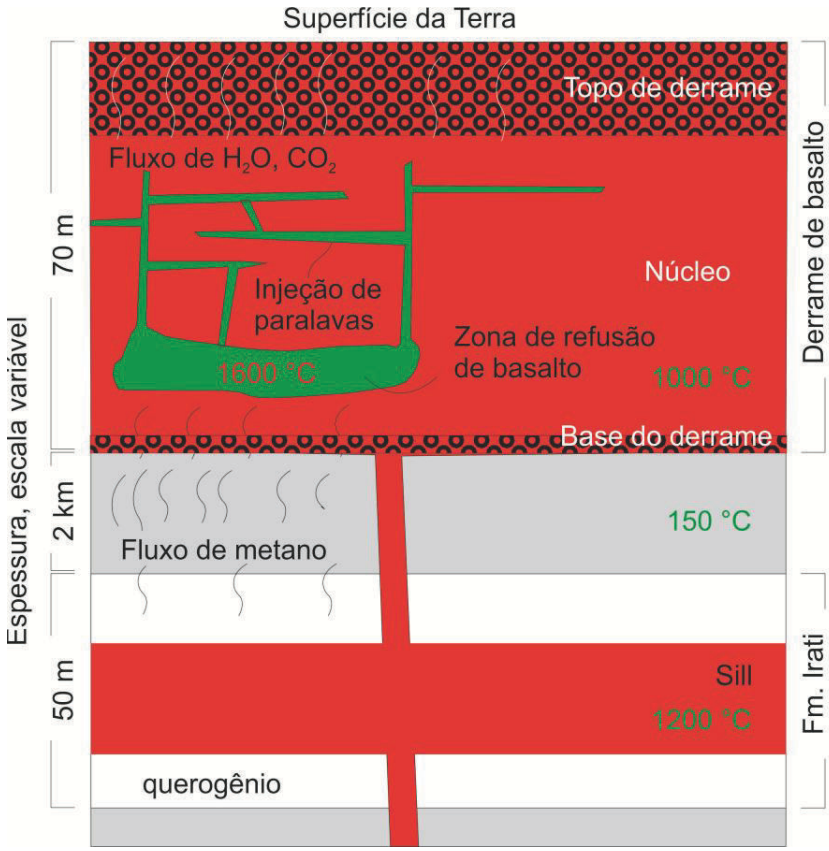

Figura 6. Modelo do processo de formação das paralavas a partir do craqueamento do querogênio da Formação Irati e geração de metano, fluxo ascendente do metano pelas formações sedimentares e vulcânicas da Bacia do Paraná. Combustão do metano na base de um derrame espesso em resfriamento (1000 ºC), refusão do basalto e injeção das paralavas em forma de sills e diques no núcleo do derrame.

O afloramento destas rochas na pedreira Dalba, mostra feições reativas importantes que foram designadas bordas de reação escura (concentração de minerais opacos) e bordas de reação clara (predominância de plagioclásio). A petrografia das paralavas mostra a magnetita e ilmenita com hábito esqueletal, fenocristais (plagioclásio e clinopiroxênio) longos e vidro na matriz com textura intersertal, que exige resfriamento muito rápido da lava. A geoquímica do basalto hospedeiro apresentou conteúdos médios de SiO_2 de 50,17 peso%, enquanto na borda escura da paralava o valor foi de 51,47 peso% e a borda de reação clara atingiu 54,96 peso%. Similar distribuição geoquímica ocorre nos óxidos K_2O, P_2O_5 e nos elementos Ba, Y, Zr, Th, U, Cu, La e demais terras raras. Em contrapartida o MgO e CaO apresentam comportamento inverso. O MgO dos basaltos hospedeiros apresenta em média de 4,84 peso% enquanto que na borda escura da paralava é 3,97 peso% e na borda clara é de 2,62 peso%. O conteúdo de CaO nos basaltos hospedeiros é em média 9,05 peso%. Na borda de reação escura o conteúdo de CaO é de 6,17 peso% e na borda de reação clara é 4,49 peso%. O estudo de D'Oriano *et al*. (2013) é relevante na avaliação geoquímica das paralavas. A refusão de fragmentos de basalto executada em laboratório pelo referido estudo, apresenta distribuição de elementos muito similar aos obtidos nas paralavas do Grupo Serra Geral, inclusive para os elementos incompatíveis. As análises de microssonda eletrônica confirmam que a magnetita das paralavas apresenta conteúdos de FeO e TiO_2 maior que na magnetita dos basaltos hospedeiros.

A análise de inclusões fluidas da amostra P1C apresentou feições sugestivas de *melt inclusions*, escape de fluidos e *necking down*. As inclusões fluidas apresentam dimensões entre 5 e10 μm principalmente e as menores são escuras e distorcidas. Uma parte das inclusões fluidas é composta por soluções aquosas salinas com 13,9 a 16,1 % em peso de NaCl equivalente. Na amostra P6 as inclusões fluidas sugeriram com cautela o sistema H_2O + NaCl + $CaCl_2$ (+/-$MgCl_2$) e salinidades variando entre 14 a 16 % em peso de NaCl equivalente. Em inclusões monofásicas o resfriamento até –180 °C não apresentou mudanças, sugerindo que podem ser constituídas por sólidos ou por fluido de baixa densidade não detectável por microtermometria (e.g., vapor de água, CO_2 gás, CH_4 gás). Na amostra P6 também foi observada uma inclusão fluida secundária maior (~100μm), com feições sugestivas de escape, baixa salinidade (2,3 % em peso de NaCl equivalente) que foi aprisionada em baixas temperatura e apresenta

morfologia, comportamento e dimensões diferentes das outras inclusões observadas. Esta avaliação indicou pelo menos duas fases de aprisionamento de inclusões fluidas na rocha. A geração de inclusões fluidas mais antigas foi aprisionada em altas temperaturas com altas salinidades que podem conter voláteis de baixa densidade relacionadas ao evento de formação das paralavas. As inclusões fluidas da geração posterior foram aprisionadas em baixas temperaturas e a partir de soluções com baixa salinidade que podem ser relacionadas com os eventos hidrotermais (item 1.3.3) do Cretáceo. Sob esta mesma ótica, a perda ao fogo e a presença de celadonita na associação das paralavas foi interpretada como forma final da alteração hidrotermal e intempérica. A perda ao fogo nos basaltos hospedeiros é de 1,6 peso% enquanto que nas paralavas a perda ao fogo chega a 2,4 peso% na borda de reação escura.

Apesar das paralavas terem ocorrência restrita, a mineralização de cobre nestas rochas é importante. A avaliação do teor médio de cobre nos basaltos hospedeiros apresenta 141 ppm. Nas paralavas observa-se um aumento significativo deste teor que passa para 236 ppm na borda de reação escura e atinge valores de 600 ppm na borda de reação clara, mostrando que a concentração do metal foi distinta e relacionada com os processos de geração das paralavas. Há ainda ocorrência de cobre nativo na superfície das disjunções colunares do mesmo derrame. Esta mineralização está associada aos eventos hidrotermais que ocorreram na evolução da província vulcânica Paraná e serão discutidos no item 1.3.4.1.

1.3.3. Eventos hidrotermais na província vulcânica Paraná

O hidrotermalismo é um processo metassomático de alteração química de minerais que compõem as rochas, relacionada com fluidos aquosos quentes com significativa inserção ou retirada de componentes químicos. A água presente nos fluidos hidrotermais comumente tem origem mista (Pirajno, 2009) e atua como fluido aquecido sob pressão. O fluido, geralmente no estado supercrítico provoca a hidratação e lixiviação de minerais silicáticos, oxidação de sulfetos e aporte de cátions metálicos de acordo com a termodinâmica e geoquímica das rochas. Além da alteração hidrotermal, lixiviação, transporte e deposição de elementos químicos e metais, frequentemente ocorre concentração de minerais de interesse econômico.

A discussão do hidrotermalismo na província vulcânica Paraná é um assunto relativamente recente, diferente dos estudos relacionados ao evento magmático que estão sendo discutidos desde o início do século passado. Porém, alguns autores a exemplo de Garcia & Marinho (1980) enquanto pesquisavam os aspectos genéticos das rochas ácidas do vulcanismo Serra Geral, indicaram evidências de hidrotermalismo na base das rochas ácidas, e feições de "*diques de arenito silicificados que gradam para diques de calcedônia e destes para geodos revestidos internamente por quartzo hialino"*. Da mesma forma, o estudo conduzido por Gomes (1996) na região de Frederico Westphalen (RS) mostra que a mineralogia dos basaltos é composta por plagioclásio (labradorita a andesina), clinopiroxênio (augita e pigeonita) e opacos representados por ti-magnetitas e ilmenitas. A autora relata que a olivina está alterada a argilominerais, enquanto os piroxênios estão parcialmente alterados a hematita e argilominerais. O plagioclásio, em geral, não está alterado, apenas nas porções superiores no derrame, há ocorrências de albitização e zeolitização. Já os óxidos de ferro e titânio, mostram-se completamente alterados nas porções superiores dos derrames, transformando-se em hematita e, localmente, em maghemita. Nos espaços intergranulares, os principais minerais precipitados são quartzo, k-feldspato e argilominerais. Nas vesículas, a autora descreve quartzo, calcita, argilominerais (esmectitas e interestratificados de clorita/esmectita) e zeolita (heulandita). Em alguns locais dos níveis vesiculares do topo do derrame há ocorrência de crisocola em virtude da desestabilização das zeolitas. A leitura destas evidências petrográficas, pela autora,

é compatível com os sistemas hidrotermais de saponitas (esmectitas) com temperaturas de cristalização entre 130°C e 170°C e heulandita com temperaturas de cristalização entre 60°C e 100°C. Os indícios hidrotermais destas pesquisas foram reavaliados em estudos recentes (e.g., Pinto *et al.,* 2006; Duarte, 2008; Hartmann, 2008a,b; Duarte *et al.,* 2009; Hartmann *et al.,* 2010a,b) que promoveram grandes avanços com a identificação e descrição dos eventos hidrotermais. Nestes estudos, a relação entre a Formação Botucatu e as rochas vulcânicas foram colocadas em evidência e tornaram-se muito importantes para o entendimento do hidrotermalismo na província. Da mesma forma, mas com objetivos diferentes, os estudos hidrogeológicos têm contribuído muito para detalhar as relações entre estas duas unidades. A complexa interação e mistura das águas do sistema aquífero Guarani e do sistema aquífero Serra Geral foram descritas em estudos a exemplo de Portela Filho *et al*. (2002) e Mocellin & Ferreira (2009). A interação é observada a partir de padrões hidroquímicos anômalos no Aquífero Serra Geral (não condizentes com a composição química dos basaltos), no arcabouço estrutural e quimismo das águas. Estes fatores sugerem zonas de conectividade que se estabeleceram entre as unidades através de sistemas de falhas verticais com soerguimento de blocos, de acordo com a evolução tectônica da Bacia do Paraná.

O estudo ao longo da calha do Rio Iguaçu, a jusante do município de Reserva do Iguaçu (Souza, 2004) avaliou várias fontes termais de água bicarbonatada sódica do Aquífero Guarani com temperaturas acima de 26 ºC. A avaliação de perfilagens de poços perfurados pela Petrobrás e por empresas de balneários da região conduziu o autor a constatar que o bloco da margem esquerda apresenta um abatimento de aproximadamente 250 m em relação ao bloco da margem direita. Com isso, as fontes localizadas na margem esquerda são mais quentes que as localizadas na margem direita. O grau geotérmico do Aquífero Guarani apontado por Araújo *et al*. (1995) é da ordem de 29 ºC/km e a temperatura da água das fontes artesianas do bloco da margem esquerda pode ser até 7,25 ºC mais quente que nas fontes do bloco da margem direita do Rio Iguaçu. Além da interconexão estabelecida pelo fluxo da água subterrânea, outro fator importante descrito em estudos é a interação das rochas vulcânicas com as areias da Formação Botucatu. No nordeste do Rio Grande do Sul, Betiollo (2006) avaliou perfis de poços tubulares denominados perfil 1 São Vedelino, perfil 2

Farropilha/Nova Roma do Sul, perfil 3 Estrela/Guaporé, perfil 4 Três Coroas/Nova Petrópolis, perfil 5 São Francisco de Paula/Três Canoas, perfil 6 Taquaras/São Francisco de Paula e perfil 7 Maquine/São Francisco de Paula. A integração dos perfis apontou interação de areia e derrames vulcânicos com mergulho para oeste além de deslocamentos, em maior ou menor escala, em todos os blocos (Fig. 7).

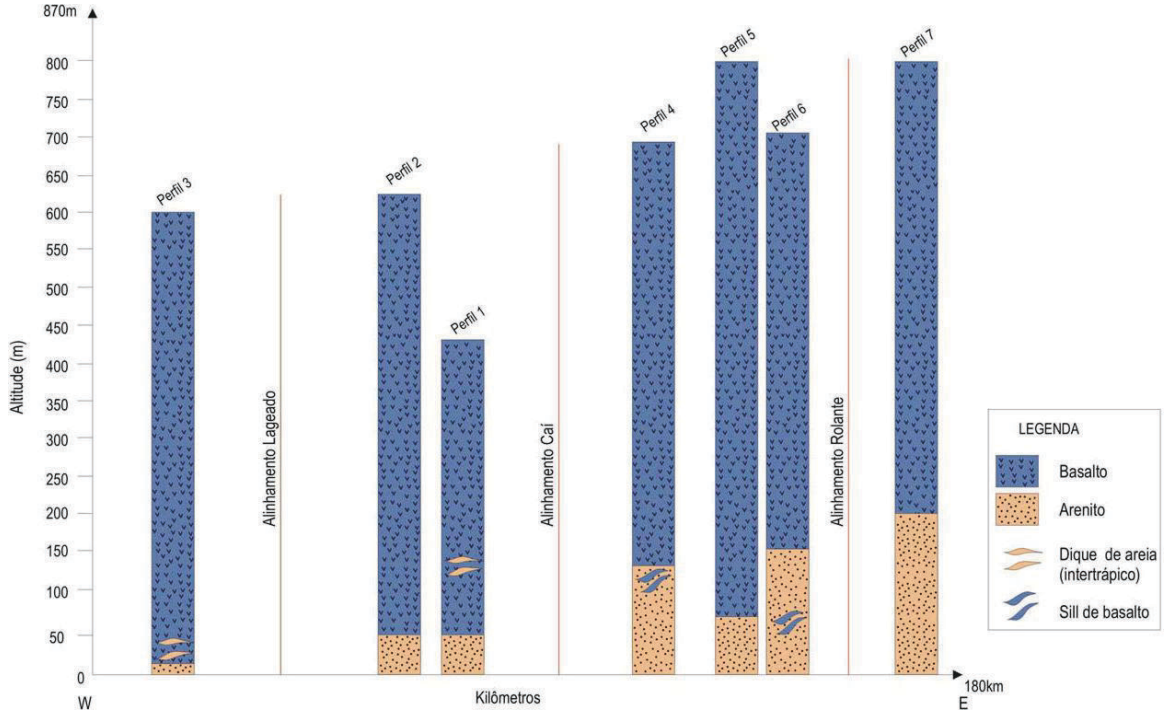

Figura 7. Perfis dos contatos entre o arenito Botucatu e os Basaltos Serra Geral (Betiollo 2006).

Da mesma maneira, o estudo de Rosenstengel & Hartmann (2012) descreveu detalhadamente a estratigrafia de 13 derrames basálticos na região Norte do Rio Grande do Sul (Alto Uruguai). Nove deles no município de Ametista do Sul (RS) e quatro no município de Frederico Westphalen (RS). Este estudo foi efetuado na parcela superior da pilha vulcânica com aproximadamente 1000 m de basalto acima da Formação Botucatu. A descrição dos autores incluiu interação de areia (silicificada) proveniente da Formação Botucatu com os derrames e deslocamentos significativos entre o bloco Frederico Westphalen, que foi abatido em mais de duzentos metros quando correlacionado com o bloco Ametista do Sul (Fig. 8). Os autores identificaram

os processos hidrotermais como agentes de transporte da areia para os níveis superiores da pilha vulcânica.

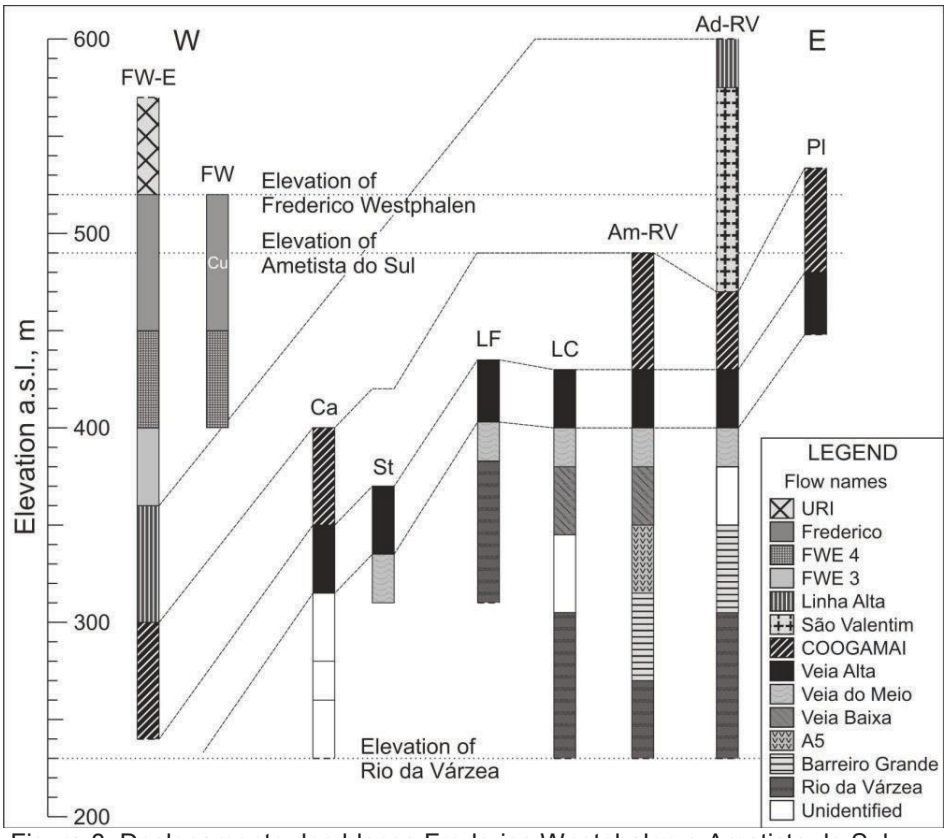

Figura 8. Deslocamento dos blocos Frederico Westphalen e Ametista do Sul (Rosenstengel & Hartmann 2012).

O entendimento dos processos de interação areia-lava foi o foco dos estudos conduzidos por Hartmann *et al*. (2012) e Duarte & Hartmann (2014). Os autores analisaram as relações da areia da Formação Botucatu com os derrames de lava nas áreas da porção sul da província (nos primeiros derrames) em afloramentos das pedreiras da região de Estância Velha e Ivoti, bem como em diversas áreas na porção superior da pilha vulcânica. As evidências observadas mostram que nos primeiros derrames ocorreu deposição de areia contemporaneamente à efusão de lavas e também hidrotermalismo com diques e sills de areia silicificada, alguns migrando lateralmente para agregados de ágata ou para veios de quartzo (Fig. 9A), falhas losangulares, areia silicificada na superfície de disjunções colunares (Hartmann *et al.,* 2012) além de mineralização de calcita e quartzo. Estas evidências podem ser compreendidas quando estabelecida a ordem dos eventos geológicos. Conforme os

derrames avançavam sobre os campos de dunas, a pilha vulcânica tornava-se mais espessa e a área fonte de retrabalhamento sedimentar menor, até que o transporte eólico cessou. O aquecimento do aquífero Guarani pelo calor residual do magmatismo desencadeou processos hidrotermais que iniciaram transporte de areia fluidizada gerando diques, sills e lacólitos de areia (Fig. 9B,C e D), incompatíveis com transporte eólico.

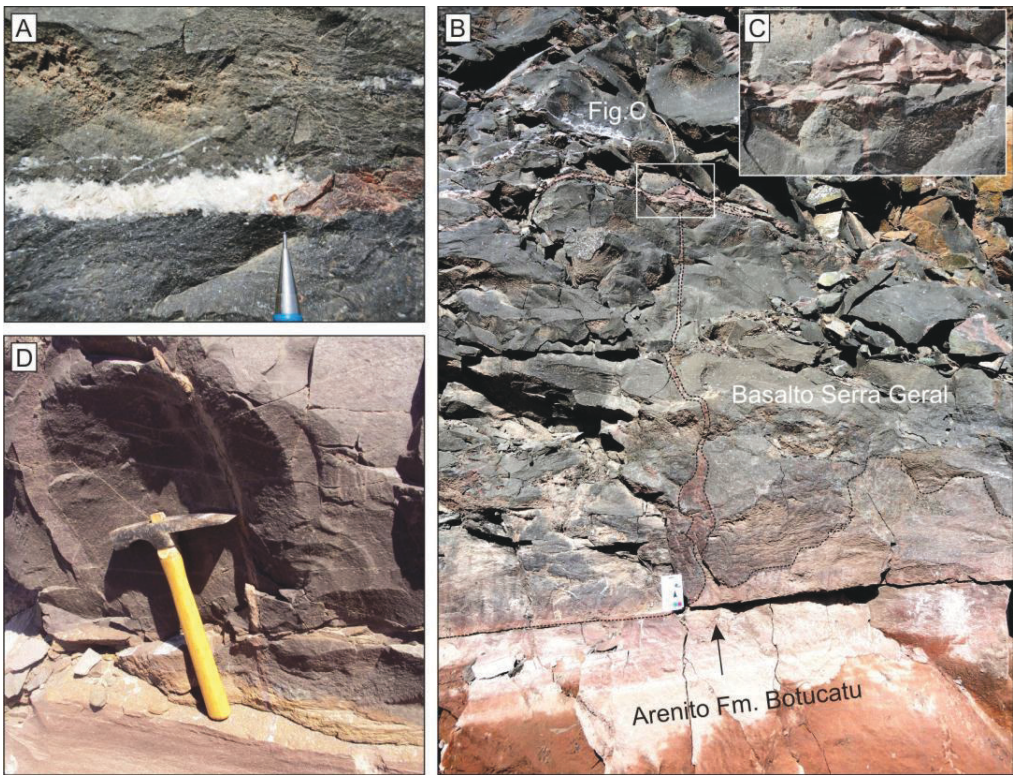

Figura 9. Pedreiras na região de Ivoti (RS). A) Dique de arenito silicificado gradando lateralmente para agregado de quartzo. B) Contato da Formação Botucatu com os basaltos do Grupo Serra Geral com injeção de areia dentro do basalto, formando um dique e um lacólito de areia. C) Detalhe do lacólito formado pela areia que foi silicificada. D) Contato do arenito com o basalto e injeção de um dique de areia.

Os eventos hidrotermais foram identificados por Hartmann (2008a, b), Duarte (2008), Duarte *et al.* (2009), Hartmann *et al.* (2010a, b) e denominados por Hartmann *et al.* (2011a) como H1, H2 e H3 (Fig. 10). A compreensão de que as rochas basálticas, após resfriamento, apresentam porosidade em torno de 30 vol.% (Flóvenz & Saemundsson, 1993) facilita o entendimento destes eventos que ocorreram na província vulcânica Paraná. O aumento da temperatura regional gerado pelo calor residual do magmatismo aqueceu de forma generalizada as litologias da Bacia do Paraná e as águas do aqüífero Guarani. A pressão do vapor de água sobre os

derrames basálticos desencadeou atividades hidrotermais, a exemplo do que acontece atualmente na Islândia e deixou evidências desde os primeiros derrames até o topo da pilha vulcânica.

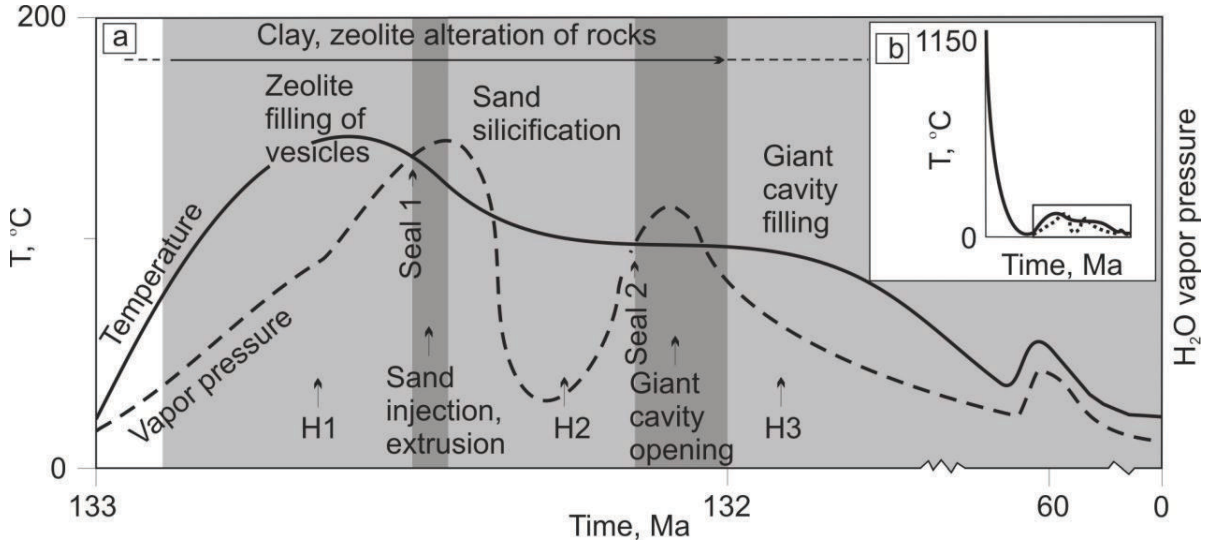

Figura 10. Eventos hidrotermais H1, H2 e H3 ocorridos na província vulcânica Paraná (Hartmann *et al*., 2011a).

O evento H1 foi marcado pela ascensão de fluido hidrotermal composto essencialmente de água quente e vapor de água (proveniente do Aqüífero Guarani). A presença de clinoptilolita e os dados de isótopos estáveis (Morteani *et al.,* 2010) indicam que o fluido apresentava temperaturas da ordem de 130ºC a 150ºC. Inclusões fluidas monofásicas em ametistas e quartzo (Gilg *et al.*, 2003; Fisher, 2004) indicam que o fluido apresentava baixa salinidade. O fluido percolou os poros das rochas da província vulcânica Paraná e promoveu a deposição de zeolitas em micro fraturas e cavidades. Argilominerais foram gerados pela interação entre as fases primárias, mesóstase e fluidos hidrotermais. Neste contexto iniciaram as mineralizações de cobre nativo que preenchem as cavidades da zona amigdaloidal e ocorrem como dendritos nas superfícies das disjunções colunares. Conforme o evento H1 se desenvolvia, a rocha era progressivamente mineralizada pelos fluidos e a porosidade diminuía. O evento H1 completou-se quando o derrame foi selado, ou seja, tornou-se impermeável. Com isso, a pressão de vapor de água foi reprimida.

O evento H2 iniciou de forma explosiva quando a pressão do vapor de água suplantou a pressão litostática. A formação de falhas losangulares em H2 é resultante deste esforço sobre as rochas sotopostas. A liberação de energia e do vapor de água

promoveu a fluidização de areia inconsolidada da Formação Botucatu que foi injetada nas rochas sobrejacentes na forma de sills, diques e principalmente brechas. Em locais onde o vapor de água atingiu a superfície a areia foi lançada sobre a superfície dos derrames basálticos. A alta porosidade da areia injetada permitiu que a água quente continuasse percolando por estas estruturas solubilizando parcialmente o quartzo, depositando calcedônia e formando algumas cavidades nas áreas mais argilizadas do derrame (preenchidas parcialmente por areia). Conforme o H2 se desenvolvia, maior era a silicificação e a porosidade tornava-se cada vez menor. O H2 finaliza com nova impermeabilização do derrame.

O aumento da pressão de vapor de água abaixo do selo formado durante H2 ocasionou o evento H3. Durante o H3 o fluido hidrotermal dissolveu as zeolitas depositadas no evento H1. Observa-se nestes casos que as cavidades foram preenchidas por areia e por minerais de sílica. O fenômeno de dissolução e substituição ocorreu apenas em locais onde o fluido de H3 teve acesso. Em muitos locais as zeolitas continuam preenchendo as cavidades e são evidências do evento H1. A contínua ação hidrotermal dos fluidos quentes sobre as rochas intensificou os processos de argilização. A rocha argilizada e saturada em água a 150ºC tornou-se dúctil. A pressão do fluido aquoso do H3 expandiu bolhas neste material argiloso formando protogeodos de diversos tamanhos, desde centimétricos até métricos, que foram preenchidos por minerais de sílica, calcita e gipsita.

1.3.4. Depósitos hidrotermais na província vulcânica Paraná

1.3.4.1. Cobre nativo

Os depósitos de cobre nativo e seus produtos oxidados geralmente ocorrem associados a lavas basálticas em várias províncias do mundo. Além do Brasil, diversos países do mundo apresentam ocorrência de cobre nativo em derrames basálticos. Alguns depósitos como Keweenaw Peninsula (Michigan - USA), Zhaotong (China), Ilhas Faroe e na província do Atlântico Norte podem ser destacados e comparados com a mineralização de cobre da província vulcânica Paraná.

O depósito de cobre nativo da Península de Keweenaw está hospedado em basaltos amigdaloidais e conglomerados da sequência vulcânica de Portage Lake. A sequência apresenta uma pilha de derrames basálticos toleíticos com mais de 200 derrames. A espessura mínima dos derrames no distrito cuprífero é de 2,5 a 5 m (White, 1968). A ganga é representada por uma grande variedade de minerais (quartzo, calcita, epidoto, clorita e argilominerais). A gênese dos depósitos de Keweenaw ainda está em discussão, porém a mais aceita é de um modelo de alteração hidrotermal relacionada a fluidos metamórficos de fácies prehnita-pumpelleyita (White, 1968; Jolly, 1974; Livnat *et al*., 1983) que mobilizou o cobre dos sedimentos abaixo da pilha basáltica. Brown (2006) demonstrou a importância dos fluidos aquosos em condições de redução e oxidação nas paragêneses da mineralização, sugerindo a possibilidade de uma interação entre os fluidos metamórficos e meteóricos na remobilização e deposição do cobre nativo dos depósitos de Keweenaw.

O depósito de cobre nativo da Província de Zhaotong na China (Wang *et al*., 2006) está associado aos derrames basálticos Emeishan. A extensão da área é superior a 500.000 km^2 e engloba o sudoeste da China e norte do Vietnã. A sequência vulcânica consiste de espessos derrames de basaltos separados por unidades sedimentares carbonáceas com espessura inferior a 50 cm e ocorrências de betume. Na porção superior dos derrames é comum a ocorrência de brechas vulcânicas. O cobre nativo ocorre no topo das sequências de derrames, na porção vesicular e brechada. O minério é associado com betume, zeolita, calcita e quartzo e configura alteração hidrotermal de baixa temperatura. O teor de cobre varia de 0,1 a 20,0 %. Segundo os autores o cobre está associado a interações orgânico-inorgânicas em ambiente reduzido de enxofre. Nas Ilhas Faroe o cobre nativo está associado à zeolitas, sendo raramente encontrado como pequenas inclusões em óxidos de Fe-Ti e, mais raramente, em piroxênios (Jensen, 1982). O autor investigou a distribuição do cobre em silicatos e óxidos nos fluxos de lava da região e utilizou técnicas de fluorescência de raios-X e microssonda eletrônica para definir os teores de cobre. Ele concluiu que, quanto maior o estado de oxidação, maior o teor de cobre no sistema. Na província vulcânica do Atlântico Norte (basaltos Terciários), o cobre nativo foi descrito em sete testemunhos de sondagem de mar profundo, e ocorre no topo dos derrames (Le Huray, 1989) preenchendo vesículas e fraturas. O autor relata que o topo dos derrames

apresenta uma coloração diferenciada devido à oxidação/hidratação dos óxidos de Fe-Ti e por interação parcial com a água do mar. A associação de alteração mineral relacionada ao cobre é composta por hidróxidos de ferro, celadonita, calcita e esmectita.

A comparação das ocorrências de cobre nestas províncias com as mineralizações da província Paraná apresenta alguns pontos em comum a exemplo das assembleias mineralógicas de baixa temperatura. Para balizar esta discussão a avaliação de estudos prévios na província Paraná (Tabela 4) remonta mais de um século. Alguns têm importância histórica descritiva a exemplo dos estudos de 1890 e 1930 que foram obtidos a partir de citações de Pinto (2010). Por outro lado, os estudos desenvolvidos a partir de 1979 iniciam as discussões sobre a mineralização e apresentam hipóteses para a origem do cobre na província.

Autor	Ano	Estudo
Hussak	1890	Primeira descrição de cobre nativo em cavidades de amígdalas.
Englert	1930	Descrição um bloco de 28 kg de cobre nativo entre as cidades de São Luiz Gonzaga (RS) e Santo Ângelo (RS).
Szubert *et al.*	1979	Projeto Cobre em Itapiranga (CPRM). Ocorrências de cobre nativo e óxidos de cobre (noroeste do RS) e em Itapiranga (SC).
Costa. A.F.U	1982	Geofísica aplicada à prospecção de cobre em basaltos na área de Vista Alegre: Frederico Westphalen (RS).
Tazaki *et al.*	1988	Basaltos da região de Três Pinheiros (noroeste de SC).
Gomes	1996	Tese de Doutorado. Mecanismo de resfriamento e cristalização dos basaltos na região de Frederico Westphalen (RS). Observação de cobre nativo e crisocola.
Mello	2000	Dissertação de Mestrado. Ocorrência de cobre nativo e cuprita em Campina da Lagoa (PR), norte do alinhamento estrutural do Rio Piquiri.
Mineropar	2001a	Projeto Riquezas Minerais. Avaliação do Potencial Mineral e Consultoria Técnica à Prefeitura Municipal de Bom Jesus do Sul (PR).
Mineropar	2002	Projeto Riquezas Minerais. Avaliação do potencial mineral e consultoria técnica à Prefeitura Municipal de Realeza (PR).
Pinto *et al.*	2006	Hydrothermal origin of native copper mineralization in Paraná Flood Basalts.
Pinto, VM.	2010	Tese de doutorado. Condições de formação do cobre nativo na região de Vista Alegre (RS).
Pinto *et al.*	2011b	Epigenetic hydrothermal origin of native copper and supergene enrichment in the Vista Alegre district, Paraná basaltic province.
Arena *et al.*	2014	Geological controls of copper, gold and silver in the Serra Geral Group, Realeza region, Paraná, Brazil.

Tabela 4. Estudos sobre mineralizações de cobre nativo desenvolvidos na província vulcânica Paraná.

As rochas basálticas da província Paraná hospedam cobre nativo nas disjunções colunares dos derrames e na zona amigdaloidal superior dos derrames. Um dos trabalhos pioneiros e que discutiu a origem da mineralização foi o Projeto Cobre em Itapiranga desenvolvido pela CPRM apresentado por Szubert *et al.* (1979). O estudo catalogou 85 ocorrências de cobre na província vulcânica Paraná. Destas, 19 foram descritas como tardi-magmáticas (ocorrência dendrítica em disjunções verticais) e 66 descritos como supergênicos preenchendo amigdalas. A mineralização descrita constitui-se cuprita, tenorita, crisocola, malaquita, azurita e cobre nativo. Os autores descrevem a morfogênese de alguns tipos de derrames mineralizados com cobre (Fig. 11). A zona amigdaloidal superior muitas vezes apresenta mineralização de cobre preenchendo as cavidades. A zona central apresenta dezenas de metros e disjunções colunares que apresentam mineralização dendrítica de cobre nativo. A zona inferior apresenta no máximo dois metros de espessura com acentuada disjunção horizontal e pequenas vesículas. A conclusão dos autores é que o cobre foi depositado por processo pós-magmático tipo epitermal.

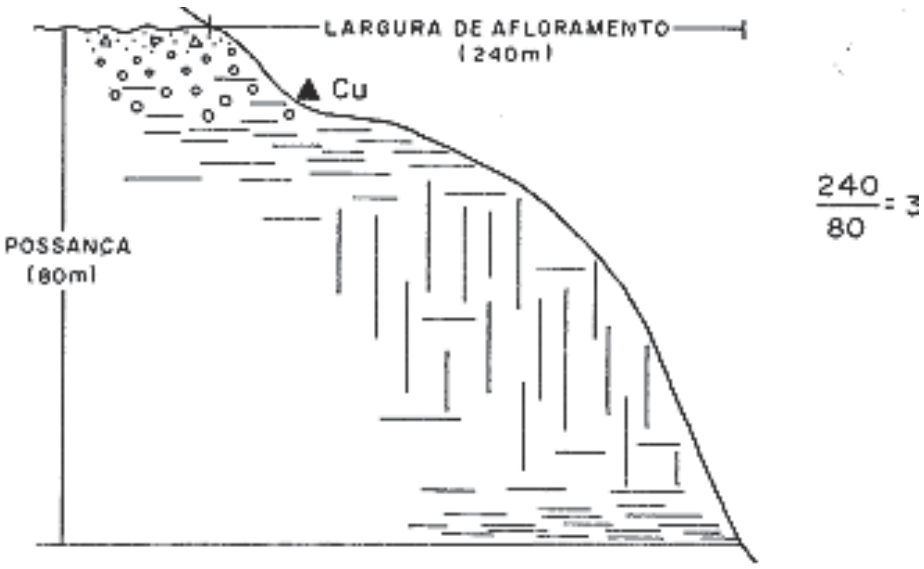

Figura 11. Derrame basáltico na região de Flor da Serra, município de Tenente Portela (RS), portador de mineralização de cobre (Szubert *et al*., 1979).

O estudo desenvolvido por Tazaki *et al.* (1988) em basaltos atravessados pela sondagem 1TP3-SC (Três Pinheiros, SC), descreve a ocorrência de filmes de cobre nativo e também de esmectita cuprífera associada a basaltos alterados. Os autores destacam que o cobre é móvel durante a alteração hidrotermal de baixa temperatura e

indicam que os padrões de condutividade elétrica podem ser potencialmente importantes para avaliação de áreas onde a circulação do fluido na rocha basáltica foi mais pronunciada. No trabalho conduzido na região de Frederico Westphalen (RS) doze derrames vulcânicos foram caracterizados por Gomes (1996) e o cobre nativo também foi descrito na disjunção colunar de alguns derrames além da ocorrência de crisocola nas cavidades da zona amigdaloidal. No Paraná, na região de Água Perdida, município de Campina da Lagoa, a ocorrência de cobre nativo foi descrita por Mello (2000) que avaliou a morfologia das disjunções colunares do derrame. O autor indicou que a temperatura de geração das disjunções foi de 750˚C e que, nesta temperatura o fluido residual imiscível, rico em cobre, migrou para estes espaços gerando a mineralização. Assim, ele sugere que a origem do cobre está diretamente relacionada com os processos de solidificação da lava.

Na região de Bom Jesus do Sul (PR), o projeto Riquezas Minerais, desenvolvido pela Mineropar (2001b) descreveu ocorrências de geodos com incrustações de cobre nativo, tenorita, cuprita e malaquita sobre cristais de quartzo e em Salto do Lontra (PR), na pedreira Bonetti, Lopes *et al.* (2008) descrevem a presença de cobre nativo e cavidades no basalto preenchidas por celadonita. Porém, as maiores ocorrências de cobre descritas no Paraná estão em Realeza. O estudo desenvolvido pela Mineropar (2002) constatou a ocorrência de cobre em brechas cimentadas por crisocola e malaquita com teores de 20% de cobre em quatro derrames. As brechas destes derrames apresentam cobre nativo, crisocola, cuprita e azurita com teores variando de 38% a 98%, em função da composição mineralógica. A reserva indicada no estudo foi da ordem de 75.419 toneladas, mas segundo a Mineropar por mais elevados que sejam os teores de cobre a composição de silicatos inviabiliza a extração do metal. Outra ressalva destacada pela Mineropar é que estes depósitos apresentam restrições de ordem metalogenética para a remobilização e concentração de depósitos econômicos. Estas restrições, segundo o estudo, ocorrem por ausência de estruturas tectono-vulcânicas, domos e falhas, em ambiente que permita a circulação de fluidos (remobilizadores e concentradores por reações epigenéticas) com complexantes (sulfatos, carbonatos, ácidos orgânicos e inorgânicos) contidos, por exemplo, nas águas de ambiente marinho e lacustre.

Na região de Vista Alegre, Frederico Westphalen e Irai (RS), o estudo de Pinto & Hartmann (2011) identificou e descreveu 13 derrames basálticos e mineralização de cobre nativo associada a alguns derrames. Os cinco primeiros derrames foram classificados com magma-tipo Pitanga, enquanto os demais derrames mostraram afinidade geoquímica com o magma-tipo Paranapanema. A ocorrência de cobre é dendrítica ao longo das disjunções colunares na porção central dos derrames mais espessos e preenchendo amigdalas de 1 a 5 cm de diâmetro nas porções superiores dos derrames, que algumas vezes estão brechados. No estudo, foram consideradas duas hipóteses principais para a origem do cobre. A primeira, embasada na deposição direta com a solidificação da lava e a segunda por processos hidrotermais. As evidências de campo, estudos em microscopia eletrônica de varredura (MEV) e assembléias minerais associadas ao cobre nativo, levaram os autores a conclusão que a origem do cobre é derivada de atividade hidrotermal epigenética de baixa temperatura (<150ºC). Da mesma maneira Arena *et al*. (2014) concluem que a origem do cobre é hidrotermal e mostram que em alguns locais da província as temperaturas foram mais elevadas que 150 ºC e geraram mineralizações de ouro e prata, associadas ao cobre nativo.

A avaliação deste estudo mostra que o cobre nativo ocorre predominantemente nos magma-tipo intermediário Ti e os derrames hospedeiros são principalmente basaltos e andesitos basálticos holocristalinos. A mineralogia dos basaltos hospedeiros é formada basicamente por plagioclásio, clinopiroxênios, ilmenita e magnetita com textura intergranular. A magnetita geralmente associada à ilmenita apresenta bordas corroídas e alteradas com textura de exsolução e formação de hematita. O clinopiroxênio apresenta-se fraturado e alterado. Os argilo-minerais são esmectitas originadas a partir da alteração dos minerais opacos e dos clinopiroxênios.

O teor médio de cobre dos basaltos hospedeiros é de 207 ppm, sendo que os menores teores ocorrem na porção sudoeste da província, 83 ppm em Dom Pedro de Alcântara (RS) e 97,7 ppm em Bom Princípio (RS), e os maiores teores ocorrem em Dionísio Cerqueira (SC) com 292.2 ppm e Frederico Westphalen (RS) com 324.4 ppm. Na amostra DC6 de Dionísio Cerqueira (SC), o teor de cobre atingiu 1114.7 ppm e foi considerado como efeito pepita porque a amostra incluiu disjunções colunares

preenchidas por cobre nativo. A perda ao fogo apresenta correlação positiva entre os teores de cobre e MnO e Fe_2O_3.

A mineralização de cobre nativo ocorre na superfície das disjunções colunares (Fig. 12A), em cavidades, associada à esmectitas ou zeolitas (Fig. 12B) e em brechas hidrotermais onde o cobre nativo está associado à crisocola e malaquita (Fig. 12C). Cobre nativo e cuprita é a associação mais frequente na província vulcânica, porém ocorrem também azurita e tenorita identificados por difração de raios-X (Tabela 5, Fig. 13) e espectrometria Raman (Tabela 5, Fig. 14).

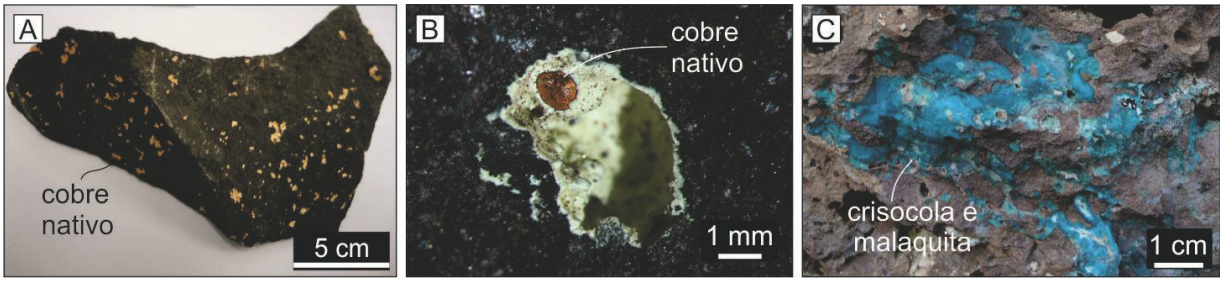

Figura 12. Formas de ocorrência do cobre nativo na província vulcânica Paraná. A) Cobre nativo dendrítico sobre a superfície de disjunções colunares do basalto. B) Cobre nativo preenchendo cavidade e associado com zeolitas. C) Brecha hidrotermal cimentada por crisocola e malaquita

MALAQUITA						CUPRITA			CRISOCOLA				TENORITA
DRX (Å)	Frequência Raman (cm^{-1})					DRX (Å)	Freq.Raman (cm^{-1})		Frequência Raman (cm^{-1})				Freq.Raman (cm^{-1})
5.95	3377.6	3310.6	1490.3	1454.5	1363	3.01	794.9	637.5	3625.6	3580.1	3440.7	2945.9	1102
5.04	1090.7	1056.1	885.3	744.7	714.6	2.46	531.5	414.2	2887.3	1459.6	1075.9	1042	630
3.68	591.8	561.6	531.5	504.7	427.7	2.13	297.9	216	910.7	862.5	790.6	675.2	342
2.51	348.5	264.8	217.6	174.8	165.1	1.50	198.5	187.5	638.4	508.9	480.9	410.5	293
2.12	138.7	127	114.9				146.9		334.5	246.6	200.2	138.6	214

Tabela 5. Espaçamento basal DRX e frequência espectroscópica Raman de minerais de cobre da província vulcânica Paraná.

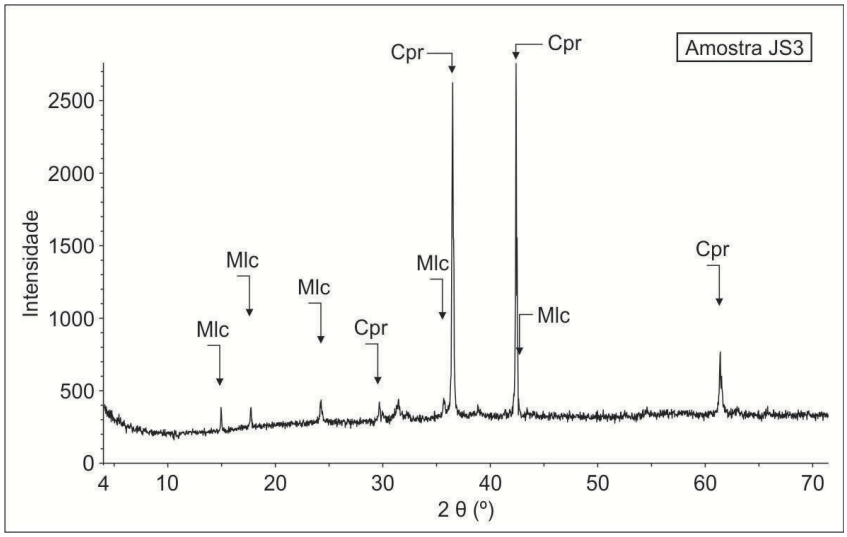

Figura 13. Difração de raios-X de minerais de cobre. Mlc = malaquita, Cpr = cuprita.

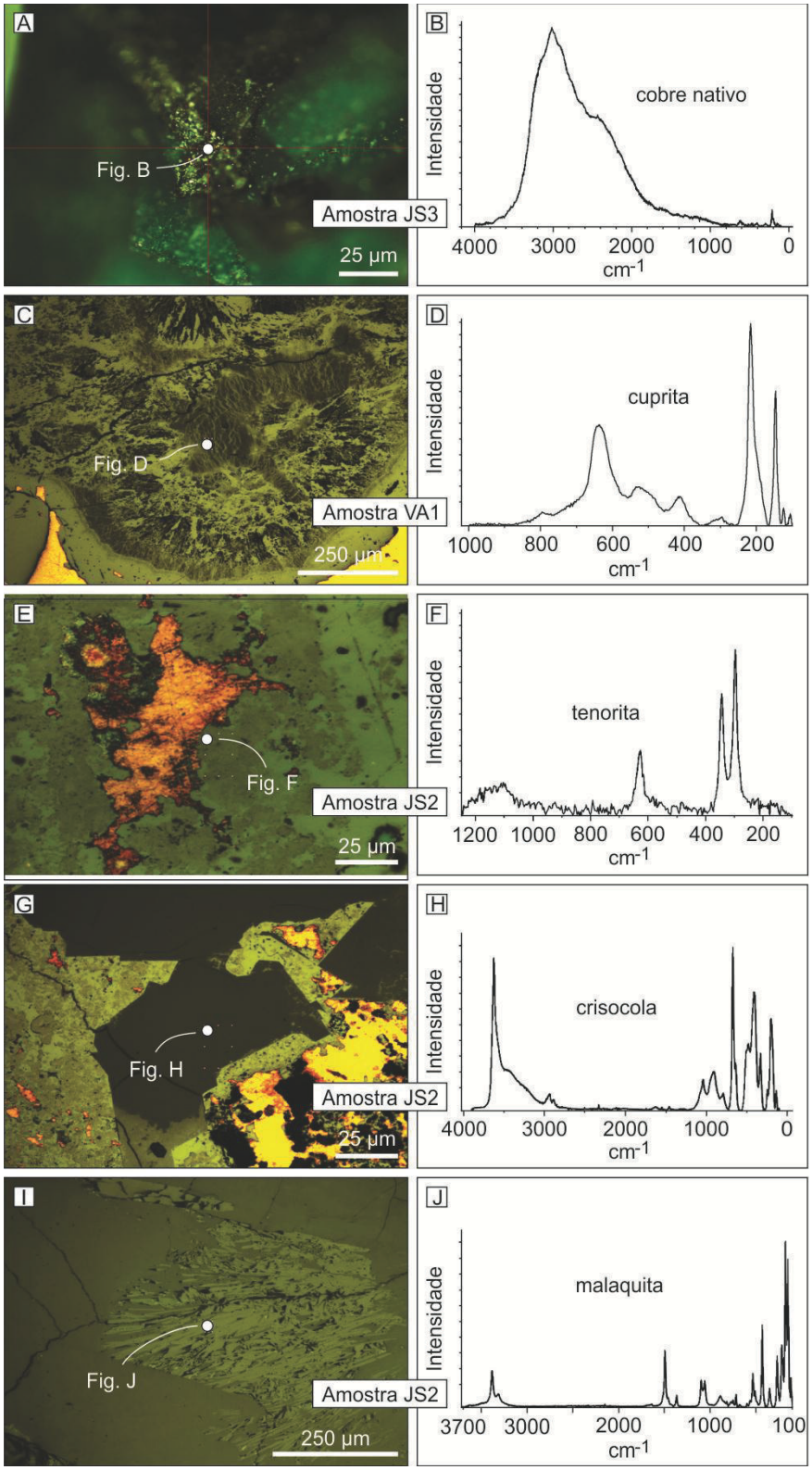

Figura 14. Fotomicrografias e espectro Raman dos minerais de cobre.

Análises de laser ablation (LA-ICP-MS) foram efetuadas para determinação do conteúdo de cobre na estrutura cristalina dos minerais. Os minerais analisados foram: magnetita (Fig. 15A), ilmenita (Fig. 15B), clinopiroxênio, plagioclásio e esmectita. Apesar da grande variação de teores observada em todos os minerais, a magnetita foi o mineral que apresentou os maiores teores (média 1085 ppm) atingindo valores superiores a 9000 ppm na amostra PQ16 de Cascavel (PR). Na mesma amostra a ilmenita apresentou valores de 3827 ppm, enquanto o clinopiroxênio apresentou a média de 97 ppm, com valores máximos de 431 ppm. O plagioclásio apresentou os teores mais baixos que variaram entre 0,02 e 91,90 ppm. Na matriz do basalto hospedeiro o valor obtido foi de 16,02 ppm de cobre.

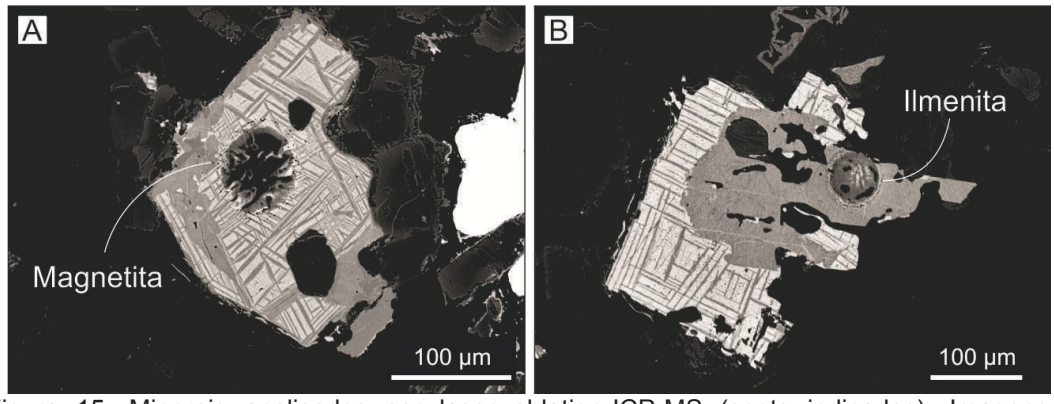

Figura 15. Minerais analisados por laser ablation-ICP-MS (spots indicados). Imagens de elétrons retroespalhados. A) Magnetita (Dionísio Cerqueira, SC). B) Ilmenita (Bom Princípio, RS

A composição química do cobre nativo foi efetuada por microssonda eletrônica. Os cristais de cobre nativo apresentam concentração de 99,7 peso % de Cu e os elementos Sn, Ca, Co, Ni and U ocorrem com teores muito baixos. Alumínio praticamente não aparece, enxofre apresenta teor médio de 0,03 peso % e o Si foi observado em apenas alguns cristais com o máximo de 0,40 peso %.

A composição isotópica do cobre foi executada em 11 amostras (64 análises) incluindo áreas do RS, SC e PR. A composição isotópica da grande maioria dos cristais de cobre nativo está entre 0.1- 0.7 ‰, mas ocorre uma variação maior desde -0.90 ‰ até 1.89 ‰ (Tabela 6, Fig. 16).

Amostra	Fig. 16	Tipo de ocorrência	Localidade	$\partial^{65}Cu/^{63}Cu$ (‰)	$2\sigma\ \partial^{65}Cu$ (‰)
FS86a	A1	Cobre nativo dendrítico	Dom Pedro	-0.83	± 0.05
FS86a	A2		de Alcântara	-0.86	± 0.05
FS86a	A3		(RS)	-0.91	± 0.06
FS86a	A4			-0.88	± 0.05
FS86a	A5			-0.59	± 0.05
FS86b	A6	Cobre nativo dendrítico		0.09	± 0.05
FS86b	A7			0.02	± 0.05
BP1	A8	Cobre nativo dendrítico	Bom Princípio	0.37	± 0.05
BP1	A9		(RS)	0.44	± 0.05
BP1	A10			0.47	± 0.05
JS3a	A11	Cobre nativo maciço	Santo Augusto	0.10	± 0.05
JS3a	A12		(RS)	0.10	± 0.04
JS3a	A13			0.13	± 0.05
JS3a	A14			0.22	± 0.05
JS3a	A15			0.17	± 0.05
JS3b	-	Crisocola		-0.27	± 0.05
JS3b	-			-0.34	± 0.05
JS3b				-0.33	± 0.05
JS4a	A16	Cobre nativo maciço	Santo Augusto	0.62	± 0.04
JS4a	A17		(RS)	0.63	± 0.04
JS4a	A18			0.69	± 0.05
JS4a	A19			0.65	± 0.05
JS4b	-	Cuprita (borda)		0.12	± 0.04
JS4b	-			0.10	± 0.04
JS4b	-			0.73	± 0.05
JS4b	-			0.32	± 0.04
JS4b	-	Cuprita (centro)		0.16	± 0.04
JS4b	-			0.21	± 0.04
JS4c	A20	Cobre nativo maciço		1.07	± 0.04
PD1a	A21	Cobre nativo dendrítico	Taquaruçu	0.70	± 0.05
PD1a	A22		do Sul	0.71	± 0.04
PD1b	A23	Cobre nativo dendrítico	(RS)	1.14	± 0.05
PD1b	A24			1.18	± 0.05
W247a	A25	Cobre nativo dendrítico (borda)	Frederico	-0.20	± 0.05
W247a	A26		Westphalen	-0.16	± 0.05
W247a	A27		(RS)	-0.05	± 0.05
W247b	A28	Cobre nativo dendrítico (centro)		0.37	± 0.05
DC6	A29	Cobre nativo dendrítico	Dionísio	1.09	± 0.04
DC6	A30		Cerqueira (SC)	1.09	± 0.05
DC6	A31			1.11	± 0.05
NZ1	A32	Cobre nativo dendrítico	Palma Sola	0.47	± 0.06
NZ1	A33		(SC)	0.48	± 0.06
NZ1	A34			0.51	± 0.05
P1C	A35	Cobre nativo dendrítico (borda)	Francisco	0.32	± 0.05
P1C	A36		Beltrão (PR)	0.37	± 0.05
P1C	A37			0.37	± 0.05
P1C	A38			0.42	± 0.05
P1C	A39			0.31	± 0.04
P1C	A40	Cobre nativo dendrítico (centro)		0.36	± 0.04
P1C	A41			0.43	± 0.05
P1C	A42			0.41	± 0.04
P1C	A43			0.38	± 0.04
CP14a	A44	Lâminas de cobre nativo (mm)	Cascavel (PR)	0.57	± 0.04
CP14a	A45			0.62	± 0.05
CP14a	A46			0.53	± 0.04
CP14a	A47			0.55	± 0.05
CP14b	A48	Cobre nativo dendrítico (cm)		1.89	± 0.05
CP14b	A49			1.50	± 0.05
CP14b	A50			1.51	± 0.05
R2P	A51	Cobre nativo dendrítico com quartzo	Cascavel (PR)	0.55	± 0.04
R2P	A52			0.56	± 0.04
R2P	A53			0.51	± 0.04
R2P	A54			0.64	± 0.04
R2P	A55			0.61	± 0.04

Tabela 6. Variação isotópica das mineralizações de cobre da província vulcânica Paraná.

A variação da composição isotópica ocorre em escala local e regional (Fig. 16A). As variações locais são com frequência na mesma amostra e algumas vezes identificam pelo menos duas mineralizações de cobre nativo que ocorreram em momentos distintos. Variações regionais destacam o fracionamento do cobre (oxidação, remobilização e deposição do cobre) e podem ser comparadas às variações dos depósitos hidrotermais da província vulcânica Keweenaw, Michigan, USA (Fig. 16B, Tabela 6) e dos depósitos supergênicos do Arizona (Fig. 16C, Tabela 7).

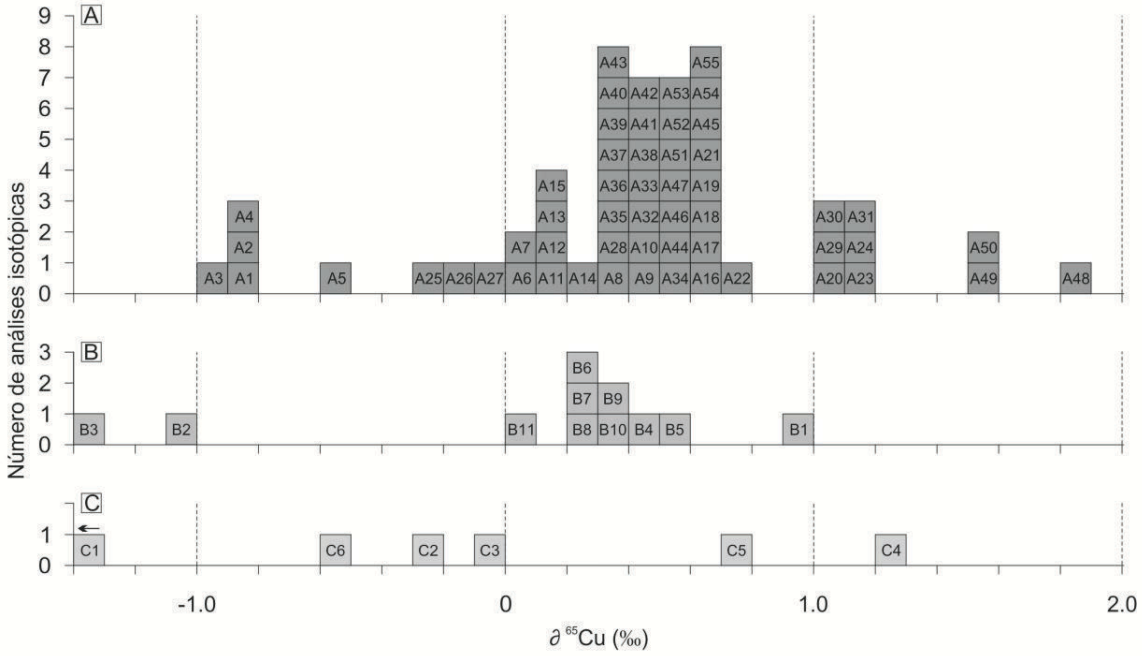

Figura 16. Variação isotópica do cobre. A) Província vulcânica Paraná B) Província vulcânica Keweenaw. C) Depósitos supergênicos do Arizona (EUA). Identificação das amostras nas tabelas 6 e 7.

Fig 13	Amostra	Mineral	Localidade	Depósito	∂^{65}Cu (‰)	Referência
B1	85	Cu nat.	Soudan mine, Minnesota, USA		0.9	Shields *et al*. (1965)
B2	88	Cu nat.	Lake Superior district, Michigan, USA	Hidrotermal	-1.0	Shields *et al*. (1965)
B3	90	Cu nat.	Painesdale, Michigan, USA	Hidrotermal	-1.3	Shields *et al*. (1965)
B4	OUM 15126	Cu nat.	Michigan, USA	Hidrotermal	0.45	Zhu *et al*. (2000)
B5	OUM 15120	Cu nat.	Lake Superior, USA	Hidrotermal	0.54	Zhu *et al*. (2000)
B6	LS-7	Cu nat.	Trimountain Mine, Michigan, USA	Hidrotermal	0.27	Larson *et al*. (2003)
B7	LS-10	Cu nat.	Baltic Mine, Michigan, USA	Hidrotermal	0.29	Larson *et al*. (2003)
B8	LS-12	Cu nat.	Centennial Mine, Michigan, USA	Hidrotermal	0.26	Larson *et al*. (2003)
B9	LS-45	Cu nat.	Isle Royale Mine, Michigan, USA	Hidrotermal	0.34	Larson *et al*. (2003)
B10	LS-48	Cu nat.	Wolverine Mine, Michigan, USA	Hidrotermal	0.30	Larson *et al*. (2003)
B11	LS-51	Cu nat.	Copper Falls Mine, Michigan, USA	Hidrotermal	0.02	Larson *et al*. (2003)
C1		Cu nat.	Ray Mine, Arizona, USA	Supergênico	-3.03	Maréchal *et al*. (1999)
C2	OUM 22647	Cu nat.	Bisbee, Arizona, USA		-0,2	Zhu *et al*. (2000)
C3	Ray-1	Cu nat.	Ray Mine, Arizona, USA	Supergênico	-0.04	Larson *et al*. (2003)
C4	Ray-2	Cu nat.+ cuprita	Ray Mine, Arizona, USA	Supergênico	1.26	Larson *et al*. (2003)
C5	Ray-2b	Cu nat.	Ray Mine, Arizona, USA	Supergênico	0.72	Larson *et al*. (2003)
C6	Arizona Cu	Cu nat.	Morenci, Arizona, USA		-0.51	Ikehata *et al*. (2011)

Tabela 7. Variação isotópica do cobre nativo em depósitos da província Keweenaw e no Arizona (EUA).

Os resultados do estudo sustentam a origem hidrotermal para as mineralizações de cobre. A estrutura cristalina dos minerais dos basaltos e andesitos basálticos é a fonte de cobre. A alteração hidrotermal da magnetita, ilmenita e clinopiroxênio para esmectitas, libera o cobre da estrutura cristalina. A remobilização e o transporte do cobre são efetuados pelos fluidos hidrotermais através da superfície das disjunções colunares, onde há alívio da pressão dos fluidos e ocorre a mineralização dendrítica do cobre. Na zona amigdaloidal o cobre preenche as cavidades e apresenta a forma de pequenas esferas maciças. As outras fases minerais do cobre advêm de sua oxidação (cuprita/tenorita) e interação do cobre nativo com fluidos hidrotermais gerando, por exemplo, crisocola e malaquita. O artigo *"Origin of native copper in the Paraná volcanic province, Brazil, integrating Cu stable isotopes in a multianalytical approach"* descreve com detalhe os resultados obtidos e apresenta uma discussão sobre a origem do cobre.

1.3.4.2. Ametista, ágata, gipsita e calcita

Os basaltos da província vulcânica Paraná são os hospedeiros das maiores jazidas de geodos de ametista e ágata do mundo a exemplo de Ametista do Sul (RS), Entre Rios (SC) e Chopinzinho (PR) no Brasil, Los Catalanes no Uruguai e Wanda na Argentina. Dentre estes, destaca-se o distrito mineiro de Ametista do Sul, no norte do Rio Grande do Sul pela produção de 400 ton/mês de geodos de ametista.

Os depósitos de geodos com ametista nos basaltos da província Paraná vem fomentando discussões científicas desde a descoberta das primeiras ocorrências no século passado. As principais discussões tratam da abertura das cavidades, dos processos de preenchimento dos geodos e também da fonte da sílica para gerar a mineralização. Para vários autores (Leinz, 1949; Franco, 1952; Szubert *et al.,* 1979; Juchem *et al.,* 1987, 1990; Correa *et al.,* 1994; Meunier *et al.,* 1988; Gomes, 1996; Scopel, 1990; Scopel *et al.,* 1998; Juchem, 1999; Gilg *et al.,* 2003; Fischer, 2004) a formação das cavidades em basaltos está relacionada à exsolução e coalescência de fases gasosas do magma. Este processo envolve temperaturas entre 1250ºC a 1150ºC e ocorre durante a cristalização e resfriamento da lava. Por outro lado, a análise do ambiente geológico que envolve sua gênese na província vulcânica Paraná começou a fornecer evidências incomuns que precisavam ser compreendidas. Uma das evidências, a presença de arenitos associados às rochas basálticas mineralizadas no Uruguai levou Bossi & Caggiano (1974) a sugerir que houve incorporação de areia da Formação Tacuarembó durante a erupção das lavas, e que a água dissolvida no magma solubilizou a sílica e gerou a mineralização dos geodos com ametista. Outra evidência observada nos derrames mineralizados é a intensa alteração das rochas basálticas marcada pela presença de celadonita e de argilominerais do grupo das esmectitas. A mineralização de ametista ocorre na porção central do derrame e a presença de celadonita ocorre na zona dos geodos e na zona amigdaloidal do topo. A partir disso Scopel (1990) sugeriu que processos hidrotermais seriam responsáveis pelo preenchimento das cavidades previamente formadas no estágio magmático.

Para explicar a abertura das cavidades dos geodos Gilg *et al.* (2003), utilizaram o modelo de exsolução de fases gasosas. Com base em estudos isotópicos, sugeriram que fluidos aquosos de baixa temperatura provenientes do Aquífero Guarani ricos em sílica, preencheram as cavidades dos geodos. Este modelo genético representa dois

estágios e insere o fator tempo entre a formação e preenchimento dos geodos. Outra interpretação é elaborada por Proust & Fontaine (2007). Eles utilizam o modelo de abertura de cavidades associado à coalescência de gases exsolvidos do magma, mas sem a necessidade de aporte externo de fluido, ou seja, a partir de um magma supersaturado em água. Já Strieder & Heeman (2006) sugerem que a areia provinda de xenólitos do arenito Botucatu seja a fonte de sílica das ágatas da região de Salto do Jacuí. Entretanto, estudos recentes (Duarte *et al.,* 2005; Pinto *et al.,* 2006; Duarte, 2008; Duarte *et al.,* 2009; Hartmann *et al.,* 2010a, Duarte *et al.,* 2011, Hartmann *et al.,* 2011a) apontaram a hipótese de formação e preenchimento das cavidades a partir de processos hidrotermais. Os resultados da pesquisa desenvolvida por Duarte (2008) no distrito mineiro de Artigas (Uruguai) sustentam um modelo epigenético de baixa temperatura e as evidências observadas nos distritos de Ametista do Sul (Brasil) e Idar-Oberstein (Alemanha) são coerentes com o modelo. Os depósitos de geodos de ametista ocorrem no núcleo dos derrames do tipo I (Gomes, 1996) que apresentam espessuras em torno de 50 m na região de Artigas (Uruguai) e de 30 m em Ametista do Sul. A interação do fluido hidrotermal com estes derrames ocorreu de maneira intensa, poro a poro promovendo alteração e argilização do basalto, tornando seu comportamento dúctil. Sob esta nova condição a intensa e contínua pressão do vapor de água a 100-150 °C sobre o basalto dúctil originou as cavidades dos proto-geodos (cm-m) e uma rede de fraturas horizontais (Fig. 17) interconectadas (Hartmann *et al*., 2012, Duarte *et al*., 2014) e facilitaram sua passagem.

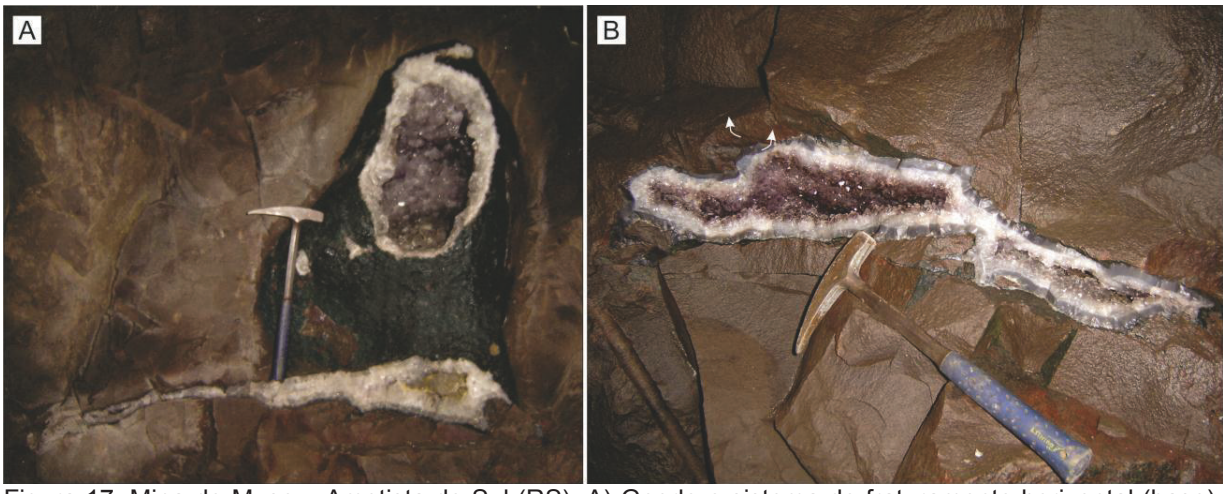

Figura 17. Mina do Museu, Ametista do Sul (RS). A) Geodo e sistema de fraturamento horizontal (base). B) Geodo formado ao longo da fratura de alimentação do fluido hidrotermal (Duarte *et al.* 2014).

Os fluidos hidrotermais continuaram percolando as cavidades e formaram os cristais de ametista, ágata, gipsita e calcita que compõem as jazidas dos distritos mineiros. Para validar o modelo, Hartmann *et al.* (2011b) apresentaram através de simulações numéricas (Fig. 18) as condições necessárias para a formação das cavidades dos geodos e as condições que controlam seus tamanhos e formas. O tamanho dos proto-geodos (centimétricos a métricos) depende da pressão do vapor de água e da espessura da pilha vulcânica que está sobre ele, e a forma das cavidades, prolatos ou oblatos (Hartmann *et al.*, 2015) depende do ângulo de cedência da rocha alterada (meta-basalto).

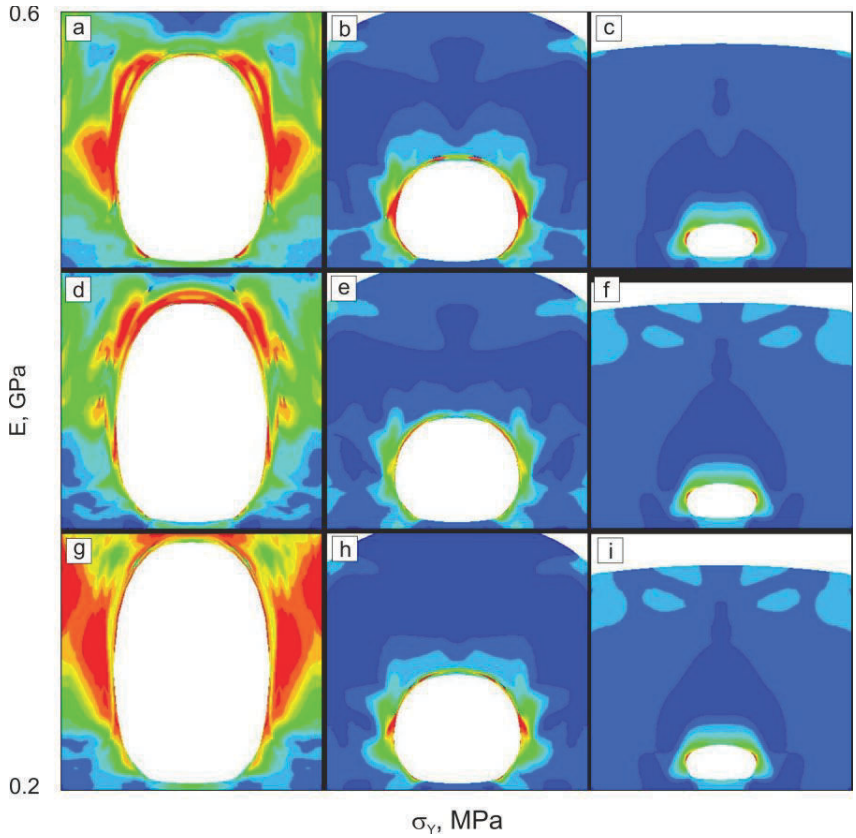

Figura 18. Simulação numérica da abertura de cavidades (módulo de Young = 1). Método dos elementos finitos (Hartmann *et al.,* 2011).

Os estudos desenvolvidos por Baggio *et al.* (2012, 2014c) nos depósitos de ametista identificaram os indicadores geológicos da presença destes depósitos nos derrames vulcânicos da província Paraná e estabeleceram os guias prospectivos destes depósitos.

1.3.5. Guias prospectivos

Os estudos prospectivos desenvolvidos na província vulcânica Paraná em sua grande maioria foram focados na busca por guias prospectivos associados a sistemas de rifteamento da Bacia do Paraná. Destaque para o estudo de Nakamura *et al*. (2003) em cooperação entre a CPRM, Japan International Cooperation Agency e a Metal Mining Agency of Japan para depósitos de Ni-Cu e EGP. O estudo gerou uma gama de informações e permitiu reconhecer duas áreas. A primeira no Arco de São Gabriel e a segunda no Arco de Ponta Grossa, e também incluiu áreas para avaliação de potenciais depósitos minerais nos estados de Goiás, Minas Gerais e Mato Grosso do Sul, além das áreas do Paraná, Santa Catarina, Rio Grande do Sul e norte de São Paulo.

Alternativamente, os estudos prospectivos na província vulcânica Paraná receberam um direcionamento baseado em modelagem 3D e estrutural (Heemann, 1997; 2005) para depósitos de ágata no distrito mineiro de Salto do Jacuí. O autor propôs um modelo de prospecção de ágata incluindo fatores estruturais, sondagem e controle 3D do basalto mineralizado. Porém somente os estudos que se seguiram colocaram em destaque os eventos hidrotermais e, neste ambiente, procuraram identificar os guias prospectivos. Os estudos pioneiros de Hartmann (2008b), Pertille *et al.* (2008a, b) e Pertille (2011) abriram novas perspectivas metalogenéticas para a província. Foram descritas estruturas com diâmetros entre 50-200 m sobre os depósitos de ametista e ágata que foram identificadas como gossans.

O termo gossan, comparativamente às pesquisas desenvolvidas para sua definição está focado em estudos de alterações intempéricas e lixiviação de rochas que formam inicialmente oxi-hidróxidos de ferro e fluidos residuais de ácido sulfúrico (Kosakevitch, 1979; Essalhi *et al.,* 2011). O estudo proposto por Blanchard (1968) trouxe grande contribuição ao estudo dos gossans com definição de terminologias, e descrição das estruturas *boxworks*, consideradas uma das principais características destas feições geológicas. Por outro lado, a caracterização do gossan é dada a partir do topo (zona oxidada) para a base, com zonação vertical bem definida sendo que na superfície a estrutura concentra minerais de ferro oxidados, resultantes de alteração supergênica. Da mesma forma Butt (2004) descreve o perfil do gossan a partir da porção superior com óxidos de ferro e baixa concentração de metais, passando para

uma zona de enriquecimento secundário com metais nativos, carbonatos e sulfatos de origem supergênica, e no final, a transição para sulfetos primários onde está a mineralização principal.

Contudo, o termo gossan tem sido discutido com recorrência na literatura com o objetivo de identificar quais as estruturas que podem ser definidas efetivamente como gossan. Um exemplo é a discriminação entre gossans e crostas lateríticas através da avaliação da geometria, dimensão, presença de substituição pseudomórfica (*boxworks*) e aspectos macroscópicos característicos (Fig. 19). Quando esses critérios são insuficientes, a análise química permite discriminá-los. Os gossans geralmente apresentam anomalias em As, Sb, Ag, Zn, Cu, Pb e Bi. Já as crostas lateríticas concentram preferencialmente Al, Si, Cr, V, Ti, Mn e Ni.

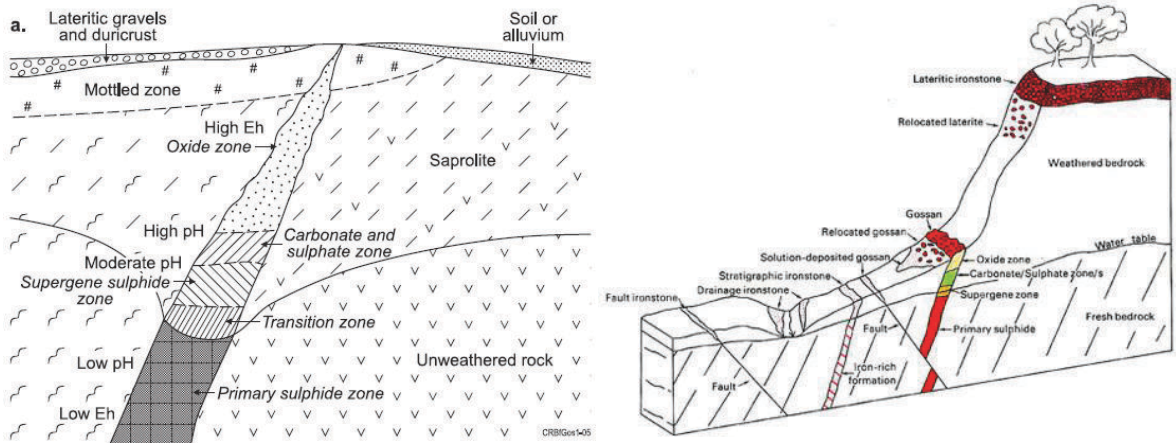

Figura 19. Caracterização de gossans e de couraças lateríticas (Butt 2004, Butt *et al.,* 2005).

Uma das escolas que mais se especializou na discriminação de gossans foi a Australiana a exemplo do estudo de Pirajno (2009). O autor descreve que os gossans apresentam crostas de óxidos de ferro e quartzo (liberação de sílica durante o processo de oxidação), porém destaca que nem todas as estruturas que apresentam óxidos de ferro associados com superfície rica em quartzo são gossans. Ele elenca e define os termos a exemplo de falsos gossans, gossans estéreis, gossans transportados entre outros. De maneira similar e com os mesmos objetivos o estudo de Blot (2004) contribuiu para a discriminação de gossans elencando as principais características e diferenças entre os gossans e as crostas lateríticas (Tabela 8).

A definição de gossan como expressão intempérica de uma rocha com substancial mineralização de sulfetos (Butt *et al.*, 2005) não tem conotação econômica e pode ser aplicado ao produto intempérico de qualquer sulfeto, incluindo pirita. Para fazer discriminações é utilizado o termo *ironstone* como qualquer afloramento intemperizado rico em ferro, incluindo nesta terminologia os gossans. Mas os autores destacam que o termo gossan representa depósitos derivados de sulfetos. Para referenciar estruturas com composição sugestiva de gossan, mas não desenvolvidas a partir de sulfetos os autores indicam o uso dos prefixos falso ou pseudo-gossans.

Característica	Crosta ferrífera laterítica	Gossan
Morfologia	Superfície mapeável	Corpos finos e alongados
Fácies	Relativamente homogênea	Variadas
Microtextura	Erosão da texturas minerais	Réplica perfeita de minerais primarios com recristalização de goetita.
Mineralogia	Frequentemente ternaria: goetita, caolinita e quartzo.	Frequentemente binária: goetita e quartzo.
Composição química e geoquímica	Fe, Al E Si predominantes. Elementos traço: V, Cr, Ti	Predominância de Fe e Si. Importância dos elementos traço: Cu, Pb, Zn, Ni, As, Mo
Composição da Goetita	Frequente substituição de Al.	Fixação de elementos traço dentro e for a da rede cristalina.
Alteração da sequência não aflorante.	Zonação oxi-hidroxi silicatada.	Zonação sulfetada, carbonatada e oxi-hidroxidada.

Tabela 8. Discriminação de gossans e crostas lateríticas (Blot 2004).

Comparativamente aos gossans observados na província vulcânica Paraná, os estudos desenvolvidos por Hanson & Keller (1966) e Keller & Hanson (1968, 1969) descrevem enormes e espessos gossans de sílica sobre depósitos hidrotermais argilosos do México. Estes mesmos autores em 1968, trabalhando com depósitos hidrotermais sobre rochas riolíticas em San Luis Potosi (México) utilizaram o termo sílica gossan para descrever a formação de uma estrutura caracterizada por intensa silicificação sobre uma jazida de caulim. Uma das características principais descritas pelos autores é a forte oxidação e mudança de coloração da superfície do sílica gossan, presença de caulinita e cavidades com calcedônia. No ano seguinte os autores referendam o termo sílica gossan como estrutura geológica utilizada como guia prospectivo para jazidas de caulim de origem hidrotermal, derivado de rochas riolíticas.

Segundo os autores sílica gossans são compostos por quartzo e calcedônia e apresentam estruturas coerentes com a ascensão de fluidos quentes ricos em sílica. A estrutura se destaca na superfície com uma zona oxidada enriquecida em ferro e coloração característica. Da mesma maneira, os estudos de Sayin (2004; 2007) descrevem a ocorrência de sílica gossan associado à ocorrência de caulim de origem hidrotermal na Turquia. A jazida ocorre em andesitos, dacitos e tufos, na localidade de Gonen (Bahkisir – Oeste da Turquia). O autor verificou que durante a alteração, a sílica dissolvida foi remobilizada por fluxos hidrotermais para as porções superiores e silicificou as rochas sotopostas às jazidas de caulin formando sílica gossans, considerados os guias prospectivos destes depósitos hidrotermais.

Na província vulcânica Paraná, Hartmann (2008b) identifica pela primeira vez a presença de gossans sobre jazidas de ametista e ágata e propõe um modelo para sua formação. A evolução dos estudos levou Pertille *et al.* (2008a, b) à descoberta de gossans em dacitos de Padre Eterno (RS), sobre depósitos de geodos de ágata. Os autores destacam que os basaltos e dacitos da região apresentam pouca alteração hidrotermal, porém dentro das estruturas geométricas (200 m x 200 m), há intensa alteração hidrotermal, característica observada também no distrito mineiro de Los Catalanes (Pertille, 2011; Pertille *et al.*, 2013) em Artigas, noroeste do Uruguai. Os estudos destacam as estruturas geométricas nos morros, sua silicificação e presença de anomalias negativas de U, Th e K. Estes guias prospectivos foram avaliados por Baggio *et al.* (2012, 2014a, 2014c) desde o sul até o norte da província e a nomenclatura “sílica gossan” foi indicada para defini-los. Sílica gossans são guias prospectivos de mineralizações de cobre nativo e de depósitos de ametista.

A formação dos sílica gossans está associada ao fluxo ascendente dos fluidos hidrotermais através da pilha vulcânica e aos eventos intempéricos principalmente os do Quaternário que redefiniram a paisagem na província Paraná. Quando os fluidos hidrotermais atravessaram os derrames vulcânicos, formaram caminhos preferenciais, como chaminés verticais com centenas de metros de diâmetro gerando depósitos minerais “derrame a derrame”. Por isso, ao longo destas chaminés hidrotermais, mineralizações de cobre e depósitos de ametista podem ocorrer em vários derrames da estratigrafia vulcânica. Os depósitos de ametista, por exemplo, podem ocorrer próximo à superfície, como nas minas de Entre Rios (SC), no primeiro derrame como em Artigas

(Uruguai) ou em várias profundidades como em Ametista do Sul (RS) onde os depósitos ocorrem em três derrames (derrames Veia Alta, Veia do Meio e Veia de Baixo). O intemperismo sobre os derrames vulcânicos promoveu erosão das rochas e oxidação da superfície das chaminés hidrotermais e deram destaque à estrutura dos sílica gossans. Eles apresentam formas geométricas, hexagonais, poligonais ou irregulares e geralmente estão localizados em altos topográficos (morros), porque a presença de diques, sills e camadas de areia silicificada deixam a sua estrutura mais resistente à erosão. Os sílica gossans se caracterizam pela concentração de óxidos de ferro na superfície (zona oxidada) que destaca sua cor vermelha amarronzada ou ocre, por apresentar áreas de banhados, lagos ou clareiras com intensa argilização e mudanças abruptas do tipo da vegetação sobre sua estrutura. Estes guias podem ser observados em imagens de satélite e apresentam texturas diferenciadas das áreas do entorno. Eles ocorrem em inúmeros locais da província Paraná (Fig. 20) e foram observadas em todos os depósitos de ametista incluindo os distritos mineiros de Artigas (Uruguai), Ametista do Sul (RS) Entre Rios (SC), Chopinzinho (PR) e Wanda (Argentina).

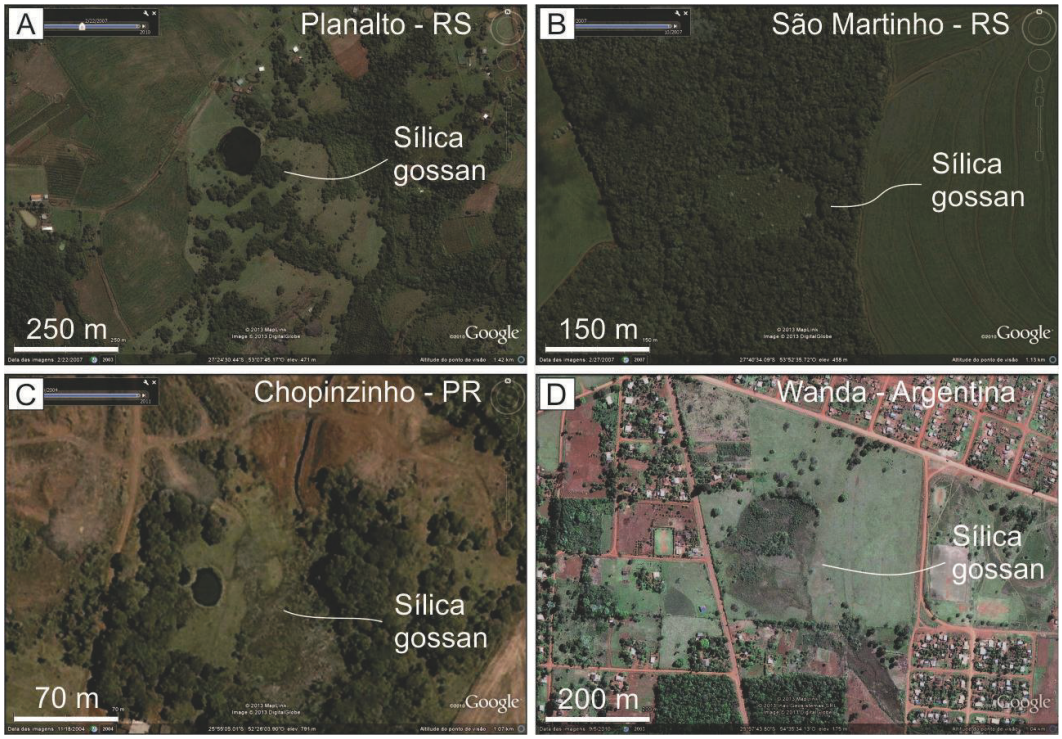

Figura 20. Textura de sílica gossans na província vulcânica Paraná (GoogleEarth). A) Planalto (RS), geodos com gipsita. B) São Martinho (RS). C) Chopinzinho (PR), geodos com ametista. D) Distrito mineiro de Wanda (Argentina) geodos com ametista. (Baggio *et al*., 2014b)

Estudos analíticos de derrames com sílica gossans reforçam sua importância como guias prospectivos de cobre e ametista e comprovam que a alteração hidrotermal e o intemperismo foram os eventos que desencadearam a sua formação. A alteração hidrotermal está representada pelos valores de perda ao fogo, ou seja, quanto maior a perda ao fogo maior a alteração hidrotermal. A avaliação comparativa de análises químicas em riodacitos, andesitos basálticos e basaltos (Baggio *et al*., 2014b) demonstra que, no mesmo derrame, as rochas localizadas dentro dos sílica gossans apresentam valores de perda ao fogo maiores do que as rochas localizadas fora do sílica gossans (Fig. 21).

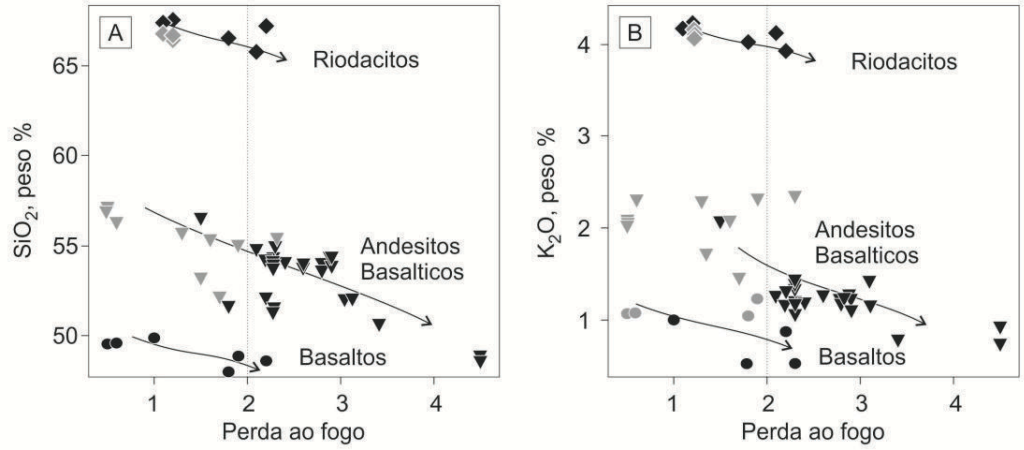

Figura 21. Diagramas de distribuição de óxidos *versus* perda ao fogo. Símbolos pretos: análises químicas de rochas de dentro do sílica gossan. Símbolos cinza: Fora do sílica gossan. (Análises: Baggio *et al*., 2014b; Rosenstengel & Hartmann 2012, Pertille *et al*., 2013)

Para exemplificar serão caracterizados os sílica gossans da Mina do Museu (geodos de ametista) em Ametista do Sul (RS) e o de Taquaruçu do Sul (RS) sobre mineralização de cobre nativo. O sílica gossan Mina do Museu está no derrame Coogamai um derrame do tipo II, localizado imediatamente acima do derrame Veia Alta, que é um derrame do tipo I (Gomes, 1996) e produtor de ametista. Os valores de perda ao fogo fora do sílica gossan são em média 0,4 peso % enquanto que dentro do sílica gossan estes valores são em média 1,5 peso %. O sílica gossan de Taquaruçu do Sul (Baggio, 2014a) está em um derrame tipo II com mineralização de cobre na superfície das disjunções colunares e nas cavidades da zona amigdaloidal. Nas áreas fora do sílica gossan os valores médios de perda ao fogo são de 0,8 peso% enquanto que dentro do sílica gossan os valores atingem 2,3 peso%. Quando avaliada a

radioatividade natural gama espectrométrica (K%, eU e eTh) dos derrames onde estão os sílica gossans observam-se anomalias negativas que se intensificam sobre as áreas mineralizadas. No derrame Coogamai, fora do sílica gossan os valores gama espectrométricos são em média 55 cps (contagem por segundo) enquanto que nas áreas dentro do sílica gossan a média é de 43,5 cps (Fig. 22).

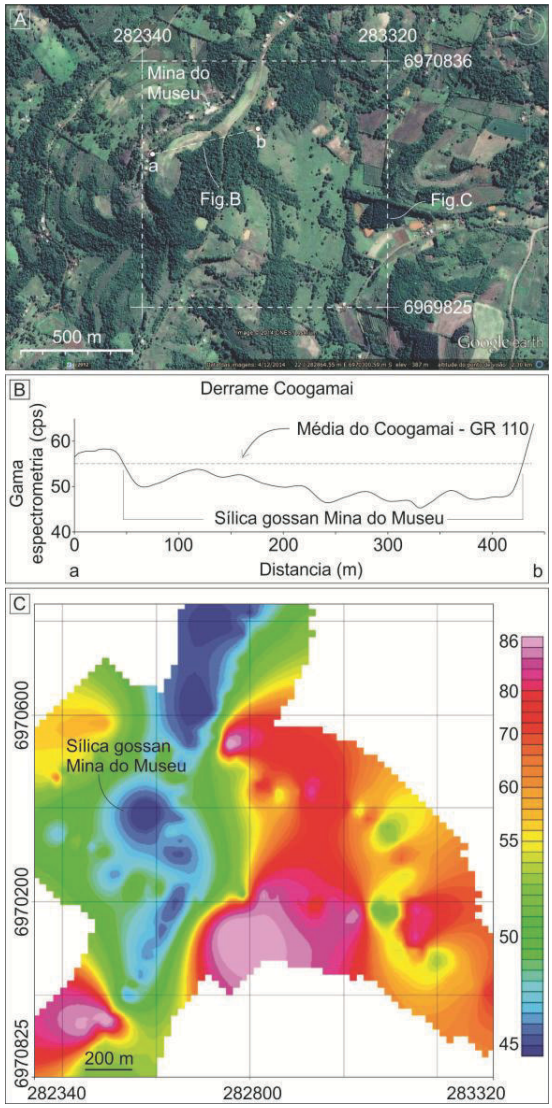

Figura 22. Área de levantamento do sílica gossan Mina do Museu. A) Imagem Google Earth da área. B) Perfil gama-espectrométrico. C) Mapa gama-espectrométrico sobre a Mina do Museu (Baggio *et al*., 2015b)

O mesmo comportamento gama espectrométrico foi observado ao longo do derrame vulcânico onde está o sílica gossan de Taquaruçu do Sul (Fig. 23). Fora da estrutura os valores gama espectrométricos apresentam em média 61 cps enquanto que no sílica gossan as médias são de 39 cps. Estas áreas com as anomalias

negativas mais expressivas correspondem às áreas onde os agricultores encontraram esferas de cobre nativo com dimensões mm-cm, durante os trabalhos de retirada de matacões de rochas para a implantação da agricultura.

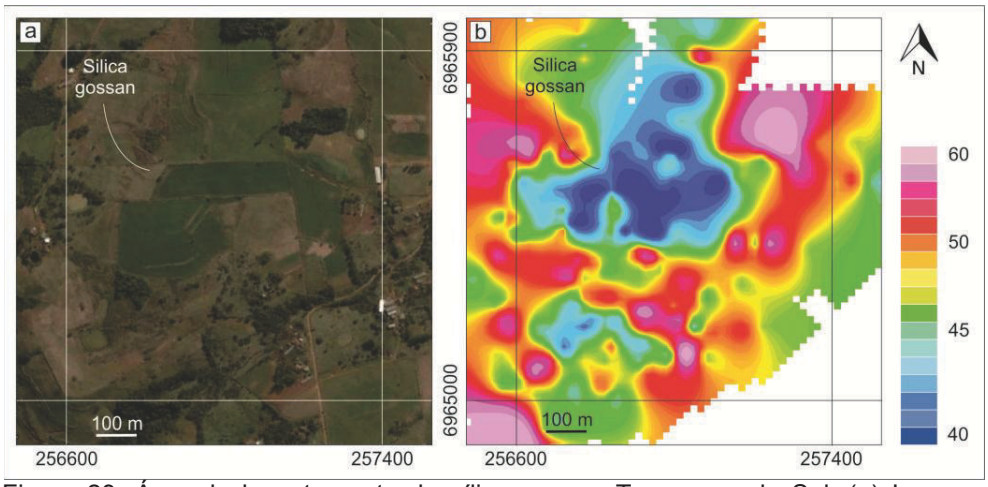

Figura 23. Área de levantamento do sílica gossan Taquaruçu do Sul. (a) Imagem GoogleEarth mostrando o sílica gossan associado a áreas com banhado e lagos. (b) Mapa gama espectrométrico mostrando as áreas com anomalias negativas sobre as mineralizações de cobre.

As áreas com as anomalias negativas são resultantes da combinação dos eventos hidrotermais e intempéricos. O hidrotermalismo foi o responsável pela alteração de minerais (piroxênio, magnetita-ilmenita) e formação de argilo-minerais do grupo da esmectita. Os eventos intempéricos desencadearam a oxidação e concentração de ferro na superfície dos sílica gossans o que facilitou a solubilidade do Th e a mobilidade do U. Estes radionuclídeos adsorvidos em argilas coloidais, soluções silicáticas complexas e óxidos-hidróxidos de ferro são lixiviados pelos processos gravitacionais, gerando áreas com anomalia negativa nos sílica gossans. A concentração superficial de ferro, além de auxiliar este processo é uma característica importante dos sílica gossans. Por vezes formam-se crostas ferruginosas na superfície do terreno (Fig. 24A) e a cor do solo e das rochas alteradas torna-se vermelha amarronzada ou ocre. A formação de áreas úmidas, banhados e lagos (Fig. 24B) ocorre em virtude da concentração de argilo minerais (esmectitas) nas áreas mais afetadas pelo hidrotermalismo sobre o sílica gossan. Estes locais naturalmente apresentam facilidade em reter a água e formar estes tipos de ambientes. As argilas predominantes foram identificadas por raios-X como montmorilonita (principalmente), nontronita e caolinita. A execução de análises por microssonda eletrônica mostrou que nas áreas fora do sílica gossan predominam as

esmectitas dioctaedrais com intercamadas dominadas por potássio e dentro do sílica gossan predominam as esmectitas trioctaedrais enriquecidas em magnésio. Esta característica é importante e serve como um indicador confiável do grau de alteração hidrotermal do basalto.

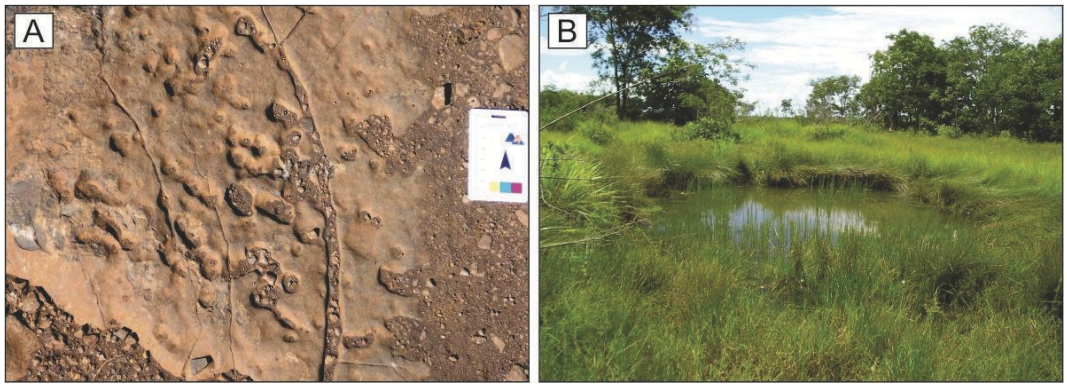

Figura 24. Feições dos sílica gossans. A) Crosta ferruginosa e coloração ocre. Mina do Museu, Ametista do Sul (RS). B) Concentração de argilo-minerais e formação de lago sobre o sílica gossan Serra de Maracaju (MS) (Baggio *et al*., 2014c).

Todas estas características que identificam os sílica gossans são praticamente comuns tanto em depósitos de ametista como em mineralizações de cobre nativo. A variação que os diferencia é basicamente o tipo de derrame (I ou II) onde a mineralização está hospedada. Os derrames do tipo I e II (Gomes, 1996) apresentam como diferenças a espessura do derrame e a existência de disjunções colunares. Esta característica altera o comportamento de um fluido hidrotermal que está agindo sobre um maciço rochoso. No caso de derrames do tipo I, portadores de depósitos de geodos de ametista, a interação do fluido com a rocha é extremamente íntima e a alteração hidrotermal ocorre poro a poro nas áreas onde o fluido perpassa. A presença de diques, sills, camadas de areia e brechas hidrotermais também são mais intensas nestes depósitos. Por outro lado, nos derrames do tipo II os fluidos hidrotermais utilizam as disjunções colunares como caminho de alívio da pressão. A interação fluido-rocha é superficial ao longo das disjunções, onde ocorre a mineralização de cobre e também deposição de areia fina. Os sílica gossans sobre depósitos hospedados em derrames do tipo I geralmente estão associados a morros topograficamente mais elevados, enquanto que sílica gossans sobre mineralizações hospedados em derrames do tipo II apresentam geomorfologia caracterizada por elevações mais suaves que muitas vezes permitem o uso e ocupação do solo para a agricultura.

2. Análise integradora

A avaliação de áreas de estudo distribuídas ao longo da província permitiu uma visão panorâmica da relação do magmatismo, hidrotermalismo e alteração supergênica com as mineralizações de cobre nativo e depósitos de ametista na província vulcânica Paraná. Na porção sul da província, no Rio Grande do Sul, o estudo foi desenvolvido nas regiões de Torres, Gramado, Novo Hamburgo, Bom Princípio, Santo Augusto, Chiapetta, Taquaruçu do Sul e Ametista do Sul. Em Santa Catarina, nas regiões de São Lourenço do Oeste, Entre Rios, Dionísio Cerqueira e Palma Sola. Na porção central da província, no Paraná, afloramentos na região de Francisco Beltrão, Ampére, Realeza e Cascavel e no Estado do Mato Grosso do Sul, norte da província, os derrames vulcânicos da região de Campo Grande, Jardim e Serra de Maracaju. Os resultados obtidos permitiram a elaboração de quatro artigos científicos que compõem esta tese, e também capítulos do livro *"Metalogenia e Exploração Mineral no Grupo Serra Geral"*.

A área no sudoeste do Paraná foi importante para esta tese primeiramente porque vários estudos regionais discutiram a geologia regional (e.g., Ferreira, 2011; Wildner *et al*., 2006) com descrição de derrames basálticos e pegmatitos. A ocorrência de cobre nativo em uma ampla área desta região motivou o detalhamento das ocorrências. No município de Francisco Beltrão (Pedreira Dalba) foi possível avaliar um espesso derrame basáltico que apresenta intrusões descritas regionalmente como pegmatitos. Porém estas rochas apresentam bordas de reação com o basalto hospedeiro. As bordas de reação clara e escura foram separadas em escala de campo, na petrografia e geoquímica e as rochas foram interpretadas como paralavas. Uma segunda área, no centro oeste do Mato Grosso do Sul, região de Jardim também ganhou destaque uma vez que ocorre um grande afloramento de paralava (pedreira Rochasul) com dimensões da ordem de 20 m de espessura e aproximadamente 200 m de comprimento contendo fenocristais longos e curvos de clinopiroxênio (até 10 cm), plagioclásio (1 cm), magnetita-ilmenita e apatita. As observações de campo motivaram a discussão sobre a origem e a formação destas rochas e serviu como ponto de partida para os estudos geoquímicos, análises de microssonda eletrônica e observações de inclusões fluidas que culminaram na obtenção de dados para o artigo ***"Paralavas in the Paraná volcanic province, Brazil – an interpretation of the basaltic rocks containing phenocrysts and glass"***. Este artigo discute a hipótese da formação das

paralavas em derrames espessos a partir da combustão do metano (CH_4) e refusão parcial do basalto. O metano, resultante do craqueamento do querogênio pelos diques e sills de lavas que intrudiram nas Formações da bacia do Paraná reage com o basalto ainda quente e eleva a temperatura local refundindo as porções afetadas. O líquido neo formado, mais leve, é injetado na parte central e superior do derrame, sofre quenching e forma as paralavas. Apesar de serem corpos restritos e identificados principalmente no noroeste do Paraná, estas rochas ganham importância econômica pela mineralização de cobre associada.

Por outro lado, mineralizações de cobre em basaltos ocorrem amplamente disseminadas ao longo da província e foram observadas no Rio Grande do Sul, Santa Catarina, Paraná e Mato Grosso do Sul. A discussão sobre a origem do cobre nativo nos basaltos da província foi desenvolvida a partir de evidências de campo e uma combinação de técnicas analíticas como petrografia, análises químicas, difração de raios-X, espectrometria Raman, microssonda eletrônica (EMPA), LA-ICPMS, e isótopos estáveis de cobre. Estas técnicas produziram dados relevantes que permitiram a elaboração do artigo intitulado ***"Origin of native copper in the Paraná volcanic province, Brazil, integrating Cu stable isotopes in a multianalytical approach"*** que foi submetido à ***Mineralium Deposita***. Os resultados obtidos mostram que não há evidências de cobre de origem magmática. Todas as evidências relacionam o cobre a uma origem hidrotermal de baixa temperatura e mostram que a fonte primária do elemento cobre é a estrutura cristalina dos minerais (magnetita, ilmenita e clinopiroxênio) do basalto hospedeiro. A alteração hidrotermal transformou estes minerais em esmectitas e liberou o cobre que foi remobilizado e transportado pelos fluidos hidrotermais. As mineralizações de cobre nativo foram geradas ao longo da rede de disjunções colunares e nas cavidades da zona amigdaloidal. As variações das razões isotópicas refletem a remobilização de cobre, seu fracionamento ao longo dos caminhos dos fluidos hidrotermais, mineralizações recorrentes (pulsos distintos de mineralização) e eventos de alteração supergênica. Minerais de cobre a exemplo da cuprita, malaquita e crisocola foram gerados a partir da interação do cobre nativo com fluidos hidrotermais e alterações supergênicas. Além das mineralizações de cobre, os eventos hidrotermais formaram jazidas de geodos de ametista hospedadas nos derrames da pilha vulcânica. Estes derrames ao serem expostos aos eventos

intempéricos geraram os sílica gossans, os guias prospectivos de mineralizações de cobre e de depósitos de ametista. Suas feições foram reconhecidas e avaliadas desde o sul até o norte da província. A área de estudo estabelecida em Ametista do Sul (RS) tornou-se extremamente importante, não apenas por ser o maior distrito mineiro de ametista do mundo em atividade, com produção média de 400 toneladas de geodos de ametista/mês, mas também pela exposição de afloramentos de rocha e de jazidas como em nenhum outro local. O reconhecimento das feições do sílica gossan Mina do Museu e os dados gerados a partir de análises químicas, levantamento gama espectrométrico, difração de raios-X e microssonda eletrônica definiram suas características e permitiram a elaboração do artigo ***"Silica gossan as a prospective guide for amethyst geode deposits in the Ametista do Sul mining district, Paraná volcanic province, southern Brazil"*** que foi submetido ao ***Journal of Geochemical Exploration***. Os resultados permitiram avançar no conhecimento geológico dos sílica gossans, principalmente na caracterização geoquímica, distribuição dos conteúdos de perda ao fogo, avaliação das anomalias negativas de K, U e Th e na identificação de esmectitas dioctaedrais (K) fora do sílica gossan e trioctaedrais (Mg) dentro do sílica gossan. O sílica gossan Mina do Museu localizado em uma área de grande produção de geodos de ametista é um modelo a ser reproduzido em outras áreas da província vulcânica Paraná. Neste sentido foi desenvolvido um estudo prospectivo em áreas-alvo na porção norte da província, nas regiões de Campo Grande (MS) e Serra de Maracaju (MS). A avaliação de imagens de satélite identificou estruturas com texturas indicativas de sílica gossans e desencadeou trabalhos de campo e aplicação de técnicas analíticas. Os resultados obtidos permitiram a elaboração do artigo intitulado ***"Basalt stratigraphy and silica gossans in Campo Grande and Serra de Maracaju, Mato Grosso do Sul, Paraná volcanic province***" publicado no ***Ore Geology Reviews***. O artigo define a estratigrafia dos derrames basálticos da região com base na geoquímica e gama espectrometria dos derrames, identifica as áreas com anomalias negativas nos sílica gossans e indica que as duas áreas-alvo apresentam depósitos hidrotermais potenciais.

3. Conclusões

O vulcanismo da província Paraná ocorreu há 135 Ma e recobriu com lavas a porção centro-sul da América do Sul e o noroeste da Namíbia. Este evento foi o responsável pelo calor residual que afetou termicamente os sedimentos da bacia do Paraná. A intrusão de sills em formações portadoras de querogênio desencadeou formação de metano, refusão parcial dos basaltos e geração das paralavas especialmente importantes por apresentar altos teores de cobre.

O calor residual afetou também as águas do Aquífero Guarani deflagrando processos hidrotermais e fluidização de areia da Formação Botucatu. Os fluidos hidrotermais alteraram os derrames da pilha vulcânica e geraram mineralizações de cobre nativo e depósitos de geodos de ametista e ágata de classe mundial. A origem dos depósitos de ametista e das mineralizações de cobre são hidrotermais. O elemento químico cobre está presente na estrutura cristalina dos minerais dos basaltos da província e é a fonte das mineralizações de cobre hidrotermal. As razões isotópicas refletem mineralização de cobre recorrente e alteração supergênica.

A associação dos eventos magmáticos, hidrotermais e de alteração supergênica estabeleceu condicionantes geológicos exclusivos na província e foi responsável pela formação dos depósitos minerais, com destaque para as maiores jazidas de ametista do mundo e mineralizações de cobre. As relações estabelecidas nestes eventos podem ser resumidas pelos sílica gossans. Estes guias prospectivos apresentam formas geométricas e podem ser reconhecidos em imagens de satélite. Eles foram identificados em todos os distritos mineiros, ocorrem aos milhares na pilha vulcânica e representam uma nova fronteira metalogenética na província vulcânica Paraná.

4. Referências

Almeida, F.F.M., 1986. Distribuição regional e relações tectônicas do magmatismo pós-paleozóico no Brasil. **Revista Brasileira de Geociências, 16**: 325-349.

Araújo, C.C., Yamamoto, J.K., Rostirola, S.P., 2004. Distribuição espacial e caracterização geológica dos arenitos asfálticos da borda leste da Bacia do Paraná no Estado de São Paulo. **Revista Brasileira de Geociências 34**: 187-200.

Araújo, L.M., França, A.B., Potter, P.E., 1995. Arcabouço hidrogeológico do aqüífero gigante do Mercosul (Brasil, Argentina, Uruguai e Paraguai): Formação Botucatu, Pirambóia, Rosário do Sul, Buena Vista, Missiones e Tacuarembó. In: Encontro nacional de perfuradores de poços, 9., 1995, Curitiba. **Anais...** poços, UFPR, p. 110-120.

Arena, K.R., Hartmann, L.A., Baggio, S.B., 2014. Geological controls of copper, gold and silver in the Serra Geral Group, Realeza region, Paraná, Brazil. **Ore geology review** 63:178-200

Assine, M.L., Perinotto, J.A.J., Alvarenga, C.J.S., Petri, S., 1998. Arquitetura estratigráfica, tratos deposicionais e Paleogeografia da Bacia do Paraná (Brasil) no Neo-Ordoviciano / Eo-Siluriano. **Revista Brasileira de Geociências 28**(I): 61-76.

Assine, M.L., Piranha, J.M., Carneiro, C.D.R., 2004. Os paleodesertos Pirambóia e Botucatu. In: Mantesso Neto, V., Bartorelli, A., Carneiro, C.D.R., Brito Neves, B.B. (orgs). **Geologia do Continente Sul-Americano: Evolução da obra de Fernando Flávio Marques de Almeida.** São Paulo: Ed. Beca, p. 77-93.

Assine, M.L., Soares, P.C., Milani, E.J., 1994. Seqüências tectono-sedimentares mesopaleozóicas da Bacia do Paraná. **Revista Brasileira de Geociências 24**(2): 77-89.

Baggio, S.B., Hartmann, L.A., Arena, K.R., Duarte, S.K., Antunes, L.M., 2014a. Sílica gossans sobre mineralizações de cobre nativo, ouro e prata no Grupo Serra Geral. In: Hartmann, L.A., Baggio, S.B. (orgs). **Metalogenia e exploração mineral no Grupo Serra Geral,** Porto Alegre, 1ª ed. UFRGS, p. 111-133.

Baggio, S.B., Hartmann, L.A., Pertille, J., Antunes, L.M., 2012. Silica gossans in the Serra Geral Group, Paraná volcanic province as guides for the discovery of new hydrothermal deposits of native copper and amethyst geodes. In: Simpósio Brasileiro de Exploração Mineral, 5., 2012, Ouro Preto, **Anais...** Ouro Preto. ADIMB.

Baggio, S.B., Hartmann, L.A., Wildner, W., 2014b. Descrição e origem das paralavas da província vulcânica Paraná. In: Hartmann, L.A., Baggio, S.B. (orgs). **Metalogenia e exploração mineral no Grupo Serra Geral,** Porto Alegre, 1ª ed. UFRGS, p. 173-202.

Baggio, S.B., Pertille, J., Antunes, L.M., Petry, T.S., Hartmann, L.A., 2014c. Sílica gossans sobre mineralizações de geodos de ametista e ágata no Grupo Serra Geral. In: Hartmann, L.A., Baggio, S.B. (orgs). **Metalogenia e exploração mineral no Grupo Serra Geral,** Porto Alegre, 1ª ed. UFRGS, p. 89-109.

Bakker, R.J., 2003. Package Fluids 1. Computer programs for analysis of fluid inclusion data and for modeling bulk fluid properties. **Chemical Geology** 194: 3-23

Barbosa, O., Almeida, F.F.M., 1949. **A Série Tubarão na bacia do Rio Tietê, Estado de São Paulo**. Boletim da Divisão de Geologia e Mineralogia, DNPM. Rio de Janeiro, 16p.

Bellieni, G., Comin-Chiaramonti, P., Marques, L.S., Melfi, A.J., Piccirillo, E.M., Nardy, A.J.R., Stofa, D., Roisenberg, A., 1984. High- and low-Ti flood basalts from the Paraná plateau (Brazil): petrology and geochemical aspects bearing on their mantle origin. **Neues Jahrbuch Für Mineralogie: Abhlandlungen, 150**: 273-306.

Bellieni, G., Comin-Chiaramonti, P., Marques, L.S., Melfi, A.J., Nardy, A.J.R., Papatrechas, C., Piccirillo, E.M., Roisenberg, A., 1986. Petrogenetic aspects of acid and basaltic lavas from the Parana plateau (Brazil): geological, mineralogical and petrochemical relationships. **Journal of Petrology 27**: 915-944.

Betiollo, L.M., 2006. **Caracterização estrutural, hidrogeológica e hidroquímica dos sistemas aquiferos Guarani e Serra Geral no nordeste do Rio Grande do Sul, Brasil.** Porto Alegre. Dissertação de mestrado em Geociências, Instituto de Geociências, Universidade Federal do Rio Grande do Sul.

Blanchard, R., 1968. Interpretation of leached outcrops. **Bulletin 66.** Nevada Bureau of mines. University of Nevada.

Blot, A., 2004. Caractérisation des chapeaux de fer en milieu latéritique cuirassé, **Comptes Rendus Geoscience 336**: 1473-1480.

Bodziak Jr, C., Maack, R., 1946. Contribuição ao Conhecimento dos Solos dos Campos Gerais no Estado do Paraná. **Arquivos de Biologia e Tecnologia** 1: 197-214.

Bortoluzzi, C.A., Piccoli, A.E.M., Bossi, G.E., Guerra-Sommer, M., Toigo, M.M., Pons, M.E.H., Wolf, M., Silva, Z.C.C., 1978. Pesquisa geológica na bacia carbonífera de Santa Catarina. **Pesquisas em Geociências** 11: 33-192.

Bossi, J., Caggiano, W., 1974. Contribuicion a la Geologia de los Yacimentos de Amatista del Departamento de Artigas. In: Congresso Brasileiro de Geologia, 28., 1974, Porto Alegre, **Anais...** Porto Alegre, SBG. p.301-317.

Brandelik, A., Massonne H.J., 2004. PTGIBBS – an EXCELTM Visual Basic program for computing and visualizing thermodynamic functions and equilibria of rock-forming minerals. **Computers & Geosciences** 30: 909-923.

Brown, A.C., 2006. Genesis of native copper lodes in the Keewenaw District, Northern Michigan: A hybrid evolved meteoric and metamorphogenic model. **Economic Geology 101**: 1437-1444.

Brückmann, M., Hartmann, L.A., Tassinari, C.C.G., Sato, K., Baggio, S.B., 2014 A duração do magmatismo no Grupo Serra Geral, província vulcânica Paraná. In: Hartmann, L.A., Baggio, S.B. (orgs). **Metalogenia e exploração mineral no Grupo Serra Geral,** Porto Alegre, 1ª ed. UFRGS, p. 233-245.

Butt, C.R.M., 2004. Understanding the regolith in tropical and sub-tropical terrais: the key to exploration under cover. **https://www.appliedgeochemists.org /index.php/events/aag-events/2-uncategorised/51-predictive-mineral-discovery-under-cover-symposium** acessado em 16/02/2015.

Butt, C.R.M., Scott, K.M., Cornelius, M. Robertson, I.D.M., 2005. Gossans and Ironstones – Sample Media. **http://crcleme.org.au/RegExpOre/5-samplemedia.pdf** acessado em 16/02/2015.

Campbell, I.H., Griffiths, R.W., 1990. Implications of mantle plume structure for evolution of flood basalts. **Earth and Planetary Science Letters 99**: 79-93.

Carneiro, C.D.R., 2007. Viagem virtual ao Aqüífero Guarani em Botucatu (SP): Formações Pirambóia e Botucatu, Bacia do Paraná. **Terræ Didatica 3**: 50-73.

Coltice, N., Phillips, B.R., Bertrand, N., Ricard, Y., Rey, P., 2007. Global warming of the mantle at the origin of flood basalts over supercontinents. **Geology 35**: 391-394.

Correa, TE., Koppe, J.C., Costa, J.F.C.L., Moraes, M.A.L., 1994. Caracterização geológica e critérios de prospecção de depósitos de ametista do tipo Alto Uruguai, RS. In: Congresso Brasileiro de Geologia, 38., 1994, Camboriú, **Anais...** Camboriú, SBG, 2, p. 137-138.

Costa, A.F.U., 1982. Geofísica aplicada à prospecção de cobre em basaltos na área de Vista Alegre: Frederico Westphalen, RS. **Acta Geológica Leopoldinense 16**: 17-36.

Daemon, R.F., Quadros, L.P., 1970. Bioestratigrafia do Neopaleozóico da Bacia do Paraná. In: Congresso Brasileiro de Geologia, 24., 1970, Brasília, **Anais...** Brasília, SBG, p.359-412.

D'oriano, C., Pompilio, M., Bertagnini, A., Cioni, R. Pichavant, M., 2013. Effects of experimental reheating of natural basaltic ash at different temperatures and redox conditions. **Contributions to Mineralogy and Petrology** 165: 863-883.

Duarte, L.C., 2008. **Evolução geológica, geoquímica e isotópica das mineralizações de geodos com ametista, Artigas, Republica Oriental do Uruguai.** Porto Alegre. 167 f. Tese de Doutorado em Geociências. Instituto de Geociências, Universidade Federal do Rio Grande do Sul.

Duarte, L.C., Hartmann, L.A., Vasconcelos, M.A.Z., 2005. Epigenetic geode formation in the world class amethyst deposit of the southern Paraná Basaltic Province. In: Simpósio Brasileiro de Metalogenia, 1., Gramado. **CD-ROM…** Gramado. SBG, 5p.

Duarte, L.C., Hartmann, L.A., Vasconcelos, M.A.S., Medeiros, J.T.N., Theye, T., 2009. Epigenetic formation of amethyst-bearing geodes from Los Catalanes gemological district, Artigas, Uruguay, southern Paraná Magmatic- Province. **Journal of Volcanology and Geothermal Research 184**: 427-436.

Duarte, L.C., Hartmann, L.A., Ronchi, L.H., Berner, Z., Theye, T. Massonne, H.J., 2011. Stable isotope and mineralogical investigation of the genesis of amethyst geodes in the los Catalanes homological district, Uruguai, southernmost Paraná volcanic province. **Mineralium Deposita 46**: 239-255.

Duarte, S.K., Hartmann, L.A., 2014. Evolução dos injetitos de areia do Complexo Novo Hamburgo, província vulcânica Paraná. In: Hartmann, L.A., Baggio, S.B. (orgs.) **Metalogenia e exploração mineral no Grupo Serra Geral**, Porto Alegre, 1ª ed. UFRGS, p. 203-232.

Essalhi, M., Sizaret, S., Barbanson, L., Chen, Y., Lagroix, F., Demory, F., Nieto, J.M., Sáez, R., Capitán, M.A., 2011. A case study of the internal structures of gossans and weathering processes in the Iberian Pyrite Belt using magnetic fabrics and paleomagnetic dating. **Mineralium Deposita 46**: 981-999.

Faria, A., Reis Neto, J.M., 1978. Nova unidade litoestratigráfica pré-Furnas no sudoeste de Goiás. In: Congresso Brasileiro de Geologia, 30., 1978, Recife, **Resumo...** Recife, SBG, p. 136-137.

Ferreira, C.N.H. 2011., **Geologia do derrame Salto do Lontra e gênese dos pegmatitos básicos associados, província magmática do Paraná, sudoeste do estado do Paraná.** Curitiba. 102 f. Dissertação de Mestrado em Geologia. Universidade Federal do Paraná.

Fischer, A.C. 2004., **Petrografia e geoquímica das fases silicosas dos geodos mineralizados à ametista (região do Alto Uruguai, RS, Brasil).** Porto Alegre. 159 f. Tese de Doutorado em Geociências. Instituto de Geociências, Universidade Federal do Rio Grande do Sul.

Flóvenz, O.G., Saemundsson, K., 1993. Heat flow and geothermal processes in Iceland. **Tectonophysics 225**: 23-138.

Franco, R.R. 1952., Zeolitas dos basaltos do Brasil meridional. **Boletim da Faculdade de Filosofia, Ciências e Letras da USP**. Mineralogia 54, v.6.

Frank, H.T., Gomes, M.E.B., Formoso, M.L.L. 2009., Review of the extent and the volume of the Serra Geral Formation, Paraná Basin, South America. **Pesquisas em Geociências 36**: 49-57.

Fúlfaro, V.J. 1971., Evolução Tectônica e Paleogeográfica da Bacia Sedimentar do Paraná pelo “Trend Surface Analysis”. **Boletim da Escola de Engenharia de São Carlos 14**: 1-111.

Gadens-Marcon, G.T., Mendonça-Filho, J.G., Guerra-Sommer, M., Carvalho, M.A., Pires, E.F., Hartmann, L.A., 2014. Relation between the sedimentary organic record and the climatic oscilations in the Holocene attested by palynofacies and organic geochemical analyses from a pond of altitude in southern Brazil. **Anais da Academia Brasileira de Ciências 86**: 1077 -1099.

Gamermann, N., 1973. Formação Rosário do Sul. **Pesquisas em Geociências 2**: 5-36.

Garcia, P.F., Marinho, D.A., 1980. Aspectos genéticos das rochas ácidas da Formação Serra Geral nas folhas de Uruguaiana (SH-21) e Porto Alegre (SH-22). In: Congresso Brasileiro de Geologia, 31., 1980, Balneário Camboriú. **Anais…** Balneário Camboriú, SBG, 4, p. 2059-2068.

Gilg, H.A., Morteani, G., Kostitsyn, Y., Preinfalk, C., Gatter, I., Strieder, A.J., 2003. Genesis of amethyst geodes in basaltic rocks of the rocks of the Serra Geral Formation (Ametista do Sul, Rio Grande do Sul, Brazil): a fluid inclusion, REE, oxygen, carbon and Sr isotope study on basalt, quartz, and calcite. **Mineralium Deposita 38**: 1009-1025.

Gomes, M.E.B., 1996. **Mecanismos de resfriamento, estruturação e processos pós-magmáticos em basaltos da Bacia do Paraná – Região de Frederico Westphalen (RS) – Brasil.** Porto Alegre. 219 f. Tese de Doutorado em Geociências. Instituto de Geociências, Universidade Federal do Rio Grande do Sul.

Gordon Jr, M., 1947. **Classificação das Formações Gondwânicas do Paraná, Santa Catarina e Rio Grande do Sul.** Boletim da Divisão de Geologia e Mineralogia, DNPM. Rio de Janeiro, 38: 1-20.

Goulart, E.P., Jardim, N.S., 1982. Avaliação geoquímica das formações Ponta Grossa e Irati - Bacia do Paraná. In: PAULIPETRO - consórcio CESP-IPT. **Geologia da Bacia do Paraná: reavaliação da potencialidade e prospectividade em hidrocarbonetos.** São Paulo, p. 41-74.

Hanson, R.F., Keller, W.D., 1966. Genesis of refractory clay near Guanajuato, Mexico. In: National Conference on Clays and Clays Minerals, 14th., **Proceedings…** minerals, pp. 259-267.

Hartmann, L.A., 2008a. **Geodos com Ametistas formados por água quente no tempo dos dinossauros.** Porto Alegre, Gráfica UFRGS, 60p.

Hartmann, L.A., 2008b. Gossan over amethyst and agate deposits in the Paraná Basaltic Province and Hexagonal geometry of hydrothermal feeding chimneys. In: Congresso Brasileiro de Geologia, 44., 2008, Curitiba. **Anais…** Curitiba, SBG, p.213.

Hartmann, L.A., Baggio, S.B., Duarte, S.K., 2012. Decoding geochemical and gamma-spectrometric signatures from lavas and sand injectites at the base of the Paraná volcanic province, Novo Hamburgo, Brazil. **International Geology Review 55**: 510-524.

Hartmann, L.A., Duarte, L.C., Massonne, H.J., Michelin, C., Rosenstengel, L.M., Bergmann, M., Theye, T., Pertille, J., Arena, K.R., Duarte, S.K., Pinto, V.M., Barboza, E.G., Rosa, M.L., Wildner, W., 2011a. Sequential opening and filling of cavities forming vesicles, amygdales and giant amethyst geodes in lavas from the southern Paraná volcanic province, Brazil and Uruguay. **International Geology Review 54**: 1-14.

Hartmann, L.A., Duarte, S.K., Pertille, J., Techera, J., 2010b. Geologia dos geodos de Ametista de Quarai, Brasil, e los Catalanes, Uruguai – Uma imersão no vulcanismo e exploração mineral na província vulcânica Paraná (Arapey). **Excursão de campo**. Porto Alegre, Gráfica UFRGS, 98p.

Hartmann, L.A., Medeiros, J.T.N., Baggio, S.B., Antunes, L.M., 2015. Controls on prolate and oblate geode geometries in the Veia Alta basalt flow, largest world producer of amethyst, Paraná volcanic province, Brazil. **Ore Geology Reviews 66**: 243-251.

Hartmann, L.A., Medeiros, J.T.N., Petruzzellis, L.T., 2011b. Numerical simulations of amethyst geode cavity formation by ballooning of altered Paraná volcanic rocks, South America. **Geofluids 12**: 133-141.

Hartmann, L.A., Wildner, W. Duarte, L.C., Duarte, S.K., Pertille, J., Arena, K.R., Martins, L.C., Dias, N.L., 2010a. Geochemical and scintillometric characterization and correlation of amethyst geode-bearing Paraná lavas from the Quaraí and Los Catalanes districts, Brazil and Uruguay. **Geological Magazine 147**: 954-970.

Heemann, R., 1997. **Geologia, controles e guias prospectivos para depósitos de ágata na região de Salto do Jacuí.** Porto Alegre. 107 f. Dissertação de Mestrado em Engenharia de Minas, Metalurgia e dos Materiais. Universidade Federal do Rio Grande do Sul.

Heemann, R., 2005. **Modelagem exploratória estrutural e tridimensional dos depósitos de ágata do distrito mineiro de Salto do Jacuí (RS).** Porto Alegre. 163 f. Tese de doutorado em Engenharia de Minas, Metalurgia e dos Materiais. Universidade Federal do Rio Grande do Sul.

Hill, R.I., 1991. Starting plumes and continental breakup. **Earth and Planetary Science Letters 104**: 398-416.

Hill, R.I., Campbell, H., Davies, G.F., Griffiths, R.W., 1992. Mantle plumes and continental tectonics. **Science 256**: 186-192.

Holz, M. França, A.B., Souza, P.A., Iannuzzi, R., Rohn, R., 2010. A stratigraphic chart of the Late Carboniferous/Permian succession of the eastern border of the Paraná Basin, Brazil, South America. **Journal of South American Earth Sciences 29**: 381-399.

Ikehata, K., Notsu, K., Hirata, T., 2011. Copper isotope characteristics of copper-rich minerals from Besshi-type volcanogenic massive sulfide deposits, Japan, determined using a femtosecond LA-MC-ICP-MS. **Economic Geology 106**: 307-316

IPT., 1981. **Mapa Geológico do Estado de São Paulo**. 1: 500.000. Divisão de Minas e Geologia Aplicada. Pró-Minério.

Janasi, V.A., Freitas, V.A., Heaman, L.H., 2011. The onset of flood volcanism, Northern Paraná Basin, Brazil: A precise U-Pb baddeleyite/zircon age for a Chapecó-type dacite. **Earth and Planetary Science Letters 302**: 147-153.

Jensen, A., 1982. The distribution of Cu across three basaltic lava flows from the Faeroe Islands. **Bulletin of the Geological Society of Denmark 31**: 1-10.

Jolly, W.T., 1974. Behavior of Cu, Zn and Ni during prehnite-pumpellyite rank metamorphism of the Keweenaean basalts, northern Michigan. **Economic Geology 69**: 1118-1125.

Juchem, P.L.,1999. **Mineralogia, geologia e gênese dos depósitos de ametista da região do alto Uruguai, Rio Grande do Sul.** São Paulo, 225 f. Tese de doutorado em Geociências. Instituto de Geociências, Universidade de São Paulo.

Juchem, P.L., Hofmeister, T., Brum, T.M., 1987. Ágata e ametista no Rio Grande do Sul. In: Simpósio Sul-Brasileiro de geologia, 3., Curitiba, **Anais...** Curitiba, SBG 2: 601-613.

Juchem, P.L., Hofmeister, T., Brum, T.M., 1990. Substâncias gemológicas no Rio Grande do Sul. Modos de ocorrência e caracterização gemológica. In: Congresso Brasileiro de Geologia, 36., 1990, Natal. **Anais…** Natal, SBG, 3, p. 1436-1449.

Keller, W.D., Hanson, R.F., 1968. Hydrothermal alteration of a rhyolite flow breccia near San Luis, Potosi, Mexico, to refractory kaolin. **Clays and Clay Minerals. 16**: 223-229.

Keller, W.D., Hanson, R.F., 1969. Hydrothermal argillation of volcanic pipes in limestone in México. **Clays and Clay Minerals 17**: 9-12.

Kosakevitch, A., 1979. “Chapeaux de fer”: problème de définition et de nomenclature pratique, **Bulletin BRGM**, n.2-3, p.141-149.

Lages, L.C., 2004. **A Formação Irati (Grupo Passa Dois, Permiano, Bacia do Paraná) no furo de sondagem FP-01-PR (Sapopema, PR).** Rio Claro. 117 f. Dissertação de Mestrado em Geociências. Instituto de Geociências e Ciências Exatas. Universidade Estadual Paulista.

Lange, F.W., Petri, S., 1967. The devonian of Paraná Basin. **Boletim Paranaense de Geociências 21/22**: 5-55.

Larson, P.B., Maher, K., Ramos, F.C., Chang, Z., Gaspar, M., Meinert, L.D., 2003. Copper isotope ratios in magmatic and hydrothermal ore-forming environments. **Chemical Geology 201**: 337-350

Le Huray, A.P., 1989. Native Copper in ODP site 642 Tholeiites. In: Eldholm, O., Thiede, J., Taylor, E. (eds.) **Proceedings of the Ocean Drilling Program**. Scientific Results 104: 411-417.

Leinz, V., 1949. Contribuição à geologia dos derrames basálticos do sul do Brasil. **Boletim da Faculdade de Filosofia, Ciências e Letras**. Universidade de São Paulo, 103 Geologia 5: 1-61.

Licht, O.A.B., Arioli, E.E., 2012. Statistic behavior of major and minor elements in basic, intermediate and acidic rocks of the Serra Geral Formation and Arapey Group, Paraná Large Igneous Province, South America. **Pesquisas em Geociências** 39: 247-267.

Livnat, A., Kelly, W.C., Essene, E.J., 1983. P-T-X conditions of sub-greenschist burial metamorphism and copper mineralization, Keweenaw Peninsula, northern Michigan. Geological Society of America. **Abstract Programs**, 15: 629.

Lopes, A.R.B.C., Vieira, S.F., Scheibe, L.F., 2008. Relatório de excursão: Geologia, Estratigrafia, Evolução Petrográfica e mineralização de gemas da Formação Serra Geral na Região Sul do Brasil. **Revista Discente Expressões Geográficas 4**: 98-118.

Lustrino, M., Melluso, L., Brotzu, P., Gomes, C.B., Morbidelli, L., Muzio, R., Ruperti, E., Tassinari, C.C.G., 2005. Petrogenesis of the early Cretaceous Valle Chico igneous complex (SE Uruguai): relationships with Paraná-Etendeka magmatism. **Lithos 82**: 407-434.

Maack, R., 1947. Breves notícias sobre a geologia dos estados do Paraná e Santa Catarina. **Arquivos de Biologia e Tecnologia 11**: 63-154.

Mantovani, M.S.M., Marques, L.S., De Souza, M.A., Civetta, L., Atalla, L., Innocenti, F., 1985. Trace element and strontium isotope constraints on the origin and evolution of Paraná continental flood basalts of Santa Catarina State (Southern Brazil). **Journal of Petrology 26**: 187-209.

Maréchal, C., Télouk, P., Albarède, F., 1999. Precise analysis of copper and zinc isotopic compositions by plasma-source mass spectrometry. **Chemical Geology 156**: 251-273

Medeiros, R.A., Thomaz-Filho, A., 1973. Facies e ambientes deposicionais da Formação Rio Bonito. In: Congresso Brasileiro de Geologia, 27., 1973, Aracaju. **Anais...** Aracaju, SBG 3: 3-11.

Melfi, A.J., Piccirillo, E.M., Nardy, A.J.R., 1988. Geological and magmatic aspects of the Paraná Basin an introduction. In: Piccirillo, E.M., Melfi, A.J. (eds.) **The Mesozoic Flood Volcanism of the Paraná Basin: Petrogenetic and Geophysical Aspects**. São Paulo, IAG-USP, p. 1-13.

Mello, K.S., 2000. **Estudo Petrológico da Região de Água Perdida no Vale do Rio Piquirí-PR: Reconhecimento das Mineralizações de Cobre e Produtos de Alteração em Rochas Básicas da Formação Serra Geral – Bacia do Paraná.** São Leopoldo. Dissertação de mestrado em Geociências, Universidade do Vale do Rio dos Sinos.

Mendonça Filho, J.G., 1999. **Aplicação de estudos de palinofácies e fácies orgânica em rochas do Paleozóico Superior da Bacia do Paraná, sul do Brasil. Porto Alegre.** 157 f. Tese de Doutorado em Geociências. Instituto de Geociências, Universidade Federal do Rio Grande do Sul.

Mendonça Filho, J.G., Sommer, M.G., Klepzig, M.C., Mendonça, J.O., Silva, T.F., Kern, M.L., Menezes, T.R., Jasper, A., Silva, M.C., Santos L.G.C., 2013. Permian carbonaceous rocks from the Bonito Coalfield, Santa Catarina, Brazil: Organic facies approaches. **International Journal of Coal Geology 111**: 23-36.

Meunier, A., Formoso, M.L.L., Patrier, P., Chies, J.O., 1988. Altération hydrotermale de roches volcaniques liées à la gênese dês améthystes – Bassin Du Paraná – sud du Brésil. **Geochimica Brasiliensis 2**:127-142.

Milani, E.J., Faccini, U.F., Scherer, C.M., Araújo, L.M., Cupertino, J.A., 1998. Sequence and stratigraphic hierarchy of the Paraná Basin (Ordocician to Cretaceous), Southern Brazil. **Boletim IG-USP 29**: 125-173.

Milani, E.J., Melo, J.H.G., Souza, P.A., Fernandes, L.A., França, A.B., 2007. Bacia do Paraná. **Boletim de Geociências Petrobrás 15**(2): 265-287.

Milani, E.J., Ramos, V.A., 1998. Orogenias Paleozóicas no domínio sul-ocidental do Gondwana e os ciclos de subsidência da Bacia do Paraná. **Revista Brasileira de Geociências 28**(4): 473-484.

Mincato, R.L., 2000. **Metalogenia dos elementos do grupo da platina com base na estratigrafia e geoquímica da Província Ígnea Continental do Paraná.** São Paulo. 172 f. Tese de Doutorado em Geociências. Instituto de Geociências, Universidade Estadual de Campinas.

Mineropar, Minerais do Paraná S/A., 2001a. **Atlas Geológico do Estado do Paraná**. Curitiba, CD-ROM.

Mineropar, Minerais do Paraná S/A., 2001b. **Avaliação do Potencial Mineral e Consultoria Técnica à Prefeitura Municipal de Bom Jesus do Sul.** Projeto Riquezas Minerais, Curitiba - PR.

Mineropar, Minerais do Paraná S/A., 2002. **Avaliação do potencial mineral e consultoria técnica à Prefeitura Municipal de Realeza.** Projeto Riquezas Minerais, Curitiba - PR.

Mineropar, Minerais do Paraná S/A., 2007. **Produção Mineral Paranaense e compensações financeiras decorrentes 1996-2005.** Programa de Economia Mineral, Curitiba - PR.

Mocellin, R.C., Ferreira, F.J.F., 2009. Conectividade e compartimentação dos sistemas aqüíferos Serra Geral e Guarani no sudoeste do estado do Paraná, Brasil. **Revista Brasileira de Geociências 39**(3): 567-579.

Morteani, G., Kostitsyn, Y., Preinfalk, C., Gilg, H.A., 2010. The Genesis of the amethyst geodes at Artigas (Uruguay) and the paleohydrology of the Guarani aquifer: structural, geochemical, oxygen, carbon, strontium isotope and fluid inclusion study. **International Journal of Earth Sciences 99**: 927-947.

Mühlmann, H., Schneider, RL., Tommasi, E., Medeiros, R.A., Daemon, R.F., Nogueira, A.A., 1974. Revisão Estratigráfica da Bacia do Paraná. PETROBRÁS. **Relatório DESUL, 444**, 186p.

Nakamura, K., Shibuya, A., Masuta, K., Murakami, T., Wildner, W., Dias A.A., Kirchner, C.A., Lessa, N., 2003. Mineral exploration in the Paraná Basin area, the Federal Republic of Brazil, phase I. Metal Mining Agency of Japan - MMAJ e Serviço Geológico do Brasil – CPRM. **Relatório interno**.

Nardy, A.J.R., Machado, F.B., Oliveira, M.A.F., 2008. As rochas vulcânicas mesozóicas ácidas da Bacia do Paraná: litoestratigrafia e considerações geoquímico-estratigráficas. **Revista Brasileira de Geociências 38**(1): 178-195.

O'Connor, J.M., Duncan, A.R., 1990. Evolution of the Walvis Ridge-Rio Grande Rise hot Spot System: Implication for African and South American Plate Motions Over Plumes. **Journal of Geophysical Research 95**(B11): 17475-17502.

Oeser, M., Weyer, S., Horn, I., Schuth, S., 2014. High-precision Fe and Mg isotope ratios of silicate reference glasses determined in situ by femtosecond LA-MC-ICP-MS and by solution nebulisation MC-ICP-MS. **Geostand Geoanal res 38**:311-328

Oliveira, E.P., 1912. O terreno Devoneano do sul do Brasil. **Annaes da Escola de Minas de Ouro Preto 14**: 31-41.

Oliveira, E.P., 1916. **Geologia do Estado do Paraná.** Boletim do Ministério de Agricultura, Indústria e Comércio. Rio de Janeiro, 5(1): 67-143.

Pacheco, J., 1927. **Relatório elucidativo do esboço geológico da região comprehendida entre o meridiano 4°, rio Itararé e os paralellos 23° 34' e 24° 38'.** Comissão Geográfica e Geológica do Estado de São Paulo, Exploração da região comprehendida pelas folhas topográficas Sorocaba. São Paulo, p. 9-12.

Paula e Silva, F., Kiang, C.H., Caetano-Chang, M.R., 2003. Perfis de referência do Grupo Bauru (K) no Estado de São Paulo. **Geociências 22**: 21-32.

Peate, D.W., 1997. The Parana-Etendeka Province. In: MAHONEY, JJ. COFFIN, MF (eds.) **Large Igneous Provinces.** American Geophysical Union. Geophysical Monograph Series 100, p. 217-246.

Peate, D.W. Hawkesworth, C.J., Mantovani, M.S.M., 1992. Chemical stratigraphy of the Paraná lavas (South America): Classification of magma types and their spatial distribution. **Bulletin of Volcanology 55**: 119-139.

Peate, D.W. Hawkesworth, C.J., Mantovani, M.S.M., Rogers, N.W., Turner, S.P., 1999. Petrogenesis and stratigraphy of the high-Ti/Y Urubuci magma type in the Paraná flood basalt province and implications for the nature of 'Dupal'-type mantle in the south Atlantic region. **Journal of Petrology 40**: 451-473.

Pertille, J., 2011. **Caracterização geofísica e geoquímica de gossans sobre jazidas de geodos de ágata e ametista na região de Quaraí, Rio Grande do Sul.** Porto Alegre. 67 f. Dissertação de mestrado em Geociências. Instituto de Geociências, Universidade Federal do Rio Grande do Sul.

Pertille, J., Hartmann, L.A., Duarte, S.K., Arena, K., Rosa M.L.C.C., Barboza, E.G., 2013. Gossan characterization in the Quarai and Los Catalanes amethyst geode districts (Brazil and Uruguay), Paraná volcanic province, using rock geochemistry and gamma-spectrometry. **Journal of Geochemical Exploration 124**: 127-139.

Pertille, J., Santos, T.C., Rosenstengel, L.M., Hartmann, L.A., 2008a. Gossans Silicosos sobre concentrações hidrotermais de geodos de ágata em Dacitos da província vulcânica Paraná em Padre Eterno, Rio Grande do Sul. In: Simpósio de Vulcanismo e ambientes associados, 4., Foz do Iguaçu, **Anais...** Foz do Iguaçu, SBG.

Pertille, J., Santos, T.C., Rosenstengel, L.M., Hartmann, L.A., 2008b. Descoberta de gossans em dacitos cretáceos de Padre Eterno, RS, mineralizados a geodos de ágata. In: Congresso Brasileiro de Geologia, 44., 2008, Curitiba. **Anais...** Curitiba, SBG, p.211.

Petri, S., 1948**. Contribuição ao estudo do Devoniano paranaense.** Boletim da Divisão de Geologia e Mineralogia, DNPM. Rio de Janeiro, 125p.

Petri, S., Fúlfaro, V.J., 1983**. Geologia do Brasil (Fanerozóico).** São Paulo, TA. Queiroz – EDUSP, 631p.

Piccirillo, E.M., Melfi, A.J., Comin-Chiaramonti, P., Bellieni, G., Ernesto, M., Marques, L.S., Nardy, A.J.R., Pacca, I.G., Roisenberg, A., Stolfa, D., 1988. Continental flood volcanism from the Paraná basin (Brazil). In: MACDOUGALL, JD. (Ed.) **Continental Flood Basalts**. Kluwer Academic Publisher, p. 195-238.

Pinto, V.M., 2010. **Condições de formação do cobre nativo, estratigrafia de derrames e geocronologia de basaltos da região de Vista Alegre, Província Magmática Paraná, Sul do Brasil.** Porto Alegre. 116 f. Tese de Doutorado em Geociências. Instituto de Geociências, Universidade Federal do Rio Grande do Sul.

Pinto, V.M., Hartmann, L.A., 2011. Flow-by-flow chemical stratigraphy and evolution of thirteen Serra Geral Group basalt flows from Vista Alegre, southernmost Brazil. **Anais da Academia Brasileira de Ciências 83**(2): 425-440.

Pinto, V.M., Hartmann, L.A., Santos, J.O.S., McNaughton, N.J., Wildner, W., 2011a. Zircon U-Pb geochronology from the Paraná bimodal volcanic province support a brief eruptive cycle at ~135Ma. **Chemical Geology 281**: 93-102.

Pinto, V.M., Hartmann, L.A., Wildner, W., 2011b. Epigenetic hydrothermal origin of native copper and supergene enrichment in the Vista Alegre district, Paraná basaltic province, southernmost Brazil. **International Geology Review 53**(10): 1163-1179.

Pinto, V.M., Hartmann, L.A., Wildner, W., Theye, T., Massonne H.J., 2006. Hydrothermal origin of native copper mineralization in Paraná Flood Basalts, Southern Brazil. Semana Acadêmica dos alunos de Pós-Graduação em Geociências. Universidade Federal do Rio Grande do Sul. Porto Alegre, **Resumos** p.117-120.

Pirajno, F., 2009. **Hydrothermal processes and mineral systems.** Geological survey of western Australia. Perth, Australia. Springer.1250p.

Portela Filho, C.V., Ferreira, F.J.F., Rosa, E.F., Buchmann, A.C., Rostirolla, S.P., 2002. Estudo preliminar da conexão entre os aqüíferos Serra Geral e Guarani com base em dados aeromagnéticos e hidroquímicos. In: Congresso Brasileiro de Águas Subterrâneas, 12., 2002, Florianópolis. **Anais...** Florianópolis, ABAS.

Proust, D., Fontaine, C., 2007. Amethyst-bearing lava flows in the Paraná Basin (Rio Grande do Sul): cooling, vesiculation and formation of geodic cavities. **Geological Magazine 144**: 53-65.

Renne, P.R., Ernesto, M., Pacca, I.G., Coe, R.S., Glen, J.M., Prévot, M., Perrin, M., 1992. The age of Paraná Flood Volcanism, rifting of Gondwanaland, and the Jurassic-Cretaceous Boundary. **Science 258**: 975-979.

Richards, M.A., Duncan, R.A., Courtillot, V.E., 1989. Flood basalts and hot-spot tracks: plume heads and tails. **Science 246**: 103-107.

Rocha-Campos, A.C., Cordani, U.G., Kawashita, K., Sonoki, H.M., Sonoki, I.K., 1988. Age of the Paraná Flood Volcanism. In: Piccirillo, E.M., Melfi A.J. (eds.) **The Mesozoic Flood Volcanism of the Paraná Basin: Petrogenetic and Geophysical Aspects**. São Paulo, IAG-USP, p. 25-45.

Rosenstengel, L.M., Hartmann, L.A., 2012. Geochemical stratigraphy of lavas and fault-block structures in the Ametista do Sul geode mining district, Paraná volcanic province, southern Brazil. **Ore Geology Review 48**: 332-348.

Rostirolla, S.P., Assine, M.L., Fernandes, L.A., Artur, P.C., 2000. Reativação de paleolineamentos durante a evolução da Bacia do Paraná – O exemplo do Domo de Quatiguá. **Revista Brasileira de Geociências 30**: 1-15.

Sanford, R.M., Lange, F.N., 1960. Basin study approach oil evalution of Parana miogeosyncline of South Brazil. **American Association of Petroleum Geologist Bulletim 44**(8): 1316-1370.

Santos Neto, E.V., 1993. **Caracterização geoquímica e paleoambiente deposicional da seqüência carbonato-pelítica superior do Membro Assistência, Formação Irati no Estado de São Paulo, Bacia do Paraná**. 203 f. Dissertação de Mestrado em Geociências, Instituto de Geociências, Universidade Federal do Rio de Janeiro.

Sayin, S.A., 2004. The role of Hydrogen – Metasomatism in the Hydrothermal Kaolin Occurrences, Gönen, Western Turkey. **Key Engineering Materials 264-268**: 1379-1382.

Sayin, S.A., 2007. Origin of Kaolin Deposits: Evidence from the Hisarcik (Emet-Kütahya) deposits, Western Turkey. **Turkish Journal of Earth Sciences 16**: 77-95.

Schneider, R.L., Mulhmann, H., Tommasi, E., Medeiros, R.A., Daemon, R.F., Nogueira, A.A., 1974. Revisão estratigráfica da Bacia do Paraná. In: Congresso Brasileiro de Geologia, 28., 1974, Porto Alegre. **Anais...** Porto Alegre, SBG, 1, p. 41-65.

Scopel, R.M., 1990. **Alteração hidrotermal das rochas basálticas associadas as ametistas.** Porto Alegre, 218 f. Dissertação de mestrado em Geociências. Instituto de Geociências, Universidade Federal do Rio Grande do Sul.

Scopel, R.M. Gomes, M.E.B. Formoso, M.L.L. Proust, D., 1998. Derrames portadores de ametistas na região de Frederico Westphalen-Iraí-Planalto-Ametista do Sul, RS-Brasil. In: Congreso Uruguayo de Geologia, 2.,1998, Punta Del Este, **Actas...** Punta Del Leste, DINAMIGE y Sociedad Uruguaya de Geologia, p.243-252.

Shields, W.R., Goldich, S.S., Garner, E.L., Murphy, T.J., 1965. Natural Variations in the Abundance Ratio and the Atomic Weight of Copper. **Journal of Geophysical Research 70**: 479-491

Sinelli, O., Davino, A., Souza A., Gonçalves, N.M.M., Teixeira, J., 1980. Hidrogeologia da região de Ribeirão Preto (SP). In: Congresso Brasileiro de Águas Subterrâneas, 1., 1980, Recife. **Anais...** Recife, ABAS, p. 319-335.

Soares, A.P., Soares, P.C., Holz, M., 2008. Heterogeneidades hidroestratigráficas no Sistema Aqüífero Guarani. **Revista Brasileira de Geociências 38**: 598-617.

Soares, P.C., 1973. **O Mesozóico gondwânico no Estado de São Paulo.** Rio Claro. 152 f. Tese de doutorado. Departamento de Geologia e Mineralogia da Faculdade de Filosofia Ciências e Letras da Universidade Estadual Paulista.

Soares, P.C., 1975. Divisão estratigráfica do Mesozóico no Estado de São Paulo. **Revista Brasileira de Geociências 5**: 229-251

Soares, P.C., Landim, P.M.B., Fúlfaro, V.J., Sobreiro Neto, A.F., 1980. Ensaio de caracterização estratigráfica do Cretáceo no Estado de São Paulo: Grupo Bauru. **Revista Brasileira de Geociências 10**(3): 177-185.

Souza, A.A., 2004. **Caracterização da Bacia do Rio Iguaçu, a jusante do município de Reserva do Iguaçu, como área de descarga do Aqüífero Guarani.** Curitiba. 92 f. Dissertação de mestrado em Ciências da Terra. Universidade Federal do Paraná.

Strieder, A.J., Heeman, R., 2006. Structural constraints on Paraná basalt volcanism and their implications on agate geode mineralization (Salto do Jacuí, Rio Grande do Sul, Brazil). **Pesquisas em Geociências 33**: 37-50.

Strugale, M., Rostirolla, S.P., Mancini, F., Portela Filho C.V., 2004. Compartimentação estrutural das Formações Pirambóia e Botucatu na região de São Jerônimo da Serra, Estado do Paraná. **Revista Brasileira de Geociências 34**: 303-316.

Szubert, E.C., Grazia, C.A., Shintaku, I., 1979. **Projeto Cobre em Itapiranga**. Relatório CPRM SUREG/PA, Porto Alegre, 246 p.

Tazaki, K., Fyfe, W.S., Tazaki, K., Bischoff, J., Rocha, B.R., 1988. Ocurrence of Copper Films in Basalt from the Serra Geral Formation, Paraná Basin, Brazil. **Revista Brasileira de Geociências, 18**(3): 332-337.

Thomaz-Filho, A., Cordani, U.G., Kawashita, K., 1976. Aplicação do método Rb-Sr na datação de rochas sedimentares argilosas da Bacia do Paraná. In: Congresso Brasileiro de Geologia, 29., 1976, Ouro Preto. **Anais...** Ouro Preto, SBG, 4: 289-302.

Wang, C.Y., Zhou, M., Qi, L., Hou, S., Gao, H., Zhang, Z., Malpas, J., 2006. The Zhaotong Native Copper Deposit Associated with the Permian Emeishan Flood Basalts, Yunnan, Southwest China. **International Geology Review 48**: 742-753.

Waichel, B.L., 2006. **Estruturação de derrames e interações lava-sedimento na porção central da Província Basáltica Continental do Paraná.** Porto Alegre. 108 f. Tese de Doutorado em Geociências. Instituto de Geociências, Universidade Federal do Rio Grande do Sul.

Waichel, B.L., Lima, E.F., Sommer, C.A., 2006. Estruturação e tipos de derrames nos basaltos da Formação Serra Geral na porção Oeste do Paraná. In: Congresso Brasileiro de Geologia, 43., 2006, Aracaju. **Anais...** Aracaju, SBG.

White, I.C., 1908. **Relatório final da Comissão de estudos das Minas de Carvão de Pedra do Brasil.** Ed. Ac-similar, DNPM, Rio de Janeiro. Parte I p.1-300; Parte II p. 201-617.

White, W.S., 1968. The native-copper deposits of northern Michigan. In: RIDGE, JD (ed.) **Ore deposits of the United States.** The American Institute of Mining, Metallurgical and Petroleum Engineers, New York, p. 303-325.

White, R.S. Mckenzie, D.P., 1989. Magmatism at rift zones: the generation of volcanic continental margins and flood basalts. **Journal of Geophysical Research. 94**: 7685-7730.

White, R.S. Mckenzie, D.P., 1995. Mantle plumes and flood basalts. **Journal of Geophysical Research 100**, 17543-17585.

Wildner, W., Santos, J.O.S., Hartmann, L.A., Mcnaughton, N.J., 2006. Climax final do vulcanismo Serra Geral em 135 Ma: primeiras idades U-Pb em Zircão. In: Congresso Brasileiro de Geologia, 43., 2006, Aracaju. **Anais...** Aracaju, SBG, p.126-131.

Wildner, W., Hartmann, L.A., Lopes, L.C., 2007. Serra Geral Magmatism in the Paraná Basin – A new stratigraphic proposal, chemical stratigraphy and geological structures. In: Workshop on problems in Western Gondwana Geology, 1., Gramado. **Extended Abstracts**, p.189-197.

Wu, F.T., Caetano-Chang, M.R., 1992. Estudo mineralógico dos arenitos das Formações Pirambóia e Botucatu no centro-leste do Estado de São Paulo. **Revista IG 13**(1): 58-68.

Zalán, P.V., Wolff, S., Conceição, J.C.J., Astolfi, M.A.M., Vieira, I.S., Appi, V.T., Zanotto, O.A., 1987. Tectônica e Sedimentação da Bacia do Paraná. In: Simpósio Sul-Brasileiro de Geologia, 3., Curitiba. **Atas…** Curitiba. SBG, 1: 441-477.

Zhu, X.K., O'Nions, R.K., Guo, Y., Belshaw, N.S., Rickard, D., 2000. Determination of natural Cu-isotope variation by plasma-source mass spectrometry: implications for use as geochemical tracers. **Chemical Geology 163**: 139-149

Artigo 1

ORIGIN OF NATIVE COPPER IN THE PARANÁ VOLCANIC PROVINCE, BRAZIL, INTEGRATING CU STABLE ISOTOPES IN A MULTIANALYTICAL APPROACH

Artigo submetido à Mineralium Deposita

Assunto	MIDE: Submission Confirmation for *Origin of native copper in the Paraná volcanic province, Brazil, integrating Cu stable isotopes in a multianalytical approach*
Remetente	MIDE Editorial Office
Para	Sérgio Benjamin Baggio
Responder para	MIDE Editorial Office
Data	02/04/2015 08:31

Dear Mr. Baggio,

Your submission entitled "Origin of native copper in the Paraná volcanic province, Brazil, integrating Cu stable isotopes in a multianalytical approach" has been received by journal Mineralium Deposita

You will be able to check on the progress of your paper by logging on to Editorial Manager as an author. The URL is http://mide.edmgr.com/.

Your manuscript will be given a reference number once an Editor has been assigned.

Thank you for submitting your work to this journal.

Kind regards,

Editorial Office
Mineralium Deposita

Now that your article will undergo the editorial and peer review process, it is the right time to think about publishing your article as open access. With open access your article will become freely available to anyone worldwide and you will easily comply with open access mandates. Springer's open access offering for this journal is called Open Choice (find more information on www.springer.com/openchoice). Once your article is accepted, you will be offered the option to publish through open access. So you might wa nt to talk to your institution and funder now to see how payment could be organized; for an overview of available open access funding please go to www.springer.com/oafunding.
Although for now you don't have to do anything, we would like to let you know about your upcoming options.

Title: **Origin of native copper in the Paraná volcanic province, Brazil, integrating Cu stable isotopes in a multianalytical approach**

Authors: **Sérgio Benjamin Baggio, Léo Afraneo Hartmann, Marina Lazarov, Hans-Joachim Massonne, Joachim Opitz, Thomas Theye, Tillmann Viefhaus**

Abstract

The origin of native copper mineralization in the Paraná volcanic province, the second largest intraplate province in the continents, still has differing opinions. The fundamental question is whether the native copper origin was related to magmatic, late-magmatic or hydrothermal events. The copper content average in the host basalts is around 207 ppm and the native copper occurs as dendrites in the cooling joints, in the fractures and also infilling cavities of amygdaloidal crust. Mineral phases such as cuprite, tenorite, chrysocolla, malachite and azurite occur in breccias at the top of the flows. Gold and silver contents were observed associated with this mineralization. A combination of chemical analyses, X-ray diffraction, raman spectrometry, electron microprobe analyses, LA-ICPMS and copper isotope analyses, were used to evaluate the origin of the copper in the province. Magnetite of the host basalt display Cu contents close to 1 wt.%. The Cretaceous hydrothermal alteration on magnetite and also clinopyroxene released the copper from its crystalline structure and generated the hydrothermal copper mineralization. The isotopic variation ($\delta^{65}Cu$) in the native copper mineralization in the Paraná volcanic province ranges from -0.59 ‰ in the southeast portion (Rio Grande do Sul state) to 1.89 ‰ in the central portion of province (Paraná state). This study supports a hydrothermal origin and supergene enrichment for native copper mineralization in the Paraná volcanic province.

Keywords

Paraná volcanic province, native copper, gold, silver, copper isotopes, hydrothermal mineralization

Introduction

Native copper constitutes significant deposits in several basaltic intraplate provinces (e.g., Emeishan, China; Michigan, North America). The abundant occurrences registered in the Paraná volcanic province of South America require the investigation of geological processes involved in the origin of the metal concentrations. The Paraná province is one of the largest in the continents (e.g., Hartmann et al. 2010) and may contain significant deposits of copper and possibly gold and silver.

Previous studies suggest conflicting origins for the native copper, including magmatic (Mello 2000) or late-magmatic (Szubert et al. 1979) deposition and hydrothermal remobilization (Tazaki et al. 1988; Pinto et al. 2011b; Arena et al. 2014).

In this study X-ray diffraction (XRD) and Raman spectrometry was used to identify the copper phase minerals. Mineral major elements composition was obtained with the electron microprobe, while mineral trace element composition was obtained by laser ablation inductively coupled plasma mass spectrometry (LA-ICP-MS). Particular emphasis is placed on copper isotopes, because this technique is currently essential to distinguish high-temperature from low-temperature deposits (e.g., Larson et al. 2003; Seo et al. 2007; Mathur et al. 2009, 2012). The integrated approach supports a hydrothermal origin for the copper mineralization.

Geology

The Paraná volcanic province in the southern portion of South America (Fig. 1) is one of the largest igneous provinces of the world (Hartmann et al. 2010) covering 917,000 km^2 of area (Frank et al. 2009) including portions in Uruguay, Argentina, Paraguay and mainly in Brazil. The volume of lava is around 450,000 km^3 at the surface and 112,000 km^3 in the subsurface (as sill and dikes). The Etendeka in Namibia, African continent, was connected to the Paraná volcanic province (Bellieni et al. 1984) before the opening of the South Atlantic Ocean. The tholeiitic lava flows in the Lower Cretaceous generated especially basalt (>90 vol.%). However, basaltic andesite, dacite, rhyodacite and andesite also occur. Rhyolites are present in the southern portion at the top of the volcanic pile (Melfi et al. 1988) along the Brazilian continental margin and in Etendeka (Peate 1997). In Brazil, these rocks belong to the Serra Geral Group (Wildner et al. 2009; Hartmann and Baggio 2014). There is a convergence that the average U-Pb age is around 130-135 Ma (zircon SHRIMP, Pinto et al. 2011a; baddelyite SIMS, Janasi et al. 2011). A recent study (zircon SHRIMP, Brückmann et al. 2014) showed that younger volcanic pulses at 119 Ma occur in the north portion of the province. The thickness of the volcanic pile is associated with the subsidence of the Paraná Basin. In Cuiabá Paulista (Fig.1) the volcanic pile reaches the highest known thickness (1723 m) and becomes thinner to the south, reaching 50 m (Almeida 1986) along the Brazil-Argentina border. According to Peate et al. (1999), the thickness of single flows ranges from 5 to 80 m and the average thickness of individual flows is about 20 m.

The geochemical subdivision of the Paraná volcanic province based on TiO_2 content was proposed by Bellieni et al. (1984) and Mantovani et al. (1985). In the southern portion, the low-Ti magmas (TiO_2 <2%) predominates, while the northern part the high-Ti magmas (TiO_2 >2%) are dominant. These two groups was reassessed by Peate et al. (1992) who proposed a new classification based on major and trace elements

and ratio of elements. The low-Ti group was divided into Gramado, Esmeralda and Ribeira magma types and the high-Ti group into Urubici, Pitanga and Paranapanema magma types. The study by Nakamura et al. (2003) added an intermediate-Ti type to this classification, mostly the Paranapanema and Ribeira magma types. The Gramado and Esmeralda remained in the low-Ti type, the Pitanga and Urubici in the high-Ti type.

The Paranapanema and Ribeira types display low contents of U and Th showing restricted crustal contamination and larger amount of partial mantle melting when compared to Pitanga magma type (Nakamura et al. 2003). In the Gramado and Esmeralda magma-types, the degree of partial melting and crustal contamination are higher because these magmas were generated in shallower portions with higher Th, U and Sr isotopic ratios, mainly in the Gramado magma type. The Esmeralda was considered the most primitive (Nakamura et al. 2003) because of low contents of light rare elements and relatively high Nd isotopic ratio.

The intermediate-Ti magma-type commonly displays higher contents of copper when compared with high-Ti and Low-Ti. Arena et al. (2014) indicated that the copper average in the Paraná volcanic province is around 177 ppm. In the intermediate-Ti host basalts, the copper content is commonly higher than this average. The largest number of copper occurrences in the volcanic province is in the Paranapanema magma-type. In addition some occurrences with native copper, cuprite, tenorite, chrysocolla, malachite and azurite have been described in hydrothermal breccias at the top of the volcanic flows and also in the Pitanga magma type as well as Gramado magma-type.

A pioneering study of native copper in the Paraná province by Szubert et al. (1979) evaluated the genesis of the ore. The study proposed some of the copper occurrences as late-magmatic (dendritic shape in cooling joints), and others as supergene (infilling the amygdales of amygdaloidal crust). Tazaki et al. (1988)

alternatively suggested that the Cu origin was associated with hydrotermal alteration at low temperature and can be derived from small amounts of copper in the titano-magnetites. The presence of copper in the Vista Alegre - Frederico Westphalen region encouraged Costa (1982) to use geophysical prospecting techniques for the characterization of the occurrences. The study obtained negative results for the correlation of high induced polarization (IP) with magnetite content of the rocks. However, high IP results requested further research in at least three flows of the region. Other studies were performed in the Paraná volcanic province with the focus on the native copper mineralization (e.g., Mello 2000). Considering the H1, H2 and H3 (Hartmann et al. 2010, 2012a, 2012b) hydrothermal events that acted on the volcanic rocks Pinto et al. (2011b) proposed a hydrothermal origin of copper with supergene enrichment in the Vista Alegre region and suggested that the hydrothermal alteration of opaque minerals and pyroxenes may have released copper to form the mineralization.

Sampling and Methods

For each occurrence of native copper, one sample from the host basalt and one from the ore were collected over the geographic distribution of the Paraná volcanic province (Table 1, Fig. 1). In Rio Grande do Sul state, native copper in dendritic shapes is present on the surface of cooling joints in quarry 86 in Dom Pedro de Alcântara, in the Brasília-Guaíba quarry, in Bom Princípio and in the David Basso quarry in Taquaruçu do Sul (Fig. 2A). In Santo Augusto region, massive balls of native copper (Fig. 2B) occur in hydrothermal breccias associated with cuprite, tenorite, chrysocolla, malachite and azurite, quite similar as the copper mineralization in Vista Alegre district (Pinto et al. 2011b).

125 In Santa Catarina state, the host basalt and the dendritic crystals of native copper
126 were collected in the locality of São Ludgero on a fracture surface (drill core at 92 m
127 depth). In the Rebelatto quarry (Fig. 2C) in Palma Sola town, a large amount of native
128 copper occur in blades and dendrites along the cooling joints of basalt (Fig. 2D). The
129 native copper occurrence in the nearby locality of Dionísio Cerqueira was also sampled.
130 In the state of Paraná, several occurrences of native copper are known. In the town of
131 Francisco Beltrão, dendritic native copper occurs in the cooling joints in Petrocon and
132 Dalba quarries. In the Quati quarry (Fig. 2E), massive native copper in association with
133 zeolites and calcite fills the central part of cavities (Fig. 2F) and also occurs as dendrites
134 in the basal portion of cavities filled later by quartz crystals (Fig. 2G). However, the
135 main mineralization in Paraná state occurs in the town of Realeza, in the locality of
136 Linha Capanema (Fig. 2H). Native copper is there associated with hydrothermal
137 breccias which additionally contain cuprite, chrysocolla and malachite (Fig. 2I). The
138 mass of chrysocolla and malachite shows a vibrant blue color and appears cementing
139 the breccias. In the northern portion of the Paraná volcanic province, in the Mato Grosso
140 do Sul state, the occurrence of copper was observed on a fracture surface of a drill core
141 at 10 m depth in the town of Amambai, locality of Jaguaretê, and also as very fine
142 dentrites in the Santo Onofre quarry, locality of Terenos (Fig. 2J) near the city of
143 Campo Grande.

144 The host basalt samples were prepared for chemical and X-ray diffraction
145 analyses. Standard polished thin sections were used for a petrographic study and for
146 petrographic analyses. Thin section with 40-50 μm thickness were prepared for LA-
147 ICP-MS analyses. Selected crystals of native copper and copper minerals were
148 embedded in epoxy mounts with 2.5 cm diameter for Raman spectroscopy, electron
149 microprobe microanalyses, BSE imaging and Cu stable isotope analyses. The analytical

work has been performed at Universidade Federal do Rio Grande do Sul, Brazil (petrography and XRD), Institut für Mineralogie und Kristallchemie of Universität Stuttgart, Germany (XRD, Raman spectrometry, Laser Ablation mass spectrometry and Electron Microprobe), Institut für Mineralogie of the Universität Hannover, Germany (Cu stable isotope compositions), and ACME Analytical Laboratories, Vancouver, Canada (major and trace elements of bulk samples).

For the analyses of major elements of bulk rock samples (n=13), the analytical method comprises melting of 0.1 g sample in lithium metaborate/ tetraborate and subsequent digestion in nitric acid. Loss on ignition (LOI) is obtained from the weight difference after heating at 1000 °C. Trace elements and rare earths were analyzed by ICP-MS following the same procedure of the major elements with the addition of 0.5 g sample digested in aqua regia. The data were integrated in Excel sheets and interpreted with support of Geochemical Data Toolkit freeware (GCDKit; http://www.gcdkit.org).

The petrography of the host basalts was studied using a Zeiss Axioplan optical microscope and the digital ProgRes Jenoptik C10 camera. Some copper minerals were first identified using an X-ray diffractometer Bruker AXS D8 Advance. To complement the copper minerals identification, an Olympus BX51 microscope coupled with a Raman spectrometer (Horiba Xplora) was used. The wavelength was 532 nm or 638 nm with a power of 0.25 to 25 mW. The exposure time for each scan was 10 s. The number of scans was between 5 and 100 depending on the laser power and the composition of the sample, acquired in the spectral range of 70 and 4000 cm^{-1}. The electron microprobe (EMP Cameca SX100) was used for chemical microanalyses with spot diameter of 1 μm with 15 kV and 5 to 15 nA and also for generation of back-scattered electron images of native copper crystals.

The determination of element concentrations in minerals of the host basalts was carried out by laser ablation combined with mass spectrometric detection with an AGILENT 7700 ICPMS and a CETAC LSX-213 laser system. The diameter of the ablated spots was 50 µm. The laser energy was set to 5% of the maximum (= 4 mJ), with a frequency of the laser shots of 20 Hz. A mixed helium/argon gas flow with 300 ml/min and 800 ml/min, respectively, served as carrier of the ablated material. A shutter delay of 10 s was selected to measure the gas blank ion intensities. The standards used were DLH7 and DLH20 from P & H (Developments Ltd.) and a NIST612 glass. The following isotopes were monitored: ^{24}Mg, ^{25}Mg, ^{27}Al, ^{29}Si, ^{39}K, ^{55}Mn, ^{56}Fe, ^{57}Fe, ^{60}Ni, ^{63}Cu, ^{65}Cu, ^{66}Zn, ^{68}Zn, ^{89}Y, ^{90}Zr, ^{91}Zr, ^{93}Nb, ^{95}Mo, ^{107}Ag, ^{109}Ag and ^{197}Au. All elemental concentrations, were calculated relative to an internal standard element (Si) assuming a natural isotopic distribution. The absolute concentration of the internal standard element was previously measured by electron microprobe. If more than one isotope of the studied element was measured, the resulting elemental concentration values were averaged. The software used for calibration and data evaluation was developed by Dr. Joachim Opitz of the Institut für Mineralogie und Kristallchemie of the Universität Stuttgart.

The copper isotope analyses were performed on the Multicollector ICP-MS (Finnigan Neptune) connected to the deep (194 nm) UV femtosecond laser ablation system (Spectra Physics Solstice, USA) at Leibniz Universität Hannover, Germany. Samples and standard were analyzed in line mode applying 35µm spot size. Laser energy of 16 A and laser pulse frequency of 2-4.5 Hz was used. Instrumental mass bias discrimination was corrected using the ^{62}Ni/^{60}Ni ratio of the Ni NIST SRM-986 (National Institute of Standards and Technology, USA) standard solution aspirated in to the plasma and monitored simultaneously with the laser ablation signal of Cu isotopes.

199 Detail instrumental and measurement settings were described by Oeser et al. (2014) and
200 Lazarov and Horn (2015, submitted).

201 The solid Cu NIST SRM976 metal standard was used for the standard-sample-
202 standard bracketing for all samples. Usually three sample measurements were run in
203 between two standards. Obtained results were reported as $\delta^{65}Cu$ in per mill (‰) as
204 follows: $\delta^{65}Cu = [((^{65}Cu/^{63}Cu)_{sample} /(^{65}Cu/^{63}Cu)_{NIST\ SRM976})-1]*1000$. Internal error for
205 standard and samples were better than 0.05‰ (2 SD) and overall precision of the
206 standard measurements was, as reported by Lazarov and Horn 2015 (submitted) for the
207 other Cu metal, better than 0.08‰ (2 SD).

208

209 **Results**

210 Petrographic description, X-Ray diffraction and Raman spectrometry

211 The basalt host rock samples of the Paraná volcanic province are holocrystalline
212 and microporphyritic with plagioclase, clinopyroxene and opaque minerals present as
213 phenocryst phases (0.6 to 1.5 mm). The intergranular texture (Fig. 3A) is usually
214 formed by small crystals of plagioclase, clinopyroxene and opaque minerals. In some
215 cases the texture is glomeroporphyritic with phenocrysts of plagioclase and opaque
216 minerals. The average mineralogical composition of the host rocks of native copper in
217 the Paraná volcanic province has 45% plagioclase, 30% clinopyroxene, 12% opaque
218 minerals, 8% microcrystalline matrix, 5% of secondary clay minerals and traces of
219 apatite.

220 The crystals of plagioclase are subhedral to euhedral platelets (Fig. 3B) with
221 random distribution and sharply defined rims. Sometimes, they display compositional
222 zoning. No alteration of plagioclase has been detected. Magnetite and Ilmenite are
223 euhedral to anhedral and frequently form poikilitic aggregates. Ilmenite usually occurs

as exsolution in magnetite hosts. Sometimes the opaque minerals show hydrothermal alteration with corroded rims (Fig. 3C). In particular, the formation of a reddish halo containing hematite can be observed (Fig. 3D). The clinopyroxene (Fig. 3E) is commonly subhedral to anhedral and usually fractured. The rims are well-defined and straight mainly near the plagioclase without any signs of corrosion. Only a few crystals show alteration.

The microcrystalline matrix (Fig. 3F) occurring in the interstitial space between phenocrysts contains tiny crystals of clinopyroxene (0.05 – 0.1 mm), K-feldspar (≤0.1 mm) and quartz (≤0.1 mm). Acicular apatite is present as accessory mineral.

The clay minerals present in the host basalts comprise smectite (and celadonite in some cases) and they are the result of alteration of primary minerals. The occurrence of native copper in the cavities or in the cooling joints of the host basalt is always associated with the presence of alteration minerals (clay minerals, zeolites and calcite). Further copper minerals were identified by XRD and Raman spectroscopy. Three samples from the Santo Augusto region (JS3a, JS3b and JS3c) in Rio Grande do Sul state were selected and prepared. The XRD analyses (Fig. 4) of unoriented powder samples allows the identification of the minerals such as cuprite and malachite. The XRD of powdered samples also show amorphous (non-crystalline) regions and were targeted for analyses by Raman spectroscopy.

For the analyses by Raman spectroscopy, in addition to the XRD samples, five more epoxy mounts (JS2, JS3, JS4, R2P and VA1) with native copper from Santo Augusto, Cascavel and Vista Alegre region were analyzed. Six copper minerals are identified: native copper, cuprite, tenorite, chrysocolla and malachite. Azurite peaks were identified in association with chrysocolla peaks. The native copper (Fig. 5A, B) shows no Raman signal but has a significant peak at frequencies between 2000 and

3100 cm^{-1}. Cuprite (Fig. 5C, D) occurs always associated directly to the native copper, representing the most frequent copper mineral association in the Paraná province and displays unambiguous Raman spectra. Tenorite (Fig. 5E, F) is not as common as cuprite but is always associated with it. Chrysocolla (Fig. 5G, H) and malachite (Fig. 5I, J) can easily be detected from the Raman spectra, in the same way as quartz, magnetite, hematite and zeolite (heulandite). Silver was also detected in the Raman spectra (frequencies at 611.5, 523.9, 207.7, 140.1, 89.1 and 52.5 cm^{-1}) and occurs in association with the native copper and copper phases in several places in the province (Fig. 6).

Chemical analyses

The volcanic rocks of the study area were chemically analyzed and the data are presented in Table 2. Analysis VA1 corresponds to sample VVA-12 of Pinto and Hartmann (2011), analysis FM79 to sample LC3B of Arena et al. (2014), and sample W247 to sample VIF11 of Pinto and Hartmann (2011).

According to the classification of Le Bas et al. (1986), the rocks are basalt and basaltic andesite (Fig. 7A) with SiO_2 contents between 49.54-50.86 wt.% for the basalts and 53 wt.% for the basaltic andesites. The content of $Na_2O + K_2O$ is between 2.81-4.5 wt.% for the basalts and 4.76 wt.% for basaltic andesite. The intermediate-Ti Paranapanema magma-type is predominant among the host basalts of native copper mineralization, but the copper also occurs in the low-Ti Gramado magma-type and high-Ti Pitanga magma-type (Fig. 7B). The chemical analyses show the lowest contents of copper in the southwest portion of province between 83 ppm (Dom Pedro de Alcântara, Rio Grande do Sul) and 97.7 ppm (Bom Princípio, Rio Grande do Sul), while the highest contents are between 292.2 ppm (Dionísio Cerqueira, Santa Catarina) and 324.4 ppm (Frederico Westphalen, Rio Grande do Sul). The average content of the

analyzed samples (n=16) is 207 ppm, slightly above the Cu average content established by Arena et al. (2014) for the Paraná volcanic province. In the sample DC6, the contents of copper reach 1114.7 ppm, and this value was considered as a nugget effect, because the sample includes fine cooling joints filled by native copper.

In the hydrothermal environments such as the Paraná volcanic province, LOI is one of the important geochemical characteristics because it is a proxy of the hydrothermal alteration (Hartmann et al. 2010; Duarte et al. 2009, 2011; Rosenstengel and Hartmann 2012) and the LOI *versus* copper contents showed great regional variation. Copper shows no correlation with oxides such as SiO_2, Al_2O, MgO, CaO, Na_2O, K_2O, TiO_2, P_2O_5 or Cr_2O_3, whereas MnO and Fe_2O_3 display positive correlation with copper (Fig. 7C). The correlation of copper with the trace elements is not significant except with rare earth elements that show a positive correlation trend, in particular with the heavy rare earth elements (Fig. 7D). This correlation indicates that the host basalts flows have mantle origin, without significant crustal contamination.

Electron probe microanalyses and LA-ICP-MS data

The electron microprobe analyses (n= 305) were performed in native copper crystals (Fig. 8) mainly with the purpose to evaluate the chemistry of copper. Additionally they were very useful for the choice of fields for analyses of minerals by LA-ICP-MS in the host basalts and also for the selection and imaging of native copper crystals for the isotopic analyses.

Representative microanalyses of native copper crystals (Table 3) from the Paraná volcanic province show that the average copper content in the native copper crystals is 99.7 wt. %. The elements Sn, Ca, Co, Ni and U show lower values with virtually no Al. The sulfur displays an average content of 0.026 wt. % (n= 270, sd=

299 0.012) and the Si was detected only in a few crystals with maximum of 0.404 wt. %.
300 The evaluation of the silver content shows large oscillations both in microanalyses of
301 the same sample and along the Paraná volcanic province. The average of silver contents
302 is 0.027 wt.%. In these native copper crystals with silver inclusions, the microanalyses
303 show the same wide variation in the contents of silver. On the other hand it was
304 observed that some analyzes are far above the average and have values up to 0.283 wt.
305 %. Similar to the behavior of silver, gold varies significantly between the smallest and
306 largest values. Furthermore, gold crystals were not observed in association with native
307 copper in the province.

308 The LA-ICP-MS analyses were performed mainly in order to evaluate the
309 content of copper within the major minerals of the host basalts. The contents of Ag and
310 Au were also evaluated to define possible relationship with the copper content. The
311 analyzed minerals are magnetite (Fig. 9A), ilmenite (Fig. 9B), clinopyroxene (Fig. 9C),
312 plagioclase and smectite (Fig. 9D). The analyzed minerals were identified by their
313 sample number followed by the number given to each mineral analysis (e.g. BP1-
314 MG7A).

315 The analyses obtained in magnetite (Table 4) show that the average content of
316 copper (n= 30 spots) is around 1085 ppm with a highly variable distribution from
317 negligible values in sample BP1 (12 ppm) to very high contents in sample PQ16 (>9000
318 ppm). Four LA spots measurements in ilmenite from sample PQ16 (Table 4) shows that
319 the distribution of copper is similar to that observed in magnetite. However, the highest
320 copper content in ilmenite is 3827 ppm, nearly three times smaller than the higher
321 copper content observed in the magnetite of the same sample. In the clinopyroxene
322 (Table 5), the copper content is smaller than that observed in the magnetite and ilmenite
323 with great variation. The average is 97 ppm (n= 28 spots) and ranges from very low

values of 0.72 ppm to maximum values of 431 ppm. Regarding the copper content of plagioclase, the observed values have the same characteristic of variation, although the range of copper content is smaller and comprises from 0.02 ppm to a maximum of 91.90 ppm. Despite the wide variation in the copper contents of the minerals, magnetite contains the largest contents of copper followed by ilmenite and clinopyroxene. The highest contents of copper obtained in magnetite are up to 3 times higher than those observed in ilmenite and up to 22 times those of clinopyroxene. The minerals that fill the interstices (matrix) of the host basalts are usually clinopyroxene, K-feldspar, apatite and in a few cases quartz with sizes from 0.05 to 0.1 mm. The LA spot in this mixed and interstitial material (sample FS86) showed 16.02 ppm copper.

Overall in the fields for LA analyses was also observed that the crystals of magnetite, ilmenite and clinopyroxene display different levels of hydrothermal alteration. Some crystals of magnetite and clinopyroxene exhibit lightly corroded rims and others crystals of magnetite-ilmenite display formation of hematite and in the extreme cases profound alteration and formation of smectites (Fig. 10 A, B and C). The presence of smectites was observed in all samples of host rock in the Paraná volcanic province.

The LA-ICP-MS analyzes in smectites (Table 6) showed that the copper content is extremely varied similar to magnetite, ilmenite and clinopyroxene. However, the higher contents of copper are observed in the smectites of host basalt with higher mineral alteration. These copper contents outweigh all other values observed in magnetite, ilmenite and clinopyroxene. From this alteration, the copper metal is released from magnetite, ilmenite and clinopyroxene and is concentrated initially in the smectites (Fig. 10 D, E and F)

348 The LA-ICP-MS analyses also indicate the contents of silver and gold in the
349 minerals. The contents of silver range from 0.04 to 1.78 ppm in magnetite, and reach
350 2.75 ppm in a crystal of ilmenite. In clinopyroxene, these values vary from 0.01 to 1.03
351 ppm and in the smectite these contents range from 0.01 to 1.84 ppm. The contents of
352 gold range from 0.01 to 0.12 ppm in magnetite, 0.01 to 0.07 ppm in ilmenite, 0.01 to
353 0.12 ppm in clinopyroxene and 0.01 to 0.14 ppm in smectites.
354
355 Cu isotope composition of Cu minerals
356 Recent advances in mass spectrometry techniques have enabled an improvement
357 in the accuracy of the ratios of the isotopes of copper and their use in studies of the
358 origin of copper. Among the methods for copper isotopic analysis, the in situ UV-
359 femtosecond laser ablation has been considered one of the most accurate (Lazarov and
360 Horn 2015, submitted). Like for studies of iron isotopes (Horn et al. 2006; Horn and
361 Von Blanckenburg, 2007), the in situ measurements of Cu isotopes (Lazarov and Horn
362 2015, submitted) by UV- femtosecond laser MC-ICP-MS showed no isotopic
363 fractionation even when the analyses were conducted without matrix match or when
364 using different protocols (spots, lines and raster) between samples and calibration
365 standards.
366 This is the first study of copper isotopes in the Paraná volcanic province and
367 allows new insights on the copper origin. Eleven samples with Cu minerals (native Cu
368 and Cu bearing samples) were selected in the states of Rio Grande do Sul (samples
369 FS86, BP1, JS3, JS4, PD1 and W247), Santa Catarina (DC6 and NZ1) and Paraná (P1C,
370 CP14 and R2P). Some of these samples had more than one analysed native copper
371 crystal, that were identified by the sample number followed by “a, b and c” (e.g.,
372 FS86a).

373 Along 1400 km of studied exposures in the host basalts, the copper isotopic
374 ratios (Table 7) display three distributions. The most frequent has values between -0.2
375 ‰ and 0.71 ‰ (n = 41). In this variation stands out the isotopic ratios between 0.4 ‰
376 and 0.7 ‰ as values more repeating in the analyses. The second shows values between
377 1.07 ‰ and 1.89 ‰ (n = 9). This variation has a discontinuous interval where the
378 greatest occurrences are between 1 ‰ and 1.2 ‰ (n = 6). The other analyses are in the
379 interval between 1.5 ‰ and 1.6 ‰ and a single analysis in 1.89‰. The third introduces
380 samples with values from -0.59 ‰ to -0.91 ‰. These negative values present an
381 analysis with isotope ratio of -0.59 ‰ and four analyzes between -0.83 ‰ and -0.91 ‰.
382 The Dom Pedro de Alcântara region in the southeastern part of the volcanic
383 province . Sample FS86 display different native copper crystals in the same sample and
384 the isotopic ratios average is -0.81‰ for FS86a and 0.06‰ for the crystal FS86b. In the
385 Bom Princípio region, the isotopic values $\delta^{65}Cu$ in the sample BP1 has isotopic ratios
386 average of 0.43‰. In the Santo Augusto region, two samples were evaluated, JS3 (a -
387 native copper and b - chrysocolla) and JS4 (a, c - native copper and b - cuprite). Sample
388 JS3a displays native copper isotopic average ratios of 0.14‰ and the average values
389 ratios for JS3b (chrysocolla) is -0.31 ‰. In sample JS4a, the isotopic average ratios for
390 native copper showed 0.64 ‰ while in cuprite the average isotopic values was 0.18 ‰
391 in the core and for the crystal rim display a isotope variation from 0.10 – 0.73 ‰. The
392 sample JS3c shows isotope ratios of 1.07‰. In the region between Taquaruçu do Sul
393 and Frederico Westphalen was observed a large isotopic variation in the native copper
394 crystals of the same sample, and regionally. The native copper in sample PD1a showed
395 isotopic average ratios of 0.70 ‰ and in sample PD1b the isotopic ratios average is 1.16
396 ‰ whereas the sample W247 shows isotopic variations between the crystal core (0.37
397 ‰) and rim (-0.14 ‰).

The region of Dionisio Cerqueira (sample DC6) and Palma Sola (sample NZ1) in Santa Catarina state, show values of $\delta^{65}Cu$ from 0.49 ‰ (NZ1) to 1.10 ‰ (DC6). Crossing to the Paraná state, the Sample P1C in Francisco Beltrão region shows $\delta^{65}Cu$ values of 0.36 ‰ in the crystal rim and 0.39 ‰ in the core. In the Cascavel region near to the depocenter (greater thickness of the volcanic pile) of the Paraná volcanic province, the sample CP14 shows two sizes of native copper crystals. The mm-sized native copper (CP14a) has isotopic average ratios of 0.57 ‰, while in the cm-sized native copper (CP14b) the isotope average ratios is 1.63 ‰ indicating at least two different native copper mineralization in the same sample. Sample R2P which presents native copper mineralization with quartz, the isotopic average ratios is 0.57 ‰. The lowest isotopic value for native copper (-0.91‰) is observed in the Rio Grande do Sul state and the highest value (1.89 ‰) in the Paraná State. These isotopic variations (Fig. 11) is here interpreted as associated with the processes that originated the copper deposits and can be compared to the isotopic data of copper deposits in the USA (Table 8) and show a quite similar variation as the hydrothermal deposits from Keweenaw volcanic province, Michigan, USA (Fig. 11) and supergene deposits (Fig. 11).

Discussions and interpretations

The origin of copper deposits has sparkled theories and genetic models that seek to explain the different processes for a wide variety of native copper deposits in host rocks such as basic and ultrabasic igneous rocks, sedimentary rocks and also in sulphide deposits. In the Paraná volcanic province, controversy was generated centered in at least three theories about the origin of native copper based on magmatic, late-magmatic, and hydrothermal models. The magmatic origin suggested by Mello (2000) was based in the native copper mineralization at the surface of cooling joints (Água Perdida region,

Paraná). According to the author the temperature of cooling joint formation was 750 ºC and at this temperature a residual and immiscible fluid, rich in copper, migrated to this space generating a native copper mineralization with timing correlated to the lava solidification processes. The late-magmatic origin indicated by Szubert et al. (1979) suggests that the native copper mineralization (Itapiranga region, Santa Catarina) in the microfractures and in the core of basaltic flows originated from late-magmatic processes (hydrothermal processes included but not detailed). The hydrothermal origin indicated by Pinto et al. (2011b) and Arena et al. (2014) is supported in the present study.

Regarding the magmatic origin, it is worth noting that the magmatic processes are conditioned to high-temperatures so the native copper crystallization occurs in equilibrium with the magma. In deposits at this temperature, copper isotopes show δ^{65}Cu ratios ~ 0‰ and no significant fractionation (Markl et al. 2006). The isotopic composition of native copper crystals in ultramafic rocks (Albarede 2004; Ikehata and Hirata 2012) shows δ^{65}Cu values between -0.03 ‰ and 0.14 ‰ supporting the absence of significant copper fractionation during magmatic, high-temperature processes, thus higher values than 0.3 ‰ cannot be expected in these temperatures. In this case, the copper mineralization in the Paraná volcanic province should have δ^{65}Cu values close to 0 ‰ but this is not the case, they are more fractionated and must have been modified during the formation of mineralization.

The study carried out by Cabral and Beaudoin (2007) in the Quebec Appalachians (Canada) suggest the occurrence of native copper crystals of magmatic origin. According to that study, the native copper occurs as inclusions (~ 50 μm in length) in feldspars and the authors present an S *versus* As diagram from the high-temperature native copper from Quebec, Canada, and the low-temperature native copper deposits from the Keweenaw volcanic province, Michigan. The comparison highlights

448 the electron probe analyses that show the high concentrations of sulfur and arsenic in
449 the high-temperature native copper from Québec and the low concentrations of sulfur
450 and arsenic in the low-temperature native copper from Michigan. In the Paraná
451 province, the host volcanic flows of copper mineralization have essentially mantle
452 origin according copper contents *versus* rare earth elements correlations. In the same
453 way, the EPMA analyses in the copper native crystals shows very low sulfur content
454 (0.03 wt. %) and is accompanied by contents of arsenic below the electron microprobe
455 detection limit, similarly to the low-temperature copper mineralization of Michigan. A
456 careful search for native copper inclusions was made by backscattered electrons images
457 in the primary minerals of the host basalt. However no evidence of magmatic copper
458 crystals associated with the primary minerals was observed. This observation requires
459 further detail. The native copper mineralization on the surface of the cooling joint in the
460 basalts of the Paraná volcanic province acts as a time marker. Surface cracking (e.g.
461 Kilauea volcano) according to Peck and Minakami (1968) starts at 900 ºC, but the
462 cooling joint is formation completed when the bulk of the flow (e.g. Big Lost River
463 flow, USA) reaches around 750ºC (Lore et al. 2000). The structure is only completed
464 when all magmatic processes come to an end and the volcanic rock is consolidated. The
465 copper mineralization in the Paraná volcanic province was generated after the formation
466 of the cooling joints. In addition, the native copper occurs associated with a low
467 temperature mineral assemblage. Other evidence can be seen in the host basalts where
468 the native copper is associated with smectite and also in cavities where the rounded
469 massive copper occurs in the core, associated with zeolites and/or calcite in the rim.
470 Accordingly, the native copper origin in the Paraná volcanic province is not compatible
471 with magmatic processes. The hydrothermal hypothesis for the copper origin in the

Parana volcanic province can explain the mineralization based on the evidence presented in this study.

The Cretaceous native copper mineralization in the study area can be compared with the Proterozoic mineralization of native copper from Keweenaw Province, USA, and also with the Upper Permian mineralization of native copper from Emeishan volcanic province in China. In the Keweenaw Province, the native copper deposits are hosted at the top of rift subaerial basaltic lava (Bornhorst and Barron 2011). Also, fluid inclusion studies (Livnat, 1983) indicated that the hydrothermal fluids at 150-200 ºC crossed the underlying sedimentary sequence (conglomerates) and the volcanic pile to deposit the native copper. In the Emeishan province, the hosting volcanic rocks (basalts, breccias and tuffs) with bitumen have Cu average contents of 200 ppm (Li et al. 2005) and are interbedded with carbonaceous sedimentary rocks. The native copper mineralization is hosted in the breccias, in the amygdaloidal crust and also in the sedimentary sequence at the top of the basalt flows. In places, the copper replaces and fills bitumenous fissures in the basaltic rock. The minerals are characterized by a low-temperature assemblage of laumontite, epidote and quartz and the hydrothermal mineralization is epigenetic (Li et al. 2005). In the Paraná volcanic province, the H1, H2 and H3 hydrothermal events were identified, defined and described by Hartmann et al. (2008, 2012a, 2012b). These events were triggered by boiling water and its vapour from the Guarani aquifer that migrated upwards into the volcanic pile and promoted alteration in the host basalts, zeolites deposition and native copper mineralization in cooling joints, fractures and cavities.

The description of hydrothermal processes in the Paraná volcanic province requires an evaluation of the copper source that generated the mineralization. In the Michigan district, one of the discussions that have permeated this issue for over a

497 hundred years is the presence of copper in the crystal structure of iron minerals
498 (magnetite) in the host basalts, its chemical changes and the concentration of copper
499 (e.g., Butler and Burbank 1929). The study performed by Cornwall (1956) in the
500 Michigan native copper describes the presence of copper in magnetite (200 – 800 ppm),
501 ilmenite (90 – 300 ppm), clinopyroxene (51 – 320 ppm) and plagioclase (20 – 73 ppm).
502 In the Paraná volcanic province some studies (e.g. Tazaki et al. 1988; Arioli 2008; Pinto
503 et al. 2011b) have also suggested the presence of copper in magnetite.

504 The LA-ICPMS analyses in this study show that the minerals of the host basalt
505 contain copper, mainly magnetite. This finding contributes to a better understanding of
506 the behavior of copper during the hydrothermal events. The chemical reactions triggered
507 by the boiling water from the Guarani aquifer in the host basalts promoted the alteration
508 of magnetite-hematite to clay minerals and released the copper from its crystal lattice.
509 The hydrothermal fluids leached the copper and promote the first concentration in the
510 clay minerals (smectites). As the hydrothermal activity was developing, copper was
511 being deposited along the cooling joints that served as a pressure relief for hydrothermal
512 fluids. Similarly, the copper mineralization was generated in the cavities in the
513 amygdaloidal crust. Studies in monophase fluid inclusions in amethyst deposits (Gilg et
514 al. 2003; Duarte et al. 2009; Morteani et al. 2010; Juchem 2014) showed that the
515 evolved boiling fluids had low salinity and temperatures up to 150 ºC, although Gilg et
516 al. (2014) determined the additional presence of high-salinity fluids. The presence of
517 heulandite identified by Raman spectroscopy and calcite means that the copper
518 mineralogical association has been formed at temperatures lower than 200 °C (Carr et
519 al. 1999). These temperatures are consistent with those indicated by Pinto et al (2011b)
520 to the copper mineralization in the Vista Alegre mining district (100 – 150 ºC) Paraná

volcanic province and also for the hydrothermal alteration assembly (smectites, zeolites, quartz and calcite).

Au and Ag contents are present both in host basalts and in the native copper crystals, but also show no clear correlation between them in the copper mineralization of Paraná volcanic province. The experimental hydrothermal mechanisms for gold and silver (transport and concentration) in epithermal systems (Cole and Drumond 1986; Williams-Jones and Heinrich 2005) are based on pressures and temperatures which coexist with boiling liquid-vapor phases. The model predicts that the vapor transport capacity of metal is greater than that of hot water. This explosive mechanism was indicated by Arena et al. (2014) for the leaching, transport and mineralization of copper, gold and silver in the Realeza region, Paraná volcanic province. At a temperature of 150 °C, the vapor carrying metal can mix with groundwater that is close to the surface and form metal mineralization as mentioned by Williams-Jones and Heinrich (2005). Similar mechanism occurred in the copper mineralization along the Paraná volcanic province. The Cretaceous hydrothermal boiling fluids with copper percolated through the cooling joints and fractures and formed the native copper mineralization.

The process of forming copper deposits trigger many fractionation mechanisms that are not fully understood. Several studies (e.g., Zhu et al. 2000; Larson et al. 2003; Markl et al. 2006) suggest that these mechanisms are influenced by redox reactions, valence of copper ions, speciation in solution and in some cases organic process. In hydrothermal deposits the most significant mechanisms are liquid-vapor separation, multi-step equilibrium processes and physical/chemical parameters (temperature, oxygen fugacity, pH and salinity of the fluid). These processes leave their marks as fingerprints in the copper isotope ratios which can be used to define the origin of the deposits (Maréchal et al. 1999; Dekov et al. 2013; Zhang et al. 2013) and also to

546 distinguish high from low-temperature processes. The Cu isotope fractionation
547 (sulfides) in hydrothermal systems (Graham et al. 2004) is associated with the process
548 of Cu leaching and by the ore-bearing fluid. The isotope fractionation is differentiated
549 for hydrothermal vapor and for fluid phase. Multiple mineralization events could occur
550 from a fluid with different Cu isotopic composition, oxygen/sulfur fugacity, temperature
551 and chemical composition. In the copper hydrothermal deposits hosted in basalts
552 (Larson et al. 2003) the copper isotopic values are more similar to the mantle (~ 0 ‰),
553 and overlap the values of chalcopyrite in mafic intrusions with isotope variation extends
554 to higher values.

555 In the supergene environments the redox processes affect strongly the copper
556 isotopic compositions (Larson et al. 2003; Maher 2005; Markl et al. 2006; Mathur et al.
557 2012) and represents varied and repetitive fractionation processes (leaching, oxidation
558 and reduction) controlled by changes in the water system over time (Maher, 2005).
559 However, extremely high fractionation (9 ‰) may reflect an open system or kinetic
560 fractionation (Sherman, 2013). The variation in δ^{65}Cu (Maher, 2005) of supergene
561 deposits involves three processes, the leaching of copper from existing minerals, the
562 change in the valence of copper and the precipitation of copper mineral. The degree of
563 leaching of ^{65}Cu in the copper precursor mineral defines the final isotope ratios.
564 Supergene copper minerals co-existing in the same sample can be isotopically heavier
565 than the copper precursor mineral (Asael et al. 2007), but the low-temperature
566 fractionation (Maréchal and Sheppard, 2002) can precipitate minerals isotopically
567 lighter than the fluid. The supergene enrichment displays oxidized secondary phases
568 (e.g., cuprite) with isotopic ratios higher than native copper. The δ^{65}Cu variation in the
569 supergene native copper deposits range between -3.03 ‰ (Maréchal et al. 1999) to 0.72
570 ‰ (Larson et al. 2003) and up to 1.26 ‰ (Larson et al. 2003) when associated with

571 cuprite. These variations overlap the isotope ratios from Michigan native copper
572 hydrothermal deposits (Larson et al. 2003; Maher 2005).

573 In the Paraná volcanic province the hydrothermal system with boiling fluids
574 (water and its vapour) generated a wide mineralization of native copper. The $\delta^{65}Cu$
575 ratios variations in the native copper was interpreted as isotopic fractionation reactions
576 during the H1, H2 and H3 (Hartmann et al., 2008, 2012a, 2012b) low-temperature
577 hydrothermal events and by the supergene environment that affected the native copper
578 mineralization. The succession of hydrothermal events, added to redox reactions in the
579 exposed volcanic flows at the surface ensured the formation of the secondary co-
580 existing copper minerals with native copper as precursor mineral and is supported by
581 the values of $\delta^{65}Cu$ from 0.3 ‰ up to 1.89 ‰. Similarly local variations occur in several
582 places of the province. In the sample JS4 the isotope ratios of 0.65 ‰ and 1.07 ‰ show
583 the fractionation of two different events of hydrothermal native copper mineralization.
584 The cuprite in this sample shows an isotope variation in the core (~ 0.18 ‰) with more
585 fractionated $\delta^{65}Cu$ (up to 0.73 ‰) in the rim. In the same region, in sample JS3, was
586 observed chrysocolla with lighter isotope ratios (~ 0.31 ‰). In the regions of Dom
587 Pedro de Alcantara (FS86a, b), Santo Augusto (JS4a, c), Taquaruçu do Sul (PD1a, b)
588 and Cascavel (CP14a, b) the variation of isotope ratios reflect multiple hydrothermal
589 mineralization with different times of copper leaching and fractionation along the fluid
590 flow pathway. Different degrees of leaching and stronger fractionation of the Cu
591 isotopes (W247, P1C) in the supergene environment were observed in the Frederico
592 Westphalen (RS), and Francisco Beltrão (PR) regions. Accordingly, in the Paraná
593 volcanic province the origin of the copper is hydrothermal. Multiple copper
594 mineralization process occurs with leaching and mineral precipitation along the time
595 and different fractionation of copper and isotope ratio variation.

Conclusions

Hydrothermal native copper mineralization is widespread in the Paraná volcanic province as dendrides and needles in the cooling joints, fractures and also filling cavities in the amygdaloidal crust. Apart from native copper, other mineral phases such as cuprite, tenorite, chrysocolla, malachite and azurite make up the copper mineralization.

The origin of copper in the Paraná volcanic province is associated with the magma that rose from the mantle to the surface and formed the basaltic flows. The copper was added in the crystal lattice of the basalt forming minerals. As a consequence, the copper content average in the host basalts is 207 ppm. The Cretaceous H1, H2 and H3 (Hartmann et al., 2008, 2012a, 2012b) hydrothermal events altered the volcanic rocks. The minerals most affected by the hydrothermal alteration were magnetite, ilmenite, clinopyroxenes and the microcrystalline matrix. From this process smectites were formed. Copper, silver and gold were released from the crystal structure of igneous minerals. The copper initially was concentrated in the smectites. The transport of copper was supported by boiling water and vapor at temperature of 100 - 150 °C. The native copper was deposited along the network path crossed by the hydrothermal fluid in the cooling joints, fractures and within the vesicles of amygdaloidal crust. The variations of isotope ratios reflect Cu-mineralization pulses that occurred during the hydrothermal and supergene events. This study thus makes a major contribution to the understanding of the hydrothermal origin of the native copper mineralization in the large Paraná volcanic province. Of particular significance is the multianalytical approach in the study, with emphasis on copper isotopes.

Acknowledgements

Financial support was provided by Project VALE / CNPq, MCT and Mineral Sector Fund (CT-Mineral) entitled "Desenvolvimento de metodologia de exploração geológica para geodos de ametista e ágata, cobre e outros bens minerais em ambiente hidrotermal do Grupo Serra Geral, sul-sudeste do Brasil" and project of excellence PRONEX-FAPERGS/CNPq on strategic minerals from southern Brazil, coordinated by Léo A. Hartmann.

References

Albarède F (2004) The stable isotope geochemistry of Copper and Zinc. Rev Mineral Geochem 55:409-427

Almeida FFM (1986) Distribuição regional e relações tectônicas do magmatismo pós-paleozóico no Brasil. Rev Bras Geociências 16:325-349

Arena KR, Hartmann LA, Baggio SB (2014) Geological controls of copper, gold and silver in the Serra Geral Group, Realeza region, Paraná, Brazil. Ore geol rev 63:178-200

Arioli, E.E. 2008. Arquitetura faciológica da sequência vulcânica e o significado exploratório das anomalias geoquímicas de elementos do grupo da platina (EGP) e metais associados no sistema magmático Serra Geral, Estado do Paraná, Brasil. PhD Thesis, Universidade Federal do Paraná, Curitiba, Brazil, 262 p.

Asael D, Matthews A, Bar-Matthews M, Halicz L (2007) Copper isotope fractionation in sedimentary copper mineralization (Timna Valley, Israel). Chem Geol 243:238-254

Bellieni G, Comin-Chiaramonti P, Marques LS, Melfi AJ, Piccirillo EM, Nardy AJ, Roisenberg A (1984) High- and low-Ti flood basalts from the Paraná Plateau (Brazil):

645 petrology and geochemical aspects bearing on their mantle origin. Neues Jahrb
646 Mineral Abh 150:272-306
647 Bornhorst TJ, Barron RJ (2011) Copper deposits of the western Upper Peninsula of
648 Michigan. Geol Soc Am 24:83-99
649 Brückmann M, Hartmann LA, Tassinari CCG, Sato K, Baggio SB (2014) The duration
650 of magmatism in the Serra Geral Group, Paraná volcanic province. In: Hartmann LA,
651 Baggio SB (orgs) Metallogeny and mineral exploration in the Serra Geral Group, 1st
652 edn. UFRGS, Porto Alegre, Brazil, pp 507-518
653 Butler BS, Burbank WS (1929) The Copper deposits of Michigan. U.S. Government
654 printing office, 238pp. Washington
655 Cabral AR, Beaudoin G (2007) Volcanic red-bed copper mineralization related to
656 submarine basalt alteration, Mont Alexandre, Quebec Appalachians, Canada. Miner
657 Deposita 42:901-912
658 Carr PF, Pemberton JW, Nunan E (1999) Low-grade metamorphism of mafic lavas,
659 upper Permian Broughton Formation, Sydney Basin. Aust J Earth Sci 46:839-849
660 Cole DR, Drumond SE (1986) The effect of transport and boiling on Ag/Au ratios in
661 hydrothermal solutions: a preliminary assessment and possible implications for the
662 formation of epithermal precious-metal ore deposits. J Geochem Explor 25:45-79
663 Cornwall HR (1956) A summary of ideas on the origin of native copper deposits. Econ
664 Geol 51:615-631
665 Costa AFU (1982) Geologia aplicada à prospecção de cobre em basaltos na área de
666 Vista Alegre: Frederico Westphalen, RS. Acta Geol Leopold 11:17-36
667 Dekov VM, Rouxel O, Asael D, Hålenius U, Munnik F (2013) Native Cu from the
668 oceanic crust: Isotopic insights into native metal origin . Chem Geol 359:136-149

669 Duarte LC, Hartmann LA, Vasconcelos MAS, Medeiros JTN, Theye T (2009)
670 Epigenetic formation of amethyst-bearing geodes from Los Catalanes gemological
671 district, Artigas, Uruguay, southern Paraná Magmatic Province. J Volcanol Geoth Res
672 184:427-436
673 Duarte LC, Hartmann LA, Ronchi LH, Berner Z, Theye T, Massone HJ (2011) Stable
674 isotope and mineralogical investigation of the genesis of amethyst geodes in the los
675 Catalanes homological district, Uruguai, southernmost Paraná volcanic province.
676 Miner Deposita 46:239-255
677 Frank HT, Gomes MEB, Formoso ML (2009) Review of the areal extend and the
678 volume of the Serra Geral Formation, Paraná Basin, South America. Pesquisas em
679 Geociências UFRGS 36:49-57
680 Gilg HA, Krüger Y, Taubald H, van der Kerkhof AM, Frenz M, Morteani G (2014)
681 Mineralisation of amethyst-bearing geodes in Ametista do Sul (Brazil) from low-
682 temperature sedimentary brines: evidence from monophase liquid inclusions and
683 stable isotopes. Miner Deposita 49:861-877
684 Gilg HA, Morteani G, Kostitsyn Y, Preinfalk C, Gatter I, Strieder AJ (2003) Genesis of
685 amethyst geodes in basaltic rocks of the rocks of the Serra Geral Formation (Ametista
686 do Sul, Rio Grande do Sul, Brazil): a fluid inclusion, REE, oxygen, carbon and Sr
687 isotope study on basalt, quartz, and calcite. Miner Deposita 38:1009-1025
688 Graham S, Pearson N, Jackson S, Griffin W, O'Reilly S (2004) Tracing Cu and Fe from
689 source to porphyry: in situ determination of Cu and Fe isotope ratios in sulfides from
690 the Grasberg Cu-Au deposit. Chem Geol 207:147-169
691 Hartmann LA (2008) Amethyst Geodes Formed from Hot Water in Dinosaur Times, 1st
692 ed. UFRGS, Porto Alegre, Brazil.

693 Hartmann LA, Baggio SB (orgs) Metallogeny and mineral exploration in the Serra
694 Geral Group, 1st edn. UFRGS, Porto Alegre, Brazil, 560 pp
695 Hartmann LA, Duarte LC, Massonne HJ, Michelin C, Rosenstengel LM, Bergmann M,
696 Theye T, Pertille J, Arena KR, Duarte SK, Pinto VM, Barboza EG, Rosa MLCC,
697 Wildner W (2012a) Sequential opening and filling of cavities forming vesicles,
698 amygdales and giant amethyst geodes in lavas from the southern Paraná volcanic
699 province, Brazil and Uruguay. Int Geol Rev 54:1-14
700 Hartmann LA, Medeiros JTN, Petruzzellis LT (2012b) Numerical simulations of
701 amethyst geode cavity formation by ballooning of altered Paraná volcanic rocks, South
702 America. Geofluids 12:133-141
703 Hartmann LA, Wildner W, Duarte LC, Duarte SK, Pertille J, Arena KR, Martins LC,
704 Dias N.L (2010) Geochemical and scintillometric characterization and correlation of
705 amethyst-bearing Paraná lavas from the Quaraí and Los Catalanes districts, Brazil and
706 Uruguay. Geol Mag 147:954-970
707 Horn I, Von Blanckenburg F (2007) Investigation on elemental and isotopic
708 fractionantion during 196 nm femtosecond laser ablation multiple collector inductively
709 coupled plasma mass spectrometry. Spectrochim Acta B 62:410-422
710 Horn I, Von Blanckenburg F, Schoenberg R, Steinhoefel G, Markl, G (2006) In situ iron
711 isotope ratio determination using UV-femtosecond laser ablation with application to
712 hydrothermal ore formation processes. Geochim Cosmochim Ac 70:3677-3688
713 Ikehata K, Notsu K, Hirata T (2011) Copper isotope characteristics of copper-rich
714 minerals from Besshi-type volcanogenic massive sulfide deposits, Japan, determined
715 using a femtosecond LA-MC-ICP-MS. Econ Geol 106:307-316

716 Ikehata K, Hirata T (2012) Copper isotope characteristics of copper-rich minerals from
717 the Horoman peridotite complex, Hokkaido, northern Japan. Econ Geol 107:1489-
718 1497
719 Ikehata K, Hirata T (2013) Evaluation of UV-fs-LA-MC-ICP-MS for precise *in situ*
720 Copper Isotopic Microanalysis of Cubanite. Anal Sci 29:1213-1217
721 Janasi VA, Freitas VA, Heaman LH (2011) The onset of flood basalt volcanism,
722 Northern Paraná Basin, Brazil: A precise U Pb baddeleyite/zircon age for a Chapecó-
723 type dacite. Earth Planet Sci Lett 302:147-153
724 Juchem PL (2014) Amethyst mineralization in rhyodacites of the Serra Geral Group,
725 Paraná volcanic Province. In: Hartmann LA, Baggio SB (orgs) Metallogeny and
726 mineral exploration in the Serra Geral Group, 1st edn. UFRGS, Porto Alegre, Brazil,
727 pp 321-334
728 Larson PB, Maher K, Ramos FC, Chang Z, Gaspar M, Meinert LD (2003) Copper
729 isotope ratios in magmatic and hydrothermal ore-forming environments. Chem Geol
730 201:337-350
731 Lazarov M, Horn I (2015) Matrix and energy effects during in situ determinations of Cu
732 isotope ratios by UV-femtosecond laser ablation MC-ICP-MS. Spectrochim Acta B,
733 submitted
734 Le Bas MJ, Lemaitre RW, Streckeisen A, Zanettin B (1986) A chemical classification
735 of volcanic-rocks based on the total alkali sílica diagram. J Petrol 3:745-750
736 Li H, Mao J, Chen Y, Wang D, Zhang C, Xu H (2005) Epigenetic hydrothermal
737 features of the Emeishan basalt copper mineralization in NE Yunnan, SW China. In:
738 Mao J, Bierlein FP (eds) Mineral Deposit Research: Meeting the Global Challenge.
739 Springer Berlin Heidelberg, Beijing pp. 149-152

740 Livnat A (1983) Metamorphism and copper mineralization of the Portage Lake Lava
741 Series, northern Michigan. PhD Thesis, University of Michigan, Ann Arbor, USA
742 Lore J, Gao H, Aydin A (2000) Viscoelastic termal stress in cooling basalt flows. J
743 Geophys Res 105:695-709
744 Maher KC (2005) Analysis of copper isotope ratios by multi-collector inductively
745 coupled plasma mass spectrometry and interpretation of copper isotope ratios from
746 copper mineralization. PhD Thesis, Washington state University, USA, 239 pp
747 Mantovani MSM, Marques LS, De Sousa MA, Civetta L, Atalla L, Innocenti F (1985)
748 Trace element and strontium isotope constraints on the origin and evolution of Paraná
749 continental flood basalts of Santa Catarina state (southern Brazil). J Petrol 26:187-209
750 Maréchal C, Télouk P, Albarède F (1999) Precise analysis of copper and zinc isotopic
751 compositions by plasma-source mass spectrometry. Chem Geol 156:251-273
752 Maréchal C, Sheppard SMF (2002) Isotopic fractionation of Cu and Zn between
753 chloride and nitrate solutions and malachite or smithsonite at 30° and 50° C. Geochim
754 Cosmochim Ac 66: A484
755 Markl G, Lahaye Y, Schwinn G (2006) Copper isotopes as monitors of redox processes
756 in hydrothermal mineralization. Geochim Cosmochim Ac 70:4215-4228
757 Mathur R, Ruiz J, Casselman MJ, Megaw P, Van Egmond R (2012) Use of Cu isotopes
758 to distinguish primary and secondary Cu mineralization in the Cañarico Norte
759 porphyry copper deposit, Northern Peru. Miner Deposita 47:755-762
760 Mathur R, Titley S, Barra F, Brantley S, Wilson M, Phillips A, Munizaga F,
761 Maksaev V, Vervoort J, Hart G (2009) Exploration potential of cu isotope fractionation
762 in porphyry copper deposits. J Geochem Explor 102:1-6
763 Melfi AJ, Piccirillo EM, Nardy AJR (1988) Geological and magmatic aspects of the
764 Paraná Basin an introduction. In: Piccirillo EM, Melfi AJ (Eds) The Mesozoic Flood

765 Volcanism of the Paraná Basin: Petrogenetic and Geophysical Aspects, IAG, USP,
766 São Paulo, pp 1-13
767 Mello SK (2000) Estudo petrológico da região de Água Perdida no vale do Rio Piquiri –
768 PR: Reconhecimento das mineralizações de cobre e produtos de alteração em rochas
769 básicas da Formação Serra Geral – Bacia do Paraná. PPGeo UNISINOS, São
770 Leopoldo, Brazil
771 Morteani G, Kostitsyn Y, Preinfalk C, Gilg HA (2010) The Genesis of the amethyst
772 geodes at Artigas (Uruguay) and the paleohydrology of the Guarani aquifer: structural,
773 geochemical, oxygen, carbon, strontium isotope and fluid inclusion study. Int J Earth
774 Sci 99:927-947
775 Oeser M, Weyer S, Horn I, Schuth S (2014) High-precision Fe and Mg isotope ratios of
776 silicate reference glasses determined in situ by femtosecond LA-MC-ICP-MS and by
777 solution nebulisation MC-ICP-MS. Geostand Geoanal res 38:311-328
778 Nakamura K, Wildner W, Shibuya A, Masuta K, Murakami T, Romanini S (2003)
779 Mineral exploration of the Cu–Ni PGE deposits in the Paraná Basin Southern Brazil,
780 phase II. Tokyo, Japan Mining Engineering Center for International Cooperation –
781 JMEC/Geological Survey of Brazil – CPRM, Porto Alegre, Brazil
782 Peate DW (1997) The Paraná-Etendeka Province. In: Mahoney JJ, Coffin MR (Eds)
783 Large Igneous Provinces: Continental, Oceanic, and Planetary Flood Volcanism:
784 Geophysical Monograph 100, American Geophysical Union, Washington DC, USA,
785 pp 217-245
786 Peate DW, Hawkesworth CJ, Mantovani MSM (1992) Chemical stratigraphy of the
787 Paraná lavas (South America): classification of magma types and their spatial
788 distribution. Bull Volcanol 55:119-139

789 Peate DW, Hawkesworth CJ, Mantovani MSM, Rogers NW, Turner SP (1999)
790 Petrogenesis and stratigraphy of the high-Ti/Y Urubuci magma type in the Paraná
791 flood basalt province and implications for the nature of 'Dupal'-type mantle in the
792 south Atlantic region. J Petrol 40:451-473
793 Peck DL, Minakami T (1968) Formation of columnar joints in the upper part of
794 Kilauean lava lakes, Hawaii. Bull Geol Soc Am 79:1151-1166
795 Pinto VM, Hartmann LA (2011) Flow-by-flow chemical stratigraphy and evolution of
796 thirteen Serra Geral Group basalt flows from Vista Alegre, southernmost Brazil. An.
797 Acad Bras Ciênc, 83:425-440
798 Pinto VM, Hartmann LA, Santos JOS, McNaughton NJ, Wildner W (2011a) Zircon U–
799 Pb geochronology from the Paraná bimodal volcanic province support a brief eruptive
800 cycle at 135 Ma. Chem Geol 281:93-102
801 Pinto VM, Hartmann LA, Wildner W (2011b) Epigenetic hydrothermal origin of native
802 copper and supergene enrichment in the Vista Alegre district, Paraná basaltic
803 province, southernmost Brazil. Int Geol Rev 53:1163-1179
804 Rosenstengel LM, Hartmann LA 2012. Geochemical stratigraphy of lavas and fault-
805 block structures in the Ametista do Sul geode mining district, Paraná volcanic
806 province, southern Brazil. Ore geol rev 48:332-348
807 Seo JH, Lee SK, Lee I (2007) Quantum chemical calculations of equilibrium copper (I)
808 isotope fractionations in ore-forming fluids. Chem. Geol 243:225-237
809 Sherman DM (2013) Equilibrium isotopic fractionation of copper during
810 oxidation/reduction, aqueous complexation and ore-forming processes: Predictions
811 from hybrid density functional theory. Geochim Cosmochim Ac 118:85-97

812 Shields WR, Goldich SS, Garner EL, Murphy TJ (1965) Natural Variations in the
813 Abundance Ratio and the Atomic Weight of Copper. Journal of Geophysical Research
814 70:479-491
815 Szubert EC, Grazia CA, Shintaku I (1979) Projeto Cobre em Itapiranga. CPRM SUREG
816 Porto Alegre, Brazil
817 Tazaki K, Fyfe WS, Tazaki K, Bischoff J, Rocha BR (1988) Occurrence of Copper
818 films in basalt from the Serra Geral Formation, Paraná Basin, Brazil. Rev Bras Geoc
819 18:332-337
820 Wildner W, Hartmann LA, Cunha-Lopes R (2009) A proposed stratigraphy for the
821 Serra Geral Group in the Paraná Basin. In: Milani EJ, Chemale Jr. F (Eds) Correlation
822 Brazil–Africa. PETROBRAS, Gramado, Brazil
823 Williams-Jones AE, Heinrich CA (2005) Vapor transport of metals and the formation of
824 magmatic-hydrothermal ore deposits. Econ Geol 100:1287-1312
825 Zhang D, Zhou T, Yuan F, Fiorentini ML, Said, N, Lu Y, Pirajno F (2013) Geochemical
826 and isotopic constraints on the genesis of the Jueluotage native copper mineralized
827 basalt, Eastern Tianshan, Northwest China. J Asian Earth Sci 73:317-333
828 Zhu XK, O'Nions RK, Guo Y, Belshaw NS, Rickard D (2000) Determination of natural
829 Cu-isotope variation by plasma-source mass spectrometry: implications for use as
830 geochemical tracers. Chem Geol 163:139-149
831

832 **Figure captions**

833 Figure 1. Geological map of southeastern South America (modified from Peate et al.
834 1992), highlighting the Paraná Basin, the Paraná volcanic province (light gray),
835 Cretaceous sedimentary rocks overlying lavas (dark gray). Older sedimentary, igneous
836 and metamorphic rocks and an extensive coastal plain covered by Cenozoic sediments

837 are shown in blank. The sampling sites of native copper crystals and the host volcanic
838 rocks are indicated.
839 Figure 2. Field photos of native copper mineralization in the Paraná volcanic province.
840 A) Dendritic shapes of native copper at the surface of cooling joints. Hand specimen
841 (sample PD1) from David Basso quarry, Taquaruçu do Sul, Rio Grande do Sul. B)
842 Massive native copper with cuprite, tenorite, chrysocolla and malachite (sample JS3)
843 from Santo Augusto, Rio Grande do Sul. The mineralization occurs in a hydrothermal
844 breccia. C) Mining front in the Rebelato quarry, in Palma Sola, Santa Catarina. D)
845 Detail of Fig. C showing the collected sample NZ1 in the Rebelato quarry, with native
846 copper in thin blades and dentrites at the surface of basalt cooling joints. E) Basalt face
847 in the Quati quarry in Francisco Beltrão, Paraná. F) Detail of Fig. E (Sample PQ16)
848 showing the mineralization of native copper infilling the central portion of a cavity in
849 association with zeolites. G) Sample R2P from the Quati quarry with native copper in
850 dentritic shape associated with crystals of quartz. H) Outcrop in Linha Capanema,
851 Realeza, Paraná, showing the intense blue and green association of malachite and
852 chrysocolla. I) Detail of Fig. H showing the chrysocolla and malachite cementing the
853 hydrothermal breccia. The copper mineralization is also infilling the cavities
854 (amygdaloidal crust) of the fragmented basalts.
855 Figure 3. Photomicrographies of basalts hosting native copper from the Paraná volcanic
856 province. A) Sample PD1. Intergranular texture of small crystals of plagioclase,
857 clinopyroxene and opaque minerals. Glomeroporphyritic texture with phenocrysts of
858 plagioclase and opaque minerals. Cross-polarized light. B) Photograph of sample
859 W247. Phenocrysts of plagioclase associated with smaller crystals of clinopyroxene
860 and plagioclase. Cross-polarized light. C) Sample PD1. Microphenocrysts of
861 magnetite partly altered to clay minerals (left), reflected light. D) Sample PD1

862 showing magnetite with reddish halo of hematite (center and left), reflected light. E)
863 and F) Sample NZ1 with clinopyroxene crystals, microcrystalline matrix in the
864 intersticial space between the phenocrysts and presence of opaque minerals in the
865 matrix. Cross polarized light in E) and reflected light in F).
866 Figure 4. X-ray diffraction of sample JS3 from Santo Augusto, Rio Grande do Sul. Mlc
867 = malachite, Cpr = cuprite.
868 Figure 5. Photomicrographies and Raman spectra of copper minerals, plane polarized
869 light.
870 Figure 6. Silver associated with copper. Backscattered electron images. A) and B)
871 Sample R2P from Dalba quarry, Francisco Beltrão, Paraná. C) and D) Sample VA1
872 from the Vista Alegre mining district, Vista Alegre, Rio Grande do Sul. E) and F)
873 Sample JS4 from Santo Augusto, Rio Grande do Sul.
874 Figure 7. Classification diagrams of basalts hosting copper from the Paraná volcanic
875 province. A) Total alkalis-silica (TAS) diagram (after LeBas et al., 1986). B) TiO_2
876 *versus* MgO diagram, showing the magma types of basalts hosting copper, after Peate
877 et al. (1992) and Nakamura et al. (2003). C) $Fe_2O_3^T$ *versus* Cu diagram showing the
878 contents of copper and iron oxide of the samples and their positive correlation. D) Yb
879 *versus* Cu diagram showing the positive correlation.
880 Figure 8. Backscattered electron images of studied copper minerals. Numbers on images
881 indicate the analytical spots of microprobe analyses.
882 Figure 9. Backscattered electron images of basalt minerals hosting native copper in the
883 studied area. Dark spots are LA-ICP-MS craters. Sample-spot numbers indicated, e.g.,
884 DC1-MG2. (A) Magnetite. (B) Ilmenite. (C) Clinopyroxene. (D) Smectite.
885 Figure 10. Backscattered electron images of basalts, displaying specific relationships
886 between several minerals. A) B) and C) Magnetite crystals altered to smectite, in

887 different contrast intensities. D) E) and F) Contact relationships between a smectite
888 crystal and native copper, clinopyroxene and magnetite-ilmenite. Mag = magnetite,
889 Ilm = Ilmenite, Cpx = clinopyroxene, Sme = smectite.
890 Figure 11. Native copper isotopic compositions. Black: This study, Paraná volcanic
891 province. Light gray: Hydrothermal native copper composition from Keweenaw
892 volcanic province, Michigan, USA. Data from Shields et al. (1965), Zhu et al. (2000),
893 Larson et al. (2003). Dark gray: Supergene native copper composition deposits. Data
894 from Maréchal et al. (1999), Zhu et al. (2000), Larson et al. (2003), Ikehata et al.
895 (2011). For details, see Tables 8 and 9.

Figure
Click here to download Figure: Figure 01 2015_04_02.jpg

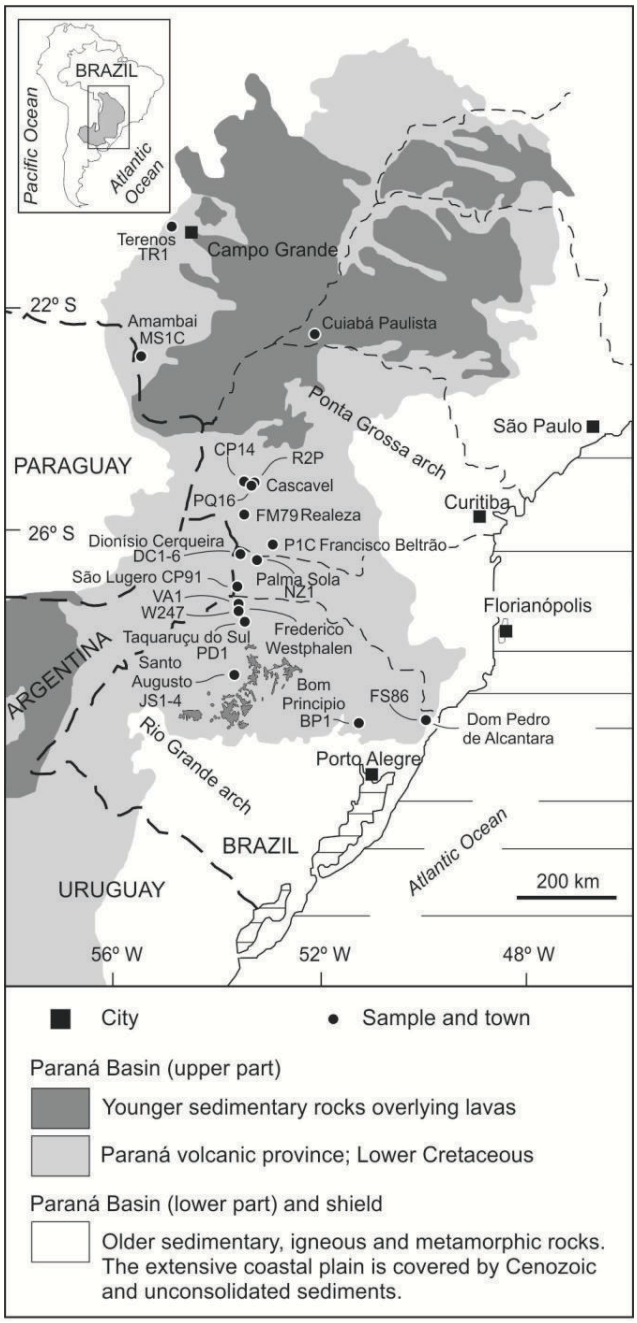

Figure
Click here to download Figure: Figure 02 2015_04_02.jpg

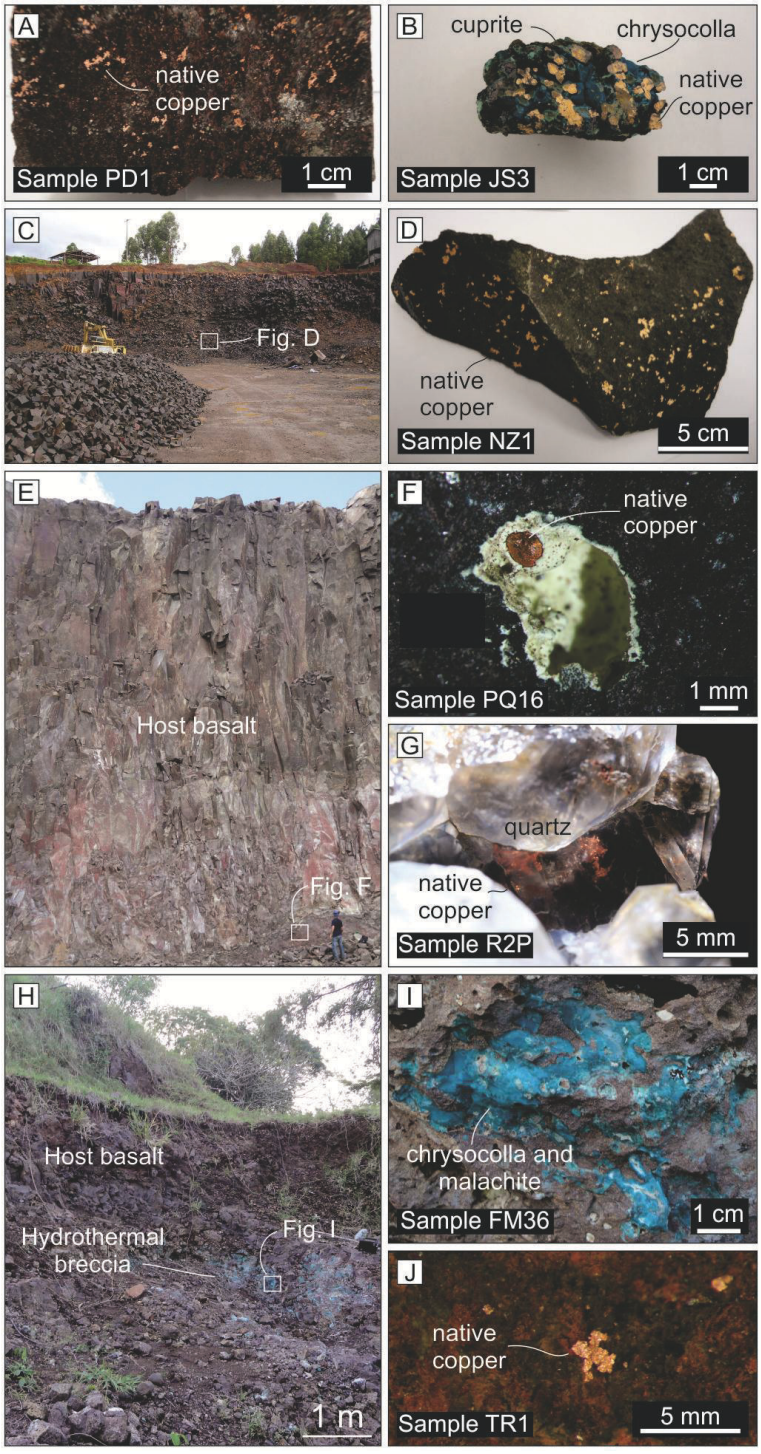

Figure
Click here to download Figure: Figure 03 2015_04_02.jpg

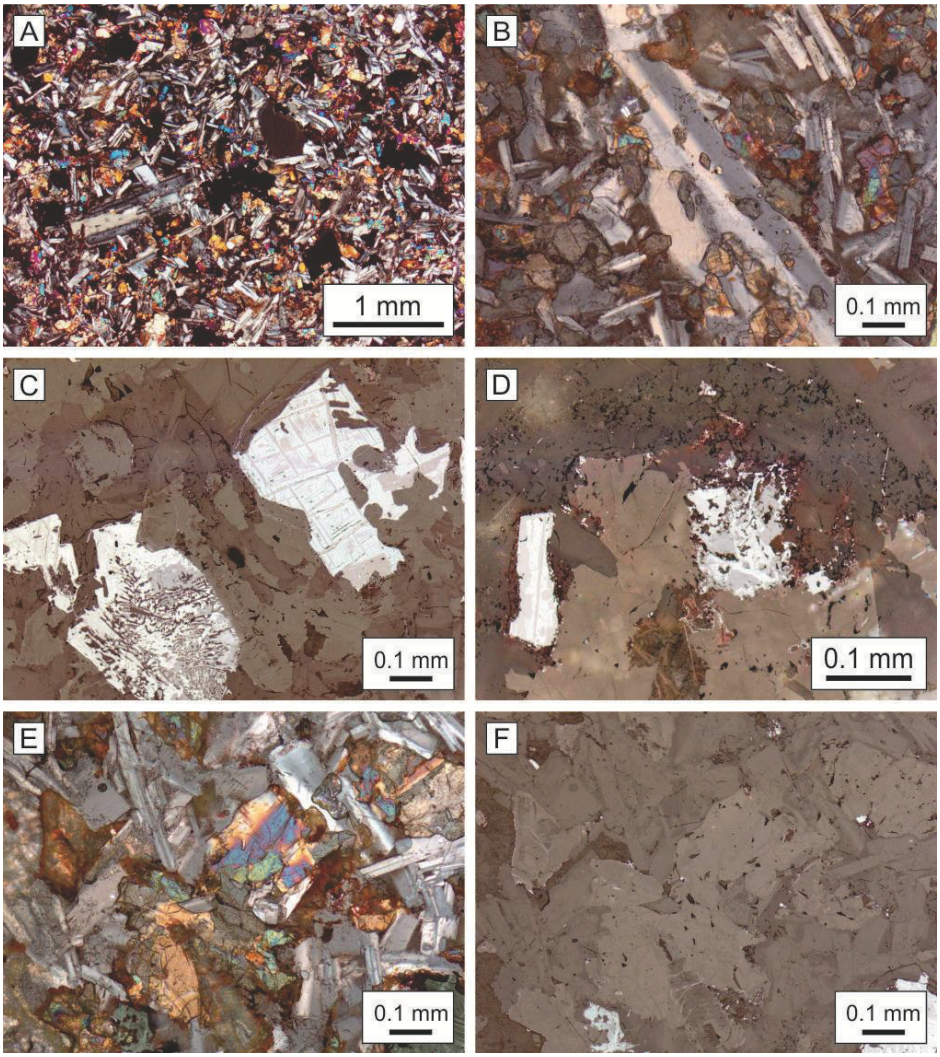

Figure
Click here to download Figure: Figure 04 2015_04_02.jpg

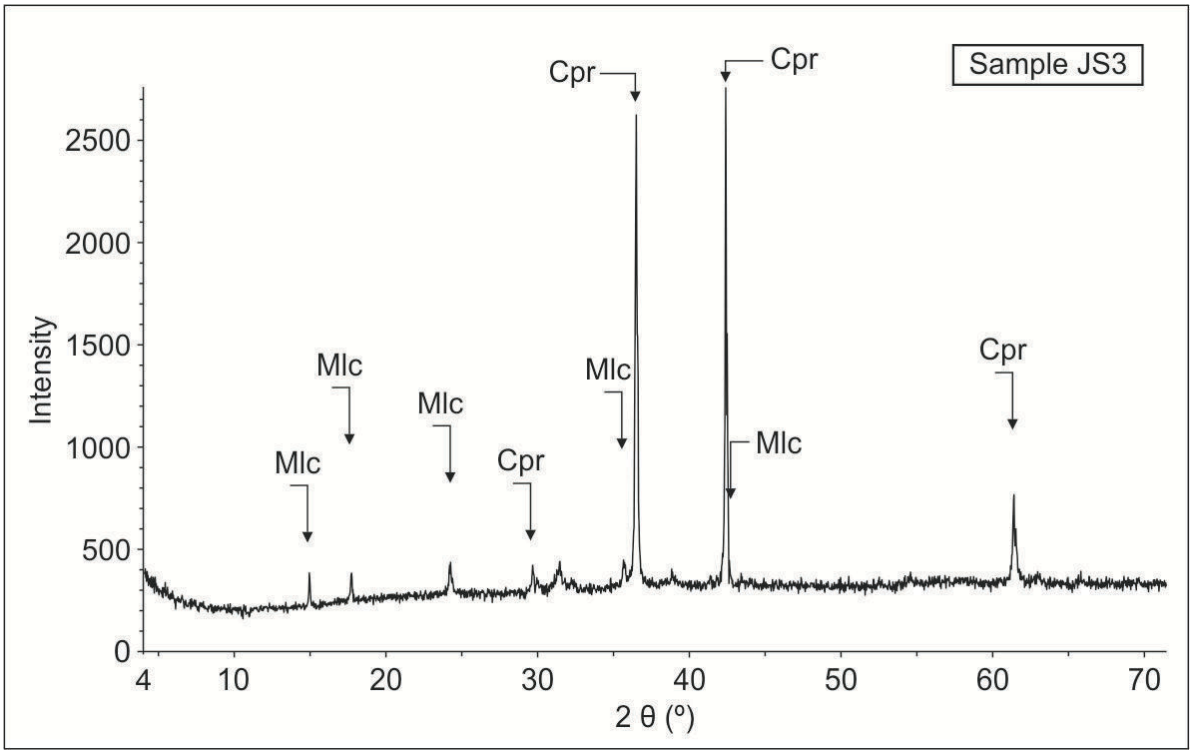

Figure
Click here to download Figure: Figure 05 2015_04_02.jpg

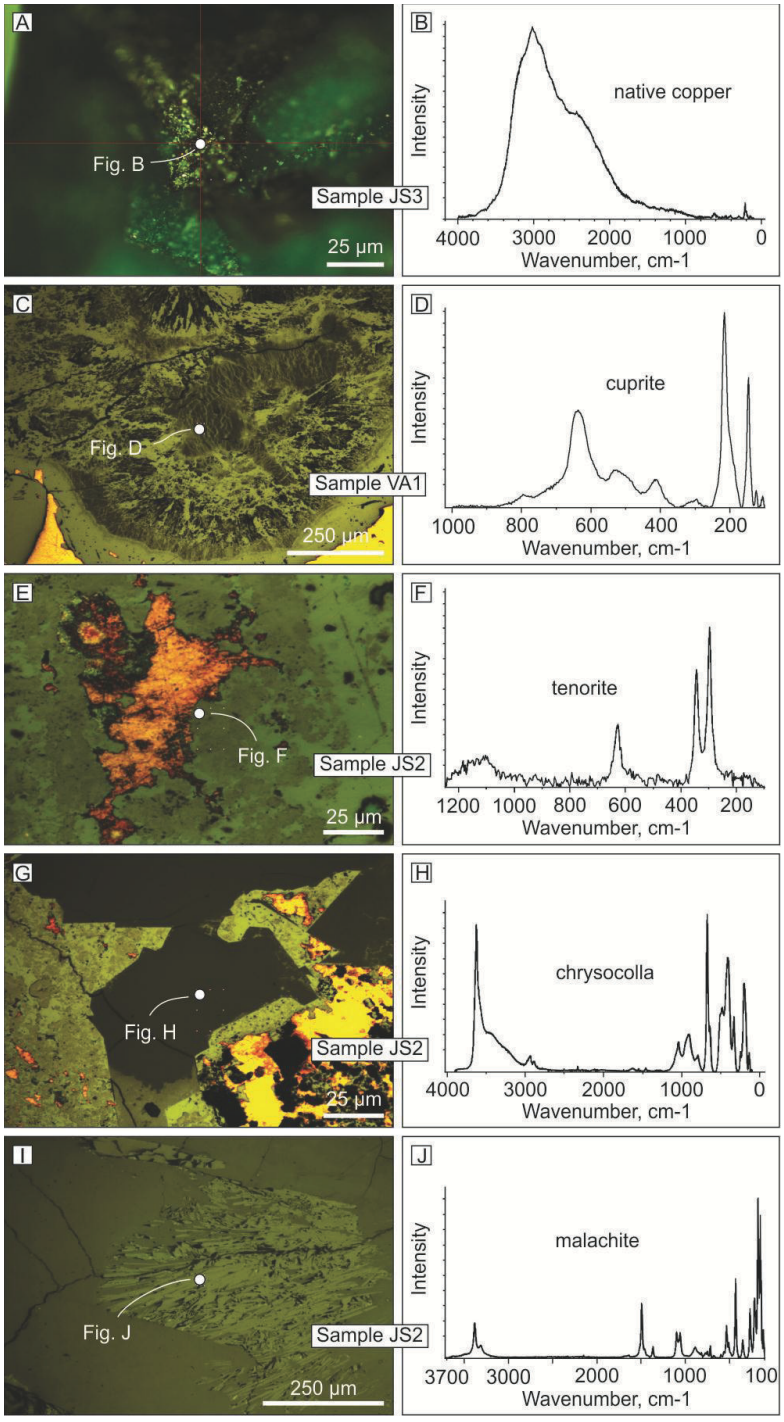

Figure
Click here to download Figure: Figure 06 2015_04_02.jpg

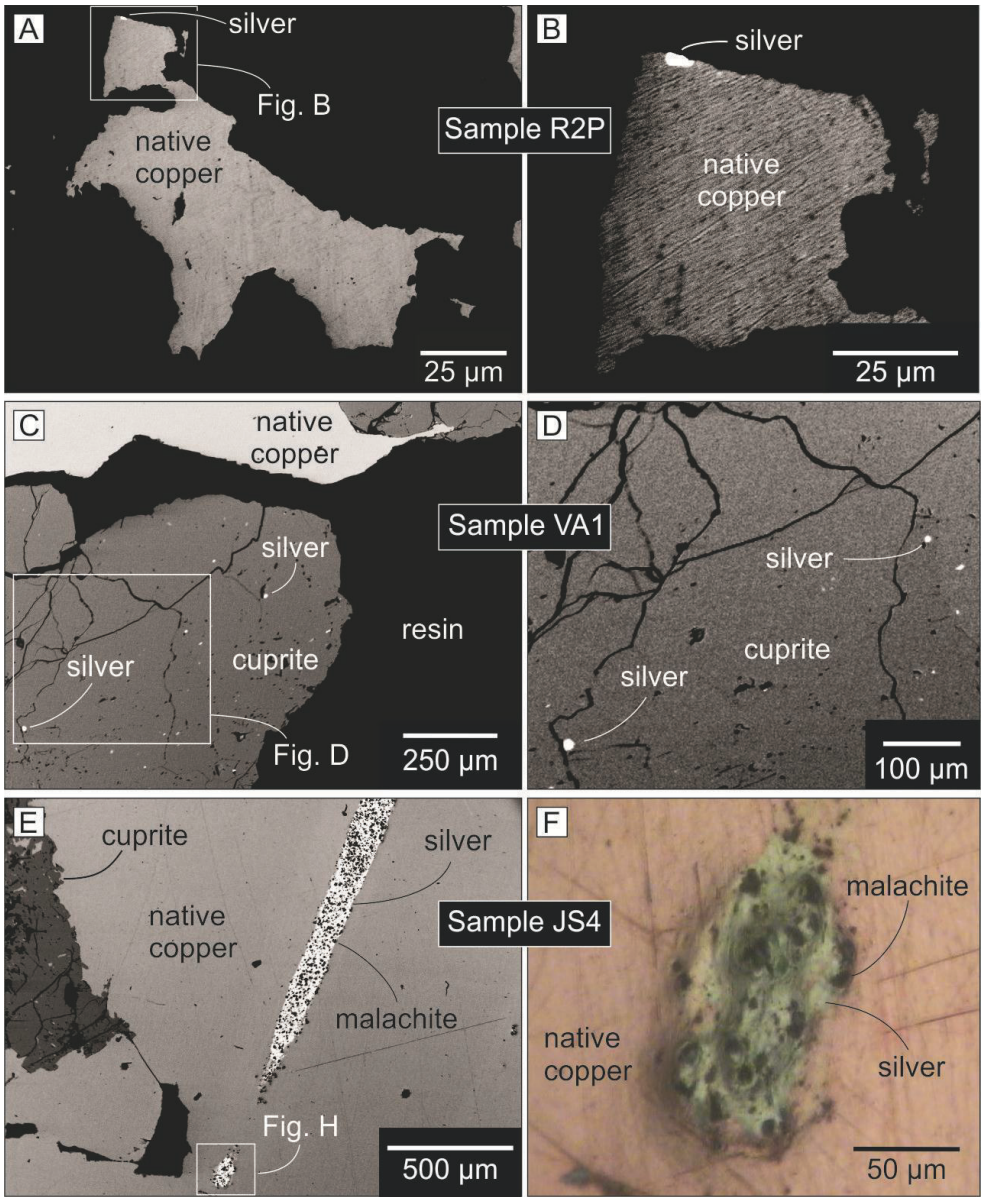

Figure
Click here to download Figure: Figure 07 2015_04_02.jpg

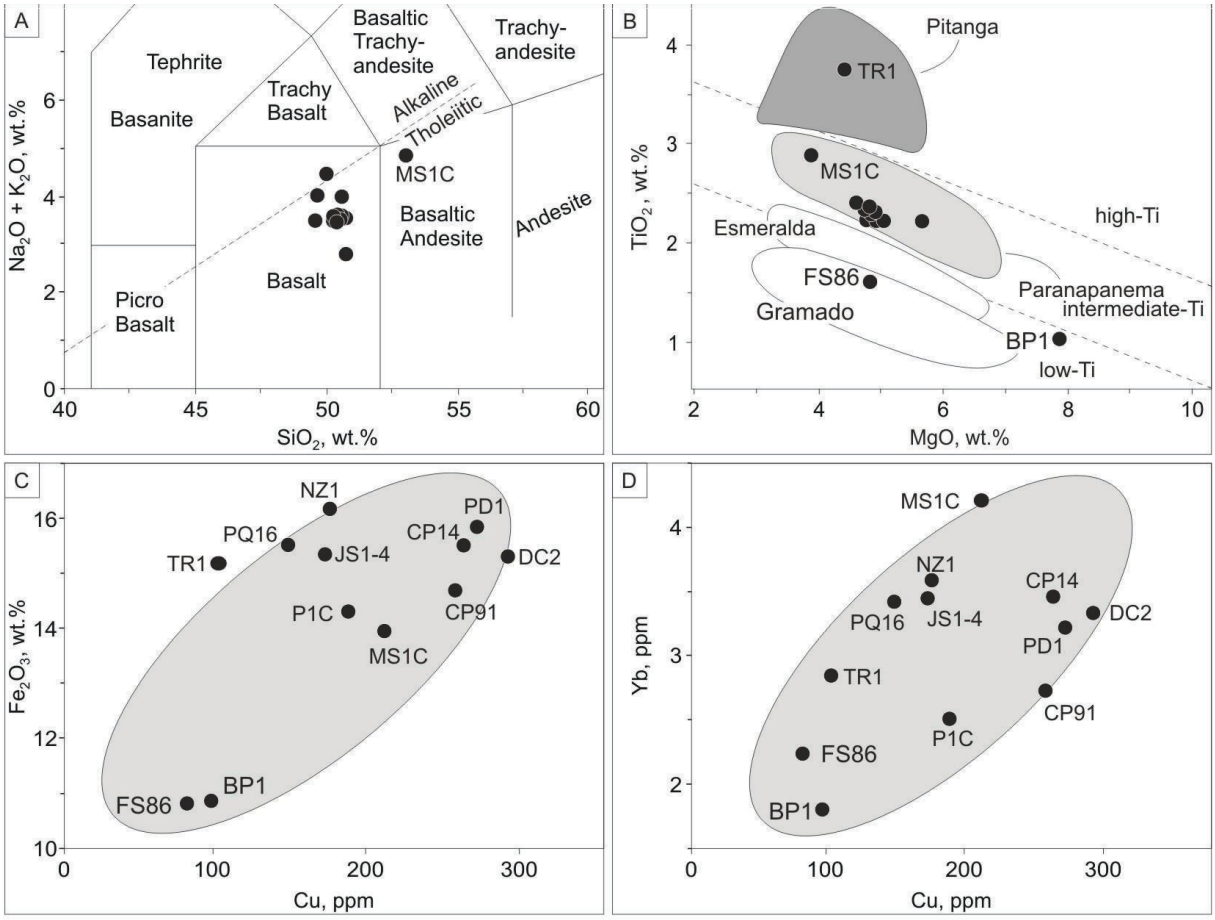

Figure
Click here to download Figure: Figure 08 2015_04_02.jpg

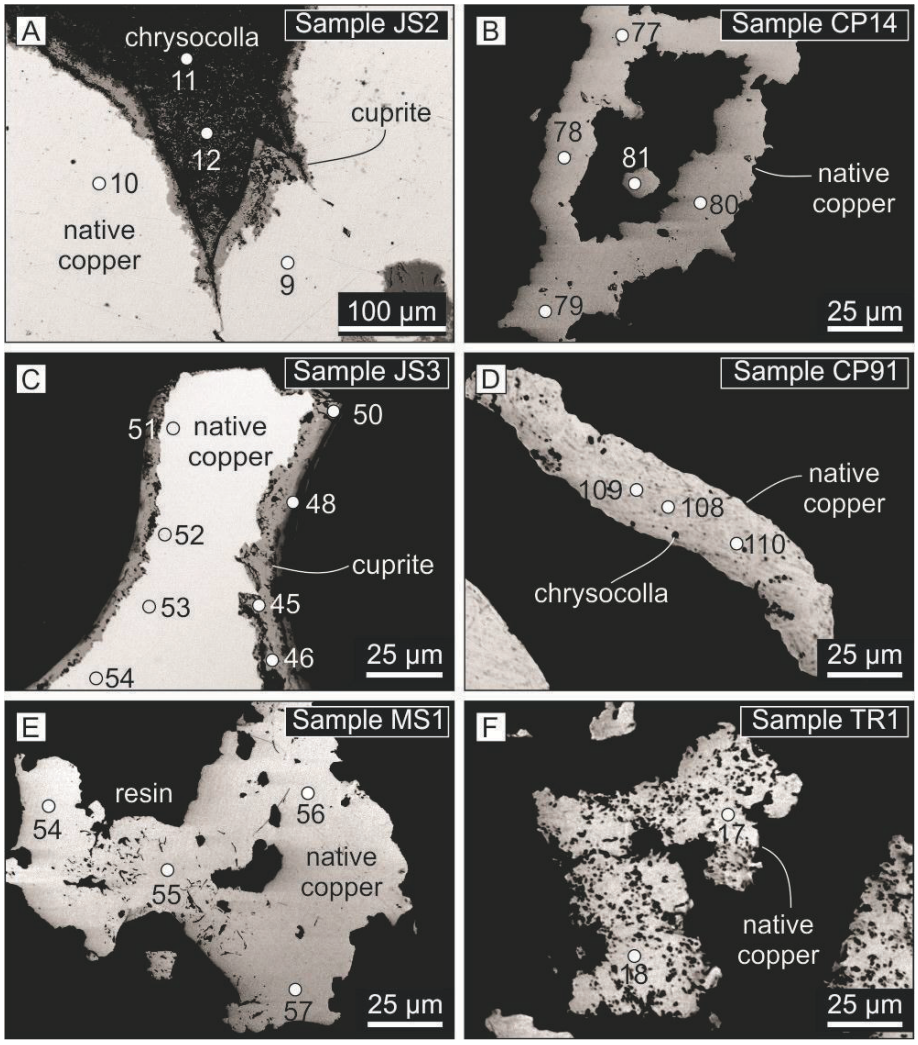

Figure
Click here to download Figure: Figure 09 2015_04_02.jpg

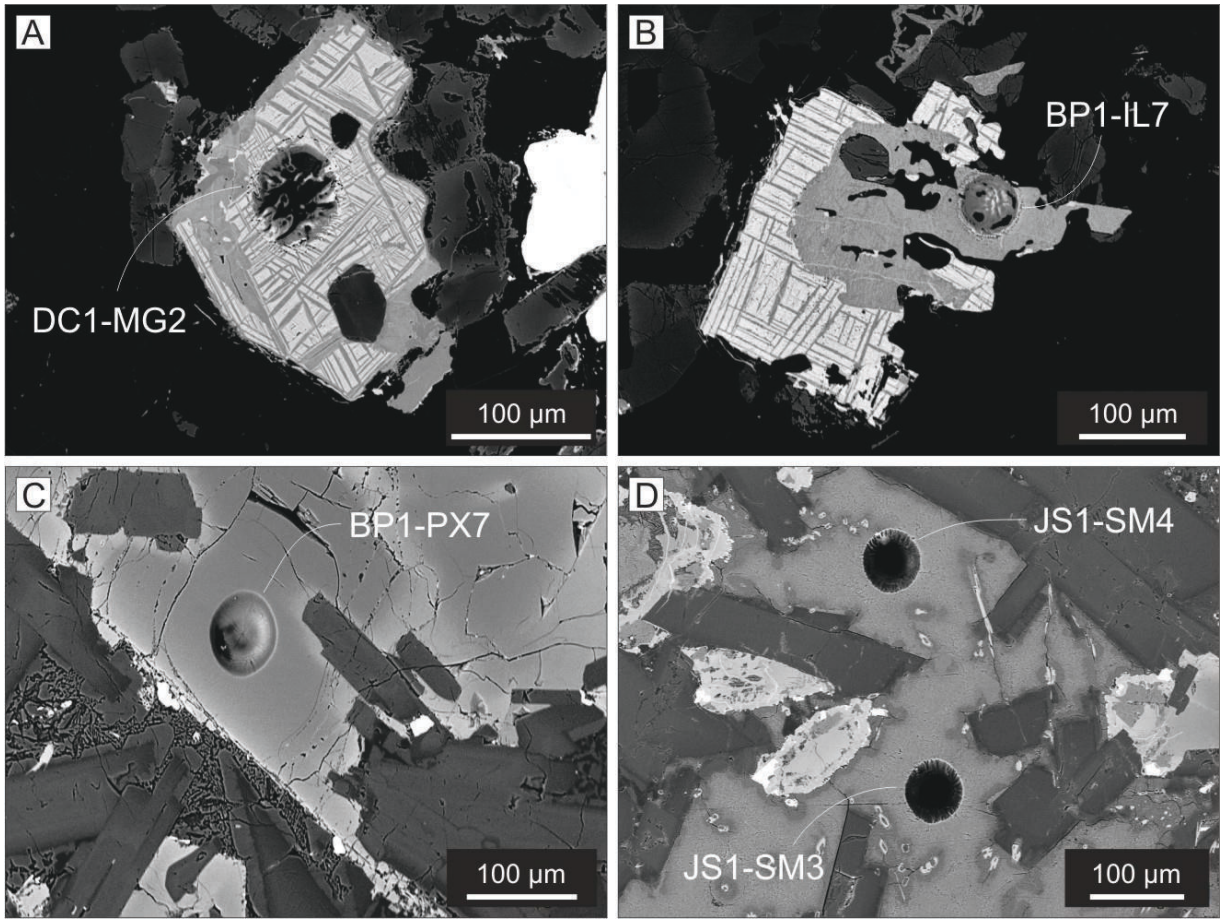

Figure
Click here to download Figure: Figure 10 2015_04_02.jpg

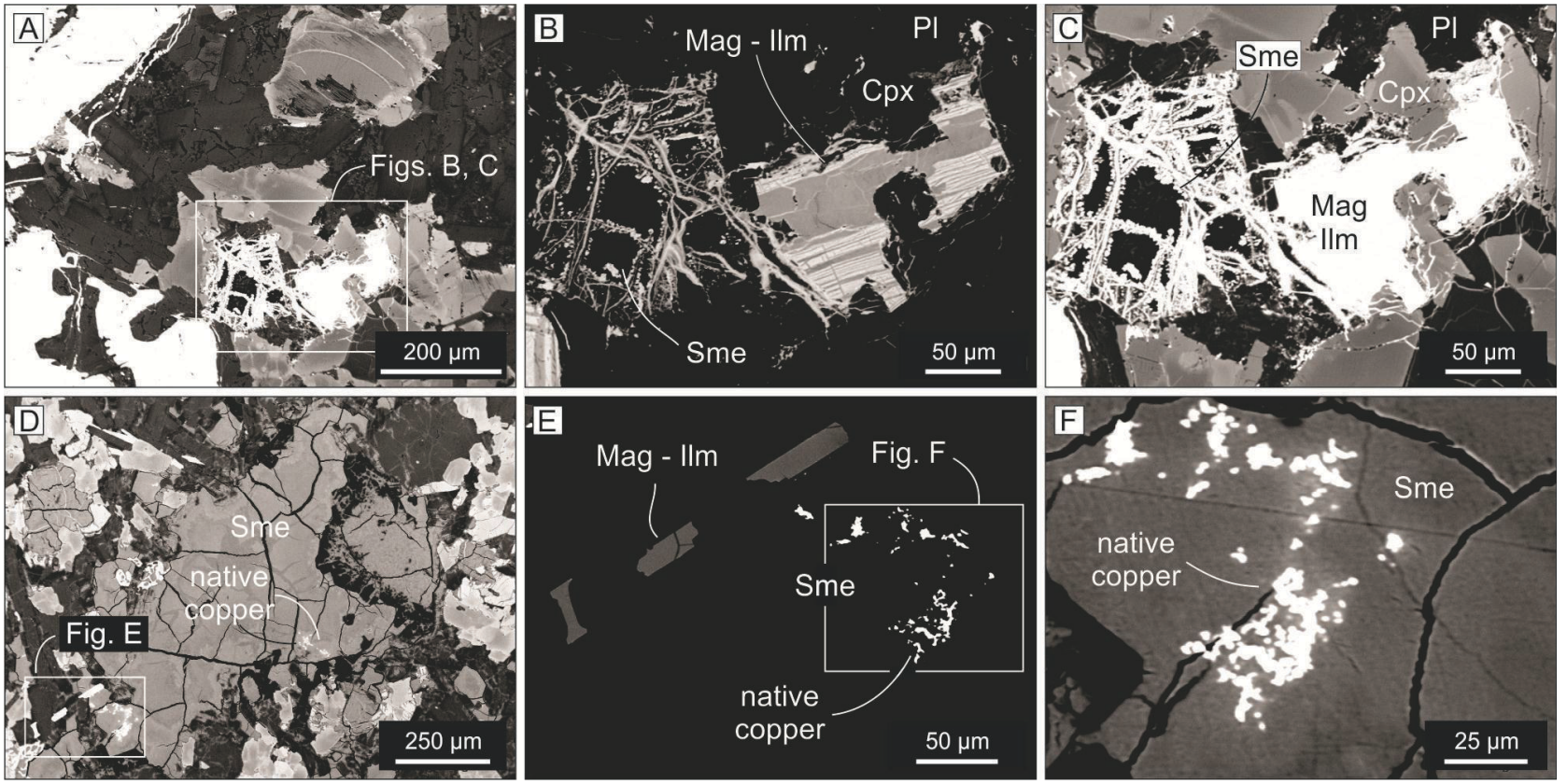

Figure
Click here to download Figure: Figure 11 2015_04_02.jpg

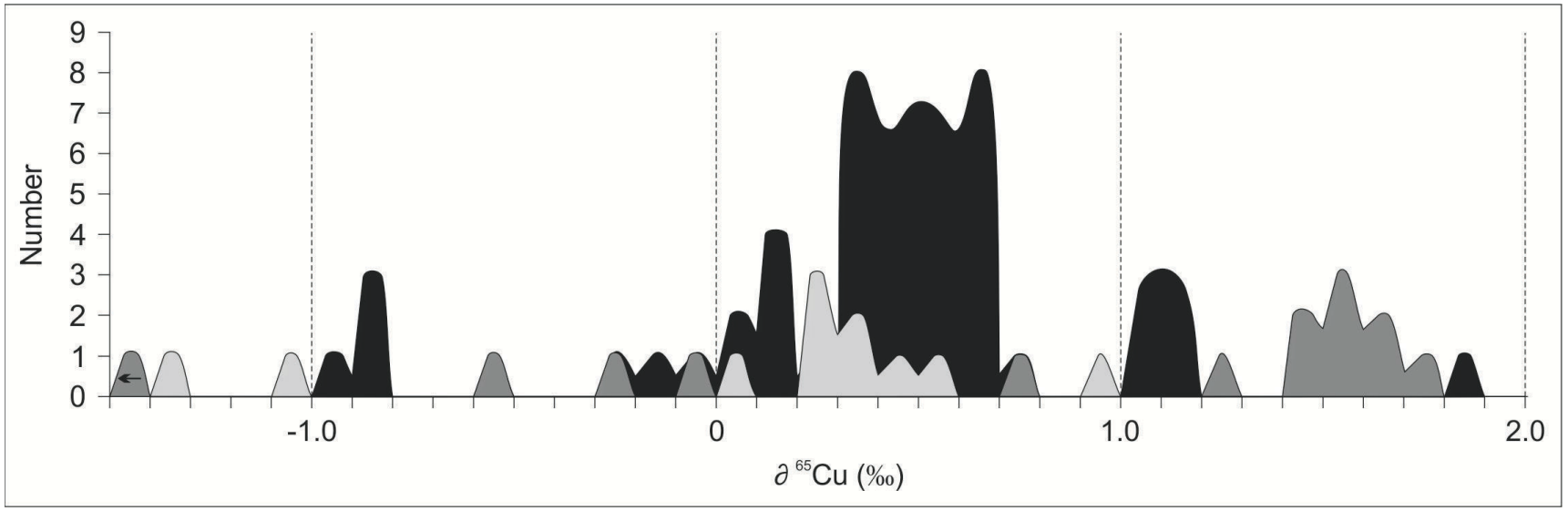

Table 1
Location of the native copper mineralization and description of its form of occurrence in the Paraná volcanic province

Sample	Location	Datum WGS84	Native Copper occurrence
FS86	Quarry 86, Dom Pedro de Alcântara, RS	22J 0611709E / 6748186S	Thin blades and dendrites (mm) in the surface of cooling jointing. Basalt.
BP1	Brasilia-Guaíba quarry. Bom Princípio, RS	22J 0465727E / 6743260S	dendrites (mm) in the surface of the cooling jointing. Basalt.
JS1-4	Property of Jair Vargas da Silva. Santo Augusto, RS	22 J 0220370E / 6909591S	Hydrothermal breccia cemented by chrysocolla, malachite (cm – m) and native copper (massive). Basalt.
PD1	David Basso quarry Taquaruçu do Sul, RS	22J 0257078E / 6965190S	dendrites and needles (mm) in the surface of the cooling jointing. Basalt.
W247	Frederico Westphalen, RS	22J 0264402E / 6956949S	dendrites (mm) in the surface of the columnar jointing. Basalt.
VA1	Vista Alegre, RS	22J 0253121E / 6971015S	Infilling cavities in the amygdaloidal crust in basaltic flows. Basalt.
CP91	Property of Tarcísio Kummer, São Lugero community	22J 0222429E / 7002086S	Needle-shape (mm) in the surface of fracture at 92m deep (drill core). Basalt.
DC1-6	Property of Cito Taper Dionísio Cerqueira, SC	22J 0238359E / 7092896S	Dendrites (mm) in the surface of the cooling jointing. Basalt.
NZ1	Rebelatto Quarry, Palma Sola, SC	22J 0273386E / 7086059S	Dendrites (mm - cm) in the surface of the cooling jointing. Basalt.
P1C	Dalba Quarry, Francisco Beltrão, PR	22J 0300442E / 7117893S	Infilling cavities (mm) in basalt.
CP14	Petrocon Quarry, Cascavel, PR	22J 0250573E / 7233062S	Long thin blades and dendrites (2-5 cm). Surface of cooling jointing and fractures in basalt.
PQ16	Quati Quarry, Cascavel, PR	22J 0250947E / 7231785S	1. Dendrites and needle-shape (mm). Surface of cooling jointing and fractures. 2. In cavities with crystals of quartz. Basalt (Sample R2P).
FM79	Property of Agostino Munaro Realeza, PR	22J 241878E / 7149156S	Associated with hydrothermal breccia. Chrisocole and malachite (cm – m)
MS1C	Locality of Jaguaretê, Amambaí, MS.	21K 651769E / 7482158S	Dendrites (mm) on a surface of fracture at 10m deep (drill core) in basaltic andesite.
TR1	Santo Onofre quarry Terenos, MS	21K 732259E / 7738169S	Very fine dendrites (1mm) in basalt.

Table 2

Chemical analyses of host volcanic rock with native copper mineralization in the Paraná volcanic province. Oxides in wt.%, trace elements in ppm except Au in ppb. (-) = below detection limit (Cs = 0.1, Au = 0.5, Ni = 20).

Sample	FS86	BP1	JS1-4	PD1	CP91	DC2	DC6	NZ1	P1C	CP14	PQ16	MS1C	TR1
SiO_2	50.26	50.74	50.38	50.59	49.54	50.52	50.39	50.53	49.95	50.86	50.16	53.00	49.62
TiO_2	1.60	1.03	2.20	2.27	2.21	2.23	2.31	2.36	2.20	2.41	2.34	2.89	3.76
Al_2O_3	16.08	14.79	12.77	12.50	13.24	12.79	12.45	12.54	13.07	12.64	12.68	12.05	12.61
Fe_2O_3	10.82	10.89	15.35	15.83	14.67	15.31	16.21	16.15	14.30	15.51	15.52	13.95	15.20
MgO	4.79	7.85	4.91	4.80	5.64	5.01	4.83	4.79	4.73	4.58	4.74	3.86	4.38
CaO	10.36	10.40	8.71	8.74	9.90	8.95	8.78	8.68	8.84	8.84	8.84	5.50	8.38
Na_2O	2.28	1.89	2.39	2.44	2.41	2.44	2.39	2.49	2.26	2.50	2.44	2.44	2.66
K_2O	1.37	0.92	1.63	1.23	1.08	1.16	1.19	1.15	2.24	1.11	1.09	2.32	1.48
P_2O_5	0.28	0.13	0.25	0.26	0.25	0.25	0.26	0.27	0.27	0.28	0.26	0.78	0.39
MnO	0.15	0.16	0.20	0.23	0.20	0.22	0.22	0.24	0.21	0.21	0.22	0.19	0.21
Cr_2O_3	0.018	0.053	0.012	0.008	0.016	0.009	0.009	0.012	0.016	0.007	0.009	0.005	0.004
LOI	1.7	0.9	0.9	0.8	0.5	0.8	0.6	0.5	1.6	0.8	1.4	2.7	1
Total	99.75	99.75	99.72	99.72	99.69	99.71	99.62	99.71	99.72	99.73	99.72	99.65	99.67
Au	-	3.0	4.0	5.3	1.1	4.1	1.2	7.2	2.4	-	-	4.7	-
Ba	349	224	316	306	320	284	287	299	310	313	311	682	451
Ce	48.9	30.5	46,7	47.7	48.3	45	45.7	48.5	47.6	50.1	50	110.2	70.2
Co	33.9	42.2	42.6	40.6	42.2	41.4	39.2	41.5	37.7	42.6	42.9	29.2	39.1
Cs	0.9	0.4	0.4	0.3	-	0.3	0.2	-	0.5	0.3	0.3	0.4	0.3
Cu	83.0	97.7	173.20	272.7	258.6	292.2	1114.7	176.5	189.0	263.8	149.3	212.2	103.6
Dy	4.98	3.37	6.58	6.57	5.29	6.48	6.52	6.64	4.76	6.52	6.96	9.92	6.64
Er	2.62	2.03	3.96	3.75	2.93	3.68	3.89	3.94	2.71	3.58	3.62	4.83	3.52
Eu	1.52	1.06	1.78	1.80	1.78	1.81	1.78	1.87	1.65	1.76	1.86	3.41	2.48
Ga	19.2	15.2	17.6	18.9	20.2	18.9	18.1	20.1	18.6	18.6	19.3	22	21.1
Gd	5.22	3.62	6.48	6.47	5.53	6.33	6.5	6.77	5.45	6.92	6.85	10.87	7.30
Hf	4.4	2.8	4.5	4.5	4.1	4.7	4.8	4.7	3.6	5.1	4.8	8.9	6.3
Ho	0.99	0.70	1.45	1.31	1.05	1.38	1.33	1.39	0.94	1.34	1.35	1.78	1.30
La	23.5	15.3	22.5	21.6	23.4	21.3	22.4	22.7	21.5	22.3	22.2	52.9	31.0
Lu	0.35	0.28	0.51	0.55	0.37	0.52	0.52	0.53	0.38	0.52	0.51	0.66	0.43
Mo	0.4	0.2	0.9	0.6	0.3	0.3	2.1	1.5	0.5	0.5	0.4	1.5	1.3
Nb	18.4	7.4	13.4	13.1	13.9	13.1	13.3	13.6	12.9	13.8	14.2	29.4	21.5
Nd	25.6	14.3	25.3	25.3	25.2	25.5	25.8	26.0	23.6	28.2	24.7	55	36.8
Ni	64	136	57	48	67	55	56	50	42	29	34	-	37
Pb	2.3	2.1	1.2	1.7	3.2	1.3	1.9	1.5	1.5	1.6	1.9	1.7	1.8
Pr	6.03	3.69	5.94	6.10	5.94	5.82	5.91	6.01	5.70	6.18	6.05	13.5	8.77
Rb	38.3	25.3	54.7	29	21.9	23.8	24	21.9	81.4	22.8	22.3	51.1	28.3
Sc	33	36	41	40	39	41	41	41	35	39	39	27	31
Sm	5.07	3.22	5.82	5.79	5.37	5.82	5.97	5.97	5.25	5.94	6.11	11.06	7.71
Sr	339.20	221.3	253.3	264.7	382.1	246.8	244.2	244.8	338.7	255.1	262.5	416,4	470.0
Ta	1.1	0.4	0.8	0.9	0.9	0.8	0.9	0.8	0.7	0.9	0.9	1.8	1.3
Tb	0.84	0.62	1.07	1.07	0.91	1.10	1.12	1.11	0.80	1.04	1.05	1.66	1.19
Th	4.3	3.0	2.3	2.4	2.4	2.5	2.2	2.5	2.7	2.8	2.6	6.1	3.1
Tm	0.37	0.30	0.56	0.57	0.43	0.57	0.53	0.55	0.41	0.54	0.57	0.69	0.45
U	0.8	0.6	0.4	0.5	0.4	0.4	0.4	0.4	0.6	0.8	0.7	1.1	0.7
V	257	272	429	445	439	408	424	442	476	474	479	294	466
Y	25.4	19.8	34.8	37.1	26.5	32.4	34.4	34.6	25.9	36.5	35.5	47.5	33.4
Yb	2.24	1.80	3.45	3.21	2.72	3.34	3.46	3.59	2.51	3.46	3.42	4.21	2.85
Zn	47	33	54	76	87	62	73	65	91	69	58	69	66
Zr	164.3	101.1	173.4	163.2	155.6	171.6	177.9	182.4	144.3	175.3	175	347.4	246.7

Table 3
Representative microprobe analyses of native copper crystals from Paraná volcanic province (wt.%). (-) Below detection limit.

Sample	Si	Sn	S	Al	Fe	Ca	Co	Ni	Ag	Au	U	Cu	Total
FS86_36	-	0.012	0.028	-	-	0.007	0.014	-	0.041	0.003	-	99.895	100
FS86_44	-	-	0.024	-	-	-	0.002	-	0.003	0.008	0.009	99.954	100
FS86_46	-	-	0.019	-	-	0.006	0.007	0.013	0.005	-	-	99.949	99.999
BP1_17	-	0.025	0.019	-	-	0.010	0.006	0.009	0.020	0.002	0.075	99.834	100
BP1_18	-	0.014	0.023	-	0.004	0.020	0.005	0.010	0.003	0.026	0.049	99.846	100
BP1_33	-	0.015	0.029	-	-	0.002	0.008	-	0.004	-	0.009	99.933	100
JS2_A1_20	-	-	0.015	-	0.003	0.001	-	-	0.004	-	0.018	99.959	100
JS3a_51	-	0.011	0.038	-	-	0.002	0.010	0.009	0.010	0.072	-	99.848	100
JS4_A2_42	0.004	0.006	0.029	-	-	0.006	0.007	0.008	0.011	0.047	-	99.883	100.001
PD1_49	-	0.016	0.019	-	-	-	-	-	0.009	0.042	0.017	99.898	100.001
PD1_132	0.060	-	0.036	-	-	0.013	0.002	0.035	0.028	-	-	99.825	99.999
PD1_151	-	-	0.023	-	0.008	0.004	0.002	0.016	0.003	0.021	0.034	99.889	100
WW247_04	-	-	0.023	-	0.001	0.007	0.012	-	0.021	-	0.046	99.890	100
WW247_05	-	-	0.013	-	-	-	0.023	0.007	-	-	0.076	99.881	100
WW247_11	-	0.020	0.024	-	-	-	-	-	0.003	0.022	-	99.931	100
VA1a_3	-	-	-	-	0.017	0.014	0.005	-	0.007	0.001	0.027	99.929	100
VA1a_5	-	-	-	-	0.008	0.001	-	-	0.283	0.062	-	99.647	100.001
VJ1_172	-	0.043	0.020	-	-	0.001	-	0.001	0.002	0.011	-	99.922	100
CP91_101	-	-	0.024	-	0.034	0.005	0.004	0.004	0.204	0.035	0.029	99.662	100.001
CP91_106	0.005	-	0.024	-	-	0.009	-	-	0.142	-	-	99.819	99.999
CP91a_112	-	0.015	0.038	-	-	0.003	0.002	-	-	0.032	-	99.910	100
DC6_08	0.010	-	0.056	-	-	0.017	-	-	0.039	0.014	0.086	99.778	100
DC6_10	-	-	0.053	-	-	0.004	0.004	-	0.004	0.015	0.022	99.898	100
DC6_22	-	0.012	0.040	-	0.009	-	-	0.001	-	0.021	0.068	99.850	100.001
NZ1_01	0.006	0.008	0.018	-	-	0.011	0.005	-	0.007	0.015	-	99.931	100.001
NZ1_12	-	0.025	0.017	-	-	0.007	0.014	-	0.022	-	-	99.914	99.999
NZ1_24	-	0.009	0.011	-	0.002	0.003	-	-	0.002	-	0.074	99.899	100
CP14_72	-	0.012	0.039	-	-	-	-	0.003	0.006	0.056	0.054	99.830	100
CP14_77	-	-	0.039	-	-	0.002	0.005	-	0.038	0.020	0.008	99.887	99.999
CP14_80	-	0.019	0.039	-	-	-	0.010	0.044	0.020	0.029	-	99.839	100
PQ16_83	-	-	0.042	-	-	0.006	0.021	-	0.009	0.004	-	99.919	100.001
PQ16_88	-	0.012	0.027	-	-	0.001	0.015	-	0.034	0.004	0.121	99.787	100.001
PQ16_95	0.005	0.031	0.028	-	-	0.001	0.011	0.020	0.034	-	0.007	99.864	100.001
R2P_6	-	-	0.012	-	-	-	0.012	-	0.149	0.019	0.025	99.783	100
R2P_9	-	0.016	0.009	-	-	0.007	0.007	0.027	0.015	0.013	-	99.906	100
FM79_72	0.003	-	0.020	-	-	0.002	-	-	0.021	-	-	99.954	100
FM79_73	-	-	0.017	-	-	0.005	-	-	0.025	0.023	-	99.930	100
FM79_75	-	0.018	0.023	-	-	0.004	0.023	0.005	0.029	-	0.100	99.799	100.001
MS1C_57	-	-	0.015	-	-	-	0.018	-	0.009	0.026	0.082	99.850	100
MS1C_58	-	0.008	0.019	-	-	0.008	-	0.022	0.004	0.009	-	99.930	100
MS1C_61	-	0.018	0.021	-	-	0.005	-	0.011	0.042	-	-	99.903	100
TR1_11	0.404	-	0.027	0.017	0.183	0.017	0.006	0.008	0.024	0.012	-	99.302	100
TR1_17	0.218	0.005	0.023	-	0.205	0.025	-	0.012	0.010	0.005	0.031	99.465	99.999
TR1_28	-	0.012	0.022	-	0.028	0.012	-	0.015	0.011	0.024	-	99.875	99.999

Table 4

Concentrations for major and trace elements (ppm) determined by LA-ICP-MS in magnetite (MG, e.g., MG7A) and ilmenite (IL, e.g., IL1A) from the Paraná volcanic province.
* Mean value of those obtained by monitoring different isotopes. (-) Not detected.

Sample	Mg *	Al	Si	Mn	Fe *	Ni	Cu *	Zn *	Y	Zr *	Nb	Mo	Ag *	Au
BP1-MG7A	11870.39	651.22	9683.38	4084.46	374097.55	243.04	12.92	240.95	4.23	942.28	221.65	3.18	0.25	-
BP1-MG7B	11306.50	858.70	6268.29	5788.82	357339.75	200.70	83.56	220.86	1.23	770.26	199.13	3.16	0.41	0.03
BP1-MG8A	9634.95	5274.67	15509.46	3675.06	366485.10	247.57	611.94	233.11	8.11	827.11	258.00	4.67	0.32	0.06
BP1-MG9A	8300.92	12072.13	25412.47	8629.59	369100.00	290.89	131.85	219.46	2.53	499.78	115.00	4.04	0.24	0.06
CP91-MG3B	7289.66	2866.88	6100.71	7584.23	446855.00	192.04	242.46	304.27	3.85	530.35	150.83	4.65	0.24	-
CP91-MG4A	9148.21	2442.17	75123.48	3301.79	336229.75	99.07	354.06	133.42	2.66	1104.78	503.16	8.50	0.76	0.10
CP91-MG5A	5364.10	5916.96	7978.94	8237.95	524584.75	285.71	141.61	845.84	3.98	179.78	34.18	3.72	0.07	0.01
CP91-MG6A	4158.99	6679.81	5915.85	7916.62	557452.10	295.06	148.95	868.98	3.31	175.04	23.43	4.49	0.11	0.03
DC1-MG1	2417.43	7082.52	2419.79	4334.17	516630.30	165.64	677.81	1001.09	0.43	208.70	54.62	5.73	1.05	-
DC1-MG2A	6765.36	3503.74	20551.61	3484.03	463479.20	151.82	294.34	348.59	9.86	371.53	83.88	10.21	0.10	0.10
DC1-MG3A	1312.59	4563.51	2854.28	1428.87	465861.00	168.78	76.45	900.07	1.01	142.53	17.26	14.88	0.07	-
DC1-MG4A	2768.16	7607.86	3584.30	4927.98	504640.20	167.82	1907.55	1018.12	1.51	155.15	32.38	8.21	0.48	0.01
DC1-MG5A	4625.78	11685.68	26174.07	3886.66	647194.05	187.64	374.46	893.84	9.97	671.50	233.01	18.27	0.22	0.02
FS86-MG1A	4417.36	102.58	2520.06	4793.51	351084.10	61.14	25.83	367.75	1.44	789.78	395.68	5.11	0.20	0.03
JS1-MG1A	1720.01	4058.06	2391.40	3068.48	344476.80	76.80	265.57	492.50	1.63	183.91	43.51	2.88	0.07	-
JS1-MG2A	2727.37	5205.05	3500.34	3959.62	462870.75	104.28	512.94	712.11	2.51	263.03	58.32	4.52	0.15	-
JS1-MG3A	2297.80	6959.16	3492.39	2800.70	516933.00	120.22	23.15	874.69	0.05	194.49	50.16	3.04	0.14	-
NZ1-MG1A	1997.63	4891.89	2704.08	2016.63	573725.85	266.51	77.36	1151.89	1.93	164.22	9.01	12.18	0.05	-
NZ1-MG2A	3732.27	1831.81	5594.55	5496.13	362746.20	103.13	460.64	521.55	6.28	669.73	112.25	8.58	1.61	0.03
NZ1-MG3A	3599.74	3452.31	4164.21	7978.23	550806.10	139.69	737.97	653.33	9.77	816.40	232.74	11.05	1.78	0.12
P1C-MG1A	1364.01	7634.67	3288.01	4211.71	456311.45	133.59	1529.19	886.28	0.83	156.39	38.04	4.76	0.10	-
P1C-MG2A	774.45	7782.16	3966.78	11724.15	493270.35	154.85	2813.82	3733.32	9.74	201.49	32.39	3.47	0.30	-
P1C-MG3A	842.87	7921.18	3844.22	13658.85	486930.65	129.95	2493.65	2158.77	5.30	213.62	40.21	3.00	0.06	0.03
P1C-MG4A	1777.15	7838.75	2912.81	9496.48	467552.40	114.04	2319.73	963.31	2.04	191.11	36.82	3.02	0.07	-
TR1-MG1A	20600.51	9540.51	63634.19	3999.16	681561.15	177.72	26.75	514.03	24.67	72.41	0.46	15.80	0.04	0.02
TR1-MG3A	7748.78	2652.28	28962.17	940.84	282170.70	33.91	58.07	105.84	18.38	1271.87	36.73	1.49	0.23	0.01
TR1-MG4A	25703.23	20192.65	81521.07	6309.46	371604.60	38.73	76.63	409.12	17.76	1266.13	313.51	6.15	0.30	0.09
PQ16-MG1A	4635.26	7746.27	6003.37	11024.06	618917.55	227.35	9325.74	4150.34	8.05	255.84	74.96	8.77	0.19	0.01
PQ16-MG2A	2676.25	8193.82	6594.82	11460.40	624780.10	233.09	5789.60	3718.23	15.88	237.00	55.86	12.86	0.17	-
PQ16-MG3A	7942.26	18106.45	38110.55	4393.57	363644.45	55.44	977.54	97.85	24.98	439.96	150.98	5.45	0.95	0.09
PQ16-IL1A	5306.13	4732.50	3349.50	7787.20	44986.74	101.36	1810.54	1067.99	11.21	737.40	217.60	8.34	0,47	-
PQ16-IL2A	5182.75	5599.50	4296.52	8080.53	479959.15	142.87	3827.32	1867.25	5.22	495.36	136.27	8.53	0.13	0.07
PQ16-IL3A	6610.70	852.36	3940.33	3831.93	360345.85	55.86	404.87	162.26	3.49	728.82	234.20	4.29	0.34	0.02
PQ16-IL4A	4781.97	1299.79	3742.17	2920.50	364952.00	55.69	584.50	213.12	4.17	553.39	161.13	4.25	2.75	0.01

Table 5

Concentrations for major and trace elements (ppm) determined by LA-ICP-MS in clinopyroxene from the Paraná volcanic province.

* Mean value of those obtained by monitoring different isotopes. (-) Not detected.

Sample	Mg*	Al	Si	Mn	Fe*	Ni	Cu*	Zn*	Y	Zr*	Nb	Mo	Ag*	Au
BP1-P7A	141536.35	53359.37	245990	1267.15	90372.88	240.76	431.08	332.15	4.46	1.85	0.48	0.08	1.03	0.12
BP1-P8A	157808.25	41961.72	245930	1551.80	121783.75	294.09	370.42	531.35	6.61	4.94	0.56	0.10	0.41	0.10
BP1-X7A	166065.25	4754.13	246660	3453.27	152294.20	325.76	0.33	161.10	6.62	3.51	0.02	0.03	0.01	-
BP1-X8A	129395.00	9468.38	246830	1807.75	65575.68	228.44	4.88	51.75	11.37	8.52	0.08	0.03	0.01	-
CP91-PX1A	65334.58	33927.43	236380	2383.92	107825.65	91.51	120.73	129.93	34.65	183.34	6.04	0.26	0.11	-
CP91-PX2A	88467.40	9476.25	235880	3097.70	139735.80	113.21	33.65	154.17	51.47	61.06	0.73	0.10	0.09	0.03
CP91-PX3A	92164.28	10696.41	238160	2586.75	114255.60	115.77	5.55	111.59	33.74	43.42	0.40	0.05	0.02	0.07
CP91-PX4A	81419.29	8874.97	232530	2734.63	136851.85	118.39	246.48	193.44	43.27	46.43	0.75	0.02	0.02	-
DC1-PX1A	95661.67	9918.87	239970	3080.59	148463.65	149.09	281.93	124.39	30.01	26.20	1.45	-	0.02	0.04
DC1-PX2A	82270.12	13979.42	217140	2896.04	153045.45	103.24	114.24	143.14	32.14	39.01	1.43	0.09	0.03	0.03
DC1-PX3A	90429.04	6917.14	224120	3971.83	223588.50	93.56	142.88	254.36	32.99	75.02	2.20	0.10	0.02	0.01
FS86-PX1B	112293.45	9208.70	235890	1855.99	76459.51	176.20	2.31	59.83	16.45	18.15	0.11	0.09	0.04	0.03
FS86-PX2A	111194.80	8084.02	237690	2224.78	90459.28	157.27	0.72	66.69	17.25	16.20	0.07	0.01	-	0.04
FS86-PX1A	99271.33	8637.94	229530	3102.52	138954.05	116.52	0.69	125.25	31.47	33.54	0.11	0.02	-	0.01
JS1-PX1A	91487.17	8977.87	234680	3324.11	161239.35	110.33	71.87	142.18	34.52	30.94	0.51	0.13	-	0.04
JS1-PX2A	104852.85	10335.43	235920	3033.94	138768.20	138.38	29.20	122.46	24.79	41.55	0.70	0.03	-	-
JS1-PX3A	98995.52	10368.02	234540	3216.18	158255.10	129.64	169.46	174.97	39.91	39.53	1.19	0.03	0.01	0.08
NZ1-PX1A	71465.56	19700.83	234330	3292.46	171174.45	76.47	20.68	162.63	71.28	499.20	4.28	0.07	0.02	0.12
NZ1-PX2A	72988.79	8135.75	233290	3341.40	213398.25	86.88	31.34	232.62	81.49	83.46	0.65	0.19	0.09	0.05
P1C-PX1A	96665.88	10296.13	230130	2963.53	144030.90	125.19	2.62	101.63	24.08	19.87	0.09	0.05	0.04	-
P1C-PX2A	60349.99	7881.63	230370	2224.45	197251.60	48.95	7.52	82.48	42.20	87.33	2.21	0.23	-	-
PQ16-PX3A	198177.80	20413.46	505090	6911.34	371608.10	246.42	132.00	325.61	92.14	181.96	6.45	0.32	0.07	-
TR1-CX1A	88706.63	6495.36	236470	4410.53	172015.80	43.68	14.53	287.11	51.23	115.93	0.16	-	0.11	0.05
TR1-CX2A	2242.05	67841.84	290280	99.53	18100.37	1.98	5.40	26.17	28.13	361.41	5.40	0.14	0.10	0.11
TR1-PX1A	91191.04	26178.48	249620	693.71	106326.85	57.41	19.49	332.69	2.43	33.72	0.04	-	0.03	-
TR1-PX2A	42390.08	54006.23	232420	357.30	60463.19	27.75	303.02	229.84	2.37	27.64	0.02	-	0.78	0.03
TR1-PX3A	3119.33	73938.45	355700	140.22	26564.15	1.65	29.00	34.05	40.08	288.84	6.18	0.24	0.05	-
TR1-CX3A	37670.91	72456.26	266620	374.22	69176.22	46.00	121.19	282.86	15.91	84.90	-	-	0.09	-

Table 6
Concentrations for major and trace elements (ppm) determined by LA-ICP-MS in smectites from Paraná volcanic province.
* Mean value of those obtained by monitoring different isotopes. (-) Not detected.

Sample	Mg*	Al	Si	Mn	Fe*	Ni	Cu*	Zn*	Y	Zr*	Nb	Mo	Ag*	Au
CP91-SM1A	88198.91	26320.00	209130	1205.28	237432.40	265.39	1112.60	687.88	4.66	177.03	160.81	3.44	0.16	0.09
CP91-SM2A	82876.24	9584.33	212220	2265.25	104054.30	126.13	482.95	112.05	20.96	21.76	0.14	0.02	0.02	0.02
CP91-SM3A	87842.87	27167.74	248150	1374.39	249288.60	243.59	4091.46	669.77	5.00	88.18	64.28	1.61	0.66	-
CP91-SM4A	100229.40	30579.04	212890	1066.09	316092.50	305.54	630.86	809.21	21.70	5.26	2.50	4.08	0.20	0.03
CP91-SM4B	66142.06	27438.23	206200	2103.95	336416.45	131.18	4762.28	287.67	40.37	30.96	2.28	6.00	1.67	0.02
CP91-SM5A	31850.77	52382.26	209060	551.50	60142.44	59.24	190.31	134.20	9.00	302.01	1.43	0.02	0.09	-
CP91-SM6A	25503.02	97148.11	242380	265.24	55655.67	63.39	123.75	183.44	1.30	10.20	0.17	0.11	0.09	-
CP91-SM8A	100096.05	45158.48	224400	1816.50	368656.80	253.69	286.12	768.02	50.60	57.31	23.12	2.60	0.10	-
DC1-SM1A	94263.07	32709.43	235590	531.11	164372.30	109.33	284.39	151.87	4.32	4.06	0.46	-	0.04	0.02
DC1-SM2A	69101.69	36433.94	241060	716.28	317823.35	94.10	265.81	175.67	29.36	65.39	4.59	0.33	0.06	-
DC1-SM3A	78433.92	25941.38	225330	186.12	168162.15	79.78	26.15	104.28	1.47	1.91	0.03	0.04	0.02	-
DC1-SM4A	104537.70	29089.91	247470	333.76	153266.05	122.10	122.54	156.70	1.42	2.04	0.01	-	0.02	0.03
DC1-SM5A	56176.81	41359.48	237650	193.64	136983.65	67.51	301.23	94.92	5.47	8.01	0.73	0.09	-	0.03
DC1-SM6A	77263.83	24561.76	234900	507.46	409074.60	88.05	115.87	117.11	24.52	15.50	1.38	0.52	0.01	0.07
DC1-SM7A	82568.08	27313.19	260570	530.36	176470.90	82.45	10.91	113.21	1.98	0.93	0.02	0.04	-	0.04
FS86-SM2A	99441.63	28595.55	206790	1951.50	147589.95	88.24	132.25	500.86	2.75	4.98	0.42	0.04	0.54	-
FS86-SM3A	94754.79	34584.33	199860	2015.70	146633.90	74.87	703.60	485.41	14.70	25.60	0.55	0.02	1.84	0.05
FS86-SM4A	88661.49	26021.87	204530	1826.83	128420.65	80.55	281.35	436.95	74.31	7.54	0.38	0.05	0.38	-
FS86-SM6A	94049.62	34098.71	207440	1347.25	131606.05	72.65	1.51	444.06	1.74	1.32	0.27	0.02	0.05	-
FS86-SM1A	84943.33	25927.05	213970	7817.47	1456004.50	299.60	31.91	558.65	89.65	2.09	0.01	6.97	0.08	0.03
JS1-SM1A	47029.01	13954.88	256490	1192.32	189957.55	35.79	27.71	394.47	0.57	0.29	0.24	-	0.01	0.05
JS1-SM2A	49292.06	21077.07	263770	640.43	187412.30	54.72	86.78	335.45	12.42	4.93	1.45	0.05	0.01	0.01
JS1-SM3A	47228.33	22432.53	258750	525.25	171480.60	71.63	215.63	346.23	37.91	9.71	0.97	-	0.03	0.01
JS1-SM4A	46311.74	18682.91	257200	744.79	174960.75	49.43	130.53	339.03	3.05	4.79	1.39	0.03	0.02	-
NZ1-SM1A	77096.25	35065.00	209430	609.94	182802.85	79.16	33.07	196.11	2.22	0.74	0.05	-	0.09	0.14
NZ1-SM2A	71408.06	41256.06	219690	738.13	157341.20	75.72	37.15	186.49	16.81	18.73	0.11	0.12	0.02	0.09
NZ1-SM3A	76792.17	43701.30	212860	513.21	130995.80	82.18	112.47	190.86	1.65	0.19	0.03	-	0.01	-
PQ16-SM1A	31324.29	72087.41	454530	79.94	200417.65	15.91	363914.65	12.21	162.58	1.22	0.02	-	0.11	-
PQ16-SM2A	43500.74	102686.80	490130	84.98	416691.10	20.52	87330.32	35.28	29.67	0.96	0.01	0.15	0.04	0.09
PQ16-SM3A	10242.33	23411.78	216010	55.18	14309.23	4.58	347389.90	4.42	167.87	0.07	-	-	0.19	0.06
PQ16-SM3Ax	24253.76	55438.90	511510	130.68	33884.14	10.84	822616.55	10.47	397.52	0.17	0.01	-	0.45	0.14
PQ16-SM4A	168338.25	39785.64	495740	6717.36	383870.45	316.95	356.93	357.26	113.61	576.01	32.07	2.86	0.18	-
PQ16-SM4B	224147.80	76839.52	479410	333.24	271796.05	358.36	11280.70	313.61	4.57	4.90	0.05	-	0.06	-
PQ16-SM5A	139059.50	68053.25	525410	1031.84	413762.35	236.56	440.66	244.30	27.41	75.58	5.21	1.84	0.22	-
TR1-SM1A	66182.55	26490.88	214710	2984.29	766474.60	90.53	424.83	684.18	64.51	32.91	1.30	1.47	0.05	0.03
TR1-SM2A	70515.35	6906.89	198520	3721.51	188065.50	42.14	25.40	263.27	47.96	57.53	0.25	0.12	0.01	-

Table 7

Results of Femtosecond-laser ablation Cu isotope measurement.
Paraná volcanic province. NIST-SRM 976 Cu standard. Plotted in Figure 11.

Sample	Type	$\partial\ ^{65}Cu/\ ^{63}Cu$ (‰)	$2\sigma\ \partial\ ^{65}Cu$ (‰)
FS86a	Nat Cu dendrite	-0.83	± 0.05
FS86a		-0.86	± 0.05
FS86a		-0.91	± 0.06
FS86a		-0.88	± 0.05
FS86a		-0.59	± 0.05
FS86b	Nat Cu dendrite	0.09	± 0.05
FS86b		0.02	± 0.05
BP1	Nat Cu dendrite	0.37	± 0.05
BP1		0.44	± 0.05
BP1		0.47	± 0.05
JS3a	Native Cu massive	0.10	± 0.05
JS3a		0.10	± 0.04
JS3a		0.13	± 0.05
JS3a		0.22	± 0.05
JS3a		0.17	± 0.05
JS3b	Chrysocolla	-0.27	± 0.05
JS3b		-0.34	± 0.05
JS3b		-0.33	± 0.05
JS4a	Nat Cu massive	0.62	± 0.04
JS4a		0.63	± 0.04
JS4a		0.69	± 0.05
JS4a		0.65	± 0.05
JS4b	Cuprite (rim)	0.12	± 0.04
JS4b		0.10	± 0.04
JS4b		0.73	± 0.05
JS4b		0.32	± 0.04
JS4b	Cuprite (core)	0.16	± 0.04
JS4b		0.21	± 0.04
JS4c	Nat Cu massive	1.07	± 0.04
PD1a	Nat Cu dendrite	0.70	± 0.05
PD1a		0.71	± 0.04
PD1b	Nat Cu dendrite	1.14	± 0.05
PD1b		1.18	± 0.05
W247a	Nat Cu dendrite (rim)	-0.20	± 0.05
W247a		-0.16	± 0.05
W247a		-0.05	± 0.05
W247b	Nat Cu dendrite (core)	0.37	± 0.05
DC6	Nat Cu dendrite	1.09	± 0.04
DC6		1.09	± 0.05
DC6		1.11	± 0.05
NZ1	Nat Cu dendrite	0.47	± 0.06
NZ1		0.48	± 0.06
NZ1		0.51	± 0.05
P1C	Nat Cu dendrite (rim)	0.32	± 0.05
P1C		0.37	± 0.05
P1C		0.37	± 0.05
P1C		0.42	± 0.05
P1C		0.31	± 0.04
P1C	Nat Cu dendrite (core)	0.36	± 0.04
P1C		0.43	± 0.05
P1C		0.41	± 0.04
P1C		0.38	± 0.04
CP14a	Nat Cu blades (mm)	0.57	± 0.04
CP14a		0.62	± 0.05
CP14a		0.53	± 0.04
CP14a		0.55	± 0.05
CP14b	Nat Cu dendrite (cm)	1.89	± 0.05
CP14b		1.50	± 0.05
CP14b		1.51	± 0.05
R2P	Nat Cu dendrite with quartz	0.55	± 0.04
R2P		0.56	± 0.04
R2P		0.51	± 0.04
R2P		0.64	± 0.04
R2P		0.61	± 0.04

Table 8

Copper isotopic data of native copper from hydrothermal and supergene deposits from USA. Plotted in Figure 11.

Sample ID	Mineral	Locality	Deposit type	∂^{65}Cu (‰)	Reference
85	Nat. Cu	Soudan mine, Minnesota, USA		0.9	Shields et al. (1965)
88	Nat. Cu	Lake Superior district, Michigan, USA	Hydrothermal	-1.0	Shields et al. (1965)
90	Nat. Cu	Painesdale, Michigan, USA	Hydrothermal	-1.3	Shields et al. (1965)
OUM 15126	Nat. Cu	Michigan, USA	Hydrothermal	0.45	Zhu et al. (2000)
OUM 15120	Nat. Cu	Lake Superior, USA	Hydrothermal	0.54	Zhu et al. (2000)
LS-7	Nat. Cu	Trimountain Mine, Michigan, USA	Hydrothermal	0.27	Larson et al. (2003)
LS-10	Nat. Cu	Baltic Mine, Michigan, USA	Hydrothermal	0.29	Larson et al. (2003)
LS-12	Nat. Cu	Centennial Mine, Michigan, USA	Hydrothermal	0.26	Larson et al. (2003)
LS-45	Nat. Cu	Isle Royale Mine, Michigan, USA	Hydrothermal	0.34	Larson et al. (2003)
LS-48	Nat. Cu	Wolverine Mine, Michigan, USA	Hydrothermal	0.30	Larson et al. (2003)
LS-51	Nat. Cu	Copper Falls Mine, Michigan, USA	Hydrothermal	0.02	Larson et al. (2003)
	Nat. Cu	Ray Mine, Arizona, USA	Supergene	-3.03	Maréchal et al. (1999)
OUM 22647	Nat. Cu	Bisbee, Arizona, USA		-0,2	Zhu et al. (2000)
Ray-1	Nat. Cu	Ray Mine, Arizona, USA	Supergene	-0.04	Larson et al. (2003)
Ray-2	Nat. Cu + cuprite	Ray Mine, Arizona, USA	Supergene	1.26	Larson et al. (2003)
Ray-2b	Nat. Cu	Ray Mine, Arizona, USA	Supergene	0.72	Larson et al. (2003)
Arizona Cu	Nat. Cu	Morenci, Arizona, USA		-0.51	Ikehata et al. (2011)
Mio 7-4	Nat. Cu	Mio Mine Sanbagawa Met. Belt Japan	Supergene	1.57	Ikehata et al. (2011)
Mio 7-5	Nat. Cu	Mio Mine Sanbagawa Met. Belt Japan	Supergene	1.71	Ikehata et al. (2011)
Mio 7-6	Nat. Cu	Mio Mine Sanbagawa Met. Belt Japan	Supergene	1.65	Ikehata et al. (2011)
Mio 7-7	Nat. Cu	Mio Mine Sanbagawa Met. Belt Japan	Supergene	1.62	Ikehata et al. (2011)
Mio 8-4	Nat. Cu	Mio Mine Sanbagawa Met. Belt Japan	Supergene	1.45	Ikehata et al. (2011)
Mio 8-5	Nat. Cu	Mio Mine Sanbagawa Met. Belt Japan	Supergene	1.54	Ikehata et al. (2011)
Mio 8-6	Nat. Cu	Mio Mine Sanbagawa Met. Belt Japan	Supergene	1.43	Ikehata et al. (2011)
Mio 8-7	Nat. Cu	Mio Mine Sanbagawa Met. Belt Japan	Supergene	1.56	Ikehata et al. (2011)

Artigo 2

SILICA GOSSAN AS A PROSPECTIVE GUIDE FOR AMETHYST GEODE DEPOSITS IN THE AMETISTA DO SUL MINING DISTRICT, PARANÁ VOLCANIC PROVINCE, SOUTHERN BRAZIL

Artigo submetido ao Journal of Geochemical Exploration

Assunto:**Acknowledgement of receipt of your submitted article**
Remetente: gexplo-eo@elsevier.com
Para: sergio.baggio@ufrgs.br
Data: February 9, 2015

Dear Mr. Baggio,

Your submission entitled "Silica gossan as a prospective guide for amethyst geode deposits in the Ametista do Sul mining district, Paraná volcanic province, southern Brazil" (Research Paper) has been received by Journal of Geochemical Exploration

Please note that submission of an article is understood to imply that the article is original and is not being considered for publication elsewhere. Submission also implies that all authors have approved the paper for release and are in agreement with its content.

You will be able to check on the progress of your paper by logging on to http://ees.elsevier.com/gexplo/ as Author.

Your manuscript will be given a reference number in due course.

Thank you for submitting your work to this journal.

Kind regards,

Journal management
Journal of Geochemical Exploration

Assunto: **GEXPLO3977 - Notice of manuscript number**
Remetente: gexplo-eo@elsevier.com
Para: sergio.baggio@ufrgs.br
Data: February 10, 2015

Dear Mr. Baggio,

Your submission entitled "Silica gossan as a prospective guide for amethyst geode deposits in the Ametista do Sul mining district, Paraná volcanic province, southern Brazil" has been assigned the following manuscript number: GEXPLO3977.

You will be able to check on the progress of your paper by logging on http://ees.elsevier.com/gexplo/ as Author.

Thank you for submitting your work to this journal.

Kind regards,
Journal of Geochemical Exploration

Title: Silica gossan as a prospective guide for amethyst geode deposits in the Ametista do Sul mining district, Paraná volcanic province, southern Brazil

Authors: Sérgio Benjamin Baggio[a*], Léo Afraneo Hartmann[a], Hans-Joachim Massonne[b], Thomas Theye[b], Lucas Machado Antunes[a]

[a] Instituto de Geociências, Universidade Federal do Rio Grande do Sul, Avenida Bento Gonçalves, 9500 Agronomia; 91501-970 Porto Alegre, Rio Grande do Sul, Brazil

[b] Institut für Mineralogie und Kristallchemie, Universität Stuttgart, Azenbergstr. 18; 70174 Stuttgart, Deutschland

E-mail addresses:

Sérgio Benjamin Baggio sergio.baggio@ufrgs.br

*Corresponding author. Telephone +55-51-33087202; fax +55-51-33087203

Léo Afraneo Hartmann leo.hartmann@ufrgs.br

Hans-Joachim Massonne h-j.massonne@mineralogie.uni-stuttgart.de

Thomas Theye thomas.theye@imi.uni-stuttgart.de

Lucas Machado Antunes lucas.antunes@live.com

Silica gossan as a prospective guide for amethyst geode deposits in the Ametista do Sul mining district, Paraná volcanic province, southern Brazil

Sérgio Benjamin Baggio[a*], Léo Afraneo Hartmann[a], Hans-Joachim Massonne[b], Thomas Theye[b], Lucas Machado Antunes[a]

[a] Instituto de Geociências, Universidade Federal do Rio Grande do Sul, Avenida Bento Gonçalves, 9500 Agronomia; 91501-970 Porto Alegre, Rio Grande do Sul, Brazil

[b] Institut für Mineralogie und Kristallchemie, Universität Stuttgart, Azenbergstr. 18; 70174 Stuttgart, Deutschland

ABSTRACT

A new frontier of amethyst geode deposits (amethyst, agate, gypsum, calcite and zeolites) driven by the prospective guides termed silica gossan may change the metallogenetic scenario previously known in the Paraná volcanic province, Brazil. The silica gossans are present throughout the province and occur in basalt, basaltic andesite and rhyodacite. In this study, we focus on the Ametista do Sul mining district, Rio Grande do Sul, Brazil, the largest producer of amethyst geodes in the world (400 t/month). Veia Alta flow is the main amethyst producer in the district. A silica gossan occurs in the Coogamai flow above the Mina do Museu, at the top of the mineralized flow. The Coogamai is a basalt (47.87 wt. % SiO_2) with columnar jointing, intermediate-Ti Paranapanema magma type (2.25 wt.% TiO_2 and Ti/Y = 416.2). The prospective guide displays polygonal shape associated with increase of clay minerals at the surface, concentration of iron oxides and the presence of silicified sandstones, in addition to marshes with ponds; a change in color (ocher to brownish) at the surface and the vegetation type are observed. The gamma spectrometry survey (counts per second) at Mina do Museu silica gossan shows negative anomalies in %K, eU and eTh above the amethyst deposits, with values of 55 cps outside silica gossan and 43 cps within the silica gossan. These anomalies are associated with a combination of factors that began in the hydrothermal events and ended with the weathering of the silica gossans. The bulk rock analyses within the silica gossan show values of loss on ignition up to 1.8

wt.% while outside the silica gossan this value is around 0.5 wt.%. SiO_2, K_2O, MgO, CaO and Na_2O display negative correlation with loss on ignition. X-ray diffraction identified the presence of montmorillonite and kaolinite in the soil of the silica gossan. EMPA in the bulk rock of Coogamai flow identified dioctaehdral and trioctahedral interlayered smectite. Mg-smectite is present in the samples within silica gossan while K-smectite is present outside silica gossan.

1. Introduction

The Ametista do Sul mining district in the Serra Geral Group, Paraná volcanic province, is located in the northwest portion of Rio Grande do Sul state, Brazil (Fig. 1) and has the largest amethyst geode deposits in the world, with a production of 400 t/month (Silva, 2010) . Silica gossans occur above all known deposits in the district and are an important prospective guide for the discovery of new deposits.

The classification of gossans is usually referred to deposits of metallic minerals (Pirajno, 2009; Scott, 2001) generated in a sulphide-rich environment and characterized by high concentrations of iron, silica and intense colors. In a specific way, the volcanic rocks of the province were generated in an intraplate environment, with low sulfur contents. This situation is unprecedented, because little information is available in the scientific literature on the occurrence of gossans in other similar volcanic provinces. Gossans were described for the first time in the southern portion of the Paraná province by Pertille et al. (2013) in Quaraí (Brazil) and Artigas (Uruguay) mining districts. The term silica gossan (Baggio et al., 2014) is used based on the similar characteristics of the gossans related to sulphides and in the silicification of the sand layers brought from Botucatu formation by the hydrothermal events. The Botucatu formation is Jurassic-Cretaceous aeolian sandstone (dune fields) from Paraná sedimentary basin which was

covered by lava flows of Paraná volcanic province and currently belongs to the Guarani aquifer system. Previous studies (Keller and Hanson, 1968; Sayin, 2007) used the term silica gossan to define hydrothermal prospective guides for kaolin.

The origin of silica gossans in the province is associated with unique geological features in the province. The large extension of the Botucatu Formation was covered by lava flows with internal structure of type I massive cores (Gomes, 1996) and thickness between 10 and 30 m that provided the transformation of a sand desert into one of the largest confined aquifers in the world: the Guarani aquifer. The Cretaceous volcanism was the heat source to boil the water from the Guarani aquifer and generate the H1, H2 and H3 hydrothermal events (Hartmann, 2008; Hartmann et al., 2010). These events altered the volcanic pile and triggered the formation of sandstone sills and dikes, basalt-sandstone breccia, amethyst epigenetic deposits and the intense silicification along the chimneys where the hydrothermal fluids percolated. The silica gossans have their origin associated with these hydrothermal events, and their structure was highlighted at the surface during the Quaternary by weathering, leaching and erosional processes. These geological controls explain the presence of these structures in the Paraná volcanic province and the lack of citation of these structures in other provinces in the world.

Because of the great economic significance of the geode deposits in the Ametista do Sul district, we conducted a survey to identify the silica gossans and their characteristics. We used mostly field mapping, field gamma spectrometry, petrography, rock geochemistry, X-ray diffraction and electron microprobe analyses of minerals. The integration of the data resulted in an advanced understanding of processes related to silicia gossan formation for their use as prospective guides of additional deposits in the Paraná volcanic province.

2. Regional Geology

The Lower Cretaceous Paraná volcanic province is the second largest province in the world covering an extensive area in southern Brazil, Uruguay, eastern Paraguay and northern Argentina. The thickness of the lava pile is correlated with the shape of the Paraná Basin. In the southern and northern boundaries only a few meters (Almeida, 1986) of lava flows occur, whereas in the center near Cuiabá Paulista the thickness reaches 1723 m in depth, with more than a hundred lava flows in the volcanic pile (Hartmann, 2014). The total area covered by the volcanic rocks is around 917,000 km^2 (Frank et al., 2009). The tholeiitic basalts represent the main chemical composition, however basaltic andesite, dacite, rhyodacite, andesite, rhyolite and pyroclastic rocks (Licht et al., 2012) also occur. These rocks were divided into a low-Ti (<2 wt. % TiO_2) and high-Ti (>2 wt. % TiO_2) group (Bellieni et al., 1984; Mantovani et al., 1985). Based on major and trace elements and ratio of elements, Peate et al. (1992) reclassified the low-Ti group into Gramado, Esmeralda and Ribeira magma-types and the high-Ti group into Pitanga, Paranapanema and Urubici magma-types. The intermediate-Ti group was proposed by Nakamura et al. (2003) and includes the Ribeira and Paranapanema magma-types. The high and low-Ti groups stayed with the remaining magma-types. Studies conducted by Licht and Arioli (2012) reassessed this geochemical division and suggested at least 12-16 chemical types. Initially the stratigraphy of the flows indicated the presence of low-Ti lavas at the base, high-Ti lavas in the center and intermediate-Ti lavas at the top; however with the evolution of the studies the intercalation of flows does not follow this model in all cases (Hartmann, 2014). The amethyst-bearing geodes in the Paraná volcanic province occur in the low-Ti, intermediate-Ti and high-Ti flows (Duarte et al., 2009; Gilg et al., 2003; Hartmann et al., 2014a; Juchem, 2010, 2014; Rosenstengel and Hartmann, 2012), and their occurrence was described in several

mining districts such as Ametista do Sul, Entre Rios and Chopinzinho in Brazil, Los Catalanes in Uruguay and Wanda in Argentina. Studies developed in some of these districts have characterized the geology of the host basalts and discussed the origin of deposits. One theory of amethyst geode deposits was attributed to lava degasification, suggesting temperatures of 1150 ºC for the formation of the cavities (Gilg et al., 2003; Morteani et al., 2010; Proust and Fontaine, 2007; Scopel et al., 1990). A study of Sr isotopes in celadonite (Gilg et al., 2003) indicated the beginning of filling of geodes at 20–30 Ma after basalt eruption (Gilg et al., 2014) and was originated by repeated injections of low- temperature sedimentary brines from deeper levels of the Paraná basin. The amethyst crystallization occurred at temperature between 40 - 80 °C (Gilg et al., 2003, 2014). In a different way, a hydrothermal model was proposed (Duarte et al., 2009, 2011, 2014) based on the H1, H2 and H3 hydrothermal events (Hartmann, 2008, 2012a, 2012b). The authors suggested the rising of hydrothermal fluids (boiling water and its vapor) with huge quantity of sand from the Botucatu Formation across the basaltic flows. As a result of hydrothermal processes, cavities were formed initially by ballooning (Hartmann et al., 2012d) followed by the epigenetic amethyst deposits (Duarte et al., 2009, 2014). In the same process, the silicified hydrothermal structures (sandstone dikes, sandstone layers and even hydrothermal breccia at the top of the flows) were also formed.

In the study area of Mina do Museu, the amethyst geode deposits are hosted in three different Pitanga type I (Gomes, 1996) high-Ti flows. From bottom to the top they are the Veia Baixa (~30 m tick), Veia do Meio (~20 m thick) and Veia Alta flow (~25 m thick) flows. The Veia Alta flow is the main amethyst producer in the district. The Coogamai flow is a barren Paranapanema intermediate-Ti flow and occurs above the Veia Alta flow. The Coogamai flow has type II core and cooling joints. The thickness of

this flow at the Mina do Museu area is 35 m but its top was eroded. However the Coogamai flow shows larger thicknesses in other areas of the mining district. Coogamai is the uppermost flow in the Mina do Museu section and displays the presence of silica gossan similar to descriptions in the Quaraí-Artigas mining district (Pertille et al., 2013) and other places (e.g., Gramado, RS) along the Paraná province (Baggio et al., 2014). The hydrothermal alteration and the weathering processes generated these structures over the amethyst deposits. The satellite image from Mina do Museu silica gossan displays a geometric structure and the different geological characteristics of the amethyst geode deposit. Studies on silica gossan were applied in the municipality of Quaraí, RS for the indication of preferred areas for exploration of amethyst geode deposits (Hartmann et al., 2014b).

3. Methodology

The study developed in the Ametista do Sul mining district was focused in the Mina do Museu, an exhausted amethyst mine turned into a museum that still retains amethyst geodes in the host basalt galleries. The genetic model assumed in this study is that described by Duarte et al. (2009, 2011, 2014). Several areas in the surroundings were visited aiming at the comparison between them. Two volcanic flows were evaluated, the Coogamai flow with the silica gossan and the Veia Alta flow, amethyst producer. The Coogamai flow is the target of this study while Veia Alta flow was used for geochemical, petrographic and gamma spectrometric comparison. The applied methodology included the assessment of altimetry and geographic coordinates with a Garmin portable GPS (Datum WGS84), description of rock outcrops and sample collection in the Coogamai flow (n=10) and Veia Alta flow (n=9). Two of the samples

175 from Coogamai flow (A3A and A1) were previously published by Rosenstengel and
176 Hartmann (2012) and used in this study for geochemical comparison.
177 The petrographic description and optical images were performed in a Zeiss
178 axioplan microscope with ProgRes Jenoptik C10 digital photographic device. The
179 chemical analyses of the bulk samples were performed by ACME Analytical
180 laboratories, Vancouver, Canada for whole rock major and trace elements. The method
181 for elemental analyses was ICP (Inductively Coupled Plasma). For major elements the
182 method comprises melting of 0.1 g sample in metaborate / lithium tetraborate and
183 dilution with nitric digestion. The loss on ignition is obtained from the weight
184 difference after combustion at 1000 °C. Trace elements and rare earths are analyzed by
185 ICP-MS (mass spectrometry), following the same procedure of the major elements with
186 the addition of 0.5 g sample digested in aqua regia for analysis by ICP-MS.
187 For the gamma spectrometry survey in the Coogamai flow and Veia Alta flow,
188 two different field techniques were used. The first included the readings of the gamma
189 spectrometry in surface sections over the Coogamai and Veia Alta flows (heterogeneous
190 material including soil, altered and fresh rocks) and the second was made exclusively in
191 the Veia Alta flow through an old gallery of amethyst extraction in the Mina do Museu.
192 The devices used were the Exploranium GR110 scintillometer (measurement time 10 s)
193 and RS-125 Gamma spectrometer (measurement time 60 s) with NaI detector crystal.
194 The size of NaI crystal is 74 cm^3 and 103 cm^3 respectively. The readings of GR-110
195 display lower values (in counts per second, cps), but are equivalent to the measurements
196 of the RS-125 which allowed managing the work and testing the similarity of the
197 responses. The GR-110 was used to record the total counting of gamma radiation from
198 the rocks and the RS-125 was used for evaluation of the contents and distribution of
199 each radionuclide, %K (mean percent potassium), eU (equivalent uranium in parts per

200 million, ppm) and eTh (equivalent thorium in ppm). The values presented in this study
201 represent the average of 5 measurements in each station. The data were used to generate
202 a cps gamma spectrometric contour map with the software Oasis Montaj® (Geosoft
203 Latinoamerica) and also for the graphs of total cps using the Excel® software.

204 X-ray diffraction was performed to identify the clay minerals present in the soil
205 at the surface of the Mina do Museu silica gossan. The clay samples were prepared with
206 particle size smaller than 4 μm. The preparation and separation of this fraction involves
207 quartering the sample, crushing in porcelain mortar. After addition of deionized water,
208 the samples were stirred for 24 h in an orbital shaker and treated with an ultrasound
209 probe during 5 minutes. The settling time for the fraction <4 μm in a water column was
210 set according Stokes' law at constant temperature. The fractions <4 μm sample fractions
211 were prepared on three glass slides with preferred (001) orientation of the clay minerals.
212 The glass slide 1 was prepared to air dry at room temperature. An oriented glycol
213 preparation was saturated with ethylene glycol to verify the presence of expansive clay
214 mineral, and the third glass slide was heated at 550 °C for 2 h (calcined) to test for clay
215 collapse under these conditions. The equipment used is a BRUKER AXS diffractometer
216 SIEMENS Model D5000 with 2θ goniometer of Universidade Federal do Rio Grande
217 do Sul. The radiation was copper Kα produced at 40 kV and 25 mA. The speed and
218 range of the goniometer scan for oriented samples were 2-3 s/0.02° 2θ in the range of 3°
219 to 28° 2θ.

220 The mineral compositions were measured with an wavelenght-dispersive
221 electron microprobe Cameca SX100 at Institute für Mineralogie und Kristalchemie of
222 Universität Stuttgart, Germany. The routine measurement protocol used for silicates
223 was 15 kV accelerating voltage, 15 nA beam current and focused beam. For clay
224 minerals, a lower beam current of 10 nA and larger beam size of 10 μm were applied. In

addition to the EMP investigation, back-scattered electron images and compositional maps of Mg, Al, Fe, Ca and Na were made to evaluate the compositional variation of smectite in different structural sites. Mineral formulae have been calculated with the Microsoft Excel based CalcMin software (Brandelik & Massonne 2004).

4. Results

Several basalt flows were mapped in the Ametista do Sul mining district (Fig. 2A) with the Mina do Museu area located in the center of the district; previous flow stratigraphy was determined by Rosenstengel and Hartmann (2012). The recognized flows are the A5 flow, Veia Baixa flow, Veia do Meio flow, Veia Alta and the Coogamai flows from bottom to top of the hills (Fig. 2B). During field work, hydrothermal breccias and silicified sandstone layers were also described; these are small bodies, not located in Fig. 2. Several results are now described, including the petrography, rock geochemistry, gamma spectrometry, X-ray diffraction and electron microprobe analyses.

4.1 Petrography

The primary minerals of Veia Alta and Coogamai flows is practically the same and the main difference between flows is the occurrence of alteration minerals (clay minerals) which is larger in the Veia alta flow. The Coogamai flow contains plagioclase (44-48 vol.%), clinopyroxene (augite and pigeonite, 23-27%), opaque minerals (magnetite and ilmenite, 10-14%), microcrystalline matrix (quartz, plagioclase and K feldspar, 5-9%), clay minerals (smectites, 2-8%) and traces of apatite. Samples LF1 and LQ1 are located outside of the silica gossan and display holocrystalline texture with microphenocrysts of plagioclase. The main texture is intergranular but in some places

glomeroporphyritic. The intergranular texture is formed by subhedral to euhedral elongated prisms of plagioclase phenocrysts (0.1-0.3 mm-size) associated with subhedral to anhedral crystals (≤0,2 mm) of clinopyroxene and rounded to subhedral crystals (≤0,2 mm) of magnetite – ilmenite. The glomeroporphyritic texture is formed mainly by plagioclase crystals surrounded by opaque minerals. In some areas, the plagioclase crystals reach up to 0.5 mm in size. Apatite is an accessory mineral and occurs as fine needle-shaped crystals. The samples B1, MM90 and MM95 within the silica gossan, shows a holocrystalline and microporphyritic texture. The content of smectite outside silica gossan (Fig. 3A, B) is comparatively less than within silica gossan. The intergranular texture is formed by subhedral to euhedral elongated plagioclase crystals (0.2-0.4 mm) in association of anhedral to euhedral clinopyroxene crystals (0.1-0.3 mm) and rounded opaque minerals (0.1-0.3mm). In some places, microphenocrysts (0.5-0.7 mm) of opaque minerals with skeletal habit are observed. The partial alteration of magnetite and clinopyroxene is highlighted by areas with red and brown stains surrounding the crystals and also in the extreme cases with formation of smectites with 0.5-0.8 mm size within silica gossan (Fig. 3C, D).

The Veia Alta flow is composed of plagioclase (36-40 vol.%), clinopyroxene (18-24 %), opaque minerals (8-13 %), microcrystalline matrix (2-7 %), clay minerals (20-30 %) and traces of apatite. The basalt is holocrystalline and microporphyritic with intergranular texture and microcrystalline matrix. The elongated plagioclase phenocrysts are euhedral to subhedral (up to 0.7 mm size) and the clinopyroxene phenocrysts are present in minor amounts. The intergranular texture is composed of subhedral to euhedral plagioclase crystals (0.2 - 0.5 mm). The subhedral clinopyroxene crystals are small (0.1-0.4 mm) and often with partial alteration in the rims. The opaque minerals show platy shape (up to 0.9 mm size) and also lozenge subhedral crystals (0.1

– 0.4 mm). The microcrystalline matrix presents quartz, plagioclase and KF in the interstices forming intersertal texture and has areas altered to clay minerals. Apatite is a needle-shaped accessory mineral. In the Veia Alta flow the formation of smectites (brown to orange color) are widely distributed and the presence of celadonite (green pockets) was observed only in this amethyst mineralized flow (Fig. 3E, F).

4.2 Rock geochemistry

The analyzed samples from the Ametista do Sul mining district represent the Coogamai flow (both outside and within Mina do Museu Silica gossan) and the Veia Alta flow. The location and chemical analyses are available in Tables 1 and 2.

Both lava flows are classified as basalt according to the total alkalis-silica (TAS) diagram (Fig. 4A; Cox et al., 1979). The Coogamai flow plots in the intermediate-Ti group (Nakamura et al., 2003) as a Paranapanema magma type (Peate et al., 1992, 1997, 1999) with TiO_2 content ranging from 2.23 - 2.34 wt.% and P_2O_5 contents from 0.27 - 0.29 wt.% (Fig. 4B, C). The Veia Alta flow belongs to the high-Ti group and displays Pitanga magma-type (Peate et al., 1992). TiO_2 content varies from 3.54 - 3.76 wt.% and P_2O_5 contents range from 0.52 - 0.57 wt.% (Fig. 4B, C). The identification and individualization of the magma-types is observed also from the distribution of TiO_2 and P_2O_5 contents and low-mobility elements Th, Hf, Nb, Y, Pr, Ce, Ta, La and Zr.

Several studies conducted in the southern portion of the Paraná volcanic province (e.g., Duarte et al., 2009; Hartmann, 2008; Hartmann et al., 2010, 2012a, 2015; Meunier et al., 1988; Pinto et al., 2011b; Rosenstengel and Hartmann, 2012) highlighted the concept of the amethyst-bearing geodes genesis based on a hydrothermal model. For instance, in the Veia Alta and Coogamai flows the hydrothermal alteration, represented by LOI is the main parameter for evaluation of the volcanic rocks and an important

amethyst prospective guide. The LOI and SiO_2 contents show negative correlation in both flows (Fig. 4D). The SiO_2 content for Coogamai flow ranges from 47.43 wt.% to 49.87 wt.% and the LOI varies from 0.2 to 0.5 wt. % for samples outside silica gossan and 0.9 wt.% to 1.8 wt.% for samples within silica gossan. In the Veia Alta flow, the SiO_2 variation is between 46.38 wt.% and 50.54 wt.% and the LOI ranges from 3.1 wt.% to 5.2 wt.% showing the expected correlation between hydrothermal alteration and the geode deposits origin (Duarte et al., 2009). However some studies (e.g., Duarte et al., 2011; Hartmann et al., 2010; Pertille et al., 2013; Rosenstengel and Hartmann, 2012) suggested that the hydrothermal alteration indicated by the LOI (>2 wt. %) can limit the reliability of the classification of the volcanic rocks, especially in cases where the separation of the flows uses small variations in the TiO_2 and P_2O_5 content and immobile trace elements (e.g., Zr and Hf). In this study, this restriction does not apply because the study focuses on only two, geochemically distinct flows. Furthermore, in the case of Veia Alta flow there is a strong field control across the amethyst gallery and also the gamma spectrometry, allowing confirm the stratigraphic position and chemical characteristics of each flow in the district.

The evaluation of the LOI indicates a gradual transition between areas with silica gossan and areas without such alteration. The negative correlation with LOI and the contents of SiO_2, K_2O (Fig. 5A), Rb and U are similar to the observations by Pertille et al. (2013) in gossans of Quaraí-Artigas region. Additionally, in the Mina do Museu silica gossan, a negative correlation of LOI was observed with the contents of MgO (Fig. 5B), CaO (Fig. 5C) and Na_2O (Fig. 5D). Despite of the increase in LOI, some elements such as Th, Ta, Tb and Sc remain almost unmodified outside and within the silica gossan.

325 4.3 Gamma spectrometry

326 Gamma spectrometric measurements decode the radiometric signature of the
327 flows as demonstrated in recent studies (e.g. Hartmann et al., 2010, 2012b; Pertille et
328 al., 2013). In the Ametista do Sul mining district, this tool was used by Rosenstengel
329 and Hartmann (2012) to separate the basaltic flows.

330 The gamma spectrometry signature of the flows in the Mina do Museu silica
331 gossan (Fig. 6A) confirms that the Pitanga basaltic flows show higher counts per second
332 than Paranapanema basaltic flow (Table 3). Two field sections were made in the gamma
333 spectrometric survey. The first was performed at the surface of volcanic flows near the
334 silica gossan of the Coogamai (Fig. 6B) and Veia Alta flows (Fig. 6C). The second was
335 made through one gallery in the Mina do Museu across the entire width of the mountain
336 in the mineralized Veia Alta flow. The result of the first section showed that the Veia
337 Alta flow gamma spectrometry average is 85 cps (GR-110), equivalent to 107 cps in the
338 readings of RS-125 and very close to the regional gamma spectrometric average
339 described by Rosenstengel and Hartmann (2012). The gamma spectrometry profile on
340 the Mina do Museu and surroundings of the Coogamai flow allows the identification of
341 negative anomalous areas at the site of the silica gossan.

342 The gamma spectrometric data of several profiles results in a map (Fig. 6D) that
343 shows the progression of negative anomalies from the rim to the core of the structure
344 with the lowest values on the amethyst deposits, whereas in areas without amethyst
345 deposits the values are close to the average of Coogamai flow (55 cps, GR-110). The
346 distribution of the radionuclides eTh, eU and %K (Table 4) in the surface sections show
347 the same negative anomalies in the Coogamai flow. The values show variation in the
348 contents of radionuclides in both flows mainly in eU and eTh while the %K shows
349 values with less variation.

350

351 4.4 X-Ray diffraction

352 The use of X-ray diffraction leads to the identification of clay minerals present
353 in the Mina do Museu silica gossan. The survey section (A1T1A=0.95m) performed for
354 a palynological study (Gadens-Marcon et al., 2014) was used also in this study. This
355 survey section included the variation from top to the bottom of the section. At the top
356 there is a grayish organic soil (0.0m – 0.15m) followed by a very plastic dark gray clay
357 (0.15 m – 0.65 m) and at the end of the section an intensely altered basalt (0.65 m – 0.95
358 m) with concentration of iron oxides (e.g. goethite) with brownish to ocher color. The
359 X-ray diffraction (Fig. 7) was performed using oriented clays method under natural
360 condition, glycol and calcinated at 550 ºC. The evaluation of the results was based on
361 the peak intensity and behavior of the interplanar distances that identify montmorillonite
362 and kaolinite. Montmorillonite shows a pattern identified by the interplanar distance of
363 14.66 Å under natural oriented condition. Under the condition of oriented glycol the
364 interplanar distance was modified to 17.12 Å due to its expandability property. When
365 subjected to heating at 550 ºC the interplanar distance increased to 10.15 Å which
366 confirmed the montmorillonite identification. In the same way, the kaolinite also
367 presented its standard behavior from the peaks of intensity that characterize the
368 interplanar distances of 7.17 Å and 3.57 Å (natural and glycol) and collapsing of the
369 structure when subjected to 550 ºC.

370

371 4.5 Electron Microprobe

372 The EMPA analyses were performed in samples from the Coogamai flow in
373 order to compare the primary mineralogy with the alteration minerals within and outside
374 Mina do Museu silica gossan (Fig. 8A, B, C, D). The most significant difference was

observed in chemical composition of smectite and in the degree of alteration of clinopyroxene, magnetite and ilmenite. The compositional range of clinopyroxene and plagioclase does not correlate with hydrothermal events.

The microphenocrysts of plagioclase don't show significant alteration and the rims are very sharp. The analyses are plotted in the ternary classification diagram Ab-An-Or (Fig. 8E) and representative EMPA results are listed in Table 5. Overall the feldspar of Coogamai flow ranges in composition from An_{32} to An_{67} (andesine and labradorite), but some analyses plot in the field of anorthite and bytownite. Samples outside silica gossan present compositions between An_{35} and An_{62} (andesine and labradorite) and some crystals display large chemical zoning from core-to-rim with variations from An_{50} to An_{32} (sample LF1). Similarly, the samples within silica gossan also display compositions between andesine An_{35-42} and labradorite An_{50-67}. The alkali feldspar (Fig. 8E) of Coogamai flow is primarily composed of sanidine Or_{56-81} Ab_{19-44}. The samples outside silica gossan present sanidine compositions between Or_{19-28} while within silica gossans the sanidine displays Or_{40-44}.

The clinopyroxene from Coogamai flow occurs in the matrix and as microphenocrysts. Both augite and pigeonite are present (Fig. 8F, Table 6). The augite composition in the Coogamai flow presents a global variation from Wo_{31-44}. In the samples outside silica gossan the variation is Wo_{37-44} while within silica gossan is Wo_{31-43}. The variation of pigeonite composition outside silica gossan is Wo_{10-15} and within silica gossan is Wo_{7-15} (Fig 8F). The clinopyroxene crystals usually display alteration and in some places are replaced by smectite.

The presence of smectite in the samples outside silica gossan is limited to a few crystals while in samples within the silica gossan the presence of clay minerals is more extensive. Representative EMPA analyses of smectite from the Coogamai flow are in

Table 7. The Si and K show positive correlation (Fig. 8G). The highest contents occur in samples from outside silica gossan and the lower values in samples within the silica gossan whereas Mg has an inverse distribution. Ca in the Coogamai flow displays a positive correlation with Mg. Despite this, two classes of Ca contents comprise this correlation. Samples from outside the silica gossan have slightly higher Ca levels than those inside the silica gossan. On the other hand, a negative correlation is observed between Mg + Fe (III) *versus* Ca + Na + K (Fig. 8H) showing the strong interference of Mg and K contents in the smectite composition. The composition of smectites (Al+Fe_{3+}Cr+Ti+Mg+Mn+Ni and Ca+Na+K+Ba) is compatible with interlayered trioctahedral and dioctahedral smectites. The spatial distribution of both elements in the smectite is shown in compositional maps. The magnesium from smectite of samples outside silica gossan shows a homogeneous distribution and concentration trend of Mg in the core of the mineral (Fig. 9) and in the samples within silica gossan the distribution of Mg confirms the trend observed with concentration of Mg contents in the core. The distribution of potassium in the smectite from outside silica gossan displays a trend towards concentration of K contents in the crystal rim (Fig. 9) while the core is depleted in K. In the samples within silica gossan, the K trend continues but with lower contents. Ca, Al and Fe have homogeneous contents, both within and outside sílica gossan and no significant changes.

5. Discussion

The Mina do Museu silica gossan is an example of prospective guide of amethyst geode deposits in the Ametista do Sul mining district. Differently from the gossans originated from sulphide mineralization, the Mina do Museu silica gossan was generated in a very low sulphide environment. The denomination silica gossan (e.g.,

425 Keller and Hanson, 1968; Sayin, 2007) was used to describe prospective guides of
426 kaolin deposits in volcanic rocks in Mexico and Turkey. The authors highlight the
427 oxidized iron-rich zone, color change on the silica gossan surface, presence of kaolinite
428 and chalcedony infilling cavities.

429 In the Serra Geral Group, Hartmann (2008) identified for the first time gossans
430 on top of the deposits of amethyst and agate in basalts and rhyodacites. The evolution of
431 this matter made Pertille et al. (2013) promote the major advance in understanding of
432 these amethyst prospective guides. The study in the Los Catalanes (Uruguay) and
433 Quarai (Brazil) mining district described gossans in the same amethyst host flow on the
434 two sides of the border. The origin of the gossans was correlated to the H1, H2 and H3
435 hydrothermal events (Hartmann 2008, 2010). The Cretaceous volcanism was the heat
436 source that affected the Guarani aquifer and generated the low salinity hydrothermal
437 fluids at temperatures below 150 ºC. The pressure exerted by the boiling water and its
438 vapor raised fluidized sand (30 vol.% in water) from the Botucatu Formation and left
439 the sand as residue forming structures such as sills and dikes of sandstone along the path
440 of the hydrothermal fluid. As time passed and the process continued active, the sand of
441 these structures was silicified by the hydrothermal fluids while the amethysts were
442 deposited within the cavities generated in the H3 event. The oxidation of clinopyroxene
443 and opaque minerals of Coogamai flow provided a large amount of free iron oxides
444 highlighting reddish to brownish spots and formation of smectite, consistent with the
445 low-temperature hydrothermal alteration (Duarte et al., 2009, 2011; Hartmann, 2008;
446 Hartmann et al., 2010, 2012c, 2012d; Pinto et al., 2011b).

447 Supergene processes in the Quaternary began to act at the surface, changing and
448 leaching elements and eroding the Coogamai flow. However, the presence of silicified
449 structures close to the amethyst geodes deposit turned these areas more resistant to

erosion. The concentration of iron-rich crusts turned the surface ocher to brownish color with development of marshes and sometimes lakes. Over the amethyst deposits, the supergene alteration caused oxidation, formation of soil, clay minerals (montmorilonite and kaolinite), and silica gossans. Therefore, the Mina do Museu silica gossan is the result of the superposition of hydrothermal alteration of basalts added by silicification of sand layers brought up by H1, H2 and H3 and weathering processes.

The Veia Alta and Coogamai flows in the Ametista do Sul mining disctrict virtually display the same primary mineral composition. However the hydrothermal activity and the composition of the fluid phase on these flows promoted the formation of clay minerals with different composition. In the Veia Alta flow were formed smectite and celadonite and in the Coogamai flow only smectite was observed. The smectite has weak chemical bonds and high cation exchange capacity and soluble elements tend to be released from the host primary minerals by hydrothermal fluids.The composition of smectite in both flows is characterized by a very low Al content. In most cases, there is not sufficient Al to fill, together with Si, the tetrahedral position, and ferric iron is entering into this position. Accordingly, the octahedral position does not contain Al and is composed of Mg and Fe. Interlayer cations comprise Ca, Na, and K. Fe and Mg may be additionally present in the interlayer. Particularly, in the Coogamai flow, the chemical analyzes of whole rock demonstrates that the SiO_2 and Al_2O_3 contents in most cases are higher outside silica gossan than inside silica gossan showing a positive correlation. Also, the Al_2O_3 x Fe_2O_3 and SiO_2 x Fe_2O_3 display slightly negative correlations. Thus, the hydrothermal fluid path across the Coogamai flow generated different smectite outside and within silica gossan. Outside silica gossan smectite are characterized by relatively low octahedral totals of 2.7 to 2.2 p.f.u., and relatively high interlayer totals (Ca+Na+K) of 0.3 to 0.5 p.f.u., which approaches to dioctahedral

member. In contrast, within silica gossan smectite has higher tetrahedral total of 2.5 to 2.9 p.f.u., and distinctly lower interlayer totals (Ca+Na+K) of 0.2 to 0.3 p.f.u., close to a trioctahedral member. Relatively the low hydrothermal activity outside silica gossan is characterized by dioctahedral smectite with an interlayer dominated by K derived from K feldspar from interstitial matrix. The incipient alteration of the basalt starts in the fine-grained portions and is characterized by a large interface surface. This interpretation is also supported by the lower K content in microcrystalline sanidine inside the silica gossan. On the other hand in the more heavily altered basalt, the decomposition of clinopyroxene and of Fe oxides delivered Fe and Mg to the fluid phase. Smectite formed in equilibrium with that hydrothermal fluid is accordingly richer in these elements. The ratio Ca/Ca+K+Na in smectite from silica gossan also indicate a Ca richer source of the fluid phase from which smectite is precipitated. In the Coogamai flow, in addition to the smectite was also observed the presence of kaolinite. The contrast between environmental conditions of formation of smectite and kaolinite was studied by Keller (1964). Smectite is formed in chemical environments characterized by high Si/Al ratio associated with the availability of elements such as Mg, Na, Fe, Ca and K and low concentration of H ions, and depends of the local climate conditions and also of the soil permeability and drainage. Humid climates associated with areas with low permeability or deficient drainage facilitates the concentration of soluble silica and cations and the environment becomes conducive to the formation of smectite clay minerals. If in these same kinds of climate, a high permeability or efficient drainage occurs, then cations can be leached and silica placed in solution, so the environment becomes conducive to the formation of kaolinite.

The study made in gossans in the Paraná volcanic province highlights the presence of smectite within the gossans and the occurrence of gamma spectrometric

anomalies over the amethyst deposits. These features distinguish the gossan structure from the other field sections. The same evidence was observed in several places (Baggio et al., 2014) in the Paraná province (e.g., Entre Rios mining district) and confirmed the gamma spectrometric variations and negative anomaly over the amethyst geode deposits. In the Quaraí and Artigas mining districts, Pertille et al. (2013) indicated that the gamma spectrometry readings are associated to the intense hydrothermal alteration, represented by the LOI > 2 wt. %. LOI contents are negatively correlated with SiO_2, K_2O, Rb contents and Rb/Sr ratios on the gossans. In these districts, the amethyst geode deposits and the gossan occur in the same volcanic flow while in the Ametista do Sul mining district, the Veia Alta flow (LOI average 4 wt.%) with the amethyst deposit geodes is stratigraphically below the Coogamai flow that displays the silica gossan. This flow with type II core is characterized by lower LOI ranging from 0.8 to 1.0 wt. %. This evaluation leads to the reassessment of the interpretation of the gamma spectrometric anomalies. Besides the hydrothermal alteration, the weathering process that highlighted the silica gossan at the surface, interferes in the U, Th and K contents in the silica gossans. The studies on Th and U mobility (Dickson and Scott, 1997; Dickson et al., 1996; Langmuir, 1980; Reiller et al., 2002) show the increase of mobility of these elements in certain conditions. These elements freed by the breakdown of minerals during weathering events are normally retained in Fe oxides-hydroxides, soluble complexes silicates and/or colloidal clays and are transported absorbed by gravitational processes (Dickson and Scott, 1997; Souza and Ferreira, 2005). The concentrations of Fe (goethite and hematite) oxides-oxyhydroxides increase the Th solubility (Reiller et al., 2002) and the U mobility. The deep alteration of pyroxene and opaque minerals caused by hydrothermal fluids initiated the argillic alteration, oxidation and concentration of Fe. The combination of these factors associated to weathering and

525 erosion events led to the development of physical and chemical conditions for the
526 leaching of the radionuclides Th and U absorbed in organic complexes, iron oxides and
527 soluble silicate complexes. The enrichment in iron is associated with decrease of Th and
528 U contents. The geochemical analyses of Th bulk rocks shows few changes in content
529 inside and outside the gossan silica in comparison with LOI, but the gamma
530 spectrometric readings show significant Th changes in the soil within the silica gossan
531 and outside silica gossan. A similar effect occurs with uranium. The U gamma
532 spectrometric readings show a larger difference between the areas with soil outside
533 silica gossan and within silica gossan. However, the primary comparison was observed
534 in potassium readings because the contents of K_2O (bulk rock) display a negative
535 correlation with the LOI, with higher K_2O contents in the samples outside silica gossan.
536 The gamma spectrometric readings confirm this distribution in all sections.
537

538 **6. Conclusions**

539 The Mina do Museu silica gossan is proposed as a prospective guide model for
540 amethyst geode deposit in the Paraná volcanic province. The Veia Alta flow is the main
541 amethyst producer in the district and displays very high values of LOI (~4 wt.%) and
542 gamma spectrometry average of 85 cps. The Coogamai flow with silica gossan exhibits
543 outside silica gossan contents of LOI of 0.2-0.5 wt.% and gamma spectrometry average
544 of 55 cps while in areas within silica gossan, on the amethyst deposits, the contents of
545 LOI varies 0.9-1.8 wt.% and the gamma spectrometry average is 43.5 cps. The presence
546 of gossans like Mina do Museu in an intraplate environment is based on the unique
547 geological features developed in the Paraná volcanic province, which explains the lack
548 of description of these structures in other provinces of the world.

549 The key features for discrimination of the Mina do Museu gossan model can be
550 separated in two groups. 1) Field features. Significant change in vegetation, marsh areas
551 with intense argillic alteration, silicified sand structures more resistant to erosion, iron-
552 rich surface on the structure forming an oxidized zone with reddish brown or ocher
553 color. 2) Survey features. Geometric structure in satellite images, increase of LOI within
554 silica gossan and negative correlation between LOI and oxides (e.g., SiO_2), presence of
555 negative anomalies of K, eU and eTh on the amethyst geode deposits and presence of
556 K-smectites outside silica gossan and Mg-smectites within the silica gossan that could
557 serve as a proxy for the degree of basalt alteration.
558

559 **Acknowledgements**

560 Financial support was provided by Project VALE / CNPq, MCT and Mineral
561 Sector Fund (edital 12/2009) entitled "Desenvolvimento de metodologia de exploração
562 geológica para geodos de ametista e ágata, cobre e outros bens minerais em ambiente
563 hidrotermal do Grupo Serra Geral, sul-sudeste do Brasil" and project of excellence
564 PRONEX-FAPERGS/CNPq (edital 008/2009) on strategic minerals from southern
565 Brazil, coordinated by Léo A. Hartmann. Special thanks to CPRM/PA by GR-110
566 scintillometer loan, to X-ray diffraction Laboratory - IG UFRGS and to Gabrielli T.
567 Gadens-Marcon by the A1T1A survey profile kindly ceded.
568

569 **References**

570 Almeida, F.F.M., 1986. Distribuição regional e relações tectônicas do magmatismo pós-
571 paleozóico no Brasil. Revista Brasileira de Geociências 16, 325-349.
572 Baggio, S.B., Pertille, J., Antunes, L.M., Petry, T.S., Hartmann, L.A., 2014. Silica
573 gossans on amethyst geode mineralization in the Serra Geral Group. In: Hartmann,

574 L.A., Baggio, S.B. (Org.), Metallogeny and mineral exploration in the Serra Geral
575 Group, IGEO, UFRGS, Porto Alegre, Brazil, pp. 369-388.
576 Bellieni, G., Comin-Chiaramonti, P., Marques, L.S., Melfi, A.J., Piccirillo, E.M., Nardy,
577 A.J., Roisenberg, A., 1984. High- and low-Ti flood basalts from the Paraná Plateau
578 (Brazil): petrology and geochemical aspects bearing on their mantle origin. Neues
579 Jahrbuch für Mineralogie Abhandlungen 150, 272–306.
580 Brandelik, A., Massonne H.-J., 2004. PTGIBBS – an EXCELTM Visual Basic program
581 for computing and visualizing thermodynamic functions and equilibria of rock-
582 forming minerals. Computers & Geosciences 30, 909–923.
583 Cox, K.G., Bell, J.D., Pankhurst, R.J., 1979. The Interpretation of Igneous Rocks.
584 George, Allen and Unwin, London.
585 Dickson, B.L., Fraser, S.J., Kinsey-Henderson., 1996. Interpreting aerial gamma-ray
586 surveys utilizing geomorphological and weathering models. Journal of geochemical
587 exploration 57, 75-88.
588 Dickson, B.L., Scott, K.M., 1997. Interpretation of aerial gamma-ray surveys-adding the
589 geochemical factors. AGSO Journal of Australian Geology & Geophysics, 17, 187-
590 200.
591 Duarte, L.C., Hartmann, L.A., Medeiros, J.T.N.M., Juchem, P.L., 2014. Hydrothermal-
592 epigenetic origin of amethyst and agate geodes in the Paraná volcanic province. In:
593 Hartmann, L.A., Baggio, S.B. (Org.), Metallogeny and mineral exploration in the
594 Serra Geral Group, IGEO, UFRGS, Porto Alegre, Brazil, pp. 303-320.
595 Duarte, L.C., Hartmann, L.A., Ronchi, L.H., Berner, Z., Theye, T., Massone, H.J., 2011.
596 Stable isotope and mineralogical investigation of the genesis of amethyst geodes in
597 the los Catalanes gemological district, Uruguai, southernmost Paraná volcanic
598 province. Mineralium Deposita 46, 239-255.

599 Duarte, L.C., Hartmann, L.A., Vasconcelos, M.A.Z., Medeiros, J.T.N., Theye, T., 2009.
600 Epigenetic formation of amethyst-bearing geodes from Los Catalanes gemological
601 district, Artigas, Uruguay, southern Paraná Magmatic-Province. Journal of
602 Volcanology and Geothermal Research 184, 427-436.
603 Frank, H.T., Gomes, M.E.B., Formoso, M.L., 2009. Review of the areal extend and the
604 volume of the Serra Geral Formation, Paraná Basin, South America. Pesquisas em
605 Geociências UFRGS 36, 49–57.
606 Gadens-Marcon, G.T., Mendonça-Filho, J.G., Guerra-Sommer, M., Carvalho, M.A.,
607 Pires, E.F., Hartmann, L.A., 2014. Relation between the sedimentary organic record
608 and the climatic oscilations in the Holocene attested by palynofacies and organic
609 geochemical analyses from a pond of altitude in southern Brazil. Annals of the
610 Brazilian Academy of Sciences, 86, 1077 -1099.
611 Gilg, H.A., Krüger, Y., Taubald, H., Van den Kerkhof, A.M., Frenz, M., Morteani, G.,
612 2014. Mineralisation of amethyst-bearing geodes in Ametista do Sul (Brazil) from
613 low-temperature sedimentary brines: evidence from monophase liquid inclusions and
614 stable isotopes. Mineralium Deposita 49, 861–877.
615 Gilg, H.A., Morteani, G., Kostitsyn, Y., Preinfalk, C., Gatter, I., Strieder, A.J., 2003.
616 Genesis of amethyst geodes in basaltic rocks of the Serra Geral Formation (Ametista
617 do Sul, Rio Grande do Sul, Brazil): a fluid inclusion, REE, oxygen, carbon, and Sr
618 isotope study on basalt, quartz, and calcite. Mineralium Deposita 38, 1009–1025.
619 Gomes, M.E.B., 1996. Mecanismos de resfriamento, estruturação e processos pós-
620 magmáticos em basaltos da Bacia do Paraná - região de Frederico Westphalen (RS)
621 Brasil. PhD Thesis, Universidade Federal do Rio Grande do Sul, Porto Alegre,
622 Brazil, 219 pp.

623 Hartmann, L.A., 2008. Amethyst Geodes Formed from Hot Water in Dinosaur Times,
624 first ed. UFRGS, Porto Alegre, Brazil.
625 Hartmann, L.A., 2014. Introduction to the natural history of the Serra Geral Group. In:
626 Hartmann, L.A., Baggio, S.B. (Org.), Metallogeny and mineral exploration in the
627 Serra Geral Group, IGEO, UFRGS, Porto Alegre, Brazil, pp. 299-302.
628 Hartmann, L.A., Antunes, L.M., Rosenstengel , L.M., 2014a. Stratigraphy of amethyst
629 geode-bearing lavas and fault-block structures of the Entre Rios mining district,
630 Paraná volcanic province, southern Brazil. Anais da Academia Brasileira de Ciências
631 86, 187-198.
632 Hartmann, L.A., Arena, K.R., Duarte, S.K., 2012a. Geological relationships of basalts,
633 andesites and sand injectites at the base of the Paraná volcanic province, Torres,
634 Brazil. Journal of Volcanology and Geothermal Research 237-238, 97-111.
635 Hartmann, L.A., Baggio, S.B., Duarte, S.K. 2012b. Decoding geochemical and gamma-
636 spectrometric signatures from lavas and sand injectites at the base of the Paraná
637 volcanic province, Novo Hamburgo, Brazil. International Geology Review 55, 510-
638 524.
639 Hartmann, L.A., Duarte, L.C., Massonne, H.J., Michelin, C., Rosenstengel, L.M.,
640 Bergmann, M., Theye, T., Pertille, J., Arena, K.R., Duarte, S.K., Pinto, V.M.,
641 Barboza, E.G., Rosa, M.L.C.C., Wildner, W., 2012c. Sequential opening and filling
642 of cavities forming vesicles, amygdales and giant amethyst geodes in lavas from the
643 southern Paraná volcanic province, Brazil and Uruguay. International Geology
644 Review 54, 1–14.
645 Hartmann, L.A., Medeiros, J.T.N., Baggio, S.B., Antunes, L.M., 2015. Controls on
646 prolate and oblate geode geometries in the Veia Alta basalt flow, largest world

producer of amethyst, Paraná volcanic province, Brazil. Ore Geology Reviews 66, 243-251.

Hartmann, L.A., Medeiros, J.T.N., Petruzzellis, L.T., 2012d. Numerical simulations of amethyst geode cavity formation by ballooning of altered Paraná volcanic rocks, South America. Geofluids 12, 133-141.

Hartmann, L.A., Pertille, J., Duarte, S.K., Arena, K.R., Baggio, S.B., 2014b. Description of geological criteria and indication of preferential areas for amethyst geode deposits in the municipality of Quaraí, Rio Grande do Sul. In: Hartmann, L.A., Baggio, S.B., Metallogeny and mineral exploration in the Serra Geral Group, IGEO, UFRGS, Porto Alegre, Brazil, pp. 411-423.

Hartmann, L.A., Wildner, W., Duarte, L.C., Duarte, S.K., Pertille, J., Arena, K.R., Martins, L.C., Dias, N.L., 2010. Geochemical and scintillometric characterization and correlation of amethyst-bearing Paraná lavas from the Quaraí and Los Catalanes districts, Brazil and Uruguay. Geological Magazine 147, 954–970.

Juchem, P.L., 2014. Amethyst mineralization in rhyodacites of the Serra Geral Group, Paraná volcanic Province. In: Hartmann, L.A., Baggio, S.B., Metallogeny and mineral exploration in the Serra Geral Group, IGEO, UFRGS, Porto Alegre, Brazil, pp. 321-334.

Juchem, P.L., Brum, T.M.M., Ripoll, V.M., 2010. O laboratório de gemologia da Universidade Federal do Rio Grande do Sul. In: Hartmann, L.A., Silva, J.T. (Org.), Tecnologias para o setor de gemas, jóias e mineração. IGEO, UGRGS. Porto Alegre, Brazil, pp. 133-147.

Keller, W. D., 1964. Processes of origin and alteration of clay minerals. Soil clay mineralogy. A symposium. C. I. Rich and Kunze. Ed. Univ. of North Carolina Press, Chape Hill.

672 Keller, W.D., Hanson, R.F., 1968. Hydrothermal alteration of a rhyolite flow breccia
673 near San Luis Potosi, Mexico, to refractory kaolin. Clays and Clay Minerals 16, 223-
674 229.
675 Langmuir, D., Herman, J.S., 1980. The mobility of Thorium in natural waters at low
676 temperature. Geochemica et Cosmochimica Acta 44, 1753-1766.
677 Licht, O.A.B., Arioli, E.E., 2012. Statistic behavior of major and minor elements in
678 basic, intermediate and acidic rocks of the Serra Geral Formation and Arapey Group,
679 Paraná Large Igneous Province, South America. Revista Pesquisas em Geociências
680 (UFRGS) 39, 247-267.
681 Licht, O.A.B., Fonseca, C.R., Moretti, M.A., Silveira, D.F., 2012. Estudo de produtos
682 hidrovulcânicos no sudoeste do Paraná. Mineropar, Curitiba, PR, Brazil, 192 pp.
683 Mantovani, M.S.M., Marques, L.S., De Sousa, M.A., Civetta, L., Atalla, L., Innocenti,
684 F., 1985. Trace element and strontium isotope constraints on the origin and evolution
685 of Paraná continental flood basalts of Santa Catarina state (southern Brazil). Journal
686 of Petrology 26, 187–209.
687 Meunier, A., Formoso, M.L.L., Patrier, P., Chies, J.O., 1988. Altération hydrotermale
688 de roches volcaniques liées à la gênese dês amethysts - Bassin du Paraná - sud du
689 Brésil. Geochimica Brasiliensis 2, 127–142.
690 Morteani, G., Kostitsyn, Y., Preinfalk, C.E., Gilg, H.A., 2010. The genesis of the
691 amethyst geodes at Artigas (Uruguay) and the paleohydrology of the Guaraní
692 aquifer: structural, geochemical, oxygen, carbon, strontium isotope and fluid
693 inclusion study. International Journal of Geological Sciences 99, 927-947.
694 Nakamura, K., Shibuya, A., Masuta, K., Murakami, T., Wildner, W., Dias, A.A.,
695 Kirchner, C.A., Lessa, N., 2003. Mineral exploration in the Paraná Basin area, the

696 Federal Republic of Brazil, phase I. Metal Mining Agency of Japan - MMAJ and
697 Geological Survey of Brazil - CPRM, internal report.
698 Peate, D.W., 1997. The Paraná-Etendeka Province. In: Mahoney, J.J., Coffin, M.R.
699 (Eds.), Large Igneous Provinces: Continental, Oceanic, and Planetary Flood
700 Volcanism: Geophysical Monograph, 100. American Geophysical Union,
701 Washington DC, USA, pp. 217-245.
702 Peate, D.W., Hawksworth, C.J., Mantovani, M.S.M., 1992. Chemical stratigraphy of the
703 Paraná lavas (South America): classification of magma types and their spatial
704 distribution. Bulletin of Volcanology 55, 119–139.
705 Peate, D.W., Hawkesworth, C.J., Mantovani, M.S.M., Rogers, N.W., Turner, S.P.,
706 1999. Petrogenesis and stratigraphy of the high-Ti/Y Urubuci magma type in the
707 Paraná flood basalt province and implications for the nature of 'Dupal'-type mantle
708 in the south Atlantic region. Journal of Petrology 40, 451-473.
709 Pertille, J., Hartmann, L.A., Duarte, S.K., Arena, K., Rosa, M.L.C.C., Barboza, E.G.,
710 2013. Gossan characterization in the Quaraí and Los Catalanes amethyst geode
711 districts (Brazil and Uruguay), Paraná volcanic province, using rock geochemistry
712 and gamma-spectrometry. Journal of Geochemical Exploration 124, 127-139.
713 Pinto, V.M., Hartmann, L.A., Santos, J.O.S., McNaughton, N.J., Wildner, W., 2011a.
714 Zircon U–Pb geochronology from the Paraná bimodal volcanic province support a
715 brief eruptive cycle at 135 Ma. Chemical Geology 281, 93–102.
716 Pinto, V.M., Hartmann, L.A., Wildner, W., 2011b. Epigenetic hydrothermal origin of
717 native copper and supergene enrichment in the Vista Alegre district, Paraná basaltic
718 province, southernmost Brazil. International Geology Review 53, 1163–1179.
719 Pirajno, F., 2009. Hydrothermal processes and mineral systems. Geological survey of
720 western Australia, Perth WA Australia. Springer. 1250pp.

721 Proust, D., Fontaine, C., 2007. Amethyst-bearing lava flows in the Paraná basin (Rio
722 Grande do Sul, Brazil): cooling, vesiculation and formation of the geodic cavities.
723 Geological Magazine 144, 53-65.
724 Reiller, P, Moulin, V., Casanova, F., Dautel, C., 2002. Retention behaviour of humic
725 substances onto mineral surfaces and consequences upon thorium (IV) mobility: case
726 of iron oxides. Applied Geochemistry 17, 1551-1562.
727 Rosenstengel, L.M., Hartmann, L.A., 2012. Geochemical stratigraphy of lavas and
728 fault-block structures in the Ametista do Sul geode mining district, Paraná volcanic
729 province, southern Brazil. Ore Geology Reviews 48, 332-348.
730 Sayin, S.A., 2007. Origin of kaolin deposits: evidence from a Hisarcik (Emet-Kütahya)
731 deposits, western Turkey. Turkish Journal of Earth Science16, 77-96.
732 Scopel, R.M., Formoso, M.L.L., Dudoignon, P., Meunier, A., 1990. Hydrothermal
733 alteration of basalts, Southern Paraná Basin – Brazil. Chemical Geology 84, 249-
734 250.
735 Scott, K.M., Ashley, D.C., Lawie, D.C., 2001. The geochemistry, mineralogy and
736 maturity of gossans derived volcanogenic Zn-Pb-Cu deposits of the eastern Lanchlan
737 Fold Belt, NSW, Australia. Journal of Geochemical Exploration 72, 169–191.
738 Silva, A.O., 2010. Mineração de geodos em Ametista do Sul. In: Hartmann, L.A. Silva,
739 J.T. (Org.), Tecnologias para o setor de gemas, jóias e mineração. IGEO, UGRGS.
740 Porto Alegre, Brazil, pp. 233-246.
741 Souza, J.L., Ferreira, F.J.F., 2005. Anomalias aerogamaespectrométricas (K, eU e eTh) da
742 quadrícula de Araras (SP) e suas relações com processos pedogenéticos e fertilizantes
743 fosfatados. Revista Brasileira de Geofísica 23, 251-274.

744

745 **Figure captions**

Figure 1. Geological map of southeastern South America highlighting the Paraná Basin. Paraná volcanic province (light gray), younger sedimentary rocks overlying lavas (dark gray), represented by the Bauru Group in Brazil, Acaray Formation in Paraguay (correlated with the bottom of Bauru Group) and as Mariano Boedo Formation and sands from the Chaco Group in Argentina. Older sedimentary, igneous and metamorphic rocks and an extensive coastal plain covered by Cenozoic sediments (blank area). Ametista do Sul mining district location indicated. Modified from Peate et al. (1992).

Figure 2. A) Geological map of the Ametista do Sul mining district with the location of the samples from Coogamai flow (A1 and A3A from Rosenstengel and Hartmann, 2012). Highway indicated (RS-591). The base map used was Ministério do Exército (1979), Diretoria de Serviço Geográfico, Folha Planalto MI-2885/4. B) Geomorphologic profile of Mina do Museu silica gossan and the stratigraphy of the flows in the Ametista do Sul mining district with the location of samples from Veia Alta flow.

Figure 3. Petrography of Coogamai and Veia Alta flows. A, B) Thin section of sample LF1, showing the texture and minerals of the Coogamai flow with low hydrothermal alteration (outside silica gossan). C, D) Thin section of sample MM90, showing areas with hydrothermal alteration in the Coogamai flow and formation of clay minerals (within silica gossan). E and F) Thin section of sample V17 showing areas with hydrothermal alteration and formation of celadonite in the Veia Alta flow (amethyst producer).

Figure 4. Geochemical diagrams. A) Total alkalis-silica (TAS) classification (after Cox et al., 1979). B) TiO_2 versus MgO diagram displaying the high-Ti, intermediate-Ti magma and low-Ti types (after Peate, 1992). C) TiO_2 versus P_2O_5 diagram, with the

771 classification of the magma types and the plotted samples of Coogamai and Veia Alta
772 flows. D) SiO_2 versus LOI showing negative correlation between samples from Veia
773 Alta flow and the plot of samples from Coogamai flow (outside and within silica
774 gossan). The dotted line at LOI 0.5 wt.% separates the samples of Coogamai flow
775 (outside and within silica gossan). The dotted line at LOI 2 wt.% separates the samples
776 of Coogamai flow and the samples of Veia Alta flow that host the amethyst deposits.
777 Figure 5. Variation diagram of loss on ignition and oxides. Negative correlation and
778 contents in the Coogamai flow (outside and within silica gossan) and Veia Alta flow
779 (amethyst producer). A) LOI *versus* K_2O. B) LOI *versus* MgO. C) LOI *versus* CaO. D)
780 LOI *versus* Na_2O.
781 Figure 6. Mina do Museu silica gossan located at 22J UTM 282559E, 6970373S
782 (Datum SAD69). A) GoogleEarth image of the Mina do Museu silica gossan. 1a-1b =
783 gamma spectrometric section for Coogamai flow presented in Fig. B. 2a-2b = gamma
784 spectrometric section for Veia Alta flow presented in Fig. C. The dotted square
785 indicates the area of gamma spectrometric survey presented in Fig D. B) Gamma
786 spectrometric behavior of the Coogamai flow. The dotted line is the gamma
787 spectrometric average of Coogamai flow. C) Gamma spectrometric behavior on the
788 Veia Alta flow across the amethyst geode gallery in the Mina do Museu. The dotted
789 line is the gamma spectrometric average of Veia Alta flow. D) Gamma spectrometric
790 contour map, showing its behavior and the negative anomalous area. The deep blue
791 color in the map corresponds to the amethyst deposit area.
792 Figure 7. X-ray diffraction of the sample A1T1A. Mina do Museu silica gossan.
793 Identification of the peaks of montmorillonite and kaolinite (natural, glycol and
794 calcinated at 550 ºC).

795 Figure 8. Back scattered electron image of Coogamai flow, outside and within Mina do
796 Museu silica gossan and the composition of feldspar, clinopyroxene and smectite. A,
797 B) Samples LQ1 and LF1 located outside silica gossan. Indicated mineral: Pl =
798 plagioclase, Mgt = magnetite, Ap = apatite, Cpx = clinopyroxene and Sm = smectite.
799 The presence of smectite is restricted to a few points where there is some change in the
800 clinopyroxene crystals. C, D) Samples B1 and MM90 located within silica gossan.
801 Indicated mineral: Pl = plagioclase, FK =potassium feldspar, Mgt = magnetite, Ap =
802 apatite, Cpx = clinopyroxene and Sm = smectite. The hydrothermal alteration on the
803 clinopyroxene and magnetite crystals generated large areas with smectite. E) Ternary
804 Ab-An-Or diagram of feldspar. Ligth gray: field of feldspar of samples outside silica
805 gossan, black: field of feldspar of samples within silica gossan. F) Ternary En-Wo-Fs
806 diagram of clinopyroxenes. Ligth gray: field of clinopyroxenes of samples outside
807 silica gossan, black: field of clinopyroxenes of samples within silica gossan. G, H)
808 Diagram Si (p.f.u) *versus* K (p.f.u) and Fe_{3+}+Mg (p.f.u) *versus* Ca+Na+K (p.f.u)
809 showing the chemical behavior of the smectites outside and within silica gossan.
810 Figure 9. Distribution of the pair K and Mg in smectites from Coogamai flow, outside
811 and within Mina do Museu silica gossan. A, B) sample LF1 (outside Mina do Museu
812 silica gossan) 20 Kv, 20 nA. C, D) Sample LQ1 (outside Mina do Museu silica
813 gossan) 20 Kv, 20 nA. E, F) Sample B1 (within Mina do Museu silica gossan), 15Kv,
814 25nA. G, H) Sample MM95 (within Mina do Museu silica gossan), 15 Kv, 20nA. The
815 dotted line represents the outline of the smectite.

Table 1
Click here to download Table: Table 1_2015_02_09.doc

Table 1
Chemical analyses of volcanic rocks from Coogamai flow, Ametista do Sul mining district.

Sample	LF1	LQ1	A3A(*)	B1	MM90	MM95	CG1	VN1	CO1	A1(*)
	Outside silica gossan			Within Mina Museu silica gossan			Within other silica gossan (mining district)			
UTM E	283538	283706	282422	282565	282649	282468	283343	282033	283605	283612
UTM S	6972249	6971440	6972129	6970452	6970500	6970507	6971537	6971918	6971932	6971961
SiO_2	49.46	49.17	49.54	49.87	49.30	49.08	47.43	48.76	48.41	47.99
TiO_2	2.25	2.30	2.32	2.25	2.34	2.25	2.23	2.25	2.28	2.34
Al_2O_3	13.01	13.06	13.03	13.23	13.09	12.91	12.82	12.92	12.94	13.11
Fe_2O_3	15.23	15.24	14.81	14.25	15.05	15.27	17.09	15.29	15.41	15.05
MgO	5.71	5.40	5.74	5.70	5.59	5.40	5.25	5.64	5.42	5.65
CaO	9.69	9.67	9.77	9.60	9.60	9.50	9.40	9.70	9.64	9.78
Na_2O	2.44	2.33	2.37	2.32	2.37	2.38	2.27	2.31	2.51	2.43
K_2O	1.17	1.20	1.07	1.01	1.06	1.32	1.37	1.12	1.10	1.04
P_2O_5	0.27	0.27	0.27	0.29	0.28	0.27	0.27	0.27	0.28	0.27
MnO	0.23	0.22	0.22	0.19	0.22	0.20	0.18	0.22	0.19	0.19
Cr_2O_3	0.018	0.018	0.016	0.016	0.016	0.018	0.017	0.018	0.018	0.016
LOI	0.2	0.5	0.5	1.0	0.9	1.0	1.4	1.2	1.5	1.8
Total	99.69	99.40	99.68	99.67	99.69	99.63	99.71	99.69	99.70	99.68
Au	3.0	3.4	1.9	22.3	3.3	2.8	1.7	2.6	4.4	3.8
Ba	316	303	308	317	311	329	324	316	326	321
Ce	45	47.6	47.3	48.6	47.7	45.6	47.7	44.1	45.2	46.2
Co	41.6	40.1	42.4	50.2	51.9	41.1	39.4	47.9	39.1	44.6
Cs	0.5	0.4	0.3	0.3	0.1	0.5	0.3	0.3	0.2	0.2
Cu	240	2607.6	236.5	263.2	260	362.2	183.4	234.1	145.3	133.5
Dy	6.39	5.24	5.23	5.59	5.92	9.43	5.62	5.55	7.05	5.24
Er	3.70	2.94	3.06	3.48	3.25	5.62	3.30	3.19	4.13	3.07
Eu	1.95	1.75	1.68	1.80	1.66	2.69	1.77	1.77	1.96	1.68
Ga	18	19.4	19.7	18.7	17.4	17.6	17.5	18.5	18	18.4
Gd	6.66	5.56	5.42	5.89	5.83	9.70	6.15	5.87	6.67	5.44
Hf	4.4	3.9	3.9	4	3.9	3:9	4	3.8	4.1	4.4
Ho	1.30	1.11	1.05	1.27	1.18	2.03	1.23	1.10	1.50	1.08
La	23.1	22.1	20.1	23.7	21.8	37	23.4	21.6	24.8	20.1
Lu	0.54	0.42	0.42	0.50	0.46	0.68	0.45	0.47	0.60	0.41
Mo	1.5	0.4	0.6	0.6	1.6	0.3	0.4	1.3	1.3	0.4
Nb	12.5	12.8	13.6	13.7	13.4	12.6	12.5	13	12.5	14.3
Nd	26.7	24.5	24.1	26.2	25.1	34.9	25.4	23.7	26.3	22.7
Ni	70	65	58	58	77	74	59	77	66	61
Pb	1.1	1.6	3.7	2.4	1.2	1.6	1.7	1.3	2.2	1.4
Pr	5.99	5.73	5.67	6.07	5.68	8.01	6.06	5.57	6.23	5.64
Rb	30.9	26.8	22.9	21.9	21.4	34.3	42.9	26.3	19.4	18.6
Sc	38	38	38	38	39	38	38	38	38	38
Sm	6	5.44	5.23	5.67	5.02	7.52	5.64	5.34	5.81	5.06
Sr	354.8	352.1	315.1	353.4	338.6	351.3	335.9	356.8	342.1	340.7
Ta	0.9	0.7	0.8	0.8	0.9	0.7	0.8	0.6	0.8	0.8
Tb	1.15	0.91	0.94	1.06	0.95	1.52	0.98	0.90	1.16	0.89
Th	2.5	2.4	2.6	2.5	2.5	2.6	2.3	2.3	2.5	3.2
Tm	0.54	0.45	0.44	0.54	0.45	0.76	0.47	0.44	0.61	0.43
U	0.5	1.1	0.5	0.6	0.5	0.5	0.5	0.5	0.4	0.5
V	449	453	477	468	452	434	433	473	452	474
Y	35.2	28.2	28.5	32.4	30.2	64.4	30	29.1	33.6	28.6
Yb	3.48	2.74	2.66	3.29	3.01	4.47	2.80	3.02	3.91	2.65
Zn	67	79	61	80	70	78	71	67	82	62
Zr	153.6	157.4	145.5	146.3	155.2	151.6	147.7	146.8	151.2	148.7

Note: Oxides in wt.%, trace elements in ppm except Au in ppb. (*) Samples from Rosenstengel and Hartmann (2012)

Table 2
Chemical analyses of volcanic rocks from the Veia Alta flow, Mina do Museu, Ametista do Sul mining district. Oxides in wt.%, trace elements in ppm except Au in ppb. (-) = below detection limit (Cr_2O_3 = 0.002, Au = 0.5, Cs = 0.1, Ni = 20).

Sample	V1	V5	V9	V13	V17	V22	V26	V30	V34
	Sample collection across Veia Alta flow inside Mina do Museu gallery.								
SiO_2	48.71	47.97	47.40	45.91	47.66	46.67	48.05	48.14	48.73
TiO_2	3.57	3.68	3.54	3.70	3.76	3.68	3.59	3.56	3.63
Al_2O_3	12.29	12.52	12.21	12.54	12.78	12.57	12.37	12.52	12.52
Fe_2O_3	14.50	14.74	14.78	15.38	15.01	15.67	15.07	15.16	14.25
MgO	3.96	4.56	4.49	4.77	4.52	4.65	4.53	4.54	4.19
CaO	7.74	8.44	8.46	8.57	8.53	8.64	8.39	8.40	8.18
Na_2O	2.18	2.28	2.19	2.13	2.43	2.38	2.36	2.40	2.39
K_2O	1.17	1.08	0.83	0.68	1.11	0.84	1.11	1.03	1.26
P_2O_5	0.52	0.53	0.54	0.57	0.55	0.56	0.55	0.54	0.56
MnO	0.20	0.21	0.19	0.20	0.22	0.23	0.21	0.18	0.16
Cr_2O_3	0.004	0.004	0.004	0.004	0.003	0.003	0.005	0.004	0.005
LOI	4.8	3.7	5	5.2	3.1	3.8	3.4	3.2	3.8
Total	99.69	99.69	99.67	99.69	99.65	99.66	99.67	99.68	99.67
Au	-	-	-	-	-	-	-	-	-
Ba	482	472	482	453	509	487	506	479	490
Ce	75.1	78	75.1	77.3	77.3	74.1	80.9	74.9	75.5
Co	34.3	39	36.5	38.1	43.2	39.6	39.8	37.8	35
Cs	0.2	0.2	0.2	0.1	-	0.2	0.1	0.4	0.1
Cu	157.7	153.4	149.4	167.9	225.6	205.3	181.1	196.6	171.1
Dy	7.13	6.88	7.23	6.73	6.99	7.42	7.49	7.36	7.27
Er	3.45	3.26	3.44	3.48	3.50	3.56	3.50	3.54	3.43
Eu	2.57	2.63	2.57	2.62	2.68	2.58	2.68	2.54	2.59
Ga	19.4	19.9	20.3	19.7	20	19.7	20.5	20.1	20
Gd	8.07	8.03	8.35	8.40	8.41	8.26	8.71	8.55	8.28
Hf	6.2	5.6	6	5.9	5.6	6.1	6	5.2	6.1
Ho	1.29	1.27	1.33	1.21	1.32	1.25	1.24	1.32	1.35
La	35.6	35.7	35.1	34.8	35.9	32.9	36.1	34.4	35.4
Lu	0.43	0.46	0.48	0.44	0.43	0.46	0.47	0.45	0.43
Mo	0.3	0.3	0.3	0.3	0.4	0.3	0.4	0.3	0.3
Nb	23.4	23	22.8	22.2	23.5	22.3	22.7	22.3	22.4
Nd	40.6	40.3	37.5	41.5	39.9	36.9	40.6	37.8	38.9
Ni	22	-	23	-	-	-	-	-	25
Pb	3	2.4	2.9	3.9	3.9	3.5	2.7	2.7	2.4
Pr	9.41	9.60	9.23	9.53	9.52	9.25	9.63	9.40	9.54
Rb	14.8	11.1	8.1	6.3	9.4	7.5	9.8	15.4	15.3
Sc	30	30	30	31	31	31	31	31	30
Sm	8.20	8.18	8.06	8.05	8.58	8.17	8.86	8.40	8.38
Sr	421.2	439.4	444.8	440.9	448.6	438.5	455.9	442.3	438.7
Ta	1.3	1.3	1.5	1.3	1.6	1.5	1.4	1.5	1.5
Tb	1.14	1.17	1.16	1.15	1.22	1.19	1.22	1.18	1.12
Th	3.8	3.8	3.7	3.8	3.8	3.8	3.8	3.7	3.6
Tm	0.53	0.48	0.50	0.52	0.48	0.50	0.53	0.49	0.47
U	0.9	0.8	0.7	0.7	0.7	0.8	0.7	0.8	0.8
V	436	455	453	431	468	460	467	439	450
Y	35.2	34.9	34.1	35.4	36.1	35.7	37.2	35.1	33.6
Yb	2.97	3.04	3.20	2.94	3.11	3.13	3.24	3.27	3.04
Zn	73	80	59	78	109	68	71	69	68
Zr	221.2	228.1	227.9	226.9	239.3	227.2	235.4	226.5	229.9

Table 3

Gammaspectrometric (cps) average of the Veia Alta and Coogamai flows (outside and within the Mina do Museu silica gossan). Based on Exploranium GR110 scintillometer readings.

Volcanic flow	Magma type	Emission rates (cps)		
		n	av	sd
Veia Alta flow	Pitanga	56	85	3.1
Coogamai flow outside silica gossan	Paranapanema	62	55	2.6
Coogamai flow within silica gossan	Paranapanema	47	43.5	1.3

Table 4
Click here to download Table: Table 4_2015_02_09.doc

Table 4

Gammaspectrometric average values of equivalent Th, equivalent U and percent K. Coogamai flow, surface section. Veia Alta flow, gallery section.
Based on RS-125 gammaspectrometer readings.

Location	n	eTh (ppm)	sd	eU (ppm)	sd	K (%)	sd
Coogamai flow within sílica gossan	65	3,07	1.09	0.62	0.32	0.76	0.14
Coogamai flow outside sílica gossan	45	5,66	1.33	0.76	0.58	0.81	0.26
Veia Alta flow - amethyst gallery	72	6,65	1,58	1,03	0.65	1,66	0,26

Table 5
Click here to download Table: Table 5_2015_02_09.doc

Table 5
Representative electron microprobe analyses of feldspar from Coogamai flow, within and outside silica gossan (wt.%).

	Coogamai flow outside sílica gossan								Coogamai flow within sílica gossan							
SiO_2	52.97	52.17	59.20	58.49	58.65	56.08	54.83	51.98	53.56	58.24	51.60	52.07	54.33	53.31	51.97	53.57
TiO_2	0.07	0.08	0.08	0.09	0.07	0.07	0.09	0.12	0.17	0.08	0.09	0.07	0.08	0.09	0.08	0.09
Al_2O_3	25.18	28.17	24.75	24.61	24.73	26.11	25.62	28.59	27.16	25.34	29.07	28.83	26.73	28.46	28.89	28.28
Fe_2O_3	1.88	0.97	0.68	0.78	0.74	0.80	0.86	1.35	1.74	0.70	1.82	0.68	2.05	1.25	1.09	0.95
Mn_2O_3	0.00	0.00	0.01	0.04	0.00	0.01	0.00	0.00	0.04	0.00	0.00	0.00	0.03	0.02	0.03	0.00
Cr_2O_3	0.00	0.00	0.00	0.00	0.00	0.01	0.00	0.01	0.00	0.00	0.00	0.00	0.00	0.00	0.00	0.00
MgO	0.49	0.09	0.02	0.04	0.05	0.04	0.04	0.06	0.31	0.05	0.23	0.08	0.45	0.06	0.30	0.04
CaO	11.16	12.92	7.75	7.71	7.63	9.57	9.74	12.49	11.00	8.08	13.08	12.69	10.78	11.89	12.64	11.76
Na_2O	4.42	4.39	6.88	6.72	6.58	6.00	5.65	4.43	4.49	6.73	3.98	4.44	4.98	4.73	4.30	4.99
K_2O	1.08	0.32	0.79	0.82	0.99	0.78	0.78	0.32	0.88	0.51	0.29	0.30	0.23	0.34	0.32	0.30
BaO	0.00	0.02	0.10	0.11	0.00	0.00	0.00	0.00	0.04	0.09	0.00	0.04	0.02	0.00	0.02	0.01
Total	97.27	99.13	100.24	99.41	99.44	99.48	97.61	99.36	99.40	99.82	100.16	99.21	99.68	100.15	99.65	99.99
Si	2.49	2.40	2.65	2.64	2.65	2.55	2.54	2.39	2.45	2.62	2.36	2.39	2.48	2.42	2.38	2.43
Al	1.39	1.53	1.31	1.31	1.32	1.40	1.40	1.55	1.47	1.34	1.56	1.56	1.44	1.52	1.56	1.51
Fe_3	0.07	0.03	0.02	0.03	0.03	0.03	0.03	0.05	0.06	0.02	0.06	0.02	0.07	0.04	0.04	0.03
Mn_3	0.00	0.00	0.00	0.00	0.00	0.00	0.00	0.00	0.00	0.00	0.00	0.00	0.00	0.00	0.00	0.00
Cr	0.00	0.00	0.00	0.00	0.00	0.00	0.00	0.00	0.00	0.00	0.00	0.00	0.00	0.00	0.00	0.00
Ti	0.00	0.00	0.00	0.00	0.00	0.00	0.00	0.00	0.01	0.00	0.00	0.00	0.00	0.00	0.00	0.00
su1	3.98	3.97	3.99	3.99	3.99	3.98	3.98	3.99	4.01	3.99	4.00	3.98	4.02	4.00	4.00	3.99
Ba	0.00	0.00	0.00	0.00	0.00	0.00	0.00	0.00	0.00	0.00	0.00	0.00	0.00	0.00	0.00	0.00
Ca	0.56	0.64	0.37	0.37	0.37	0.47	0.48	0.61	0.54	0.39	0.64	0.62	0.53	0.58	0.62	0.57
Na	0.40	0.39	0.60	0.59	0.58	0.53	0.51	0.39	0.40	0.59	0.35	0.40	0.44	0.42	0.38	0.44
K	0.06	0.02	0.04	0.05	0.06	0.05	0.05	0.02	0.05	0.03	0.02	0.02	0.01	0.02	0.02	0.02
su2	1.03	1.05	1.02	1.01	1.00	1.04	1.04	1.03	0.99	1.01	1.01	1.04	0.98	1.02	1.02	1.03
Components																
An	0.55	0.61	0.37	0.37	0.37	0.45	0.47	0.60	0.55	0.39	0.63	0.60	0.54	0.57	0.61	0.56
Ab	0.39	0.37	0.59	0.58	0.57	0.51	0.49	0.38	0.40	0.58	0.35	0.38	0.45	0.41	0.37	0.43
Or	0.06	0.02	0.04	0.05	0.06	0.04	0.04	0.02	0.05	0.03	0.02	0.02	0.01	0.02	0.02	0.02

Table 6
Click here to download Table: Table 6_2015_02_09.doc

Table 6
Representative microprobe analyses of clinopyroxenes from Coogamai flow, within and outside silica gossan (oxides in wt.%).

	Coogamai flow outside sílica gossan								Coogamai flow within sílica gossan							
	Augite				*Pigeonite*				*Augite*				*Pigeonite*			
SiO_2	50.41	47.40	50.02	49.22	49.70	50.14	50.35	49.75	50.38	50.01	49.59	49.68	50.70	49.93	50.27	50.06
TiO_2	0.80	1.73	0.79	0.81	0.61	0.52	0.39	0.51	0.81	0.91	0.95	0.95	0.51	0.57	0.56	0.50
Al_2O_3	1.37	3.66	1.87	0.97	0.73	0.89	2.34	0.62	1.18	1.91	1.89	1.81	0.99	0.72	0.66	0.63
Cr_2O_3	0.03	0.17	0.18	0.01	0.00	0.00	0.00	0.00	0.00	0.11	0.00	0.01	0.03	0.00	0.02	0.00
FeO_{tot}	15.07	15.05	10.35	18.05	25.09	24.00	20.86	25.47	16.85	12.70	15.85	15.68	27.21	23.98	24.36	23.38
MnO	0.35	0.35	0.20	0.47	0.55	0.55	0.40	0.55	0.42	0.38	0.35	0.34	0.46	0.52	0.53	0.62
MgO	13.97	11.51	15.15	11.99	16.46	17.39	17.21	16.43	12.69	14.28	12.89	12.88	13.26	18.46	16.97	18.34
CaO	17.39	18.14	19.86	16.94	5.26	5.19	4.99	5.27	17.21	18.65	17.74	18.09	6.08	4.63	5.08	4.54
Na_2O	0.21	0.39	0.25	0.23	0.11	0.44	0.57	0.05	0.26	0.24	0.19	0.21	0.11	0.08	0.11	0.09
K_2O	0.03	0.05	0.00	0.02	0.01	0.04	0.34	0.04	0.02	0.02	0.01	0.03	0.02	0.00	0.00	0.03
Total	99.63	98.45	98.67	98.71	98.53	99.15	97.45	98.69	100.02	99.21	99.46	99.68	99.37	98.88	98.56	98.20
Atoms per formula unit calculated on the basis of 6 oxygen																
Si	1.93	1.85	1.90	1.93	1.94	1.94	1.95	1.95	1.94	1.91	1.91	1.91	1.98	1.93	1.96	1.95
Ti	0.02	0.05	0.02	0.02	0.02	0.02	0.01	0.02	0.02	0.03	0.03	0.03	0.01	0.02	0.02	0.01
Al	0.06	0.17	0.08	0.04	0.03	0.04	0.11	0.03	0.05	0.09	0.09	0.08	0.05	0.03	0.03	0.03
Cr	0.00	0.01	0.01	0.00	0.00	0.00	0.00	0.00	0.00	0.00	0.00	0.00	0.00	0.00	0.00	0.00
Fe_{2+}	0.48	0.49	0.33	0.59	0.82	0.78	0.68	0.83	0.54	0.40	0.51	0.50	0.89	0.78	0.79	0.76
Mn	0.01	0.01	0.01	0.02	0.02	0.02	0.01	0.02	0.01	0.01	0.01	0.01	0.02	0.02	0.02	0.02
Mg	0.80	0.67	0.86	0.70	0.96	1.00	0.99	0.96	0.73	0.81	0.74	0.74	0.77	1.06	0.98	1.06
Ca	0.71	0.76	0.81	0.71	0.22	0.22	0.21	0.21	0.71	0.76	0.73	0.74	0.25	0.19	0.21	0.19
Na	0.02	0.03	0.02	0.02	0.01	0.03	0.04	0.00	0.02	0.02	0.01	0.02	0.01	0.01	0.01	0.01
K	0.00	0.00	0.00	0.00	0.00	0.00	0.02	0.00	0.00	0.00	0.00	0.00	0.00	0.00	0.00	0.00

Table 7
Click here to download Table: Table 7_2015_02_09.doc

Table 7
Representative electron microprobe analyses of the smectite group. Coogamai flow, within and outside silica gossan (wt.%).

	Coogamai flow outside sílica gossan								Coogamai flow within sílica gossan							
SiO_2	52.12	50.60	51.10	53.69	50.84	49.97	53.98	52.25	48.02	47.18	46.91	46.04	46.13	52.04	50.34	51.13
Al_2O_3	2.72	3.64	3.05	2.46	4.47	4.58	2.42	2.79	4.35	5.35	4.39	4.70	4.64	3.51	4.79	4.58
FeO	21.02	19.41	20.52	22.73	17.07	16.06	23.23	22.07	23.78	24.66	27.37	27.08	28.09	15.55	5.04	5.48
MgO	10.23	13.78	11.98	8.99	16.32	16.85	8.80	10.40	11.32	12.11	10.89	11.96	11.22	14.46	24.22	24.25
TiO_2	0.07	0.02	0.04	0.03	0.02	0.00	0.06	0.06	0.12	0.10	0.02	0.02	0.06	0.01	0.00	0.02
MnO	0.01	0.04	0.00	0.01	0.02	0.00	0.00	0.00	0.00	0.08	0.06	0.06	0.07	0.00	0.04	0.00
CaO	1.29	1.46	1.62	1.28	1.64	1.79	1.19	1.42	1.75	1.40	1.77	1.72	1.79	0.90	1.38	1.58
Na_2O	0.19	0.19	0.20	0.18	0.24	0.23	0.18	0.16	0.05	0.35	0.06	0.08	0.09	0.21	0.13	0.13
K_2O	3.40	2.21	2.58	3.83	1.20	0.91	4.02	3.17	0.88	1.43	0.10	0.24	0.21	2.62	0.34	0.40
Total	91.04	91.35	91.09	93.21	91.82	90.39	93.89	92.33	90.28	92.65	91.57	91.89	92.29	89.31	86.28	87.57
Calculated based on 11 oxygen																
Si	3.71	3.57	3.63	3.75	3.54	3.52	3.74	3.67	3.45	3.33	3.35	3.28	3.28	3.71	3.61	3.62
Al_{IV}	0.23	0.30	0.26	0.20	0.37	0.38	0.20	0.23	0.37	0.45	0.37	0.39	0.39	0.29	0.39	0.38
$Fe_{3+,\ IV}$	0.06	0.12	0.11	0.05	0.10	0.10	0.06	0.09	0.18	0.22	0.29	0.32	0.33	0.00	0.00	0.00
$Sum_{(IV)}$	3.94	3.88	3.89	3.95	3.90	3.90	3.94	3.91	3.82	3.78	3.71	3.68	3.67	4.00	4.00	4.00
Al_{VI}	0.00	0.00	0.00	0.00	0.00	0.00	0.00	0.00	0.00	0.00	0.00	0.00	0.00	0.01	0.01	0.00
$Fe_{3+,\ VI}$	1.25	1.15	1.22	1.33	0.99	0.95	1.35	1.30	1.43	1.46	1.63	1.61	1.67	0.93	0.30	0.32
Ti	0.00	0.00	0.00	0.00	0.00	0.00	0.00	0.00	0.01	0.01	0.00	0.00	0.00	0.00	0.00	0.00
Mg	1.09	1.45	1.27	0.94	1.69	1.77	0.91	1.09	1.21	1.28	1.16	1.27	1.19	1.54	2.59	2.56
Mn	0.00	0.00	0.00	0.00	0.00	0.00	0.00	0.00	0.00	0.00	0.00	0.00	0.00	0.00	0.00	0.00
$Sum_{(VI)}$	2.34	2.60	2.49	2.26	2.69	2.72	2.26	2.39	2.65	2.74	2.79	2.89	2.87	2.47	2.91	2.88
Ca	0.10	0.11	0.12	0.10	0.12	0.14	0.09	0.11	0.13	0.11	0.14	0.13	0.14	0.07	0.11	0.12
Na	0.03	0.03	0.03	0.02	0.03	0.03	0.02	0.02	0.01	0.05	0.01	0.01	0.01	0.03	0.02	0.02
K	0.31	0.20	0.23	0.34	0.11	0.08	0.36	0.28	0.08	0.13	0.01	0.02	0.02	0.24	0.03	0.04
sum	0.44	0.34	0.39	0.46	0.26	0.25	0.47	0.41	0.22	0.28	0.15	0.16	0.17	0.34	0.16	0.18

Figure 1
Click here to download high resolution image

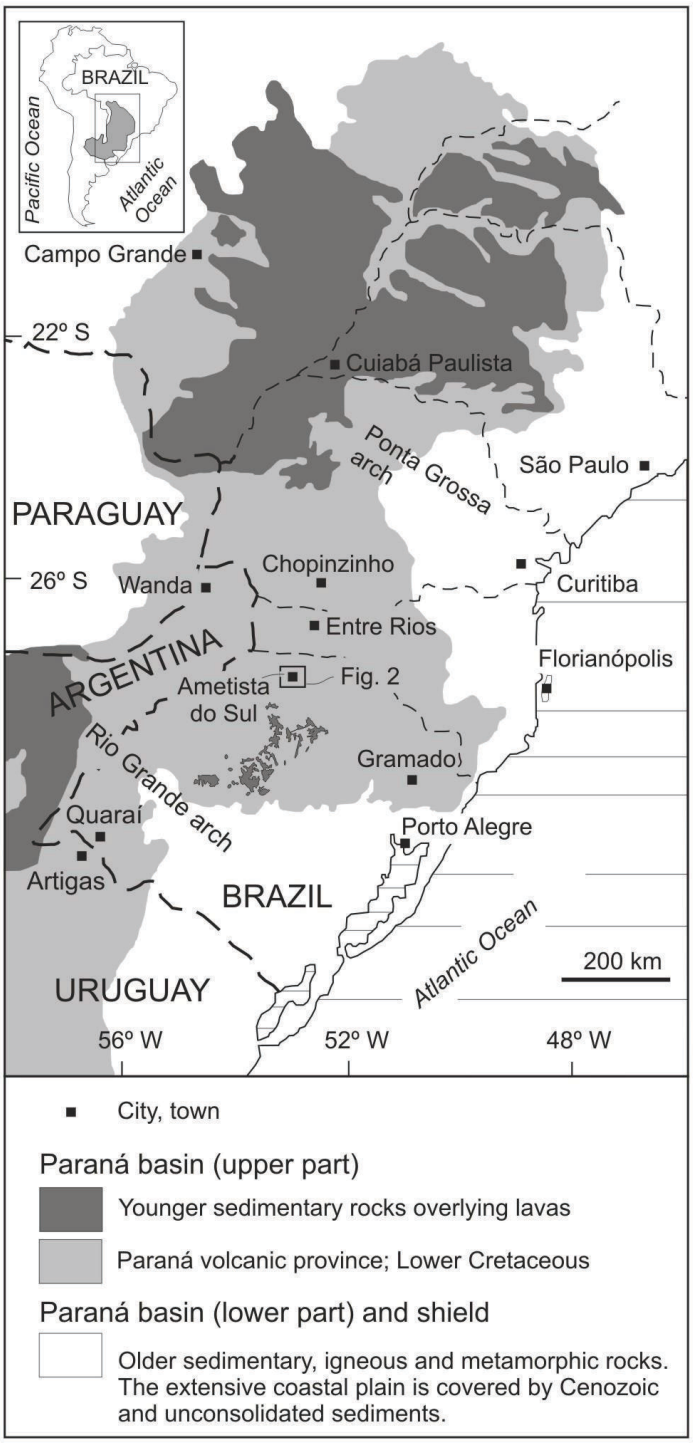

Figure 2
Click here to download high resolution image

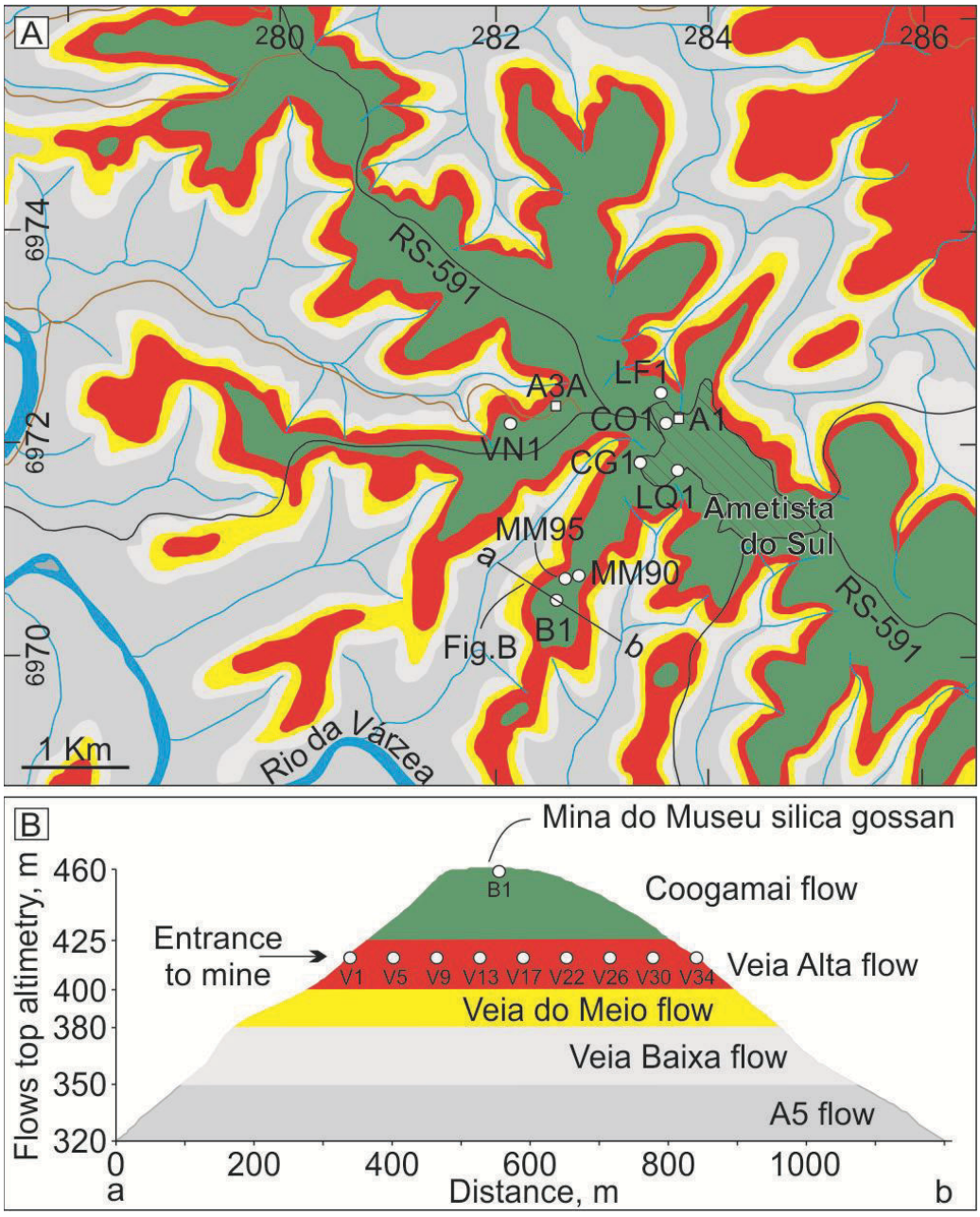

Figure 3
Click here to download high resolution image

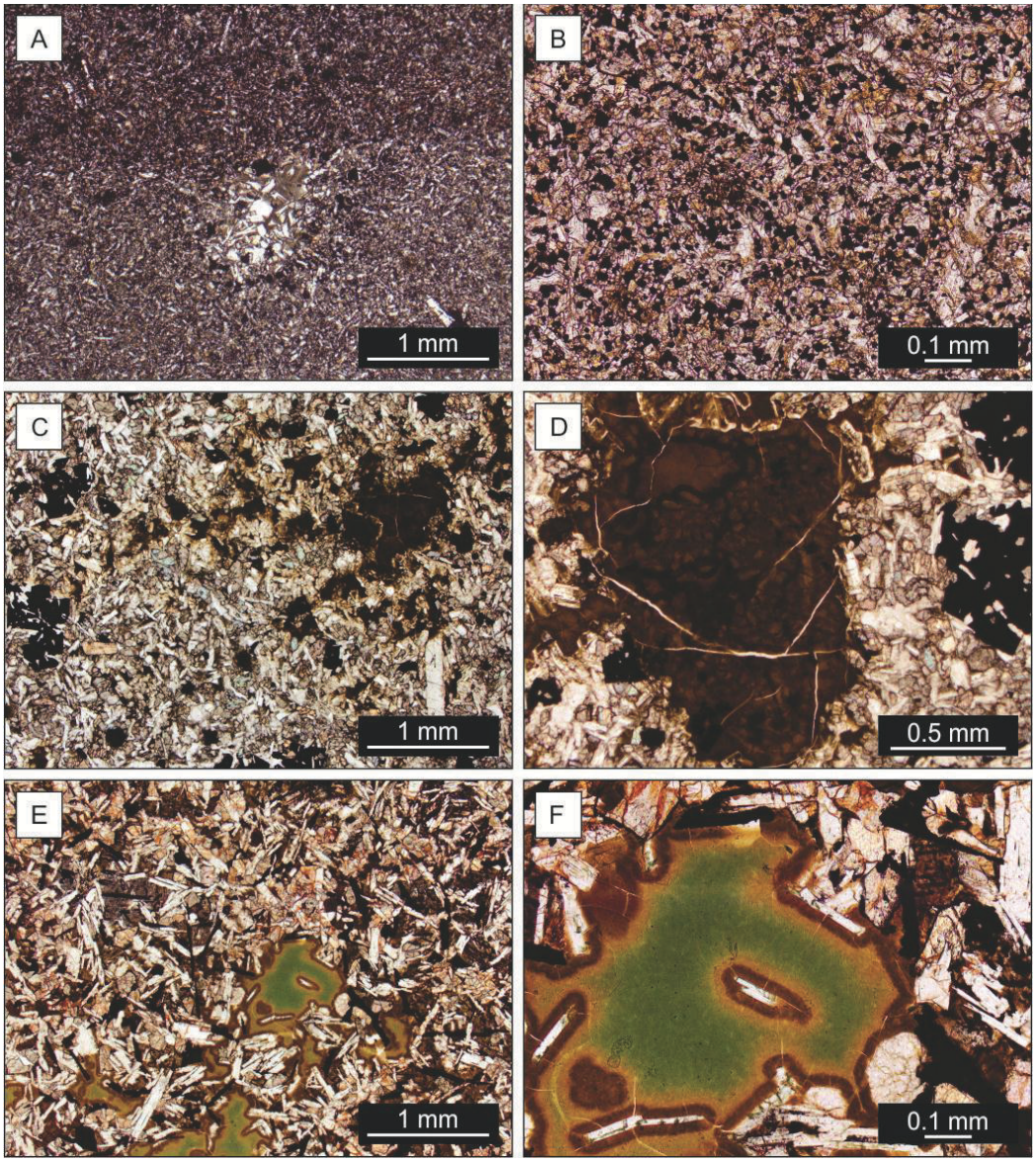

Figure 4
Click here to download high resolution image

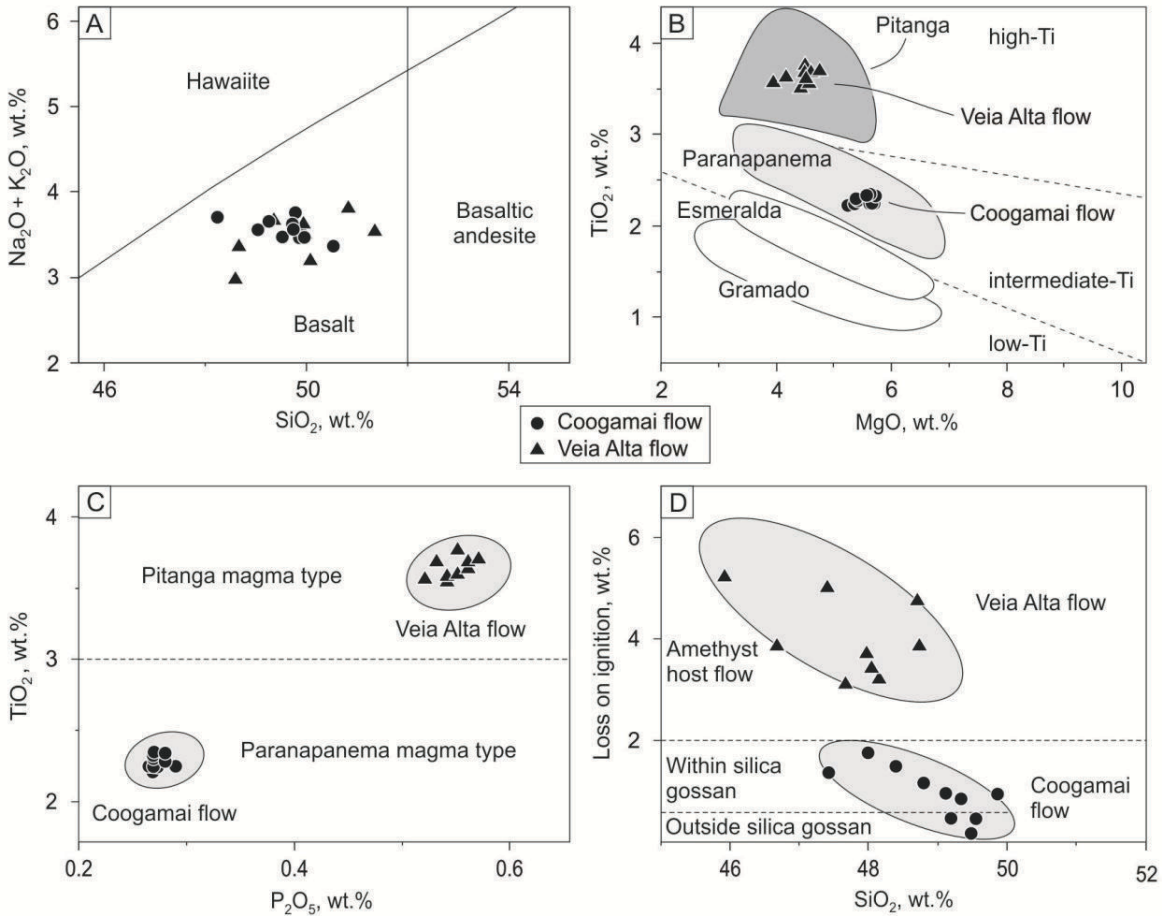

Figure 5
Click here to download high resolution image

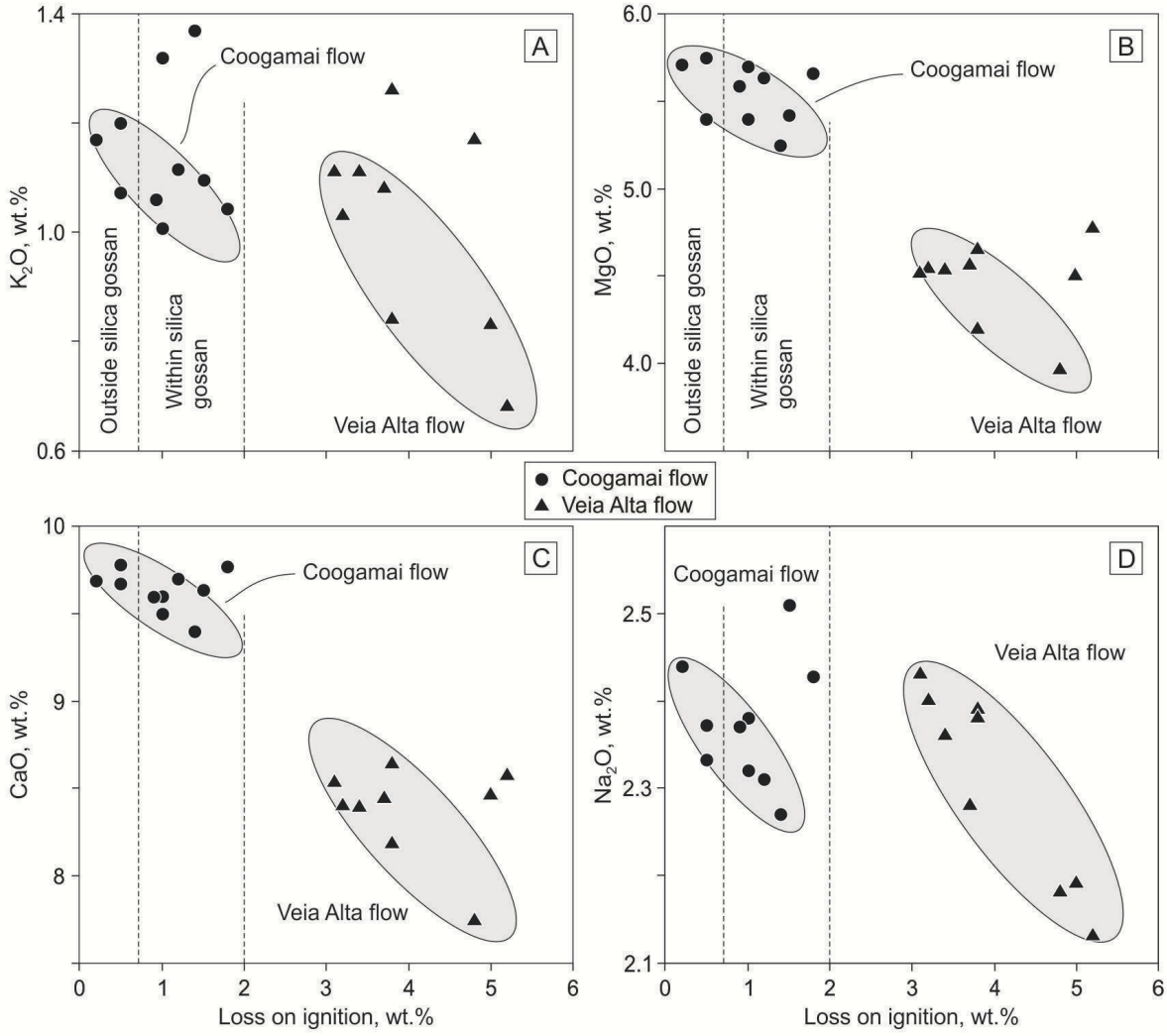

Figure 6
Click here to download high resolution image

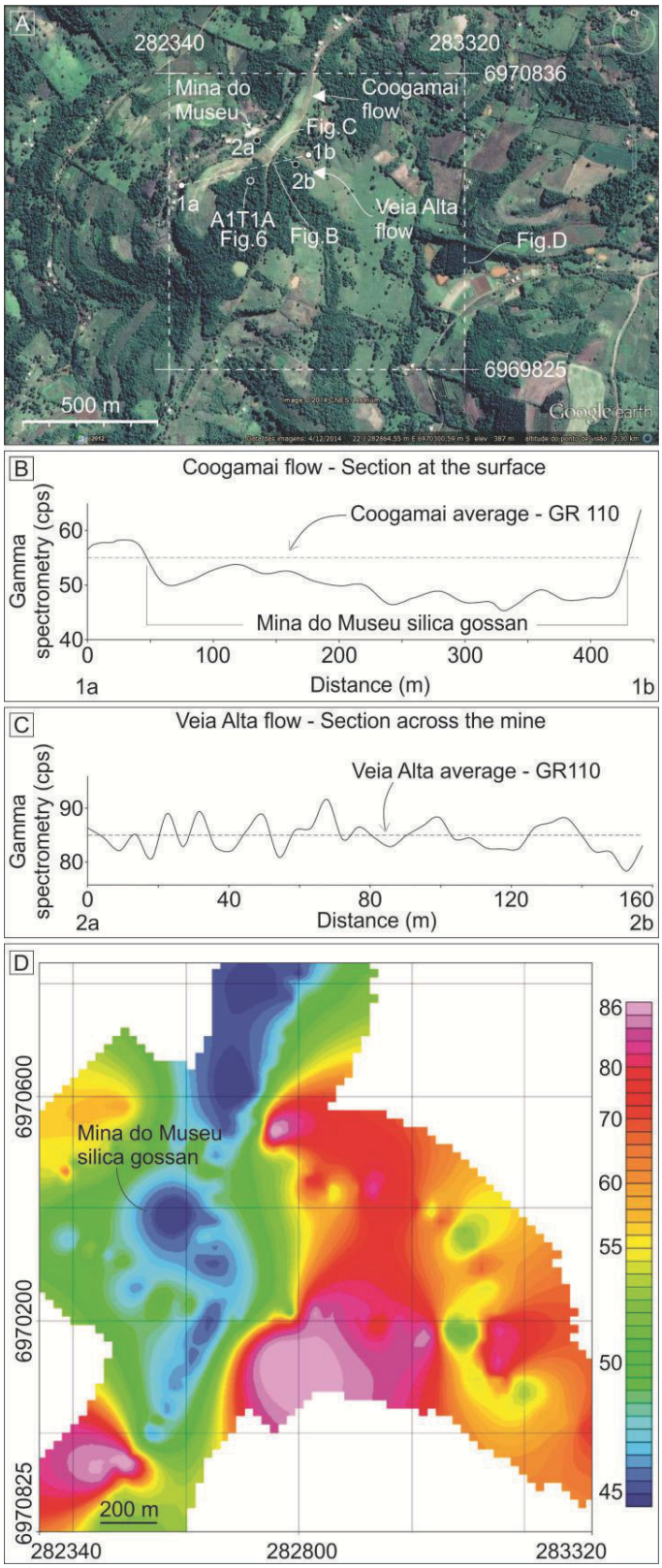

Figure 7
Click here to download high resolution image

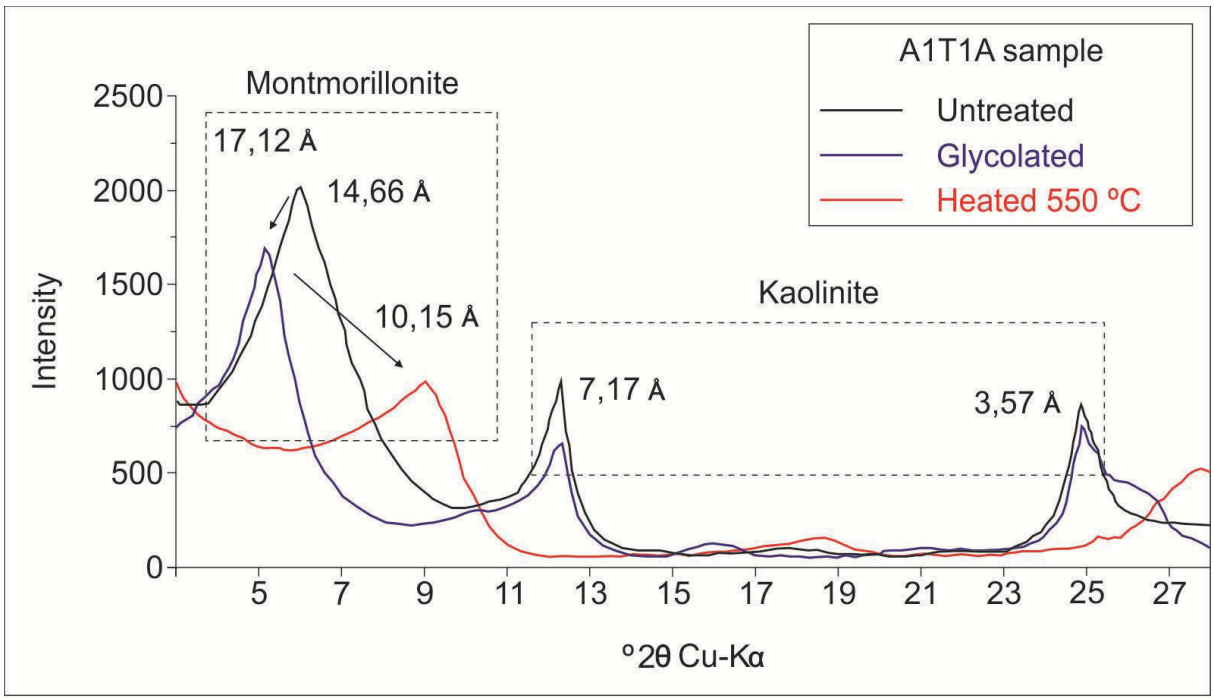

Figure 8
Click here to download high resolution image

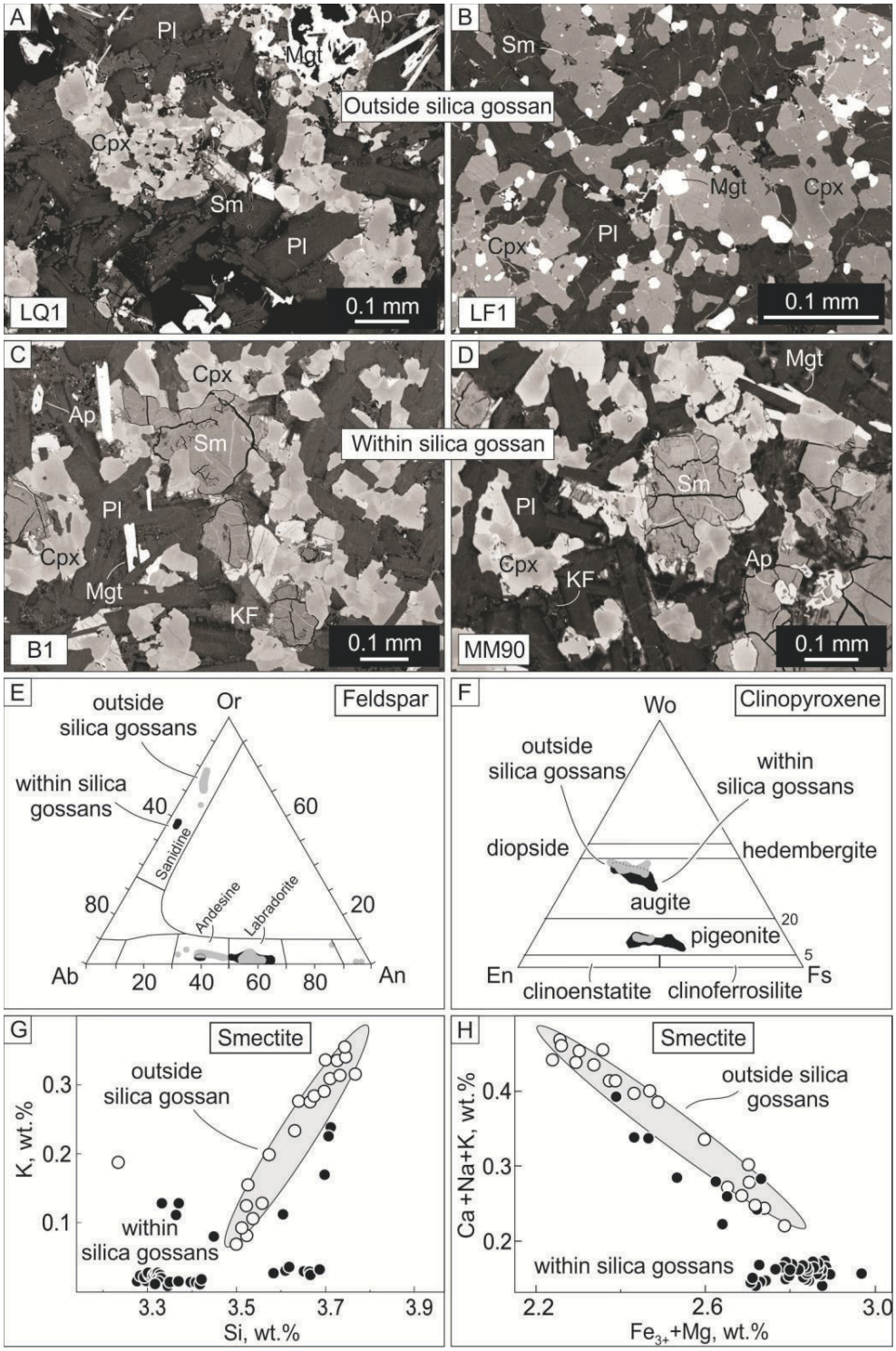

Figure 9
Click here to download high resolution image

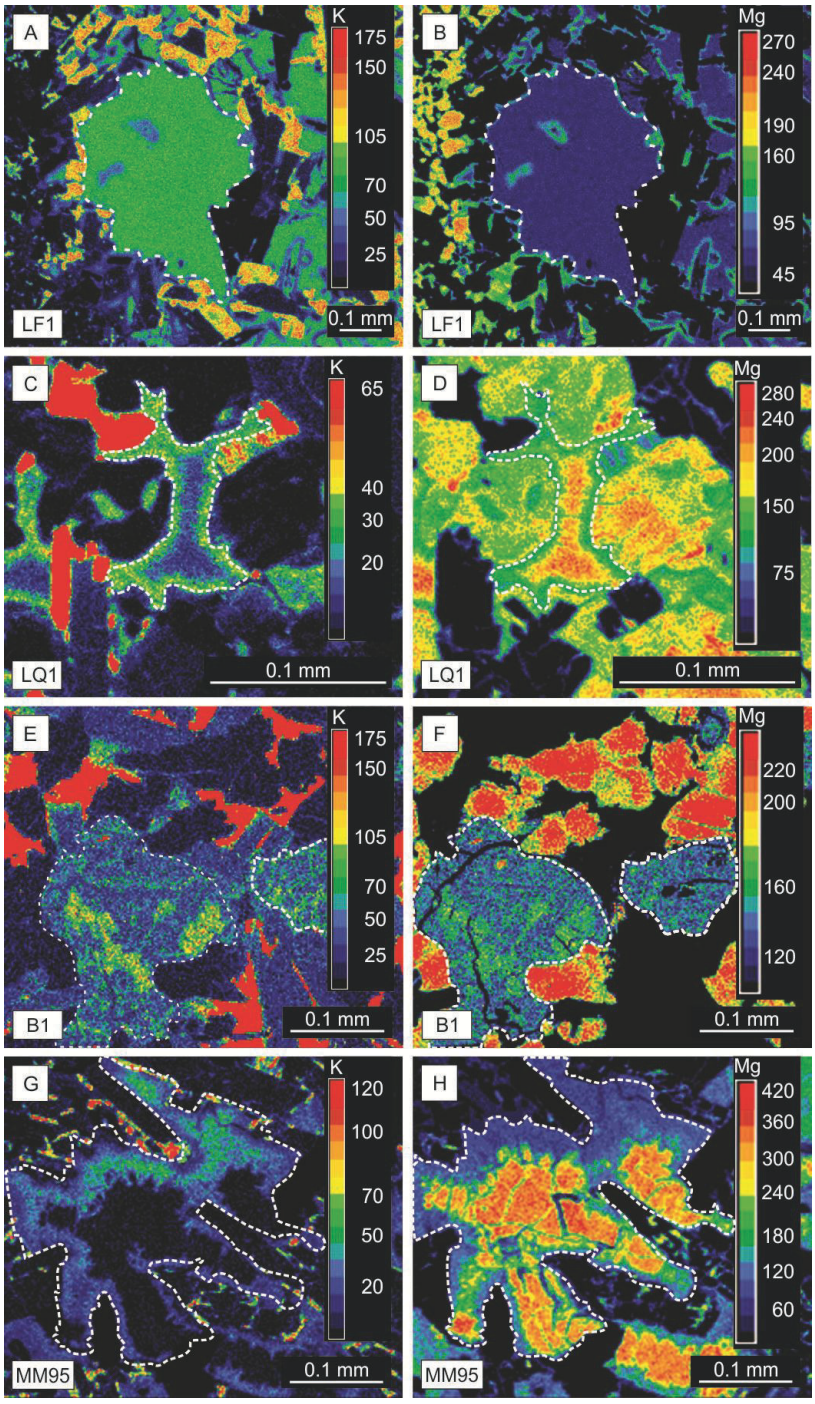

Artigo 3

BASALT STRATIGRAPHY AND SILICA GOSSANS IN CAMPO GRANDE AND SERRA DE MARACAJU, MATO GROSSO DO SUL, PARANÁ VOLCANIC PROVINCE, BRAZIL

Artigo publicado na Ore Geology Reviews

Ore Geology Reviews 69 (2015) 73–87

Contents lists available at ScienceDirect

Ore Geology Reviews

journal homepage: www.elsevier.com/locate/oregeorev

Basalt stratigraphy and silica gossans in Campo Grande and Serra de Maracaju, Mato Grosso do Sul, Paraná Volcanic Province

S.B. Baggio [a], L.A. Hartmann [a,*], R.H.P. Andrade [b], G.J. Rizzotto [c], S.K. Duarte [a], D.B. Knijnik [a], J.A. Simões-Neto [b]

[a] Instituto de Geociências, Universidade Federal do Rio Grande do Sul, Avenida Bento Gonçalves, 9500, Bairro Agronomia, 91501-970 Porto Alegre, Rio Grande do Sul, Brazil
[b] Departamento Nacional de Produção Mineral, Superintendência do Mato Grosso do Sul, Rua General Odorico Quadros, 123, 79020-260 Campo Grande, Mato Grosso do Sul, Brazil
[c] Geological Survey of Brazil (CPRM), SUREG-GO, Rua 148, 485, Setor Marista, 74170-110 Goiânia, Goiás, Brazil

ARTICLE INFO

Article history:
Received 18 April 2013
Received in revised form 20 January 2015
Accepted 22 January 2015
Available online 23 January 2015

Keywords:
Silica gossan
Paraná volcanic province
Hydrothermal deposits
Volcanic stratigraphy
Serra Geral group
Geochemistry

ABSTRACT

Thousands of silica gossans are exposed at the top of the Lower Cretaceous basalt hills in the Paraná volcanic province, strongly indicating the presence of calcite, amethyst and agate geode deposits along with native copper mineralization. The Embrapa silica gossan in the northwestern portion of the province (Campo Grande region) is an excellent example of such novel geological structure in the continental flood basalts. This silica gossan has a size of 450 × 350 m standing out as a treeless area in the densely wooded savanna and makes part of the stratigraphy of six basalt flows of Paranapanema intermediate-Ti chemical type. The base of the volcanic column is constituted by two Pitanga types and the overlying column is Paranapanema type. Every basalt flow has a silicified sand layer or breccia at the top and these are fed by abundant sand dikes. The Anel Viário Norte (AVN) flow is the most intensely altered by hydrothermal fluids producing voluminous secondary calcite infillings in the amygdales and fractures. In this region the basalts contain higher copper content than the average of the volcanic province. The studied silica gossans display negative anomalies in gamma spectrometry as a response to K, U and Th depletion during alteration. We propose a new exploration methodology by observing GoogleEarth images complemented with field studies and geochemistry to readily locate favorable areas for amethyst and agate geode deposits and native copper mineralization.

1. Introduction

The identification of silica gossans in the Paraná continental flood basalt (CFB) province (Fig. 1) of South America opens the possibility of the existence of many hitherto unsuspected hydrothermal deposits. Almost every erosional remnant hill in the province seems to contain silica gossans. Gossans commonly occur above high-sulfidation ore deposits (Scott et al., 2001; Pirajno, 2009), but the low-sulfide gossans in the Paraná volcanic province are also enriched in goethite-limonite, clay minerals and silica (silicified sandstone dikes and sills). This leads to the use of the expression "silica gossan" as an adequate name for the geological structure resulting from supergene alteration of the hydrothermal deposits. An extensive literature survey did not provide any additional information on silica gossans within continental basaltic provinces. This is thus a novel approach to a common geological structure, because a low-sulfide intraplate volcanic province hosts many hydrothermal deposits and associated silica gossans.

The earlier study of gossans in the southern part of the province (Pertille et al., 2013) is extended with the present investigation to the northwestern extreme of the Paraná basin. Because silica gossans in the Campo Grande region may contain unexplored deposits, the basalt stratigraphy is here established with the use of field description, gamma-spectrometry and rock geochemistry to adequately position the gossans in the host basalt flow.

2. Regional geology

The Paraná continental flood basalt (CFB) province of South America is one of the largest igneous provinces in the world and covers an area of 917,000 km^2 (Frank et al., 2009) in Brazil, Uruguay, Argentina and Paraguay (Fig. 1) with a lava volume of 450,000 km^3 at the surface in addition to 112,000 km^3 of lava that remained in the subsurface as sills and dikes. The Cuiabá Paulista borehole suggests the total thickness of the volcanic pile to be 1723 m. To the south, the lava pile becomes progressively thinner reaching 50 m along the Brazil–Argentina border (Almeida, 1986). The thickness of individual flows (Peate et al., 1999) is 5 to 80 m, with an average of 20 m. Although the most abundant rocks are basalt and basaltic andesite, dacites, rhyodacites and rhyolites do occur in the upper part of the volcanic pile in the southern portion of

* Corresponding author.
E-mail addresses: sergio.baggio@ufrgs.br (S.B. Baggio), leo.hartmann@ufrgs.br (L.A. Hartmann), romualdo.andrade@dnpm.gov.br (R.H.P. Andrade), gilmar.rizzotto@cprm.gov.br (G.J. Rizzotto), sandrokduarte@hotmail.com (S.K. Duarte), Daniel_bk@live.com.au (D.B. Knijnik), jose.simoes@dnpm.gov.br (J.A. Simões-Neto).

http://dx.doi.org/10.1016/j.oregeorev.2015.01.015
0169-1368/

Fig. 1. Geological map of southeastern South America highlights the Paraná Basin. The Paraná volcanic province in light gray. Younger sedimentary rocks overlying lavas (dark gray), represented by the Bauru Group in Brazil, Acaray Formation in Paraguay (correlated with the bottom of Bauru Group) and as Mariano Boedo Formation and sands from the Chaco Group in Argentina. Older sedimentary, igneous and metamorphic rocks and an extensive coastal plain covered by Cenozoic sediments (blank area). Campo Grande city is at the center of the study area. Hydrothermal deposits (amethyst and agate) and native copper occurrence are shown.
Modified from Peate et al. (1992).

the province (Melfi et al., 1988). Pyroclastic rocks are also described by some authors (e.g. Licht et al., 2012) but their occurrence is restricted.

The volcanic rocks constitute the Serra Geral Group in Brazil (Wildner et al., 2009). The age of the group is under debate (e.g., Mantovani et al., 1985; Rocha-Campos et al., 1988; Mincato, 2000; Lustrino et al., 2005; Wildner et al., 2006) and recent studies (Pinto et al., 2011a, zircon U–Pb SHRIMP; Janasi et al., 2011, baddeleyite TIMS) confirmed the age of 133–135 Ma for the peak of volcanism. The geochemical subdivision of the Serra Geral Group was made based on the TiO_2 content of the rocks (Bellieni et al., 1984; Mantovani et al., 1985) into high-Ti (TiO_2 >2%) in the north and low-Ti (TiO_2 <2%) in the south. Peate et al. (1992) reassessed these two groups and proposed a new classification based on major and trace elements and element ratios. The low-Ti group was divided into Gramado, Esmeralda and Ribeira magma types and the high-Ti group into Urubici, Pitanga and Paranapanema magma types. The world's largest deposits of amethyst and agate are hosted in rocks from the two magma types. The main exploration areas are concentrated in Ametista do Sul in Brazil and Los Catalanes in Uruguay (Juchem et al., 2010; Silva, 2010). Native copper mineralization hosted in basalts and in hydrothermal breccias is also widespread.

Until recently, the Serra Geral Group was studied mostly with respect to magmatic interactions (temperatures around 1150 °C), but from 2005 a new aspect of the Serra Geral Group was evaluated (e.g. Duarte et al., 2009; Hartmann et al., 2010, 2012a, 2012b; Pinto et al., 2011b) with the identification of low temperature hydrothermal events (150 °C). This new approach to studies of the Serra Geral Group allowed the understanding of a set of unique geological features such as the heat source, the water source in the Guarani aquifer, the unconsolidated sands of the Botucatu desert, the type I basalt flows (Gomes, 1996) and the intraplate tectonic environment (horizontal lavas). The combination of these factors triggered intense hydrothermal events defined as H1, H2 and H3 (Hartmann, 2008; Hartmann et al., 2012a, 2012b) which were responsible for the rising of hydrothermal fluids (boiling water and its vapor) that transported upward through the basalt flows a huge quantity of sand from the Botucatu Formation. Evidence of the injected sand is widespread in several areas of the province (Hartmann et al, 2013) forming silicified hydrothermal structures as sand dikes, sand sills, sand layers and even hydrothermal breccia at

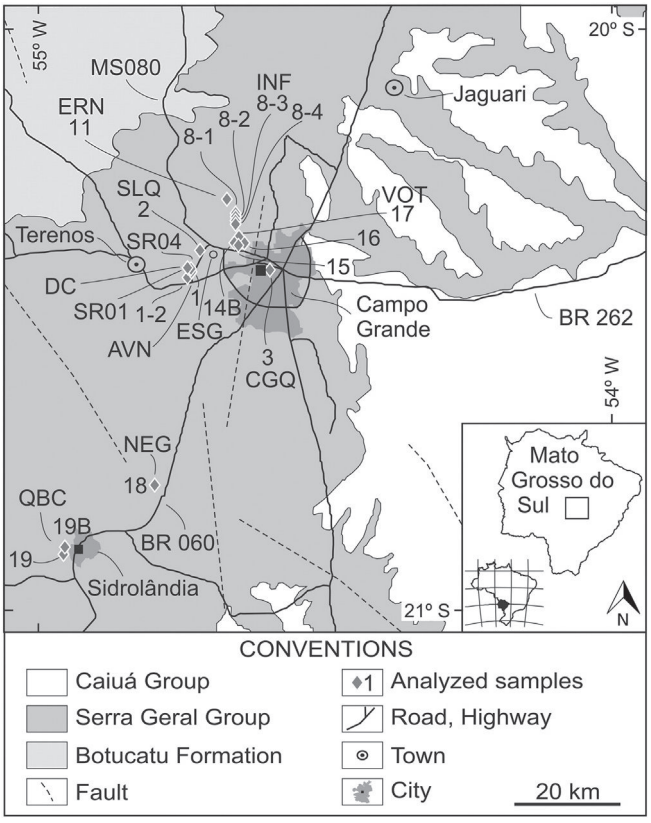

Fig. 2. Geological map of the Campo Grande region (modified from Lacerda Filho et al., 2006) with the location of the analyzed samples (all sample numbers have an MS prefix; e.g., 17 = MS17). Symbology used: AVN — Anel Viário Norte section, ESG — Embrapa silica gossan, SLQ — São Luiz quarry, VOT — Votorantim quarry, CGQ — Campo Grande quarry, INF — Cascata Infernihno section, ERN — Ernesto section, DC — Drill cores (SR1 and SR4), NEG — Negrimaq quarry, and QBC — Quebra-Coco quarry. Highways indicated (e.g., BR060, MS080). The studied area is indicated by the square in the inset map.

the top of the flows. The silicification of the sand was promoted by the continued percolation of hot water. The hydrothermal alteration modified the volcanic rocks, transforming pyroxenes and opaque minerals into clay minerals, mostly smectites and zeolites. The hydrothermal deposits associated with these events correspond to the largest amethyst-agate geode deposits in the world (Hartmann, 2008; Duarte et al., 2011; Rosenstengel and Hartmann, 2012) and also resulted in the formation of native copper mineralization (Pinto et al., 2011b). The silicified structures and their association with hydrothermal deposits are observed in the entire stratigraphy of the volcanic pile from less than 50 m thick to the top of the sequence at 1000 m elevation.

In the Campo Grande region (Fig. 2), the little-studied basaltic rocks from the Serra Geral Group display a thickness of about 100 to 300 m (Lastoria, 2002). A reconnaissance study (Machado et al., 2009), however, indicated the predominance of high-Ti basalts of the Pitanga type. The volcanic rocks are nearly horizontal which extend for large distances and are cut by large vertical faults. The Campo Grande is at an elevation of 600 m, whereas the top of the Serra de Maracaju is at 500 m. The low-lying sedimentary plain in front of the cuesta is at 350 m (Campo Grande) and 250 m (Maracaju). The thickness of the basalt group is therefore nearly 250 m in the entire plateau of the region. Classical geomorphological features are present, because the present surface is more steeply inclined at the flow cores than in their contacts. Many polygonal or irregular areas display no trees on top of the basalt hills in the savanna of the region, so we selected a few of these structures for detailed investigations.

3. Methodology

The areas chosen for this study are from Campo Grande and Serra de Maracaju, Mato Grosso do Sul state. The methodology used for basalt stratigraphy and description of silica gossans involved the observation of anomalies in GoogleEarth images, field investigations including measurement of gamma-spectrometry emission rates, collection of representative rock samples and their chemical analyses. Two drill cores in the Campo Grande region and two sections in the Sidrolândia region were also sampled and studied. The altitude and geographic coordinate of each sample were obtained with a hand-held Garmin GPS while the total emission of gamma radiation (U, K and Th) was measured with a

Table 1
Chemical analyses of volcanic rocks from the Campo Grande region. Oxides in wt.%, trace elements in ppm except Au in ppb. (–) = below detection limit (Cr_2O_3 = 0.002, Cs = 0.1, Au = 0.5). All sample numbers have an MS prefix.

Sample	1	1–2	2	3	8–1	8–2	8–3	8–4	11	14B	15	16B	17B
SiO_2	50.80	48.54	49.62	50.11	47.29	46.84	47.88	48.83	51.25	48.09	50.10	50.14	48.52
TiO_2	3.61	1.84	1.81	2.06	2.50	2.31	3.44	3.70	3.08	2.30	1.82	1.67	2.09
Al_2O_3	12.17	13.18	12.95	12.34	12.27	12.44	11.97	11.96	12.62	12.26	12.86	13.30	13.30
Fe_2O_3	15.23	13.68	13.72	15.00	15.68	15.43	14.92	15.99	13.47	15.04	13.52	12.45	15.42
MgO	2.96	6.26	5.92	5.45	4.74	5.54	4.05	4.06	4.48	4.28	6.20	6.60	4.05
CaO	7.34	10.15	9.94	8.90	7.87	8.78	7.20	7.47	7.77	9.43	9.81	10.35	7.67
Na_2O	2.79	2.32	2.32	2.55	1.86	2.08	2.19	2.39	2.64	2.46	2.30	2.28	2.41
K_2O	1.98	0.89	0.98	0.99	1.63	0.70	1.69	1.80	1.71	1.56	0.97	0.82	1.52
P_2O_5	0.72	0.21	0.21	0.24	0.29	0.27	0.62	0.59	0.48	0.28	0.22	0.19	0.31
MnO	0.15	0.21	0.20	0.22	0.19	0.20	0.18	0.30	0.21	0.24	0.21	0.20	0.19
Cr_2O_3	–	0.011	0.012	0.010	0.019	0.010	0.002	0.003	0.011	0.009	0.012	0.017	0.008
LOI	1.9	2.4	2.0	1.8	5.3	5.1	5.5	2.6	1.9	3.7	1.7	1.7	4.2
Total	99.67	99.71	99.73	99.70	99.62	99.67	99.65	99.66	99.68	99.66	99.70	99.71	99.72
Au	1.9	5.7	6.8	5.1	1.0	14.5	0.9	–	–	–	6.0	4.5	4.9
Ba	598	268	245	282	502	341	548	492	435	424	255	234	345
Ce	87.6	33.6	32.5	41.2	48.5	46.1	91.2	85.9	69.8	46.1	38.1	33.9	50.7
Co	32.8	45.9	45.0	46.2	39.5	45.4	32.9	34.5	31.7	40.8	45.5	46.5	38.6
Cs	0.5	0.2	0.2	0.1	0.2	–	–	0.3	0.8	0.1	2.1	0.1	0.3
Cu	97	222	131	224	281	210	258	152	97	214	268	249	219
Dy	9.27	5.12	5.24	6.12	7.01	7.28	8.59	8.64	7.09	6.64	5.06	4.87	7.00
Er	5.44	3.24	3.56	3.76	4.59	4.40	4.77	4.39	3.75	3.88	2.91	2.85	4.70
Eu	3.38	1.51	1.51	1.72	1.98	2.00	3.14	3.07	2.68	1.94	1.54	1.45	2.15
Ga	24.9	20.7	18.9	18.0	19.3	20.6	22.3	21.2	20.7	18.2	17.1	16.9	19.8
Gd	10.73	4.92	5.26	6.26	7.55	7.09	10.35	9.88	8.29	6.53	5.18	4.62	7.34
Hf	9.2	3.9	3.4	4.4	5.0	4.2	7.6	7.1	5.7	4.4	3.7	3.4	4.7
Ho	1.72	0.86	0.98	1.24	1.58	1.54	1.73	1.72	1.38	1.37	1.14	1.01	1.50
La	47.7	17.5	17.5	19.9	25.8	23.8	42.3	40.3	33.7	22.9	18.1	16.6	27.9
Lu	0.54	0.37	0.38	0.55	0.63	0.62	0.54	0.50	0.46	0.54	0.43	0.38	0.65
Mo	0.5	0.6	0.3	0.4	0.8	0.3	0.3	0.3	0.5	0.2	0.3	0.4	0.6
Nb	29.1	11.5	10.9	12.5	15.1	14.6	28.2	26.5	23.0	13.7	11.9	9.7	15.6
Nd	54.3	22.8	20.7	25.1	28.7	27.7	48.0	49.4	40.3	27.3	20.8	20.1	31.1
Ni	22	60	63	45	44	50	21	30	40	43	60	77	47
Pb	1.3	0.6	0.8	0.9	1.3	1.7	2.1	1.4	1.1	1.1	0.7	0.7	1.2
Pr	12.13	4.60	4.50	5.49	6.71	6.42	11.59	11.33	9.51	6.31	4.98	4.35	7.24
Rb	47.8	22.7	22.8	19.9	27.0	7.4	18.6	36.8	36.3	25.2	36.8	16.5	28.7
Sc	28	42	42	42	40	41	28	29	28	40	42	42	41
Sm	10.93	4.55	4.49	5.40	6.74	6.51	10.34	9.95	8.31	5.83	4.80	4.20	6.92
Sr	416	263	264	259	817	334	451	420	437	671	287	282	288
Ta	1.5	0.6	0.6	0.8	0.9	0.7	1.8	1.5	1.6	0.9	0.6	0.6	1.0
Tb	1.52	0.77	0.79	1.04	1.22	1.15	1.58	1.48	1.33	1.08	0.88	0.78	1.26
Th	4.4	1.6	2.0	2.2	2.5	2.5	4.3	3.9	3.5	2.6	2.0	1.9	2.9
Tm	0.61	0.39	0.39	0.54	0.64	0.63	0.64	0.60	0.52	0.57	0.44	0.44	0.63
U	0.8	0.3	0.4	0.5	0.8	0.5	0.8	0.8	0.8	1.0	0.4	0.4	0.9
V	376	423	424	462	470	494	358	393	443	445	426	397	416
Y	44.9	26.6	25.7	33.2	39.5	41.1	43.0	39.6	35.1	33.8	27.5	24.8	38.6
Yb	4.23	3.05	3.06	3.37	4.02	4.19	3.86	3.82	3.18	3.41	2.80	2.54	4.20
Zn	60	56	54	58	79	75	67	85	69	71	48	57	79
Zr	321	133	134	147	171	161	283	265	234	170	133	117	184

scintillometer exploranium GR-110 (measurement time 10 s) with results in counts per second (cps).

The gamma spectrometry evaluation of the Embrapa silica gossan was performed on a regular grid of 50 × 50 m (77 stations, 5 gamma-spectrometry readings at each station) covering an area of 550 × 450 m. In the Maracaju silica gossan we surveyed longitudinal sections that include the gossans and their immediate surroundings. The radiometric maps of gamma spectrometry were generated with software Oasis Montaj ® (Geosoft Latinoamerica) and the longitudinal section was calculated and drawn with the use of Excel and CorelDraw software.

Bulk rock samples from the Campo Grande region (n = 22) and from the Serra de Maracaju (n = 3) were chemically analyzed (Tables 1 and 2) at the ACME Analytical Laboratories, Vancouver, Canada for major and trace elements. The method used for the major elements comprises melting of 0.1 g sample in metaborate/lithium tetraborate and dilution with nitric digestion. Loss on ignition is obtained from the weight difference after combustion at 1000 °C. Trace elements and rare earth elements were analyzed by ICP–MS (mass spectrometry) following the same procedure of the major elements with the addition of 0.5 g sample digested in aqua regia for analysis by ICP–MS. The data were integrated in Excel spread sheets and interpreted with the support of Geochemical Data Toolkit freeware (GCDKit).

Soil samples (n = 2) in Embrapa (S6D) and Serra de Maracaju (S7B) were collected inside the structure of silica gossans. These samples were grinded and sieved following standard procedures and aiming to identify the mineralogy by X-ray diffraction (XRD). Each prepared powder was placed in a sample holder and the analyses of XRD were performed. For the confirmation of the identification of clay minerals, the <4 μm fraction was used in oriented natural, oriented glycol and oriented calcinated (550 °C) thin sections. XRD were carried out in a Siemens Bruker-AXS D5000 diffractometer with 2θ goniometer, radiation Kαl copper tube under conditions of 40 kV and 25 mA. The speed and the interval scanning of the goniometer for each type of analysis were as follows. Powder samples: 2 s to 0.02 of step goniometer 2θ 2° to 72°. Oriented natural samples: 2 s to 0.02 for the second step of the goniometer 2θ 2° to 28°. Oriented glycol samples: 3 s to 0.02 for the second step of the goniometer 2θ 2° to 28°. Oriented calcinated samples: 2 s to 0.02 for the second step of the goniometer 2θ 2° to 28°. The mineralogical interpretation was based on standards of PDF2 database DIFFRAC^{PLUS}

Table 2
Chemical analyses of volcanic rocks from the Campo Grande region. Oxides in wt.%, trace elements in ppm except Au in ppb. (–) = below detection limit (Cr_2O_3 = 0.002, Cs and Mo = 0.1). Sample numbers 16B, 17B, 18, 19 and 19B have an MS prefix. Sample numbers 1A, 1B, 1C, 4A, 4B and 4C have an SR prefix. Samples R4F, R7B and R11A are from basalt outcrops in the context of Maracaju silica gossan.

Sample	18	19	19B	1A	1B	1C	4A	4B	4C	R4F	R7B	R11A
SiO_2	50.31	49.72	48.52	48.43	46.38	49.33	49.89	48.05	49.89	50.54	49.68	49.36
TiO_2	1.77	2.11	2.07	1.83	2.50	3.53	1.82	2.35	3.56	3.65	3.94	3.92
Al_2O_3	12.91	12.68	12.92	12.96	11.82	12.05	12.91	12.57	12.21	11.95	12.27	12.27
Fe_2O_3	14.01	14.51	13.96	14.04	15.76	14.83	13.84	15.03	15.35	15.20	14.82	15.43
MgO	5.92	5.72	5.79	5.75	5.58	3.47	5.80	5.03	3.21	3.80	3.89	3.77
CaO	9.83	9.64	9.52	9.45	8.80	7.60	9.78	9.22	6.91	7.52	7.64	7.44
Na_2O	2.32	2.32	2.20	2.32	1.98	2.43	2.35	2.22	2.62	2.57	2.55	2.59
K_2O	0.88	0.95	0.93	1.05	0.33	1.67	1.03	0.44	2.14	1.62	1.71	1.82
P_2O_5	0.21	0.23	0.23	0.19	0.27	0.63	0.21	0.27	0.65	0.61	0.64	0.63
MnO	0.22	0.22	0.17	0.19	0.20	0.22	0.21	0.19	0.19	0.20	0.28	0.30
Cr_2O_3	0.016	0.012	0.010	0.013	0.009	0.003	0.012	0.007	–	0.003	–	–
LOI	1.3	1.6	3.4	3.5	6.1	3.9	1.8	4.3	2.9	2.0	2.2	2.1
Total	99.72	99.69	99.69	99.72	99.71	99.67	99.71	99.68	99.66	99.63	99.64	99.63
Au	2.7	3.9	2.2	1.9	6.8	2.0	4.2	7.2	2.6	2.3	2.0	5.1
Ba	258	305	328	286	209	530	266	354	561	597	585	626
Ce	37.5	43.2	43.6	30.8	45.5	79.1	35.3	44.3	86.6	86.2	83.2	90.3
Co	46.1	46.5	46.0	46.3	45.3	34.1	47.3	41.4	34.3	38.3	39.1	38.6
Cs	0.3	0.2	0.3	0.3	0.1	0.3	1.3	–	0.7	0.2	0.3	0.2
Cu	160	239	179	114	126	135	107	223	156	260.7	194	194.9
Dy	5.37	5.36	4.92	5.07	6.93	8.52	5.44	5.76	8.52	9.49	9.17	10.29
Er	3.22	3.11	2.86	3.39	4.58	4.47	3.47	4.01	4.76	5.19	5.35	5.66
Eu	1.51	1.74	1.71	1.53	1.85	3.06	1.55	1.81	3.26	3.34	3.34	3.63
Ga	17.4	18.5	18.6	19.3	20.0	22.7	18.1	19.7	23.2	23.9	23.5	24.7
Gd	5.44	5.74	5.16	5.19	6.44	9.73	5.30	6.35	10.36	10.72	10.80	11.65
Hf	3.7	4.0	3.4	3.4	4.5	7.6	3.5	4.7	8.1	8.0	7.4	7.7
Ho	1.12	1.09	1.02	0.98	1.39	1.48	0.98	1.17	1.52	1.72	1.67	1.97
La	18.6	21.5	20.7	18.0	23.0	41.9	18.8	22.9	44.3	48.0	45.5	52.3
Lu	0.44	0.43	0.42	0.38	0.50	0.50	0.36	0.46	0.56	0.59	0.60	0.60
Mo	0.3	0.5	0.3	0.3	0.5	0.5	0.4	–	0.6	0.7	0.8	0.7
Nb	11.6	12.0	12.5	11.0	16.1	27.9	11.2	14.2	31.1	30.3	30.9	30.9
Nd	19.3	23.6	24.2	21.4	26.8	47.4	21.1	23.6	48.7	50.3	58.0	58.7
Ni	67	63	60	28.6	17.5	10.1	22.2	21.5	10.3	14.5	13.7	12.4
Pb	0.7	0.9	1.3	0.5	2.3	1.5	0.7	2.2	1.7	1.6	1.7	1.5
Pr	4.79	5.72	5.73	4.62	5.99	10.88	4.90	6.12	11.77	12.06	12.16	13.17
Rb	19.4	18.6	17.8	20.4	5.0	21.6	37.8	4.4	60.9	38.1	38.1	41.1
Sc	41	39	37	43	40	28	42	40	28	30	30	30
Sm	4.81	5.21	5.07	4.58	5.98	9.56	5.01	5.64	10.57	11.49	11.06	11.72
Sr	285	347	360	252	259	394	270	416	410	422	427	453
Ta	0.7	0.8	0.7	0.7	0.9	1.6	0.6	1.0	1.5	1.6	1.8	1.8
Tb	0.90	0.90	0.91	0.78	1.03	1.39	0.86	0.96	1.52	1.58	1.52	1.73
Th	2.1	2.2	2.2	1.9	2.5	3.9	2.0	2.4	4.4	3.9	3.9	3.9
Tm	0.44	0.44	0.44	0.45	0.53	0.55	0.43	0.51	0.62	0.66	0.69	0.66
U	0.5	0.4	0.5	0.4	0.3	0.6	0.2	0.4	0.6	0.8	0.6	0.7
V	423	449	447	398	473	359	453	477	394	420	406	428
Y	28.0	27.3	27.3	29.3	36.2	39.5	30.9	32.2	43.5	48.7	47.1	52.6
Yb	2.88	2.74	2.91	2.83	3.73	3.84	3.41	3.11	3.73	4.67	4.46	5.01
Zn	43	61	65	62	57	43	39	69	69	93	82	82
Zr	129	148	143	131	176	292	141	167	317	311	299	313

software and from the database available at http://database.iem.ac.ru/mincryst.

4. Silica gossans

Our usage of "silica gossan" finds support in previous studies. The expression has been applied to prospective guides of hydrothermal kaolin deposits hosted either in Lower Tertiary rhyolites in San Luis Potosi, Mexico (Keller and Hanson, 1968) or in Lower Miocene andesites, dacites and tuffs in Turkey (Sayin, 2007). The main characteristics of these prospective guides are intense silicification, formation of oxidized iron-rich zones and change of color on the surface.

Studies carried out in Quaraí (Brazil) and Artigas (Uruguay) in basaltic andesites showed the occurrence of gossans not related to sulfides in an intraplate continental environment (Pertille et al., 2013). Silica gossans register the presence of channelized hydrothermal deposits. The deposits are either silica minerals (also calcite) or native copper. The origin of silica is associated with the H2 and H3 events (Hartmann et al., 2010) that promoted the formation of veins, dikes and sills of silicified sand. The subsequent silicification of these bodies, in the Lower Cretaceous, was generated by the boiling fluids (150 °C) derived from the Guarani aquifer along hydrothermal chimneys. In many parts of the Serra Geral Group, the silicification was very intense and made free silica available for the formation of agate and amethyst deposits.

Quaternary weathering (Hartmann et al, 2010) led to the intense alteration of the volcanic rocks. In amethyst-agate deposits and native copper mineralization, the supergene alteration caused oxidation, formation of clay minerals, soil and silica gossans. Therefore, a silica gossan is the result of the superposition of hydrothermal alteration of basalts with silicification and weathering. The altered volcanic flows display depletion in the content of some chemical elements including silica. Soils in the gossan are enriched in clay minerals with concentration of iron oxides and modification of the gamma spectrometry readings.

The evidence observed in the Campo Grande region and Serra de Maracaju is similar to the mining districts of Los Catalanes (Duarte et al., 2009, 2011), Ametista do Sul (Rosenstengel and Hartmann, 2012) and Entre Rios (Antunes et al., 2012; Hartmann et al., 2014) in the southern portion of the Paraná volcanic province.

5. Results

The fieldwork was directed to two targets. The first was focused in the local volcanic stratigraphy based in outcrops and quarries in the Campo Grande region and the second in the structures of silica gossans in the Campo Grande and Serra de Maracaju regions. The outcrops and quarries in the Campo Grande region (Fig. 3) are divided into sections designated AVN, Cascata Inferninho, rampa do Ernesto, São Luiz quarry, Campo Grande quarry (inactive, located in the São Francisco neighborhood of Campo Grande) and Votorantim quarry. The two Sidrolândia quarries are Negrimaq (active) and Quebra-Coco (inactive).

The AVN section (Fig. 4) has three lava flows, namely Abelha, AVN and Campo Grande. The São Luiz and Campo Grande quarries have exposures of the Campo Grande flow while the Abelha and AVN flows occur in the Cascata Inferninho and the Ernesto flow in the Ernesto section. The Votorantim quarry (Fig. 5) presents the AVN, Campo Grande, Pintado and Topo flows. In the Sidrolândia region (Fig. 6) the Quebra-Coco and Negrimaq quarries display the Campo Grande flow.

The six basaltic flows identified in this study show evidence of strong hydrothermal activity mainly at flow contacts. The hydrothermal events that generated these features resulted in varied gamma spectrometry values along the stratigraphic profile because of the modification in geochemistry and mineralogy of the rocks. Weathering and erosion in these areas highlighted the silica gossan structures which are guides for low-temperature (150 °C) hydrothermal deposits. No rock outcrops were observed in the Embrapa silica gossan, whereas three outcrops were collected in the Serra de Maracaju gossan.

5.1. Basalt stratigraphy

The present study establishes the volcanic stratigraphy of the region, so that studied gossans can be placed in the respective lava flow. In the Campo Grande region, six basaltic flows are identified from gamma spectrometry in the field and also by chemical analyses. The basaltic flows were named from bottom to top as: (1) Ernesto, (2) Abelha, (3) AVN, (4) Campo Grande, (5) Pintado and (6) Topo.

The Ernesto flow is exposed at the base of the hill that has the rampa do Ernesto on top; it is somewhat altered with lozenge fracturing. The

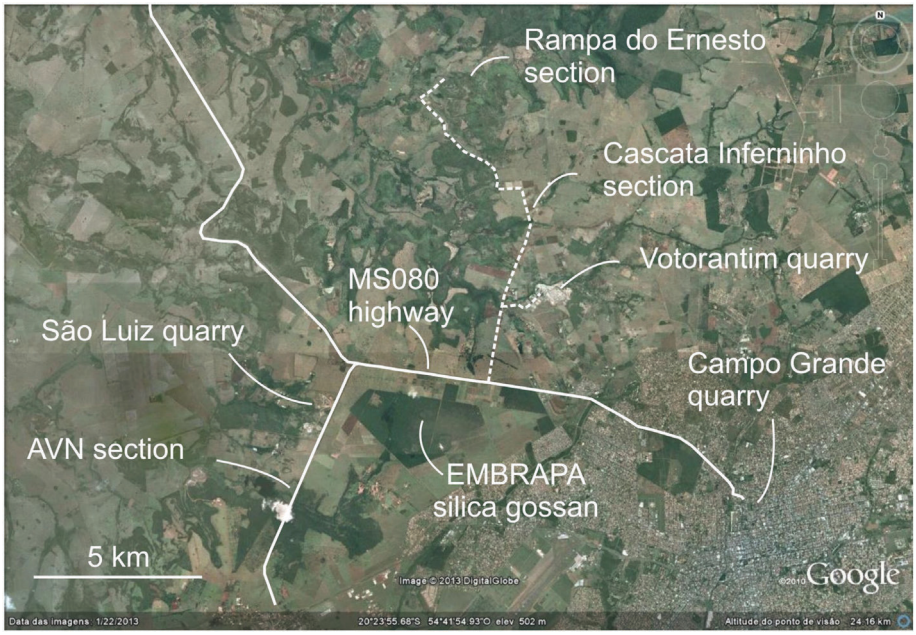

Fig. 3. GoogleEarth image with location of study sections in the Campo Grande region. The city of Campo Grande surrounds the Campo Grande quarry.

gamma spectrometry average of the Ernesto flow is 57 cps (full data in Table 3). Silicified sand dikes and loose quartz and cornelian crystals occur in this site.

The Abelha flow (Fig. 4A and C) is basaltic in composition and occurs in the Anel Viário Norte road and in the Cascata Inferninho. The gamma spectrometry average of Abelha is 68 cps. Silicified sand dikes are more resistant to erosion than the altered basalt. Cavities are present in the amygdaloidal crust and small veins interconnected the cavities. The contact between the AVN and Abelha flows in the Cascata Inferninho is marked by hydrothermal breccia and silicified sand with a gamma spectrometry average of 69 cps.

The AVN flow (Fig. 4A, B and D) crops out in the Anel Viário Norte road and in the Cascata Inferninho. It is a basaltic rock with columnar jointing that is crossed by silicified sand dikes and displays horizontal veins with calcite deposition (Fig. 4D). Cooling joints are covered by thin (1 mm) films of fine-grained, reddish-colored sand in many places. The basalts are altered along curved planes into reddish minerals. The gamma spectrometry of AVN is 65 cps. The contact between the AVN and Campo Grande flows (Fig. 4B) has commonly hydrothermal breccia and silicified sand layers with a gamma spectrometry average of 80 cps.

The Campo Grande flow is of major geological and stratigraphic significance in the Campo Grande region, because it covers a large area and is intensely exploited for construction materials mostly crushed stone. It was described in several places, including the Anel Viário Norte (Fig. 4A, B and D) and the São Luiz, Campo Grande, Votorantim (Fig. 5A, B and C), Negrimaq and Quebra-Coco (Fig. 6A, B and C) quarries. The flow is dark gray basalt with vertical cooling joints and display gamma spectrometry average of 45 cps. The thickness of the Campo Grande flow reaches 30 m in the Votorantim quarry and the cooling joints present typically a thin, reddish film of fine sand and crosscutting silicified sand dikes. Horizontal calcite veins cross the silicified sand dikes and interconnect the cavities (volcanic amygdales and hydrothermal geodes). These correspond to hydrothermal events H1 and H2 (Hartmann, 2008); H1 is the filling of amygdales with calcite and H2 is the dissolution of calcite and filling of the same space with sand. The contact between the Campo Grande and Pintado flows (Votorantim quarry) is characterized by the presence of hydrothermal breccia and silicified sand with a gamma spectrometry average of 79 cps.

The Pintado flow was only described in the Votorantim quarry (Fig. 5A) as basalt with greenish gray color and a gamma spectrometry average of 35 cps. The contact between the Pintado and Topo flows (Votorantim quarry) is characterized by the presence of hydrothermal breccia with approximately 3 m thickness and silicified sand layer with 65 cps.

The uppermost flow observed (only in the Votorantim quarry) in the sequence is the Topo flow (Fig. 5A). This intensely altered basalt displays a gamma spectrometry average of 29 cps; evidence of water infiltration during weathering is the presence of soil blocks contained in hard rock.

The description of two drill cores (SR1 and SR4) (Fig. 7) supports the definition of the basalt stratigraphy. Three samples were collected from each core for chemical analyses. The Abelha, AVN and Campo Grande flows are present in the cores. Their relative positions confirm the information obtained from the outcrops.

5.2. Geochemistry

The lava flows in the Campo Grande region are all made up of basalts according to the total alkalis-silica (TAS) diagram (Fig. 8A) from Cox et al. (1979). The location of the analyzed samples is given in Table 4.

One of the geochemical characteristics is the intense hydrothermal alteration of the basalts in the Campo Grande region. The variation in the content of SiO_2 is 46.38–51.25 wt.% and LOI from 1.3–6.1 wt.%. A strong negative correlation is observed between the SiO_2 and LOI (Fig. 8B). The basalt magmas (Fig. 8C and D) in the region are intermediate-Ti Paranapanema and high-Ti Pitanga types, based on Peate et al. (1992, 1999) and Peate (1997).

Recent studies in the southern portion of the Paraná volcanic province (Hartmann et al., 2010; Duarte et al., 2009, 2011; Rosenstengel and Hartmann, 2012; Pertille et al., 2013) delimited the use of samples

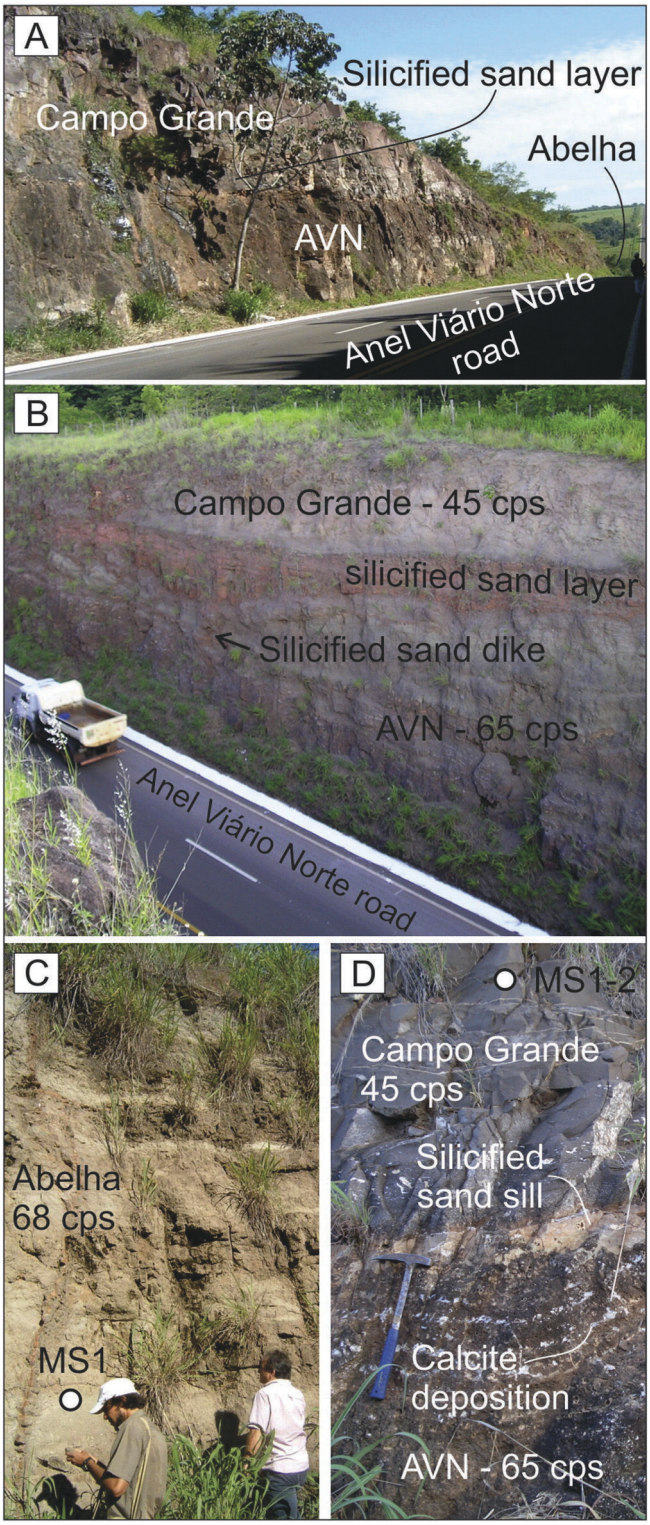

Fig. 4. Rock exposures in the AVN section. Flow names (e.g., AVN) and sampling sites of chemical analysis rocks (e.g., MS1) indicated. A) Stratigraphy of volcanic lava flows in the Anel Viário Norte. B) Silicified sand dikes and sand layer crossing and covering the lava flows. C) Detail of Abelha flow. D) Contact between the Campo Grande flow and the AVN flow showing the silicified sand sill and calcite deposition.

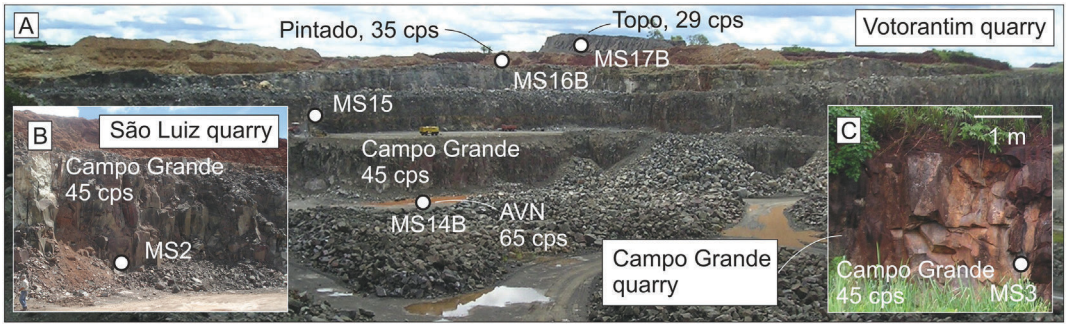

Fig. 5. Field photos of three studied quarries. Flow names (e.g., AVN) and sampling sites of chemical analysis rocks indicated (e.g., MS15). A) Votorantim quarry; B) São Luiz quarry; C) Campo Grande quarry.

with LOI <2 wt.% for the classification of volcanic rocks. The magmatic composition of the volcanic rocks can be thus estimated including the modifications caused by hydrothermal alteration. The basaltic rocks in the Campo Grande region display intense hydrothermal alteration in the same manner as observed in the southern portion of the province (Meunier et al., 1988; Hartmann, 2008; Duarte et al., 2009; Hartmann et al., 2010, 2012a; Pinto et al., 2011b) with formation of hydrothermal deposits and also the prospective guides.

The individualization of the flows in the Campo Grande stratigraphy was established by taking into consideration variations in the contents of TiO_2, P_2O_5 and low-mobility elements such as Zr, Th, Hf and Nb. TiO_2 and P_2O_5 contents allow the division of the basalts into two distinct

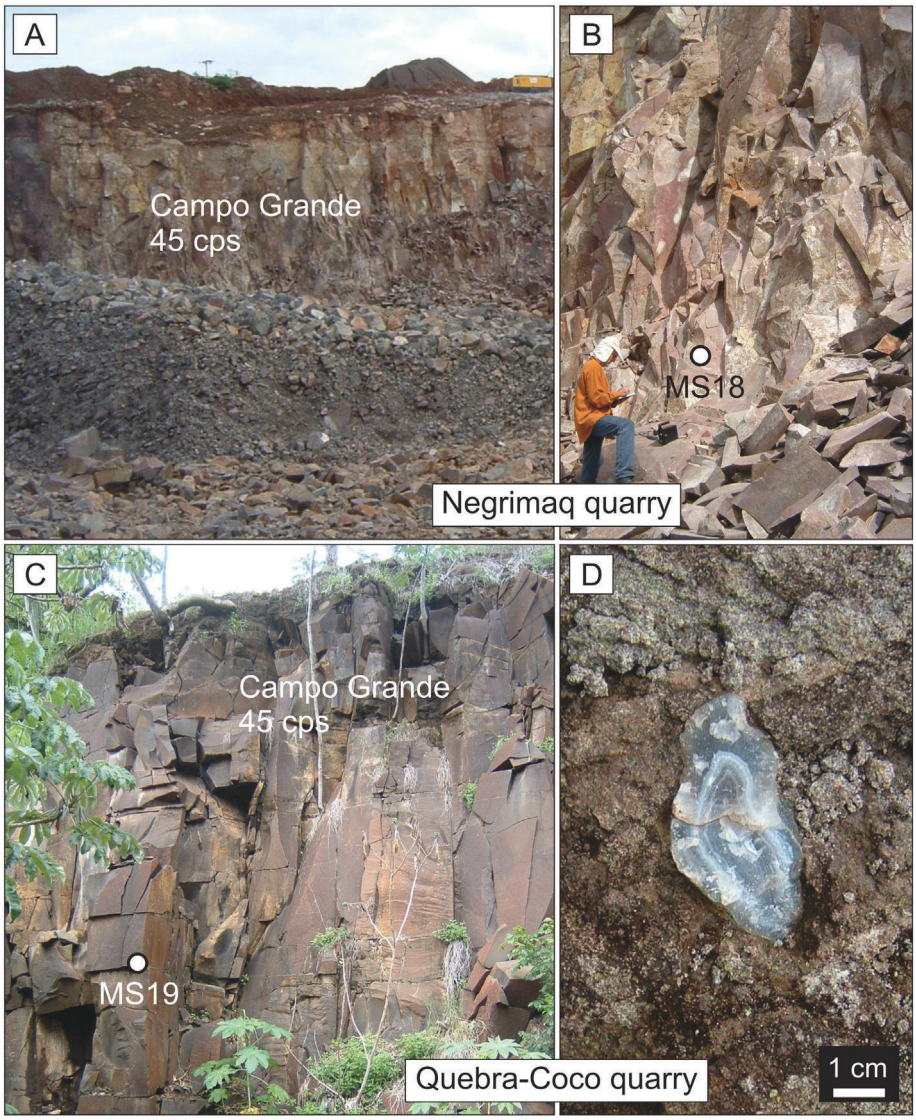

Fig. 6. Field photos of Negrimaq and Quebra-Coco quarries. Flow names (e.g., Campo Grande) and sampling sites of chemical analysis rocks are indicated (e.g., MS19). A) Negrimaq quarry; B) columnar jointing in Negrimaq quarry; C) Quebra-Coco quarry; D) Agate geode in the Quebra-Coco quarry.

Table 3
Gamma spectrometry of basaltic flows from the Campo Grande region. The geological units are in the correct stratigraphic sequence from bottom to top.

Geological unit	Emission rates (cps)		
	n	av	sd
Topo flow	11	29	1.2
Hydrothermal breccia	10	65	1.4
Pintado flow	14	35	2.8
Hydrothermal breccia	22	79	4.9
Campo Grande flow	61	45	2.2
Hydrothermal breccia/sandstone extrudite	7	80	3.8
AVN flow	28	65	2.4
Hydrothermal breccia/sandstone extrudite	10	69	5.0
Abelha	21	68	2.2
Ernesto	11	57	2.0

cps — counts per second.; n — number of measurements; av — average; sd — standard deviation.

groups (Fig. 9A). In the analyzed samples, one group has TiO_2 <2 wt.% (Paranapanema type) and another has TiO_2 >2 wt.%. Accordingly, one group has P_2O_5 <0.31 ppm and another >0.48 ppm. Other trace elements also exhibit two distinct chemical groups. Zr <200 ppm and >230 ppm, Nb <17 ppm and >23 ppm, Th <3 ppm and >3.5 ppm and Hf <5 ppm and >5.7 ppm.

Binary graphics of TiO_2, P_2O_5, Zr, Th, Nb and Hf show positive correlations between pairs of elements (Fig. 9A, B, C and D). This corroborates the separation of Paranapanema and Pitanga magma types (Fig. 9A and B). The chemistry of the rocks individualizes each of the six basalt flows and displays the geochemical evolution of the flows (Fig. 9C and D). The integrated use of geochemistry with field relationships and drill core descriptions results in the lava stratigraphy (Fig. 10A) of the Campo Grande region. The Paranapanema magma-type flows overly Pitanga magma-type flows (Fig. 10B).

The contents of Al_2O_3, Fe_2O_3, MgO, and MnO were also modified in the rocks, similar to the processes described by Franzson et al. (2008) in Iceland. Some mobility of elements such as Ca and Na in addition to Cs, Rb, Ba, K and Sr also occurred, similar to the descriptions of Wang et al. (2007). The plots of MgO versus TiO_2, P_2O_5, Zr, Th, Nb and Hf show a tendency to inverse correlation typical of magmatic fractionation, although MgO seems altered in some samples.

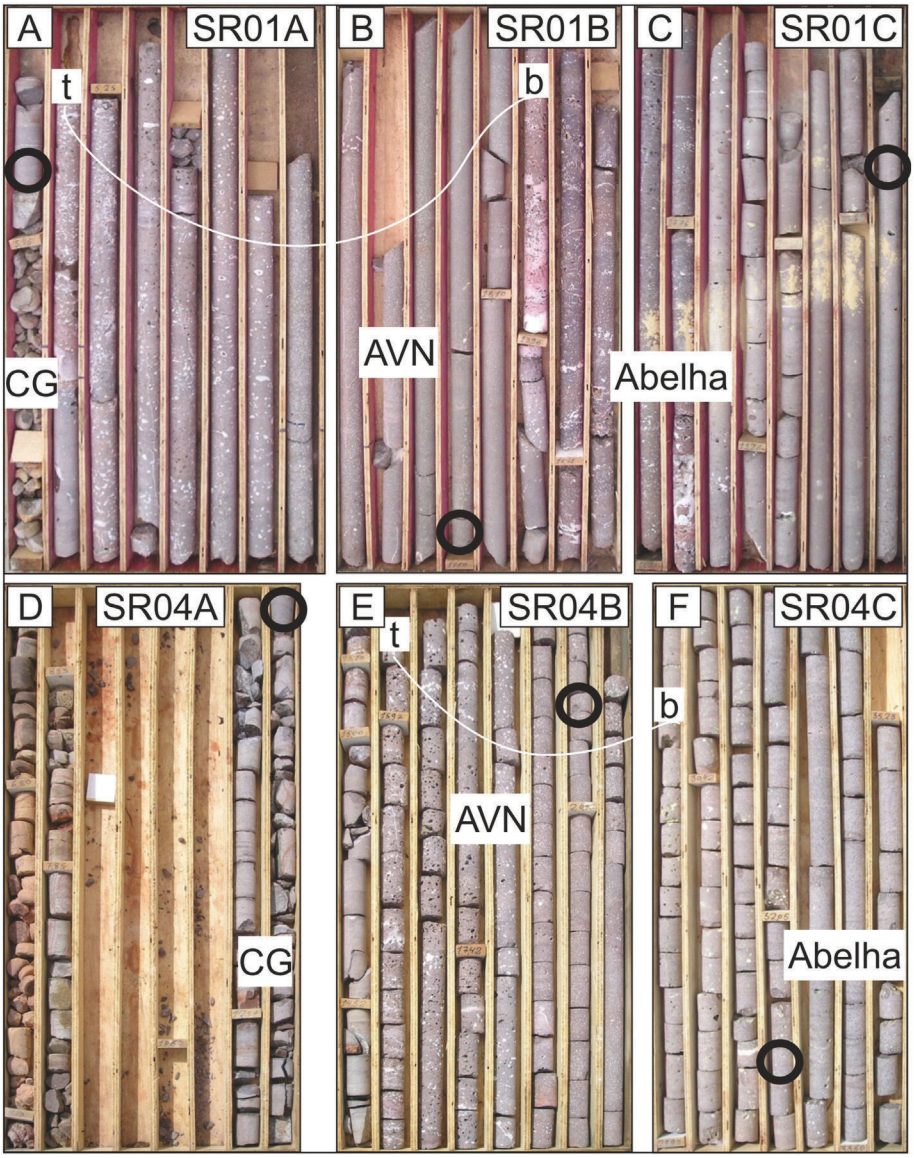

Fig. 7. SR1 and SR4 drill cores. Flow names indicated (e.g., Abelha; CG = Campo Grande flow). A) Sample SR1A (3.5 m depth). B) Sample SR1B (11.7 m depth). C) Sample SR1C (20.3 m depth). D) Sample SR4A (12.8 m depth). E) Sample SR4B (20.1 m depth). F) Sample SR4C (32.4 m depth). Top (t) and bottom (b) of AVN flow indicated by the white line in the upper three boxes and again in the lower three boxes. Collected samples indicated by black circles.

5.3. Embrapa silica gossan

The Embrapa silica gossan (Figs. 11 and 12) occurs in a topographic low (556 m) in the surrounding flat plateau (560 m), displays different texture in GoogleEarth images compared to the surroundings and has a hexagonal geometry (overall size ~450 × 350 m). Field features nearby the silica gossan include intense silicification of the sand dikes and sills, occurrence of hydrothermal breccia, and loose fragments of quartz and agate crystals in the soil. In the Embrapa silica gossan, a sudden change occurs in the type of vegetation as the silica gossan is approached from the surrounding wooded savanna. The soil becomes reddish brown with surface iron oxide alteration and has abundant kaolinitic clay where only grass (Fig. 11C) grows. In the rainy season, part of the silica gossan is covered by a lake. The total thickness of the silica gossan has not been assessed in this study. One soil sample S6D (Fig. 12A) was collected at a depth of 75–80 cm for mineralogical identification. The XRD analysis (Fig. 12C) of this disaggregated sample yielded a well-defined pattern, showing quartz as the principal mineral together with plagioclase, goethite, kaolinite and zeolites. The XRD analysis of oriented thin sections (<4 μm) helped the identification and confirmation of the clay minerals as kaolinite and gibbsite. Kaolinite showed basal spacing (001) 7.2 Å and (002) 3.57 Å in air-dried thin section. The basal spacing did not change in ethylene glycol, but in the calcinated sample the clay structure collapsed and confirmed the identification of kaolinite. The gibbsite showed basal spacing (001) 4.86 Å in air-dried thin section. The basal spacing did not change in ethylene glycol, but in the calcinated sample the clay structure collapsed and confirmed the identification of gibbsite.

This mineralogical association within the silica gossan structure changed the gamma spectrometry emission rate by increasing the negative anomaly from the edge to the center of the structure (Fig. 12B). Outside the Embrapa silica gossan, the gamma spectrometry measurements are up to 82 cps with an average of 75 cps (Fig. 11C). Within the structure, the measurements reach minimum values near 45 cps with an average of 55 cps. None of the six identified flows have comparable low gamma spectrometry values. Field observations display breccia (angular basalt fragments in silicified sand matrix), sand dikes and silicified sand layers occurring between successive basalt flows (Fig. 11B). These hydrothermal breccia have gamma spectrometry measurements around 76–85 cps. In the Embrapa silica gossan, the weathering acting on the surface reached the stratigraphic level of hydrothermal breccia between the Pintado flow and the Campo Grande flow and the gamma spectrometry values in the gossan are similar to the hydrothermal breccia. We thus interpret the geological relationships as indicating that the Embrapa silica gossan was developed at the top of the Campo Grande flow.

5.4. Serra de Maracaju silica gossans

Two silica gossans with different texture (~100 × 80 m each) were studied in the Serra de Maracaju (Fig. 13A). They are located at an intermediate elevation on a flat-lying plateau (450 m). The chemical analyses of three rock samples show that the lava flow is basalt (R11A 49.36 wt.% SiO_2, R7B 49.68 and R4F 50.54), Pitanga chemical-type with little hydrothermal alteration (LOI around 2 wt.%). Outside the silica gossans, especially in places with creeks, natural dump areas were observed with large amount of agate fragments. As the Maracaju silica gossans are approached, a first abrupt change is observed in the savanna which passes into a grassy vegetation. Towards the gossan structure, there is an increase in clay minerals content and surface ferruginisation and the soil color becomes reddish brown. The mineralogy identified in sample S7B (collected at a depth of 80–85 cm) by X-ray diffraction (Fig. 13C) includes quartz, plagioclase, goethite, kaolinite and zeolites.

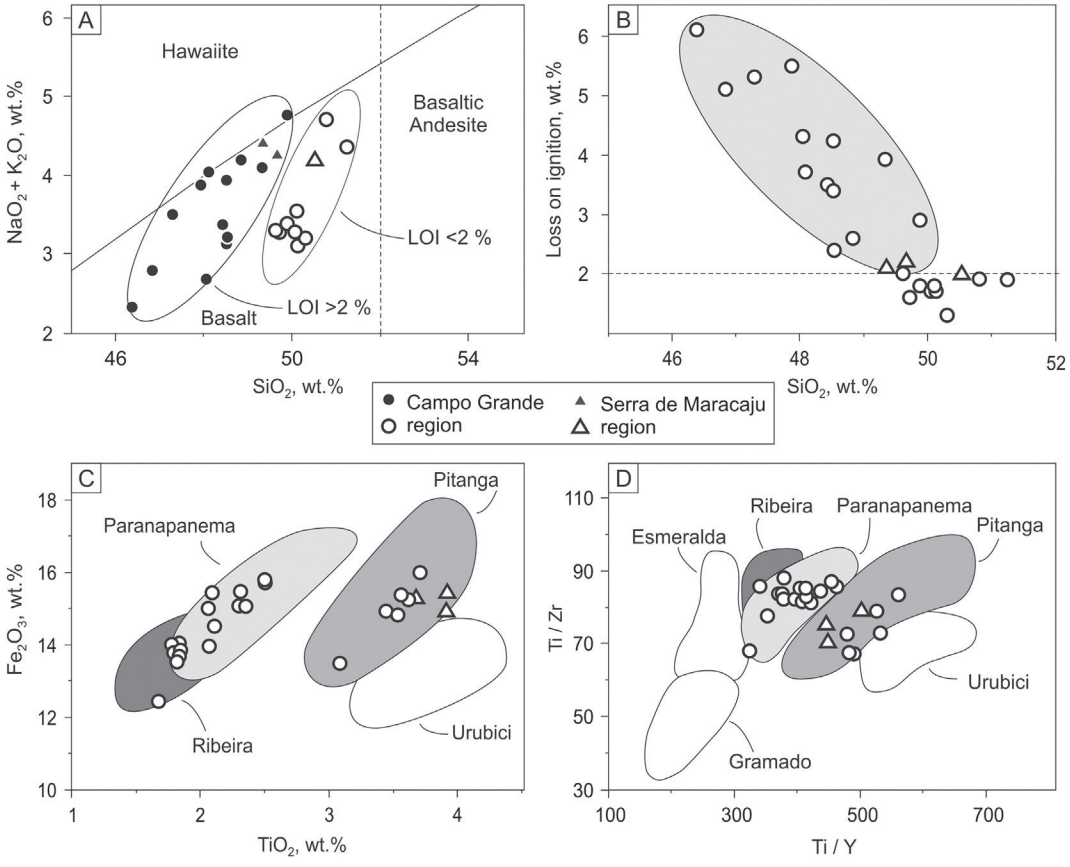

Fig. 8. Binary geochemical diagrams. A) Total alkalis-silica (TAS) classification (after Cox et al., 1979) displaying samples >2% LOI (light gray field) and samples <2% LOI. B) SiO_2 versus LOI showing negative correlation. C) TiO_2 versus Fe_2O_3 diagram displaying the high-Ti and intermediate-Ti magma types (after Peate et al., 1992). D) Ti/Y versus Ti/Zr diagram, with the classification of the magma types from the Campo Grande and Maracaju regions.

Table 4
Location of samples from the Campo Grande (MS and SR prefix) and Serra de Maracaju (R prefix) regions. Datum WGS 84. Zone 21 K.

Sample	UTM E	UTM S
MS1	734726	7736587
MS1—2	734583	7736265
MS2	736154	7740397
MS3	748836	7737016
MS8—1	742419	7745615
MS8—2	742409	7745602
MS8—3	742403	7745590
MS8—4	742397	7745577
MS11	740705	7749951
MS14B	743015	7743399
MS15	742916	7743197
MS16B	743254	7743240
MS17B	743410	7743254
MS18	726759	7696594
MS19	709611	7683700
MS19B	709865	7683752
SR1A	734392	7736325
SR1B	734392	7736325
SR1C	734392	7736325
SR4A	733576	7736944
SR4B	733576	7736944
SR4C	733576	7736944
R11A	652050	7667800
R7B	652250	7667850
R4F	652400	7668050

The clay minerals identified by oriented thin sections are compatible with smectites and kaolinites. For the smectites, the basal spacing (001) observed in a well-oriented layer (air-dried thin section) was 14 Å. The use of ethylene glycol expands the basal spacing to 17.2 Å and the thermal effect treatment (calcinated at 550 °C) led the basal spacing to 10 Å. For the kaolinite the basal spacing (001) observed was 7.2 Å in air-dried thin section. The basal spacing did not change in the ethylene glycol and in the calcinated sample the clay structure collapsed, confirming the presence of kaolinite. The occurrence of this mineralogy within silica gossans changed the gamma spectrometry as seen by the presence of two anomalies in the surveyed profile (A–B section in Fig. 13B). The readings outside the silica gossan structure show values around 60 cps while within the structures the readings reached minimum values of 42 cps.

5.5. Mineral resources

The mineral resources of Mato Grosso do Sul (Boggiani et al., 1998; Lacerda Filho et al., 2006) include the Serra Geral Group mostly for the use of basalt for construction, the occurrences of zeolites and agate near Serra de Maracaju and native copper associated with basalt dikes and sills. In this study, we identified calcite and agate in outcrops and quarries in the Campo Grande region, Serra de Maracaju and Quebra-Coco quarry.

In the Campo Grande flow, two phases of calcite deposition have been identified. The first is associated with the filling of cavities and the second of vertical cooling joints. At the top of the AVN flow, we

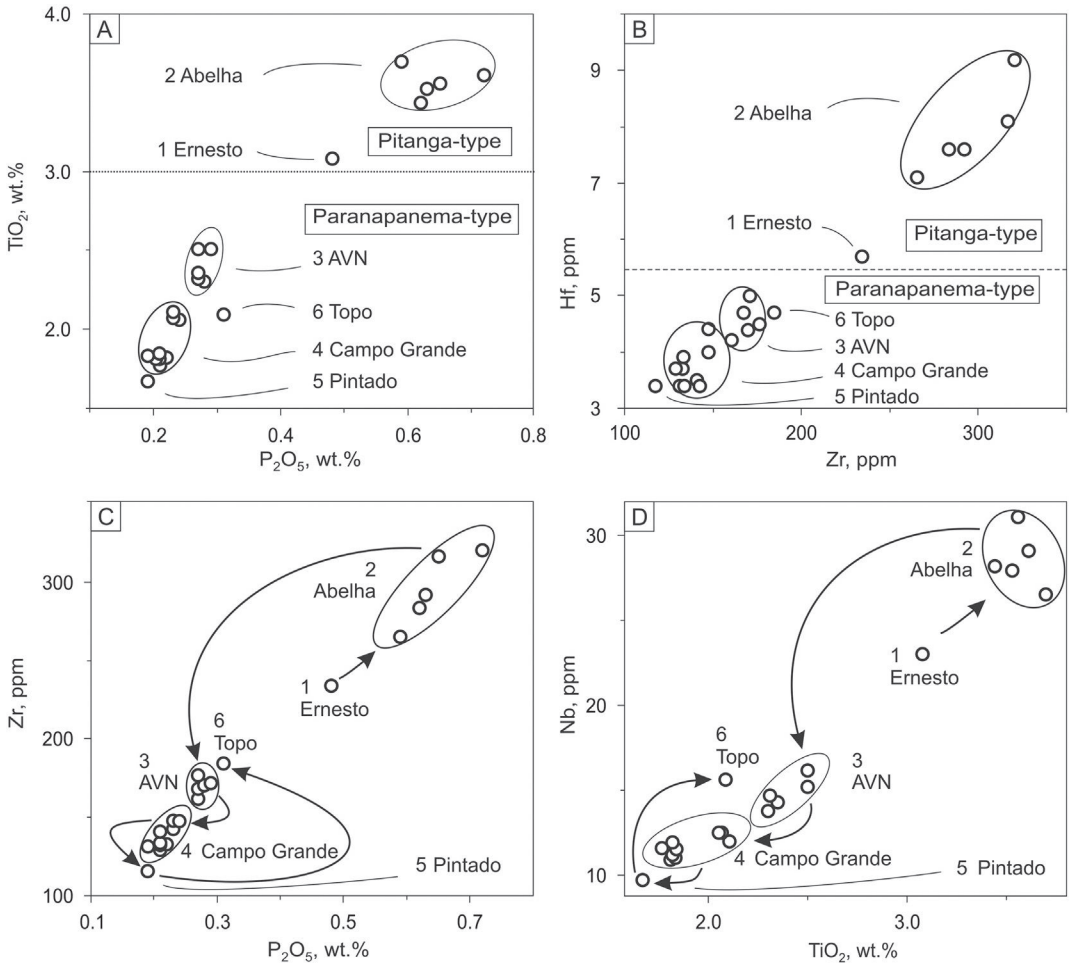

Fig. 9. Geochemical diagrams enabling the recognition of individual lava flows. A) TiO_2 versus P_2O_5 characterizing six volcanic flows of high-Ti (Pitanga) and intermediate-Ti (Paranapanema) magma types. B) Zr versus Hf diagram, identifying six volcanic flows. C) Zr versus P_2O_5 diagram, characterizing the six flows and indicating their sequence. D) Nb versus TiO_2 diagram showing the six lava flows.

observed amygdales filled with calcite and the presence of calcite in thin veins parallel to the top of the flow.

The occurrence of agate was observed in the Quebra-Coco quarry, in the Serra de Maracaju and also in the surroundings of the Maracaju silica gossan. These occurrences are associated with the filling of cavities in the amygdaloidal zone (H1) and of geodes (1 mm–10 cm) with quartz and agate (H3).

The copper contents of the rocks indicate some significant parameters, particularly when a comparison is made between the Campo Grande region and the entire Serra Geral Group. The studies of Pinto et al. (2011b) of native copper occurrences in the Serra Geral Group identified the epigenetic origin thus developing a new prospecting model for this metal. The copper content average of rocks from the Paraná volcanic province was defined by Crockett (2002) as 152 ppm and 177 ppm by Arena et al. (2014). In the southern portion of the Paraná volcanic province, the massive basalts have a copper content average of 197 ppm (Vista Alegre, n = 4, minimum 133 and maximum 245) and 208 ppm (Taquaruçu do Sul, n = 7, minimum 168 and maximum 272). In the Campo Grande region, the average content of copper is 190 ppm, therefore above the average contents of basalts in the southern portion of the province; four basalt samples show copper contents around 250 ppm. These high copper values are also present in the outcrops near the Maracaju silica gossan (194 ppm in sample R7B, 194.9 ppm in sample R11A and 260 ppm in sample R4F). We thus characterize the Serra Geral Group basalts from Mato Grosso do Sul as high-copper, a potential target for exploration.

6. Interpretation

Several aspects of the geology of the Campo Grande region are most significant for the understanding of the evolution of the Paraná volcanic province and related hydrothermal deposits. These include the chemical composition, gamma spectrometry and stratigraphy of the basalt lava flows, the basalt chemical types present and their stratigraphy, the hydrothermal alteration of the rocks, and most importantly, the description of the silica gossans.

Although the volcanic rocks are all basalts (SiO_2 = 46.38–51.25 wt.%), six individual lava flows are characterized, based on field stratigraphy, chemical and gamma spectrometry characteristics. Every basalt flow has a silicified sand layer or breccia on top. The lava stratigraphy is thus established in the region.

Following the proposition of Peate et al. (1999), we recognize two magma types. The high-Ti Pitanga type is present in the Ernesto and Abelha flows at the bottom of the stratigraphy. The remaining four flows are intermediate-Ti type; because Machado et al. (2009) considered these flows as Ribeira type, a more detailed examination is required.

According to Peate (1997), the Ribeira, Paranapanema and Pitanga magma types exhibit large TiO_2 compositional variation (1.5–4.1 wt.%) and share many compositional characteristics. They have similar primitive-mantle-normalized, trace element patterns, differing only in the Ti/Y ratios (Ribeira magma type ~360, Paranapanema ~410 and Pitanga ~530). In the studied region, most of the intermediate-Ti rocks are Paranapanema-type (Fig. 8C and D), but the compositions of some samples overlap with the Ribeira type. For instance, the magma types are distinguished in Sr versus Fe_2O_3 diagram (Peate et al., 1999), but six of our samples (MS15, MS2, MS1-2, SR1A, MS 18 e SR4A) plot in the fields shared by the Ribeira and Paranapanema magma types. In the same diagram, sample MS16B plots in the field of Gramado magma type, but in the TiO_2 versus Fe_2O_3 diagram the same sample plots in the field of Ribeira magma type (Fig. 8C), and in the Ti/Y versus Ti/Zr plots in the fields shared by Ribeira and Paranapanema magma types (Fig. 8D). We make an evaluation below and position the samples in their correct chemical types.

The bottom flow (Ernesto) is a Pitanga magma type. Sample MS11 has LOI <2 wt.%. The contents of TiO_2 (3.08 wt.%), Ba (435 ppm) Sr (437), Zr (234) and Sr/Y (12.4) e Ba/Y (12.4) ratios were decisive for the identification. The contents of SiO_2 (51.25 wt.%), Fe_2O_3 (13.47), P_2O_5 (0.48) and the Ti/Y (526), Zr/Y (6.7) and Ti/Zr (78.9) ratios are also supportive of the interpretation.

The Abelha flow is also a Pitanga magma type, as indicated by all five collected samples. Sample MS1 has LOI <2 wt.% and the remaining four samples >2 wt.% (MS8-3, MS8-4, SR1C and SR4C). The magma type was identified from TiO_2 (3.61 wt.%, 3.44, 3.70, 3.53, 3.56), Sr (416 ppm, 451, 420, 394, 410), and Sr/Y (9.3, 10.5, 10.6, 9.9, 9.4) and Ba/Y (13.3, 12.7, 12.4, 13.4, 12.9) ratios.

The AVN flow is interpreted as Paranapanema magma type. Five analyzed samples have LOI >2 wt.% (MS8-1, MS8-2, SR1B, SR4B, MS14B). Some of the contents (Peate et al., 1992) are shared with the Paranapanema and Ribeira magma types (e.g., Fe_2O_3, P_2O_5, Ba). The TiO_2 contents are similar in samples MS8-2 (2.31 wt.%), SR4B (2.35) and MS14B (2.30), either Ribeira or Paranapanema type. TiO_2 of samples MS8-1 (2.50 wt.%) and SR1B (2.50) indicate the Paranapanema type. The Ti/Y ratios of samples SR1B (414), SR4B (437) and MS14B (408) display a degree of enrichment compatible with Paranapanema magma type; Ribeira types have lower ratios. Although sample MS8-2 has TiO_2 contents and Ti/Y ratios similar to both magma types, its stratigraphic position indicates that it is also Paranapanema type. Overall,

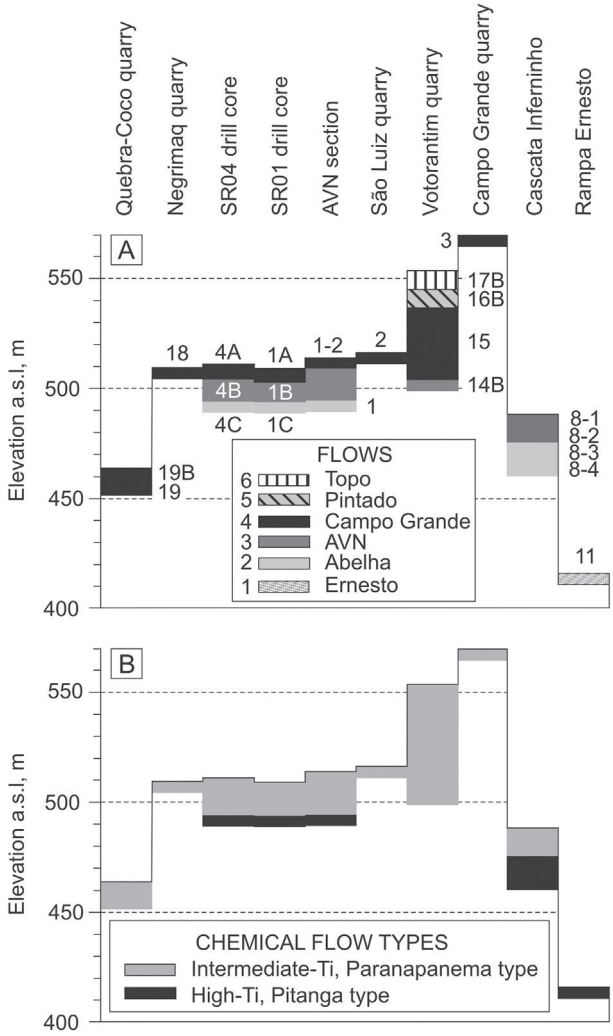

Fig. 10. Stratigraphy and chemical lava types. A) Stratigraphy of study sections, indicating the names of sections (e.g., Quebra-Coco quarry). Analyzed samples 4A, 4B, 4C, 1A, 1B, and 1C have the SR prefix. All other samples have the MS prefix. B) Stratigraphy of chemical lava types, showing the high-Ti Pitanga lavas at the base and the intermediate-Ti Paranapanema types at the top.

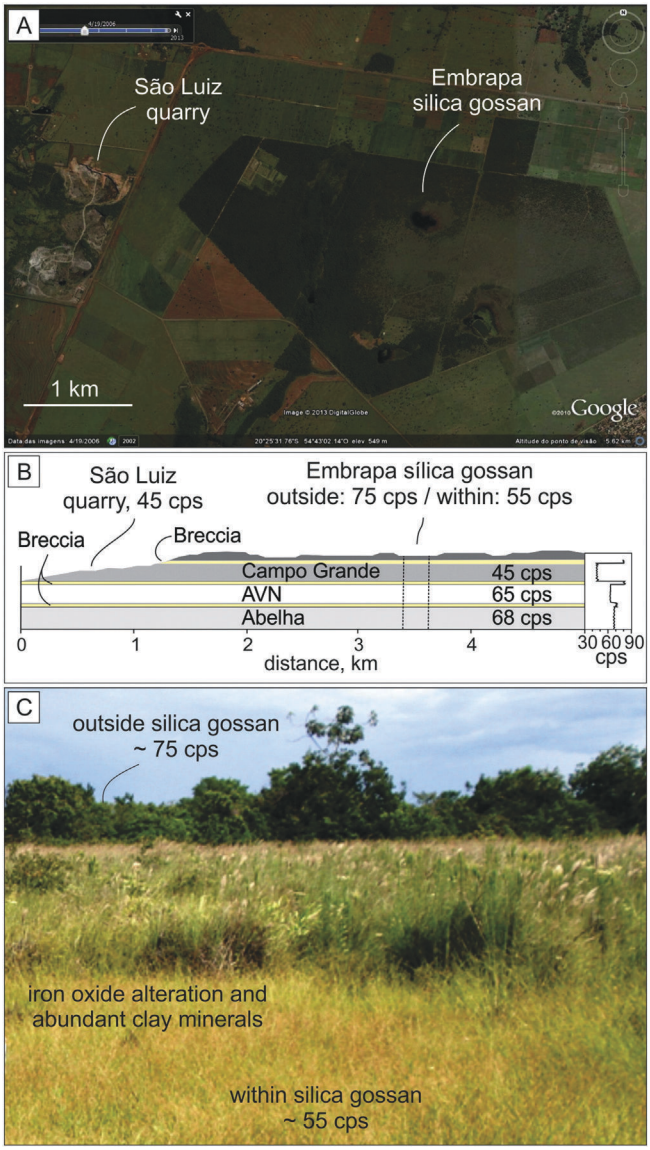

Fig. 11. Embrapa silica gossan. A) Location of the Embrapa silica gossan and São Luiz quarry; B) geological profile indicating the stratigraphy of flows and average gamma spectrometry; breccia = amygdaloidal, angular basalt blocks in silicified sand matrix; C) field photo of Embrapa silica gossan showing the average cps within and outside the gossan, and the sudden change of vegetation within and outside the gossan structure.

the chemical composition and stratigraphic position lead to the interpretation that the AVN flow is Paranapanema type.

We collected nine samples from the Campo Grande flow which is interpreted as Paranapanema magma type. Six samples showed LOI <2 wt.% (MS2, MS3, MS15, MS18, MS19, SR4A) and three >2% (MS1-2, MS19B, SR1A). Most of the contents and ratios (Peate et al., 1992) are shared by Paranapanema and Ribeira magma types, e.g., SiO_2, Fe_2O_3, TiO_2, P_2O_5, Ba, Sr, Zr, Zr/Y, Sr/Y and Ba/Y. Thus, the distinction between the two types was based on the Ti/Y ratios (Peate, 1997) of samples MS1-2 (414), MS2 (422), MS19 (463), MS19B (454) and MS15 (397), typical of Paranapanema type (~410) magma type. Samples MS3, MS18, SR1A and SR4A have somewhat lower Ti/Y, but the stratigraphic control indicates that they belong to the same flow. The Ti/Y ratios integrated with correct stratigraphic and gamma spectrometry controls of the sample allow us to interpret the Campo Grande flow as Paranapanema type.

Sample MS16B has LOI <2 wt.% and is the only sample analyzed from the Pintado flow. This is also a Paranapanema magma type. Some of the contents of this sample are shared by Ribeira and Paranapanema types, such as SiO_2 (50.14 wt.%), Ba (234 ppm), Sr (282), Zr/Y (4.7), Ti/Zr (85.4), Sr/Y (11.4) and Ba/Y (9.4). Other compositional values are close to the lower limit of the Paranapanema type, such as F_2O_3 (12.5 wt.%), TiO_2 (1.7), P_2O_5 (0.2) and Zr (117 ppm) that might be Ribeira type but is not conclusive. On the other hand, the Ti/Y ratio is 404, and according to Peate (1997) this is the Paranapanema magma type.

Sample MS17B has LOI >2 wt.% and is the only one analyzed from the Topo flow, interpreted as Paranapanema magma type. This flow has some geochemical characteristics that require examination. It shares many aspects with the Ribeira magma type, such as SiO_2 (48.52 wt.%), Fe_2O_3 (15.42), TiO_2 (2.09), P_2O_5 (0.31), Ba (345 ppm), Sr (288), Zr (184), Zr/Y (4,7), Ti/Zr (67.9), Sr/Y (7.4) and Ba/Y (8.9). The Ti/Y ratio (325) indicates Ribeira type, but is close to the lower limit of the Paranapanema (330); the ratio is therefore not conclusive. Because these criteria still overlap for the two magma types, we used the average contents of the two magma types established by Peate et al. (1999).

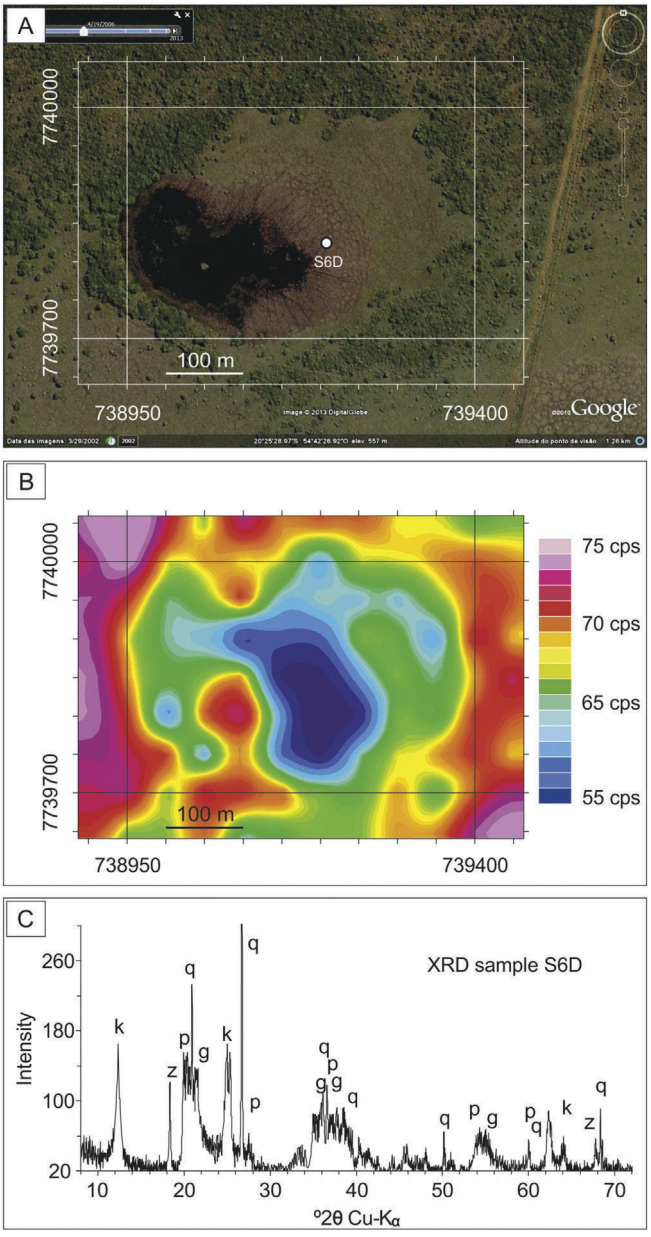

Fig. 12. Embrapa silica gossan. A) GoogleEarth image of the Embrapa silica gossan showing its hexagonal shape and brownish tint. Location of soil sample S6D indicated. B) Gamma spectrometry contour map, showing the negative anomalous area. C) X-ray diffractogram (interval 2θ 8° to 72°) of sample S6D showing the mineralogy on the Embrapa silica gossan. Symbols: (q) quartz, (p) plagioclase, (g) goethite, (k) kaolinite, (z) zeolite.

These indicate that Na_2O (2.41 wt.%), MnO (0.19), Ba (345 ppm) and Sr (288) are similar to the Ribeira type but all remaining oxides and elements SiO_2 (48.52 wt.%), Al_2O3 (13.30), MgO (4.05), CaO (7.67), K_2O (1.52), TiO_2 (2.09), P_2O_5 (0.31), Ni (47 ppm), Y (38.6), Zr (184), Rb (28.7), and Nb (15.6) are closer to the Paranapanema type. We therefore interpret the Topo flow as Paranapanema type.

From this evaluation, the basalt chemical types present in the Campo Grande region are high-Ti Pitanga type at the base (two flows) and intermediate-Ti Paranapanema type at the top (four flows). This is a consistent result from many sections of the cuesta.

Each pair of basalt flow and silicified sand layer constitutes a guide horizon for field surveys. The respective gamma spectrometry is a stratigraphic signature that can help identify the flows in the field even in areas with the presence of vertical faults.

The hydrothermal alteration of the volcanic rocks in the Campo Grande region generated calcite deposition in addition to other minerals (agate, native copper, zeolites) but calcite here is described in more detail. The AVN flow presents the most intense hydrothermal alteration, as indicated by the high LOI (3.7–6.1 wt.%) in the analyzed samples. This factor indicates that the AVN flow can be the host of hydrothermal

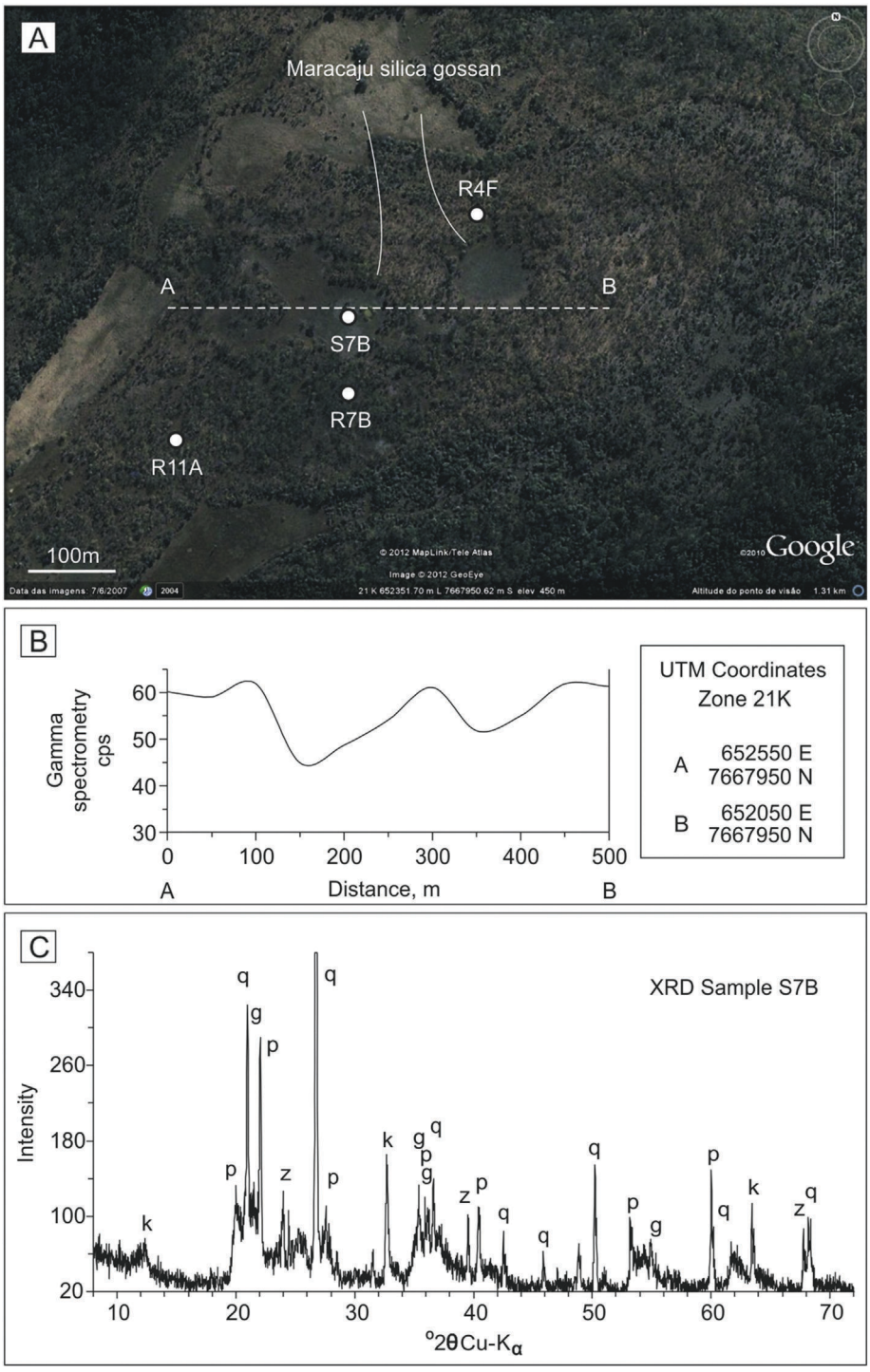

Fig. 13. Maracaju silica gossan. A) GoogleEarth image of the Maracaju silica gossan; A–B section and the location of rock samples (e.g. R11A) and soil sample (S7B) indicated; B) gamma spectrometry profile and coordinates of Maracaju silica gossan. C) X-ray diffractogram (interval 2θ 8° to 72°) of sample S7B showing the mineralogy on the Maracaju silica gossan. Symbols: (q) quartz, (p) plagioclase, (g) goethite, (k) kaolinite, (z) zeolite.

deposits in the Campo Grande region. This high LOI makes the AVN flow a prime target for mineral exploration. Calcite occurs in cavities, at the surface of vertical cooling joints and in thin veins parallel to the top of the flow. The vapor pressure of hot water in H1, H2 and H3 hydrothermal events can explain calcite deposition. In H1 the calcite filled the cavities of the amygdaloidal crust and sealed the host rock. The H2 event initiated explosively when water vapor pressure was greater than the lithostatic pressure. The release of energy and water vapor promoted the fluidization of unconsolidated sand from the Botucatu Formation paleoerg which injected sand into the overlying rocks forming sills, dikes and breccias. In places like the Campo Grande region, where the water vapor reached the surface, the sand was thrown on top of the basalt flows (paleosurface) and also filled vertical cooling joints. During H3, the hydrothermal deposits were formed in geode cavities and in subhorizontal fractures as thin calcite veins parallel to the top of the AVN flow. The proposed model (Duarte et al., 2009) incorporates vapor pressure of water at 150 °C under a 20-m basaltic column, and 100 °C for a 5-m basalt column. When the vapor pressure of hot water exceeds the pressure exerted by the column of rock, it can lift this column generating subhorizontal fractures. The CO_2-rich fluid had access to these fractures and filled them with calcite.

The weathering of the host volcanic flows generated the silica gossans as prospective guides in the mining districts of the southern Paraná volcanic province. In our interpretation, many erosional remnant hills in the Paraná volcanic province seem to be sustained by the presence of silica gossans and silica alteration. These hills are enriched in silica minerals as a hydrothermal alteration, so they are more resistant to erosion than the barren basalt.

The peculiar characteristics of the silica gossans allow their straightforward identification and positions the Serra Geral Group in a scenario of numerous, potential hydrothermal deposits, mostly amethyst and agate but also possibly metals such as copper.

7. Conclusions

This study aimed the establishment of the stratigraphy of the Paraná volcanic province (Serra Geral Group) in the Campo Grande region by integrating field geology with gamma spectrometry and rock geochemistry. This procedure allowed the understanding and localization of silica gossans, which are proposed as guides for prospecting hydrothermal deposits in the province. The detailed studies on these silica gossans can help in the discovery of new hydrothermal deposits such as amethyst, agate, gypsum, calcite and copper in the northern portion of the Paraná volcanic province. The study indicates the following.

1. A total of six basalt flows occur in the Campo Grande region; the lowest two flows are of Pitanga magma type (high-Ti) and the upper four flows are of Paranapanema magma-type (intermediate-Ti).
2. The AVN flow is the best prospective target in the Campo Grande region, because of the intensity of alteration caused by the H1, H2 and H3 hydrothermal events.
3. Based on the high contents of Cu in the rocks, the Campo Grande and Maracaju regions are identified as favorable target areas for copper mineralization.
4. The field and gamma spectrometry characteristics of the studied silica gossans are similar to the southern Paraná volcanic province, including Los Catalanes, Ametista do Sul and Entre Rios for amethyst and agate and Taquaruçu do Sul for native copper.

Acknowledgments

Financial support was provided by the Project VALE/CNPq, MCT and the Mineral Sector Fund (CT-Mineral) process 550199/2010-1 entitled "New exploration model in the hydrothermal environment of Serra Geral Group" and project of excellence PRONEX-FAPERGS/CNPq (edital 008/2009) on strategic minerals from southern Brazil, both coordinated by Léo A. Hartmann. The Campo Grande office of DNPM (Departamento Nacional de Produção Mineral, Ministério de Minas) offered support for field work; a field vehicle from the Goiânia office of CPRM (Geological Survey of Brazil) and a scintillometer GR-110 from CPRM/PA were used. The SR1 and SR4 drill cores were kindly provided by Hidrosul Ambiental from Campo Grande. Thanks to the journal reviewers for significant contributions to the improvement of the paper.

References

Almeida, F.F.M., 1986. Distribuição regional e relações tectônicas do magmatismo pós-paleozóico no Brasil. Rev. Bras. Geociênc. 16, 325–349.
Antunes, L.M., Hartmann, L.A., Rosenstengel, L.M., Baggio, S.B., Knijnik, D.B., Bruckmann, M.F., 2012. Stratigraphy and hydrothermal alteration of amethyst-geode mineralized basalt flows, Serra Geral Group, Entre Rios, Santa Catarina, Brazil. Anais do XLVI Congresso Brasileiro de Geologia e I Congresso de Geologia dos Países de Língua Portuguesa, Santos, SP.
Arena, K.R., Hartmann, L.A., Baggio, S.B., 2014. Geological controls of copper, gold and silver in the Serra Geral Group, Realeza region, Paraná, Brazil. Ore Geol. Rev. 63, 178–200.
Bellieni, G., Comin-Chiaramonti, P., Marques, L.S., Melfi, A.J., Piccirillo, E.M., Nardy, A.J., Roisenberg, A., 1984. High- and low-Ti flood basalts from the Paraná Plateau (Brazil): petrology and geochemical aspects bearing on their mantle origin. N. Jb. Mineral. Abh. 150, 272–306.
Boggiani, P.C., Coimbra, A.M., Riccomini, C., Gesicki, A.L.D., 1998. Recursos minerais não metálicos do Estado de Mato Grosso do Sul, Brasil. Revista IG, São Paulo 19, pp. 31–41.
Cox, K.G., Bell, J.D., Pankhurst, R.J., 1979. The Interpretation of Igneous Rocks. George, Allen and Unwin, London.
Crockett, J.H., 2002. Platinum-group element geochemistry of mafic and ultramafic rocks. In: Cabri, L.J. (Ed.), The Geology, Geochemistry, Mineralogy and Mineral Beneficiation of Platinum-Group Elements. Canadian Inst. of Min. Metallurgy and Petroleum, Special Volume 54 Ontario, Canada, pp. 177–210.
Duarte, L.C., Hartmann, L.A., Vasconcelos, M.A.Z., Medeiros, J.T.N., Theye, T., 2009. Epigenetic formation of amethyst-bearing geodes from Los Catalanes gemological district, Artigas, Uruguay, southern Paraná Magmatic-Province. J. Volcanol. Geotherm. Res. 184, 427–436.
Duarte, L.C., Hartmann, L.A., Ronchi, L.H., Berner, Z., Theye, T., Massone, H.J., 2011. Stable isotope and mineralogical investigation of the genesis of amethyst geodes in the los Catalanes gemological district, Uruguai, southernmost Paraná volcanic province. Mineral. Deposita 46, 239–255.
Frank, H.T., Gomes, M.E.B., Formoso, M.L., 2009. Review of the areal extend and the volume of the Serra Geral Formation, Paraná Basin, South America. Pesquisas em Geociências (UFRGS) 36, pp. 49–57.
Franzson, H., Zierenberg, R., Schiffman, P., 2008. Chemical transport in geothermal systems in Iceland. Evidence from hydrothermal alteration. J. Volcanol. Geotherm. Res. 173, 217–229.
Gomes, M.E.B., 1996. Mecanismos de resfriamento, estruturação e processos pós-magmáticos em basaltos da Bacia do Paraná - região de Frederico Westphalen (RS) Brasil. (PhD Thesis), Universidade Federal do Rio Grande do Sul, Porto Alegre, Brazil (219 pp.).
Hartmann, L.A., 2008. Amethyst Geodes Formed from Hot Water in Dinosaur Times. 1st ed. UFRGS, Porto Alegre, Brazil.
Hartmann, L.A., Wildner, W., Duarte, L.C., Duarte, S.K., Pertille, J., Arena, K.R., Martins, L.C., Dias, N.L., 2010. Geochemical and scintillometric characterization and correlation of amethyst-bearing Paraná lavas from the Quaraí and Los Catalanes districts, Brazil and Uruguay. Geol. Mag. 147, 954–970.
Hartmann, L.A., Duarte, L.C., Massonne, H.J., Michelin, C., Rosenstengel, L.M., Bergmann, M., Theye, T., Pertille, J., Arena, K.R., Duarte, S.K., Pinto, V.M., Barboza, E.G., Rosa, M.L.C.C., Wildner, W., 2012a. Sequential opening and filling of cavities forming vesicles, amygdales and giant amethyst geodes in lavas from the southern Paraná volcanic province, Brazil and Uruguay. Int. Geol. Rev. 54, 1–14.
Hartmann, L.A., Medeiros, J.T.N., Petruzzellis, L.T., 2012b. Numerical simulations of amethyst geode cavity formation by ballooning of altered Paraná volcanic rocks, South America. Geofluids 12, 133–141.
Hartmann, L.A., Baggio, S.B., Duarte, S.K., 2013. Decoding geochemical and gamma-spectrometry signatures from lavas and sand injectites at the base of the Paraná volcanic province, Novo Hamburgo, Brazil. Int. Geol. Rev. 55, 510–524.
Hartmann, L.A., Antunes, L.M., Rosenstengel, L.M., 2014. Stratigraphy of amethyst geode-bearing lavas and fault-block structures of the Entre Rios mining district, Paraná volcanic province, southern Brazil. An. Acad. Bras. Cienc. 86, 187–198.
Janasi, V.A., Freitas, V.A., Heaman, L.H., 2011. The onset of flood basalt volcanism, Northern Paraná Basin, Brazil: a precise U Pb baddeleyite/zircon age for a Chapecó-type dacite. Earth Planet. Sci. Lett. 302, 147–153.
Juchem, P.L., Brum, T.M.M., Ripoll, V.M., 2010. O laboratório de gemologia da Universidade Federal do Rio Grande do Sul. In: Hartmann, L.A., Silva, J.T. (Eds.), Tecnologias para o setor de gemas, jóias e mineração. IGEO, UGRGS, Porto Alegre, Brazil, pp. 133–147.
Keller, W.D., Hanson, R.F., 1968. Hydrothermal alteration of a rhyolite flow breccia near San Luis Potosi, Mexico, to refractory kaolin. Clay Clay Miner. 16, 223–229.
Lacerda Filho, J.W., Brito, R.S.C., Silva, M.G., Oliveira, C.C., Moreton, L.C., Martins, E.G., Lopes, R.C., Lima, T.M., Larizzatti, J.H., Valente, C.R., 2006. Geologia e Recursos Minerais do Estado de Mato Grosso do Sul. Programa Integração, Atualização e Difusão de Dados de Geologia do Brasil. Convênio CPRM/SICME, MS, MME, p. 121.

Lastoria, G., 2002. Hidrogeologia da Formação Serra Geral no Estado de Mato Grosso do Sul. (PhD Thesis), IGCE, Universidade Estadual Paulista, Rio Claro, SP, Brazil (133 pp.).
Licht, O.A.B., Fonseca, C.R., Moretti, M.A., Silveira, D.F., 2012. Estudo de produtos hidrovulcânicos no sudoeste do Paraná. Mineropar, Curitiba, PR, Brazil (192 pp.).
Lustrino, M., Melluso, L., Brotzu, P., Gomes, C.B., Morbidelli, L., Muzio, R., Ruberti, E., Tassinari, C.C.G., 2005. Petrogenesis of the early Cretaceous Valle Chico igneous complex (SE Uruguai): relationships with Paraná-Etendeka magmatism. Lithos 82, 407–434.
Machado, F.B., Nardy, A.J.R., Rocha Júnior, E.R.V., Marques, L.S., Oliveira, M.A.F., 2009. Geologia e Litogeoquímica da Formação Serra Geral nos Estados de Mato Grosso e Mato Grosso do Sul. UNESP, Geociências 28, pp. 523–540.
Mantovani, M.S.M., Marques, L.S., De Sousa, M.A., Civetta, L., Atalla, L., Innocenti, F., 1985. Trace element and strontium isotope constraints on the origin and evolution of Paraná continental flood basalts of Santa Catarina state (southern Brazil). J. Petrol. 26, 187–209.
Melfi, A.J., Piccirillo, E.M., Nardy, A.J.R., 1988. Geological and magmatic aspects of the Paraná Basin an introduction. In: Piccirillo, E.M., Melfi, A.J. (Eds.), The Mesozoic Flood Volcanism of the Paraná Basin: Petrogenetic and Geophysical Aspects. IAG, USP, São Paulo, pp. 1–13.
Meunier, A., Formoso, M.L.L., Patrier, P., Chies, J.O., 1988. Altération hydrotermale de roches volcaniques liées à la gênese dês amethysts - Bassin du Paraná - sud du Brésil. Geochim. Bras. 2, 127–142.
Mincato, R.L., 2000. Metalogenia dos elementos do grupo da platina com base na estratigrafia e geoquímica da Província Ígnea Continental do Paraná. (PhD Thesis), IG, Universidade Estadual de Campinas, SP (172 pp.).
Peate, D.W., 1997. The Paraná-Etendeka Province. In: Mahoney, J.J., Coffin, M.R. (Eds.), Large Igneous Provinces: Continental, Oceanic, and Planetary Flood Volcanism: Geophysical Monograph, 100. American Geophysical Union, Washington DC, USA, pp. 217–245.
Peate, D.W., Hawksworth, C.J., Mantovani, M.S.M., 1992. Chemical stratigraphy of the Paraná lavas (South America): classification of magma types and their spatial distribution. Bull. Volcanol. 55, 119–139.
Peate, D.W., Hawkesworth, C.J., Mantovani, M.S.M., Rogers, N.W., Turner, S.P., 1999. Petrogenesis and stratigraphy of the high-Ti/Y Urubuci magma type in the Paraná flood basalt province and implications for the nature of 'Dupal'-type mantle in the south Atlantic region. J. Petrol. 40, 451–473.
Pertille, J., Hartmann, L.A., Duarte, S.K., Arena, K., Rosa, M.L.C.C., Barboza, E.G., 2013. Gossan characterization in the Quaraí and Los Catalanes amethyst geode districts (Brazil and Uruguay), Paraná volcanic province, using rock geochemistry and gamma-spectrometry. J. Geochem. Explor. 124, 127–139.
Pinto, V.M., Hartmann, L.A., Santos, J.O.S., McNaughton, N.J., Wildner, W., 2011a. Zircon U–Pb geochronology from the Paraná bimodal volcanic province support a brief eruptive cycle at 135 Ma. Chem. Geol. 281, 93–102.
Pinto, V.M., Hartmann, L.A., Wildner, W., 2011b. Epigenetic hydrothermal origin of native copper and supergene enrichment in the Vista Alegre district, Paraná basaltic province, southernmost Brazil. Int. Geol. Rev. 53, 1163–1179.
Pirajno, F., 2009. Hydrothermal processes and mineral systems. Geological Survey of Western Australia, Perth WA Australia. Springer (1250 pp.).
Rocha-Campos, A.C., Cordani, U.G., Kawashita, K., Sonoki, H.M., Sonoki, I.K., 1988. Age of the Paraná flood volcanism. In: Piccirillo, E.M., Melfi, A.J. (Eds.), The Mesozoic Flood Volcanism of the Paraná Basin: Petrogenetic and Geophysical Aspects. IAG, USP, São Paulo, pp. 25–45.
Rosenstengel, L.M., Hartmann, L.A., 2012. Geochemical stratigraphy of lavas and fault-block structures in the Ametista do Sul geode mining district, Paraná volcanic province, southern Brazil. Ore Geol. Rev. 48, 332–348.
Sayin, S.A., 2007. Origin of kaolin deposits: evidence from a Hisarcik (Emet-Kütahya) deposits, western Turkey. Turk. J. Earth Sci. 16, 77–96.
Scott, K.M., Ashley, D.C., Lawie, D.C., 2001. The geochemistry, mineralogy and maturity of gossans derived volcanogenic Zn–Pb–Cu deposits of the eastern Lanchlan Fold Belt, NSW, Australia. J. Geochem. Explor. 72, 169–191.
Silva, A.O., 2010. Mineração de geodos em Ametista do Sul. In: Hartmann, L.A., Silva, J.T. (Eds.), Tecnologias para o setor de gemas, jóias e mineração. IGEO, UGRGS, Porto Alegre, Brazil, pp. 233–246.
Wang, C.Y., Zhou, M.F., Qi, L., 2007. Permian flood basalts and mafic intrusions in the Jinping (SW China)–Song Da (northern Vietnam) district: mantle sources, crustal contamination and sulfide segregation. Chem. Geol. 243, 317–343.
Wildner, W., Santos, J.O.S., Hartmann, L.A., McNaughton, N.J., 2006. Serra Geral volcanic climax at 135 Ma: first U–Pb isotopic results on zircon. Anais do XLIII Congresso Brasileiro de Geologia, Aracaju 1, p. 126.
Wildner, W., Hartmann, L.A., Cunha-Lopes, R., 2009. A proposed stratigraphy for the Serra Geral Group in the Paraná Basin. In: Milani, E.J., Chemale Jr., F. (Eds.), Correlation Brazil–Africa. PETROBRAS, Gramado.

Artigo 4

PARALAVAS IN THE PARANÁ VOLCANIC PROVINCE, BRAZIL – AN INTERPRETATION OF THE BASALTIC ROCKS CONTAINING PHENOCRYSTS AND GLASS

Artigo submetido aos Anais da Academia Brasileira de Ciências

Anais da Academia Brasileira de Ciências

Submission Confirmation

Thank you for submitting your manuscript to *Anais da Academia Brasileira de Ciências*.

Manuscript ID: AABC-2015-0088

Title: Paralavas in the Paraná volcanic province, Brazil – An interpretation of the basaltic rocks containing phenocrysts and glass

Authors: Baggio, Sérgio
Hartmann, Léo
Bello, Rosa

Date Submitted: 10-Feb-2015

Print Return to Dashboard

Paralavas in the Paraná volcanic province, Brazil – An interpretation of the basaltic rocks containing phenocrysts and glass

SÉRGIO B. BAGGIO[1], LÉO A. HARTMANN[1], ROSA MARIA DA SILVEIRA BELLO[2]

[1] Instituto de Geociências, Universidade Federal do Rio Grande do Sul, Avenida Bento Gonçalves, 9500 Agronomia; 91501-970 Porto Alegre, Rio Grande do Sul, Brazil

[2] Instituto de Geociências, Universidade de São Paulo, Rua do Lago, 562; 05508-080 São Paulo, São Paulo, Brazil

Keywords: Paralava, Paraná volcanic province, pyrometamorphism, remelting, metal remobilization

ABSTRACT

The occurrences of glassy rocks containing long, curved clinopyroxene and plagioclase phenocrysts in the Paraná volcanic province, South America, are here interpreted as paralavas. The large number of thin (0.1-0.5 m) dikes and sills of glassy basaltic rocks with hopper, hollow or curved, large crystals of clinopyroxene (up to 10 cm), plagioclase (up to 1 cm), magnetite and apatite are contained in the core of thick (>70 m) pahoehoe flows. They are strongly concentrated in the state of Paraná, coincident with the presence of the large number of dikes in the Ponta Grossa arch. These rocks were previously defined as pegmatites, although other names also have been used. Paralavas is here interpreted as the product of varied, successive processes of sill emplacement in high-kerogen bituminous shales followed by the ascent of the resultant

methane. As the gas reached the bottom portion of the most recent lava flow of the volcanic pile, the methane reacted with the silicate and oxide minerals of the host basalt (1,000 ºC) and thus elevated the local temperature to 1,600 ºC. The affected area of host basalt remelted (possibly 75 wt.%) and injected buoyantly the central and upper portion of the core. This methane-related mechanism explains the evidence found in the paralavas from this volcanic province, which is one of the largest in the continents.

INTRODUCTION

In the Paraná volcanic province (Figure 1), there are occurrences of paralavas formed by remelting of holocrystalline host rock to 1,600 ºC. These rocks, previously denominated pegmatites or segregations sheets, occur in all continental volcanic provinces and plutonic rocks of basaltic composition from many igneous provinces in the continents. The formation of these rocks is usually ascribed to magmatic processes that involve crystal fractionation and the filter-pressing ascent of the fractionated liquid to form dikes and sills within the mother flow or intrusion. The universal presence of long, thin, hollow crystals in a glassy matrix (quenched melt) is a common description of paralavas that resulted from quenching in pyrometamorphism (Grapes et al. 2013).

The presence of the voluminous, glassy matrix in coarse-grained basalt is a recurring feature in the large volcanic provinces but is still a paradox that remains to be solved. Several questions arise and remain unanswered from the presence of quenched paralavas in thick basalt flows: (1) Processes that caused a strong, local increase in temperature, so the nearly solid basalt again melted; (2) The chemical fractionation of the paralava as compared to the host basalt; (3) The rise of the newly-formed magma through the solid, hot basalt; (4) The quenching of the ascending liquid in strong thermal disequilibrium with the host basalt; and (5) The initial reduced composition of

the paralava. We presently address all these questions and interpret them into a unified model.

In occurrences of gabbroic pegmatites from Skaergaard (Larsen et al. 1992), fluids are dominated by H_2O, CO_2 and CH_4 in fluid inclusions of plagioclase, quartz and apatite. The source of carbon component was inferred from assimilation of sedimentary blocks from the volcanoclastic sequence, but the hypothesis of magmatic origin of carbon in silicate glass inclusions (MORB type magma) is not ruled out. Although this evaluation is close to the actual process involved in the formation of these rocks, it is likely that the processes involved in their origin are variable, particularly the types of fluids present. All evaluations rely on the mobility of the fractionated fluid by the presence of gases, but the provenance of the gases is commonly attributed to degassing of the host magma (Puffer and Horter 1993). Evidence evaluated thus far relies on a single source of energy, namely the heat liberated from the cooling magma. An additional source of energy is suggested to remelt the host basalt, and this adds complexity to the processes involved. We propose a unifying description of processes which include field evidence and the interpretation of geochemistry in the scenario of methane generation in the basin and its ascent and reaction in the hot lava. We encountered the evidence in outcrops of the Paraná volcanic province that exposes the reactive relationships between the host basalt and the surrounding paralava reaction rim. We describe here the evidence, including field relationships in Francisco Beltrão (near the depocenter of the Paraná Basin), petrography, rock geochemistry, electron microprobe and fluid inclusions in quartz and plagioclase. The origin of these rocks constitutes a significant problem not yet entirely solved in igneous petrology. The copper enrichment in the paralavas gives economic significance to these rocks.

SAMPLING AND METHODS

The study of paralavas in the Paraná volcanic province derived from several years of research of hydrothermal mineralization hosted in volcanic rocks (e.g., Duarte et al. 2009, 2011; Hartmann et al. 2012a, 2012b; Rosenstengel and Hartmann, 2012) and injection sand structures (Hartmann et al. 2013). The field studies were focused in two areas (Figure 1) that provided significant evidence for the interpretations during the fieldwork. The first area is located in the southwest Paraná limited initially by regional studies of Wildner et al. (2006) and include the occurrences of paralavas in the Dalba quarry in the municipality of Francisco Beltrão. The second area is located in the city of Jardim in the center west of Mato Grosso do Sul in the Rochasul quarry.

The methodology used in the study included evaluation and description of paralavas outcrops indicating the elevation and geographical coordinates (Garmin portable GPS), sampling of host basalts (n = 13) and paralavas (n = 14) sent for chemical analysis of major and trace elements in ACME laboratories, Canada. Thin sections from these samples were prepared at UFRGS and Geological Survey of Brazil (CPRM / PA). In the laboratories of UFRGS was performed X-ray diffraction (n = 1) in a Siemens Bruker-AXS D5000 with 2θ goniometer, radiation Kαl copper tube. Microprobe analyses and backscattered electrons images for magnetite-ilmenite, augite-pigeonite and feldspar were executed in a Cameca SX-100 of the Institut für Mineralogie und Kristallchemie of Stuttgart University, Germany. The routine measurement protocols used were 15 kV accelerating voltage, 15 nA beam current and a beam size around 1 μm. The fluid inclusions study was developed in the laboratory of fluid inclusions of the Núcleo de Apoio à Pesquisa Geoanalítica of the Instituto de Geociências da Universidade de São Paulo (Geoanalítica - USP Facility). Four thin sections were prepared from sample PD1 with polishing on both sides, suitable for the

fluid inclusions analyses. The studies were initiated with the petrographic description using a microscope Leitz Wetzlar. The fluid inclusions were assessed in their characterization, distribution and mode of occurrence in order to identify their possible origin (primary, secondary or pseudo-secondary), and also the selection of the best fields for microthermometric analysis. The microthermometry of fluid inclusions was carried out in cooling and heating platinum CHAIXMECA MTM 85 that was calibrated with chemical compounds of Merck MSP to temperatures higher than 40 °C. For negative temperatures and high positive temperatures, the platinum calibration was performed using standard synthetic Syn Flinc (Synthetic Fluid Inclusions). The calibration was performed for the following temperatures, -56.6 °C - Standard 1: composition 75 mol % H_2O and 25 mol % CO_2, -21.2 °C - Standard 2: Eutectic composition of H_2O + NaCl system with 23.2% in weight of NaCl, -10.7 °C - Standard 3: Eutectic composition of H2O + KCl system with 19.65 in weight of KCl, 0 °C and 374.1 °C – Standard 4 :Pure water (triple point and critical point, respectively) and 573.0 °C - Standard 5: Transition of α quartz to β quartz.

The information processing was performed by software GCDKit for chemical analysis, DIFFRAC^{PLUS} software (standards of PDF2 database) for X-ray diffraction and Microsoft Excel worksheet CalcMin (for EPMA data) developed by Dr. Andreas Brandelik of Mineralogy and Crystal chemistry University Stuttgart. Interpretations with determination of fluid inclusions salinity were performed by thermodynamic equations inserted in the software FLUIDS (Bakker 2003) and the CorelDraw software were used for preparation of figures.

GEOLOGY

The largest number of occurrences of paralavas in the Paraná volcanic province (n = 38) are located in the southwestern state of Paraná and they were described primarily as pegmatites (Arioli 2008). Their occurrences in other portions of the province are less abundant. The paralavas occur mostly in thick (~70 m) lava flows. and usually form small (0.1-2.0 m thick, mostly 1-10 m and maximum 100 m long), consisting of vertical, inclined or horizontal bodies, including stockworks. The contacts of the intrusive bodies are either sharp or gradational with the host rocks.

Different names have been used to describe these rocks most commonly pegmatite (Table 1). But the common presence of glass in the groundmass (intersertal texture) precludes the use of the word pegmatite for classification. The presence of long (10 cm), curved, skeletal and hollow crystals immersed in glass requires quenching of the lava. Although the Paraná volcanic province has 2.5 vol.% of silicic rocks (Wildner et al. 2006) no paralavas have been described in rhyodacites. Paralavas occurrences were described in basalt, basaltic andesite and andesite. Overall field relationships of these rocks are comparable to the description of segregation sheets in the Holyoke flood-basalt flow in the Hartford Basin, Connecticut (Philpotts et al. 1996). For instance, paralavas in the Paraná volcanic province were generated in the lower third of the flow core and occur only in intrusions or thick lava flows displaying vertical cooling joints (Figure 2A, B). This seems a requirement for the formation of the paralavas. Rapid cooling in thinner flows precludes the formation of the paralavas.

There is no occurrences of injected paralavas into the columnar jointing of the host basalt, suggesting that the formation of paralavas is earlier than the columnar disjunctions. The contacts between the paralavas and host basalt are sharp but gradational and the coarse-grained host basalt is holocrystalline. Also, the paralavas does not cross the lower or upper contact of the flow; it is confined to the flow.

For the full understanding of the paralavas process generating, is necessary to examine the sedimentary rocks of the Paraná Basin, located underneath the Paraná volcanic province. These rocks are composed mostly by fine to medium-grained sandstones with some siltites, and minor limestones. On the other hand, the Ponta Grossa Formation (states of Paraná and São Paulo) and the Irati Formation (entire basin) have thick layers of bituminous shales (e.g., Goulart and Jardim 1982). For example, "the Irati Formation, a well-known unit for its oil-prone rocks …, extends almost throughout the entire Paraná Basin. It has an average thickness of 40 m, with peaks of about 70 m..." (Holz et al. 2010). Permian sequences (e.g., Irati Formation) of the Paraná Basin are well represented in the underburden of the Paraná volcanic province in the Rochasul quarry and in the western border of the basin (e.g., Simas et al. 2012; their Figure 1). An example along the eastern border is the description of a drill core near Torres, Rio Grande do Sul (Aborrage and Lopes 1986). At 600 m depth, the core displays 35 m of dark siltites and clayey limestones of the Permian Irati Formation. It is most relevant for the origin of the paralavas that the Irati Formation contains pyrobituminous shales, from which kerogen is extracted by PETROBRAS in São Mateus do Sul (Paraná). Kerogen (particularly type III) is known to liberate large volumes of methane when intensely heated (Grapes 2011). Twenty six occurrences of oil in the eolian sandstones near the top of the Paraná Basin in the state of São Paulo were atributed to the intrusion of diabase sills into the black shales of the Irati Formation deeper in the basin (Araújo et al. 2004). As indicated by Aarnes et al. (2010), oil is formed in bituminous shales at a larger distance from the sill and methane is formed closer to the sill contact during the same pyrometamorphic event.

The lower Taquaral Member of the Irati Formation comprises siltstones and gray to black mudstones, and the upper Assistência Member has organic-rich mudstones and

shales interbedded with limestones (Holz et al. 2010).The upper Assistência Member is rich in total organic carbon (TOC = 10-25 %; e.g., Lauro Müller region, TOC = 20%). This high-TOC kerogen is known to crack into 95% methane when sujected to temperature >200 °C. Several other formations in the basin also contain black shales. For example, the Serra Alta Formation overlies the Irati Formation and also contains marine shales that contributed to the kerogen budget for methane generation during basalt sill injection. In the Ponta Grossa Formation, TOC seems to be lower between 0.1-0.6 % (Goulart and Jardim 1982).

The host basalts of paralavas in the province are holocrystalline, fine to medium-grained rocks. In this type of basalt in Dalba quarry (Francisco Beltrão region) outcrops a thick basaltic flow with paralavas intrusions. Both paralavas and host basalt are cut by the cooling joints showing that the formation of paralavas is prior to formation of cooling structures of the volcanic flow. The geological relations between the host basalt and paralavas exhibit distinct reaction rims (Figure 2C, D) that could be separated in the field scale, petrography and geochemistry including green core and two intervening light and dark grey portions in a reaction rim. The light portion is made up mostly of plagioclase passing gradually to dark grey portion with opaque, plagioclase and pyroxene. The constitution of the green core is dominated by celadonite, as determined by x-ray diffraction. However, Arioli (2008) has described these cells as being dark glass containing about 5% H_2O. It is known that the alteration of volcanic glass can generate celadonite. In the Rochasul quarry (Figure 2E, F) near the town of Jardim, Mato Grosso do Sul state occurs the largest body of paralavas observed in the Paraná volcanic province. The dimensions are approximately 20 m thick and 200 m long (Brückmann et al. 2013). The paralavas display long and curved clinopyroxene with lengths up to 10 cm. The host rock does not outcrop in the quarry. The geological

contact of basalts from Paraná volcanic province with the eolian sandstone of Botucatu Formation is exposed in a higher topographic level along the BR267 highway, eight kilometers away from the quarry.

RESULTS

PETROGRAPHIC DESCRIPTION

The host basalts and also paralavas mineralogical composition (Figure 3) present plagioclase, clinopyroxene, ilmenite, magnetite and accessory minerals (apatite and eventually olivine). The host basalt is a mesocratic rock, greenish gray color, with fine grain size and the mineralogical composition shows approximately 48% of plagioclase, ~ 26% of clinopyroxenes, ~ 16% of opaque minerals and ~ 10% of clay minerals (smectite and celadonite). The plagioclase appears as elongated crystals (≤ 0.3 mm) subhedral to euhedral with intergranular texture, where the crystals of pyroxene and opaque fill the interstices. When in direct contact with the smectite or celadonite the plagioclase crystals present their borders slightly corroded, but the contacts with pyroxene and the opaque minerals are well defined and usually show no rims alterations. Clinopyroxene display subhedral to anhedral crystals (0.2-0.3 mm) and can have poiquitithic texture with opaque minerals. They are usually fractured with alteration to clay minerals. The opaque minerals have sizes ranging from 0.2 mm to ≤ 0.5 mm with shapes ranging from euhedral (lozenge to hexagonal shapes), spherical to anhedral with changes in red iron oxide (hematite) which can be observed in the contours of the crystals. This alteration percolates through fractures and spreads to other crystals. The textures vary from sub ophitic to ophitic. The opaque minerals display

euhedral crystals (hexagonal or rectangular ~0.3 mm) usually with rims well defined and no alteration.

The paralavas comprise horizontal thin bodies sometimes interconnected by vertical veins and in dalba quarry (sample PD1) exhibit dark and light reaction rims. The mineralogical composition of the dark reaction rim is basically the same as the host basalt with 45% of plagioclase, ~ 20% of clinopyroxene, ~ 22% of opaque minerals, ~ 10% of clay minerals (smectite and celadonite) and ~ 3% of accessory minerals (apatite and quartz) and traces of carbonates. The opaque minerals (0.1 to 0.2 mm) are concentrated on the matrix and also in the surrounding of the pockets of celadonite as if they were oriented. There are phenocrysts of opaque minerals with anhedral and also skeletal habit showing alteration in red iron oxide (hematite). The plagioclase occurs in three distinct ways. The most significant display very fine crystals associated with quartz (anhedral) forming cryptocrystalline matrix in the interstices of the minerals. This mass of plagioclase is usually surrounding the occurrences of celadonite. The second form has elongated plagioclase embedded in the matrix (0.1 to 0.2 mm) and the third form is fractured phenocrysts, also immersed in the matrix. The clinopyroxenes crystals (0.1 to 0.2 mm) are associated with plagioclase and opaque minerals. They also occur as sparse phenocrysts showing intense fracturing. The celadonite also occurs in a scattered way. The mineralogy of the light reaction rim comprises ~ 50% of plagioclase, ~ 23% of clinopyroxenes, ~ 20% of opaque minerals, ~ 5% of celadonita, <1% of native copper and traces of apatite and quartz. This mineral assemblage is characterized by the presence of phenocrysts of plagioclase, clinopyroxenes and opaque minerals larger than 0.5 mm. The predominant textures are the sub-ophitic, ophitic and intersetal. The plagioclase is elongated and its major axis can display larger than 1 mm and show no reaction rims. The clinopyroxene are characterized by intense fracturing, while the

opaque are characterized by their skeletal habit. Apatite occurs as accessory mineral and stands out in the paralavas for its occurrence (greater than the host basalts), by a needle-shaped and hexagonal basal section. The celadonite occurs at concentrations forming green pockets, from where veins of celadonite come out and fill the fractures and sometimes cross the fracture minerals and interconnect other pockets of celadonite. The native copper mineralization in the paralava (Figure 4) occurs usually associated with this reaction rim, filling millimetric cavities associated with smectite or celadonite (Figure 4A, B, C) and also associated with the clinopyroxene (Figure 4D, E, F). The copper content of this reaction rim assessed by chemical analysis showed 600 ppm, however the analyzed sample not visually presented the native copper. Thus the copper content may vary locally for higher contents.

X-RAY DIFFRACTION

The preparation of sample P4 from Dalba quarry was performed from scraping, separation and concentration of the green core material. The mineralogical determination was performed by powder method (whole rock) and the X-ray diffraction was performed in the scan range (2θ) from 2 ° to 72 °. The evaluation of the results of X-ray diffraction of the sample P4 was based on the peak intensity and the interplanar distances. The main peak intensity presented the set of interplanar distances of 9.97 Å, 4.53 Å, 4.35 Å, 3.63 Å, 3.08 Å, 2.57 Å, 2.40 Å e 1.51 Å which identified the celadonite. Other peaks confirmed the presence of plagioclase, quartz and calcite.

ROCK GEOCHEMISTRY

The evaluation of the geochemistry of paralavas requires prior understanding of geochemical of the host basalts, once they occur strictly in thick flows (> 70 m). The

observation of reaction rims between the host basalt and the paralavas, in the Dalba quarry motivated us to perform differentiated chemical analyzes in the reaction rims. The evaluation presented herein makes a comparison of the geochemical behavior in the host basalt and in the paralavas in the studied areas. The chemical analyzes are available in Tables 2 and 3. In addition were used the chemical analyses from the study of Ferreira (2011) close to the study area in southwestern Paraná. The host volcanic rocks are classified as basalts (Figure 5) with Paranapanema intermediate-Ti chemical type (Nakamura et al. 2003) whereas in the paralavas the increase of SiO_2 content displays composition similar to basaltic andesite and basaltic trachyandesite and higher content of incompatible elements, including TiO_2. This behavior is observed also in the samples from Ferreira (2011). On the other hand, the geochemical compositions of host basalts and paralavas are also similar to those observed in the study of D'Oriano et al. (2013) which remelted basalt tephra in the laboratory and obtained liquids enriched in incompatible elements (Figure 5). Comparatively, the analyzes performed on samples from the Dalba quarry show that the average content of SiO_2 from the host basalt is 50.17 wt.%, similar to the other analyses of the host basalts of the Paraná volcanic province. However, the reaction rims of paralava have increments of 2.6 wt.% in the dark reaction rim and 9.5 wt.% in the light reaction rim with contents of 51.47 wt.% and 54.96 wt.% respectively. This same geochemical distribution occurs in K_2O, P_2O_5 and Ba, Y, Zr, Th, U, Cu, La and other rare earths. They feature an enrichment of contents in the paralavas. In analyzes of Dalba quarry this behavior is evident and shows that when compared to the host basalts the enrichment increases to the dark reaction rim, but it is still higher in the light reaction rim where there is occurrence of plagioclase phenocrysts. In contrast, MgO and CaO exhibit the opposite behavior. The MgO content (Figure 5) in the host basalts ranges from 6.87 wt.% to 4.93 wt.% and in the paralavas

these contents decrease to values ranging from 4.93 wt.% to 1.38 wt.%. Analyses performed on samples from the Dalba quarry show that the host basalt presents the content of MgO average around 4.84 wt.%. The MgO behavior shows gradual decrease in the paralava with levels of 3.97 wt.% in the dark reaction rim and 2.62 wt.% in the light reaction rim, in other words, the decrease is greater in portions where the plagioclase phenocrysts occur. The same behavior is observed for CaO that has the highest concentration in the host basalts, varying between 10.97-9.05 wt.% while in the paralavas this content ranges from 7.89 to 5.5 wt.%. In samples from the Dalba quarry, the content of CaO in the host basalts showed an average of 9.5 wt.% whereas the behavior in paralava presents successive decrease from the dark reaction rim (6.17 wt.%) to the light reaction rim (4.49 wt.%).

The assessment of loss on ignition of the host basalts presented values between 0.5-1.8 wt.% and the paralavas this values range between 0.9-2.4 wt.%. In the analysis performed in the Dalba quarry the host basalts display an average loss on ignition of 1.6 wt.%. In the dark reaction rim, the content of loss on ignition showed values of 2.4 wt.% and in the light reaction rim, the content of loss on ignition was 1.5 wt.%. These loss on ignition distribution show that these rocks also suffered the effects of H1, H2 and H3 hydrothermal events described in detail by Hartmann et al. (2012a, 2012b, 2013).

ELECTRON MICROPROBE

The electron microprobe analyses were performed in samples of host basalts and paralavas in order to compare their mineralogy. The composition of feldspar is plotted in the ternary classification diagram Ab-An-Or (Figure 6A, B) and representative EMPA results are listed in Table 4. Overall the feldspar of host basalts ranges in

composition from An_{50} to An_{70} (labradorite), but several analyses are more sodic. On the other hand, the plagioclase analyses in the paralavas present compositions between An_{30} and An_{50} (andesine) and some analyses fall in the field of labradorite, showing a more sodic composition than the host basalts. The alkali feldspar of host basalt and paralavas is primarily composed by sanidine. Most analyses of KF in the host basalt present sanidine compositions between Or_{55-80}. Some analyses are Or_{99} and also individual analyses plot in the orthoclase field. In the paralavas, the sanidine displays Or_{35-85} and a few analyses fall in the orthoclase field.

Clinopyroxene was observed in both host basalt and paralava. According to the classification of Morimoto et al. (1988) in the host basalt, augite and pigeonite are present while in the paralavas only augite (Figure 6C, D, Table 5). In the host basalt, the clinopyroxene is present in the matrix and also as sparse microphenocrysts; in the paralavas, only clinopyroxene occurs as phenocrysts. The variation of pigeonite composition in the host basalt is Wo_{7-20} (Figure 6D). The augite composition in the host basalt ranges from Wo_{26-41} with slightly larger Mg content than those observed in the augite from paralavas. On the other hand the augite composition in the paralavas display composition between Wo_{27-42} and in general have higher iron content than augite from host basalt.

The opaque minerals display sizes around 0.1 to 0.2 mm in the matrix and occur also as anhedral phenocrysts with skeletal habit showing alteration. The electron microprobe analyses of magnetite and ilmenite are plotted in the binary diagram FeO *versus* TiO_2 (Figure 6E, F) that shows positive correlation magnetite and ilmenite. Representative EMPA results are listed in Table 6. Magnetite-ilmenite has similar compositional distribution in both the host basalts and the paralavas. However, the magnetite from paralavas displays FeO and TiO_2 content slightly higher than the host

basalt. The analyses of ilmenite from paralavas have a wide distribution of FeO and TiO_2 contents but in the analyses with high FeO and high TiO_2, the ilmenite of paralavas have higher FeO content than the host basalts while the distribution of TiO_2 is similar in both. The evaluation of magnetite and ilmenite shows close correlation with the presence of native copper in paralavas (Figure 7) in a similar way that was observed between the copper mineralization with clinopyroxenes, smectite and celadonite.

FLUID INCLUSIONS

Four thin sections with polishing on both sides from sample PD1 (P1C, P5, P6 and P7) were prepared for analyses of fluid inclusions. The most common size of fluid inclusions in the thin sections is 5-10 μm. In the P1C were evaluated 8 (eigth) fluid inclusions although the data were obtained in only 4 fluid inclusions due to their tiny dimensions. In these inclusions salinities ranging from 5.6 to 7.3 wt.% eq. NaCl equivalent, but the results were disregarded because many of these inclusions have suggestive behavior of metastability. In the thin section P5 were investigated 57 fluid inclusions. Although the majority of fluid inclusions display small dimensions between 5 and 10 μm some of them reach 12 μm, 17 μm and 25 μm. Some of them have suggestive features of melt inclusions (Figure 8A) while the largest fluid inclusions have leakage features and necking down and were not measured. One part of the fluid inclusions is composed of aqueous saline solutions, although some of them are metastable. The Tfg (ice melting temperature) in negative temperature was repeated in various assays. In these cases the salinity ranged from 13.9 to 16.1 wt.% eq. NaCl. Some of the fluid inclusions are dark and distorted but cooling to -180 ° C, done several times, showed no change in temperatures, which seems no indicate the presence of CO_2 or mixtures of CO_2 with other volatile unless they have extremely low densities as water

vapor, CO_2 gas or CH_4 gas. It was not possible to observe phase changes with microthermometry. In the thin section P6 were analyzed 43 fluid inclusions. The fluid inclusions are rounded and few of them are black, elongated or distorted (Figure 8B). The main size of fluid inclusions range from 5 - 15 μm, but some of them have sizes from 20 to 40 μm. The microthermometric measures in this fluid inclusion present dubious results. The system H_2O + NaCl + $CaCl_2$ (+/- $MgCl_2$) was cautiously suggested with salinity ranging approximately from 14 to 16 wt.% eq. NaCl. In a very clear single-phase inclusions cooling down to -180 °C and presented no changes, showing that these fluid inclusion may consist of solid or by a low density fluid undetectable by microthermometry (CO_2 gas, CH_4 gas or water vapor). There is also a secondary fluid inclusion (~100 μm), entrapped at low temperatures with suggestive leakage features, low salinity (2.30 wt.% eq. NaCl), morphology, behavior and size very different from other fluid inclusions observed.

In the thin section P7, 18 fluid inclusions were analyzed. The sizes of fluid inclusions vary from 5 to 10 μm and only one showed 17 μm in size with suggestive features of melt inclusions. The bubbles within the fluid inclusions are even smaller. During the heating of these fluid inclusions the temperature was raised to 600 °C and there was no change in any of the fluid inclusions analyzed. In all of the thin sections the eutectic temperatures of the aqueous phase that range mainly from – 60 °C to – 50 °C, are suggestive of an aqueous system comprising NaCl + H_2O + $CaCl_2$ (+/- $MgCl_2$) although the results are often dubious due to the small size of the inclusions and the occurrence of metastability in many cases.

DISCUSSION AND INTERPRETATIONS

The field observation of the formation of paralavas as reaction rims wrapped by the host basalt precludes any interpretation of the paralavas as products of fractional crystallization. Although the products of remelting of the host basalt are similar to fractional crystallization, the process is overall comparable to the remelting of volcanic blocks entrained in lava (D´Oriano et al., 2013). All previous investigations considered fractional crystallization as the main process responsible for the enrichment of the lava in incompatible elements and its ascent to the upper part of the lava core (Table 7). But some geochemical features cannot be explained entirely with use of fractional crystallization. For instance, the study of Greenough and Dostal (1992a) showed that the presence of the rhyolite layers and pegmatite in the North Mountain basalt flows cannot be explained by fractional crystallization. Mass balance calculations of the major elements have missing phase, which in that study is represented by stilpnomelane. The authors suggested that the rhyolite layers and the pegmatite are product of silicate liquid immiscibility. The study of Hartley and Thordarson (2009) concluded that although "...crystal fractionation exerts a first-order control on the Grande Ronde basalt composition, it is generally agreed that fractional crystallization alone is not sufficient to explain the compositional and isotopic variations observed in the Grande Ronde basalt. Both mantle heterogeneity and crustal contaminations are advocated as possible explanations for these variations."

The abundant glass observed in the groundmass of all pegmatite lenses and the presence of large (10 cm), curved, hollow crystals requires quenching of the lava. This texture is observed in all pegmatite lenses described in continental basalts in other provinces and in the Paraná volcanic province. For instance, in Hawaii, segregation veins occur in entirely crystalline diabase and contain ~30 vol.% glass matrix (Fodor and Bauer 2014). The geochemistry of these veins and host basalts is similar to the

Paraná volcanic province occurrences. The reason for the presence of undevitrified glass in these pyrometamorphic rocks remains largely unexplained in general (Grapes, 2011).

There is no reasonable explanation for the presence of higher temperature liquid lava in the lower core of a thick, solid lava flow, or for its quenching against similar-temperature host rock. There is also no known fractional crystallization process that would raise the temperature of cooling basalt above its liquidus temperature to cause remelting of the lower core. An extraneous source of energy seems required to cause remelting of the crystalline basalt. We suggest the combustion of methane as the cause of remelting of basalt and formation of the paralava. It is therefore necessary to examine the steps involved in the process, including the source of the methane, its non-reactive ascent in the crust, spontaneous combustion in the lower core of the lava, the temperature attained during combustion, remelting of the crystalline basalt (paralava formation), and injection of the paralava upwards into the core and quenching of the paralava.

The methane present in sedimentary basins in general may have originated from mantle degassing, anaerobic bacterial reduction of organic matter or thermal cracking of kerogen. The Paraná Basin contains several sedimentary formations rich in kerogen under the Paraná volcanic province. The two most significant ones are the coal-rich, Permian Rio Bonito Formation present in 10% of the basin in its southeastern portion, and the Devonian Ponta Grossa Formation and Permian Irati Formation present along the basin. Bituminous shales are also present in the Serra Alta Formation higher up in the stratigraphy.

The injection of basaltic sills into coal seams turns kerogen mostly into CO_2. "Humic coals are mainly composed of Type III kerogen from which 10–25% of the carbon mass can be converted into gas" whereas "…type I and II kerogen commonly

found in organic-rich shales have the potential of converting up to 95% of the TOC to hydrocarbons…" (Aarnes et al. 2010). Because the coal seams cover a minor area of the Paraná Basin and coal generates mostly CO_2, the bituminous shales of the Irati Formation seem more significant. In several continental volcanic provinces, "in shales with total organic carbon content (TOC) of >5 wt.%, CH_4 is the dominant volatile ... generated through organic cracking, relative to H_2O generation from dehydration reactions ..." (Aarnes et al. 2010). Type I and II kerogen is commonly found in organic-rich shales such as the Irati Formation and may convert up to 95% of the TOC to hydrocarbon. Low oxygen fugacity in organic-rich shales will originate fluid dominated by CH_4–H_2O rather than H_2O–CO_2 in contact aureoles (Aarnes et al. 2010). It can be assumed therefore that kerogen will convert mostly into CH_4 rather than CO_2 in contact metamorphism of shale. CH_4 will dominate for TOC contents of >5 wt.%, while H_2O will dominate for TOC contents of <1 wt.%. In the Paraná Basin, particularly in the state of Paraná, TOC contents of the bituminous shales of the Assistência Member (Irati Formation) have TOC contents between 10-25% (Pereira 2013).

Basaltic sills are present under the Paraná volcanic province in a large volume. Mariani et al. (2013) concluded from gravimetric modeling that sills adding to 10,000 m in thickness are present in the crust below the 1,500 m thick lavas. Extensive drilling (n = 1424 holes) for coal-seam evaluation by the Geological Survey of Brasil in 1986 resulted in a clear picture of the number and thickness of sills (Table 8) injected into the sedimentary basin (southeastern coal-bearing portion). The examination of 835 logs that include the Irati Formation and the Rio Bonito Formation shows that basaltic sills are present dominantly in the Irati Formation, followed by the Rio Bonito Formation and the other formations. The field observation in quarries confirms the dominance of sills in the Irati Formation over the other formations. The fissile nature of the Irati Formation

shales seems to have facilitated the injection of the magmas (e.g., Araújo et al. 2004) compared to the dominantly fine-grained sandstones of the other formations. The average thickness of the sills is near 20 m for all formations. The Irati Formation thus emerges as one target for the observatin of pyrometamorphism of bituminous shales in the Paraná Basin.

The sedimentary rocks of the Paraná Basin contain therefore the necessary large volume of kerogen spread over the entire basin as potential generator of methane; part of the kerogen was cracked and a large volume still remains in the basin. The large number of basaltic sills injected into the bituminous beds offers additionally the necessary heat for the secondary cracking of kerogen into methane. The newly-formed gas has to migrate upwards unreactive through the sedimentary and the consolidated volcanic pile. The temperature of the sedimentary rocks, and contained (and ascending) fluids including methane, was 60 °C above the temperature expected for intraplate basins, and this was probably caused by the additional heat from volcanism, mostly from sills. Microthermometric studies in primary fluid inclusions in calcite from fractures (Cesário Lange region, São Paulo state) indicate aqueous fluids that were trapped at 70-141 °C with the highest mode at 105 °C; salinity is between 5.33-0.0 wt.% eq. NaCl" (Sawakuchi et al. 2011). The highest temperature attained is constrained by mineral assemblies and oxygen isotopes at <200 °C. At this temperature methane is not affected and runs through the sedimentary layers toward the top, much higher temperature is required to ignite methane. The autoignition temperature of methane is 580 °C in air, which is the minimum temperature required to ignite the gas in air without a spark or flame being present (Wikipedia). As mentioned by Caron et al. (1999), "the autoignition temperature ... is strongly pressure-dependent and decreases with increasing pressures", but is not expected to decrease down to the temperature

present in the Paraná Basin sedimentary rocks below the Paraná volcanic province. Methane gas was thus able to migrate upwards through the sedimentary package without spontaneous reaction with oxygen present in pores and in mineral lattices.

As the gas reached the base of the flow that was still cooling with temperature around 1000 ° C (without having yet developed columnar jointing) the scenario became entirely different. A coincidence of timing occurred between the processes of methane generation in the Irati Formation and its arrival at the base of the cooling basalt. According to Aarnes et al. (2010), "the generation of volatiles is occurring on a time-scale of 10–1000 years within an aureole of a single sill…" This is the same time-scale of cooling of basalt lava. In the studies of a 45 m thick basaltic andesite flow from the Paraná volcanic province, Schenato et al. (2003) estimated the time for complete solidification as 35 years, corresponding to cooling processes between the liquidus (1200 °C) and the solidus (1000 °C) of the lava. During cooling, the two solidus curves approaching from above and below intersected at two-thirds distance from the top of the flow; this is the level where the temperature reached 1000 °C and the flow became solid. This level coincides with the position commonly attributed by many authors to the origin of the segregation melts. Cooling of the 45 m thick lava to ambient temperature probably took 560 years.

Only very few thin basalt lavas have pegmatite seams, and these are of the order of millimeters in thickness; we interpret this as due to the faster cooling of the lava. Thicker (>70 m) lavas and mafic plutonic complexes remain at a high temperature for a longer period of time. Because the vertical cooling joints of thick lava flows begin to form at 1,000-900 °C and do not contain injected paralavas, these must have formed at a temperature >900 °C. In one study, the initiation of surface cracks in a cooling lava lake

from Hawai was observed to occur at 900 ℃ for a lava emplacement temperature of 1090 °C (Peck and Minakami 1968).

Methane is extremely flammable and is violently reactive with oxidizers (e.g., Wikipedia). In the cooling basalt, little free oxygen (the prime example of oxidizer agent) is present so methane reacts with the oxygen in the mineral lattices in a reaction of "reduced burning". This is a strongly exothermic chemical reaction. Local temperature in the holocrystalline, cooling (1,000 °C) basalt is raised because of CH_4 oxidation. Several geological estimates have been made on the temperature attained during methane burning. For instance, Grapes (2011) estimates the temperature in air up to 1,600 °C, whereas Sokol et al. (2010) refer to ultrahigh temperature up to 1,500 ℃ in ignition foci of sedimentary rocks by combustion metamorphism. A detailed study of mud melting by methane ignition established the temperature at 1,400-1,800 ℃, with the resultant formation of glass at 1,400 ℃ and lower. From this, we model the remelting of the base of the basalt lava core because of the rise of temperature from the local 1,000 °C up to 1,600 ℃. At this very high temperature, the affected basalt would melt extensively, possibly 75% liquid with 25% remaining solid. This is the inverse proportion commonly mentioned for the extent of fractional crystallization required to generate the pegmatite sheets in other provinces. The description of segregation sheets by Philpotts et al. (1996), for example, concludes from fractional crystallization modelling that "the composition of the segregations corresponds to liquids that can form by as little as 25% crystallization of the initial basalt." The resultant new magma would be overall similar by the two processes. The mixed rock that remains in place would be composed of a larger portion of crystallized new magma and a smaller portion of remnant, unfused solid. In the terminology of Grapes (2011), this may be called a buchite, which is a partially fused rock by pyrometamorphism.

In a relevant study for the present interpretation, D'Oriano et al. (2013) remelted Etna, Vesuvius and Stomboli basalt tephra in the laboratory and obtained liquids enriched in incompatible elements and SiO_2 while the Mg content decreased. In the present study similar results was observed in EMPA analyses of magnetite, which display higher contents of TiO_2 in the paralavas than in the host basalt and also in the chemical analyses of samples P1 (host basalt), P2 and P3 (reaction rims of paralavas) including Zr and Y. This observations support the comparison between remelting occurred in paralavas of Paraná volcanic province with those obtained in the laboratory.

This overall process is shown in the model (Figure 9) that explains the reason for the origin of the newly-formed liquid in the lower portion of the lava core, as described in many lava flows. The paralava contains a higher proportion of light elements, so it is more "differentiated" and rises buoyantly to the central and upper portion of the core. Dikes, sills and stockworks of paralava are thus formed in the core of thick basaltic lava flows. The columnar jointing will be formed by cooling of the flow below 900 °C, with the paralava already solid with intersertal texture and also the coarse-grained host basaltic rock.

We envisage the occurrence of similar processes of basalt or gabbro remelting to form paralavas in other continental provinces whenever methane streaming occurs through solid rock portions at 1000 °C so methane autoignition can occur. The recognition of the process is important both for petrology and economic geology. The presence of CH_4 in fluid inclusions (Larsen et al. 1992) was attributed to carbon assimilation from sedimentary blocks. In the fluid inclusions evaluated in the paralavas from Paraná volcanic province the $NaCl+H_2O+CaCl_2$ system was suggested as a hypothesis. This system can be observed in a wide range of geological environments and also in the sedimentary basins with hydrocarbon occurrences (Steele-MacInnis et al.

2011) like the Paraná Basin. Overall the evaluation performed in this study indicates that there are at least two distinct phases of trapping fluid inclusions. The older generation was trapped at higher temperatures with higher salinity fluid which may contain a volatile of low density besides single-phase inclusions consisting only of such volatile. Fluid inclusion of later generation were entrapped in low temperature conditions from low salinity solutions which can be related to the hydrothermal events Cretaceous described by Hartmann et al. (2012a) and are superimposed on these rocks. On the other hand, the presence of CH_4 in the fluid inclusions in the paralavas of Paraná volcanic province has not been definitively identified due the small size of fluid inclusions. However, the cooling results indicate that the fluid inclusions can be constituted by a low density fluid such as water vapor, CO_2 or CH_4 undetectable by microthermometry. Further study with Raman technique in fluid inclusion with appropriate size may identify the presence of CH_4.

The economic importance of paralavas opens a new frontier for studies related to mineral exploration. This can be illustrated with the copper mineralization in the paralava of Dalba quarry, in which the copper content average in the host basalts is 141 ppm (n = 2), slightly below the average (152 ppm) established for the volcanic province (Crocket, 2002). On the other hand, in the dark reaction rim the copper content increase for 236 ppm and in the light reaction rim the content reaches 600 ppm, showing that the concentration of metal was related with the paralava generation process. The host basalt presents LOI of 1.6 wt. %, similar to the LOI of the light reaction rim (1.5 wt.%), while the LOI of the dark reaction rim is 2.4 wt.%. The native copper mineralization in the host basalt is associated to the dendritic form on the surface of the columnar jointing and is consistent with the epigenetic hydrothermal mineralization generated during the H1,H2 and H3 Cretaceous hydrothermal events (for details see Hartmann et al. 2012a,

b) which promoted hydrothermal alterations on the host basalts and in the paralavas. The native copper occurrences observed in the paralavas fill microcavities in the light reaction rim and the higher Cu contents are associated with the extensions of paralavas bodies.

The geological and mineralogical evidence thus far described in pegmatites and some segregation sheets in thick basalt lavas and in intrusions were previously attributed to fractional crystallization, but may be alternatively explained by partial melting process, including the Paraná basaltic province and possibly other similar flood basalt and mafic intrusions in the world. We thus use "paralava" for these geological bodies, as an interpretation of the remelting portions of the host Basalt by the heat generated by the combustion of methane inside a thick, cooling basalt or intrusion.

CONCLUSIONS

1. Rocks from the Paraná volcanic province previously called pegmatites or segregation sheets are presently interpreted as paralavas, the result of melting of hot host basalts by methane combustion.
2. The paralavas formed from remelting (1,600 ºC) of the lower portion of the still-hot (1,000 ºC) core of the host basalt and rose buoyantly to inject the core of the flow.
3. The external source of energy required to raise the temperature was the reaction of methane with the hot minerals (silicate and oxides).
4. The methane was originated deeper in the Paraná Basin from the cracking of kerogen in bituminous shales (Ponta Grossa, Irati Formation and others).

ACKNOWLEDGMENTS

Financial support was provided by Project CNPq/VALE, MCT and Mineral Sector Fund (CT-Mineral) entitled "Desenvolvimento de metodologia de exploração geológica para geodos de ametista e ágata, cobre e outros bens minerais em ambiente hidrotermal do Grupo Serra Geral, sul-sudeste do Brasil" and project of excellence PRONEX-FAPERGS/CNPq on strategic minerals from southern Brazil, coordinated by Léo A. Hartmann. Thanks to CPRM (Geological Survey of Brazil) and Dr. Wilson Wildner by chemical analyzes ceded.

RESUMO

Na província vulcânica Paraná, há inúmeras ocorrências de rochas vítreas contendo fenocristais longos e curvos de clinopiroxênio (até 10 cm), plagioclásio (1 cm), magnetita e apatita, intrusivas em derrames de basalto. Estas rochas são aqui consideradas paralavas e ocorrem sob a forma de diques e sills finos (0,1-0,5 m) no núcleo de espessos derrames pahoehoe (>70 m). A ocorrência de paralavas está concentrada principalmente no estado do Paraná em decorrência do grande número de diques associados ao arco de Ponta Grossa. Estudos prévios denominaram estas rochas principalmente como pegmatitos, embora outras designações também tenham sido utilizadas. As paralavas foram interpretadas como sendo o produto de processos sucessivos e diversificados de injeção de sills do vulcanismo Serra Geral em formações sedimentares compostas por camadas de folhelhos betuminosos ricos em querogênio. A temperatura das intrusões provocou o craqueamento do querogênio e geração de gás metano que fluiu através das rochas sedimentares e vulcânicas. Ao atingir a parte inferior do núcleo do derrame de lava mais recente do Grupo Serra Geral, ainda quente (1.000 ºC), o metano reagiu com silicatos e óxidos, elevando a temperatura local até 1.600 ºC. O basalto hospedeiro foi refundido (possivelmente 75% do volume) e injetado

por flutuação na parte central e superior do núcleo. Este mecanismo relacionado à geração e oxidação do metano explica todas as evidências encontradas nas paralavas da província vulcânica, uma das maiores do mundo.

Palavras-chave: Paralava, província vulcânica Paraná, pirometamorfismo, refusão, remobilização de metais

REFERENCES

AARNES I, SVENSEN H, CONNOLLY JAD AND PODLADCHICOV, YY. 2010. How contact metamorphism can trigger global climate changes: Modeling gas generation around igneous sills in sedimentary basins. Geochim Cosmochim Ac 74: 7179-7195.

ABORRAGE AM AND LOPES RC. 1986. Projeto Borda Leste da Bacia do Paraná: integração geológica e avaliação econômica. DNPM/CPRM, São Paulo, final report, 18 v.

ARAÚJO CC, YAMAMOTO JK AND ROSTIROLA SP. 2004. Distribuição espacial e caracterização geológica dos arenitos asfálticos da borda leste da Bacia do Paraná no Estado de São Paulo. Rev Bras Geocienc 34: 187-200.

ARIOLI EE. 2008. Arquitetura faciológica da sequência vulcânica e o significado exploratório das anomalias geoquímicas de elementos do grupo da platina (EGP) e metais associados no sistema magmático Serra Geral, Estado do Paraná, Brasil. PhD Thesis, Universidade Federal do Paraná, Curitiba, Brazil, 262 p.

BAKKER RJ. 2003. Package Fluids 1. Computer programs for analysis of fluid inclusion data and for modeling bulk properties. Chem Geology 194: 3-23

BRÜCKMANN M, HARTMANN L.A, KNIJNIK D.B, ANDRADE R.H.P, SATO K. 2013. Extended duration of Paraná volcanism 135-119 Ma. Annals, XIV Simpósio Nacional de Estudos Tectônicos, Chapada dos Guimarães. Mato Grosso, abs., 1 p.

CARON M, GOETHALS M, DE SCHMEDT G, BERGHMANS J, VLIEGEN S, VAN'T OOST E AND AARSSEN A. 1999. Pressure dependence of the auto-ignition temperature of methane/air mixtures. J Hazard Mater 65: 233-244.

CHEADLE MJ, ELLIOT MT AND MCKENZIE D. 2004. Percolation threshold and permeability of crystallizing igneous rocks: the importance of textural equilibrium. Geology 32: 757-760.

CORNWALL HR. 1951. Differentiation in lavas of the Keweenawan Series and the copper deposits of Michigan. Geol Soc Am Bull 62: 159-202.

CROCKET JH. 2002. Platinum-group element geochemistry of mafic and ultramafic rocks. In: Cabri LJ (Ed), The geology, geochemistry, mineralogy and mineral beneficiation of platinum-group elements: Ontario, Canada. Canadian Institute of Mining, Metallurgy and Petroleum 54: 177-210.

D'ORIANO C, POMPILIO M, BERTAGNINI A, CIONI R AND PICHAVANT M. 2013. Effects of experimental reheating of natural basaltic ash at different temperatures and redox conditions. Contrib Mineral Petrol 165: 863-883.

DRAGOVIC B AND PHILPOTTS A.R. 2002. Degree of crystal-mush compaction in the Holyoke basalt, CT, as inferred from overgrowths on plagioclase phenocrysts. Geological Society of America, 37th Annual Meeting.

DUARTE LC, HARTMANN LA, VASCONCELOS MAZ, MEDEIROS JTN AND THEYE T. 2009. Epigenetic formation of amethyst-bearing geodes from Los Catalanes gemological district, Artigas, Uruguay, southern Paraná Magmatic-Province. J Volcanol Geoth Res 184: 427-436.

DUARTE LC, HARTMANN LA, RONCHI LH, BERNER Z, THEYE T. AND MASSONNE HJ. 2011. Stable isotope and mineralogical investigation of the genesis of amethyst geodes in the los Catalanes gemological district, Uruguai, southernmost Paraná volcanic province. Miner Deposita 46: 239-255.

FERREIRA CNH. 2011. Geologia do derrame Salto do Lontra e gênese dos pegmatitos básicos associados, província magmática do Paraná, sudoeste do estado do Paraná. Master of Science Dissertation. Universidade Federal do Paraná, Curitiba, Brazil, 102 p.

FODOR RV AND BAUER, G.R. 2014. Diabasic intrusion and lavas, segregation veins, and magma differentiation at Kahoolawe volcano, Hawaii. Miner Petrol 108: 269–286.

GOULART EP AND JARDIM NS. 1982. Avaliação geoquímica das Formações Ponta Grossa e Irati – Bacia do Paraná. In: Instituto de Pesquisas Tecnológicas do Estado de São Paulo (Ed.) PauliPetro Consórcio CESP/IPT, p. 41-74.

GRAPES R. 2011. Pyrometamorphism. Springer-Verlag, Berlin. 365p.

GRAPES R, SOKOL E, KOKH S, KOZMENKO O AND FISHMAN O. 2013. Petrogenesis of Na-rich paralava formed by methane flares associated with mud volcanism, Altyn-Emel National Park, Kazakhstan. Contrib Mineral Petr 165: 781-803.

GREENOUGH JD AND DOSTAL J. 1992a. Layered rhyolite bands in a tick North Mountain Basalt flow: the products of silicate liquid immiscibility? Mineral Mag 56:309-318.

GREENOUGH JD AND DOSTAL J. 1992b. Cooling history and differentiation of a thick North Mountain basalt flow (Nova Scotia, Canada). B Volcanol 55: 63-73.

GREENOUGH JD, LEE CY AND FRYER BJ. 2004. Evidence of volatile-influenced differentiation in a layered alkali basalt flow, Penghu Islands, Taiwan. B Volcanol 60: 412-424.

HARTLEY ME AND THORDARSON T. 2009. Melt segregations in a Columbia River Basalt lava flow: A possible mechanism for the formation of highly evolved mafic magmas. Lithos 112: 434-446.

HARTMANN LA, BAGGIO SB AND DUARTE SK. 2013. Decoding geochemical and gamma-spectrometric signatures from lavas and sand injectites at the base of the Paraná volcanic province, Novo Hamburgo, Brazil. Int Geol Rev 55: 510-524.

HARTMANN LA, DUARTE LC, MASSONNE HJ, MICHELIN C, ROSENSTENGEL LM, BERGMANN M, THEYE T, PERTILLE J, ARENA KR, DUARTE SK, PINTO VM, BARBOZA EG, ROSA MLCC AND WILDNER W. 2012a. Sequential opening and filling of cavities forming vesicles, amygdales and giant amethyst geodes in lavas from the southern Paraná volcanic province, Brazil and Uruguay. Int Geol Rev 54: 1-14.

HARTMANN LA, MEDEIROS JTN AND PETRUZZELLIS LT. 2012b. Numerical simulations of amethyst geode cavity formation by ballooning of altered Paraná volcanic rocks, South America. Geofluids 12: 133-141.

HOLZ M, FRANÇA AB, SOUZA PA, IANNUZZI R, ROHN R. 2010. A stratigraphic chart of the Late Carboniferous/Permian succession of the eastern border of the Paraná Basin, Brazil, South America. J S Am Earth Sci 29: 381-399.

KONTAK DJ, DE WOLFE MY, YOUNG DE AND DOSTAL J. 2002. Late-stage crystallization history of the Jurassic North Mountain basalt, Nova Scotia, Canadá. I.Textural and chemical evidence for pervasive development of silicate-liquid immiscibility. Can Mineral 5: 1287-1311.

LARSEN RB, BROOKS CK AND BIRD D. 1992. Methane-bearing, aqueous, saline solutions in the Skaergaard intrusion, east Greenland. Contrib Mineral Petrol 112: 428-437.

MARIANI P, BRAITENBERG C AND USSAMI N. 2013. Explaining the thick crust in Paraná basin, Brazil, with satellite GOCE-gravity observations. J S Am Earth Sci 45: 209-223.

MARSH BD. 1995. Solidification fronts and magmatic evolution. Mineral Mag 60: 5-40.

MORIMOTO N, FABRIES J, FERGUSON AK, GINZBURG IV, ROSS M, SEIFERT FA, ZUSSMAN J, AOKI K AND GOTTARDI G. 1988. Nomenclature of pyroxenes. Am Mineral 73: 1123-1133.

NAKAMURA K, SHIBUYA A, MASUTA K, MURAKAMI T, WILDNER W, DIAS AA, KIRCHNER, CA, LESSA N. 2003. Mineral exploration in the Paraná Basin area, the Federal Republic of Brazil, phase I. Metal Mining Agency of Japan - MMAJ and Geologycal Survey of Brazil - CPRM, internal report.

PEATE DW, HAWEKSWORTH CJ AND MANTOVANI MSM. 1992. Chemical stratigraphy of the Paraná lavas (South America): classification of magma types and their spatial distribution. B Volcanol 55: 119-139.

PECK DL AND MINAKAMI T. 1968. The formation of columnar joints in the upper part of Kilauean lava lakes, Hawaii. Geol Soc Am Bull 79: 1151-1168.

PEREIRA R. 2013. Evolução da bacia do Paraná no Rio Grande do Sul. Master of Science Dissertation, Universidade do Estado do Rio de Janeiro, Rio de Janeiro, Brazil, www.fgel.uerj.br/prh17/renatapereiracsampaio_prh17_uerj_fgel_monografia.pdf (accessed february 26, 2014).

769 PHILPOTTS AR, CARROLL M AND HILL JM. 1996. Crystal-mush compaction and
770 the origin of pegmatitic segregation sheets in a thick flood-basalt flow in the
771 Mesozoic Hartford basin, Connecticut. J Petrol 37: 811-836.
772 PHILPOTTS AR, BRUSTMAN CM, SHI J, CARLSON WD AND DENISON C. 1999.
773 Plagioclase-chain networks in slowly cooled basaltic magma. Am Mineral 84: 1819-
774 1829.
775 PHILPOTTS AR AND DICKSON LD. 2002. Millimeter-scale modal layering and the
776 nature of the upper solidification zone in thick flood-basalt flows and other sheets of
777 magma. J Struct Geol 24: 1171-1177.
778 PUFFER JH AND HORTER DL. 1993. Origin of pegmatitic segregation veins within
779 flood basalts. Geol Soc Am Bull 105: 738-748.
780 ROSENSTENGEL LM AND HARTMANN LA. 2012. Geochemical stratigraphy of
781 lavas and fault-block structures in the Ametista do Sul geode mining district, Paraná
782 volcanic province, southern Brazil. Ore Geol Rev 48: 332-348.
783 SAWAKUCHI AO, BELLO RM, NOMURA SF, OLIVEIRA AF, FERREIRA MP,
784 FUZIKAWA K, SAYEG IJ AND GIANNINI PCF. 2011. Paleotermometria das
785 unidades permotriássicas da borda leste da Bacia do Paraná (SP). Analls, XIII
786 Simpósio Nacional de Estudos Tectônicos**,** Campinas, São Paulo, 4 p.
787 SCHENATO F, FORMOSO M, DUDOIGNON P, MEUNIER A, PROUST D AND
788 MAS A. 2003. Alteration processes of a thick basaltic lava flow of the Paraná Basin
789 (Brazil): petrographic and mineralogical studies. J S Am Earth Sci 16: 423-444.
790 SILVA KFB. 2011. Caracterização petrográfica e geoquímica de pegmatitos básicos,
791 encaixados em derrames basálticos do Grupo Serra Geral, no Estado do Paraná.
792 Course conclusion monograph. Universidade Estadual de Campinas, Campinas,
793 Brazil, 94 p.

SIMAS MW, GUERRA-SOMMER M, CAZZULO-KLEPZIG M, MENEGAT R, SANTOS JOS, FERREIRA JAF AND DEGANI-SCHMIDT I. 2012. Geochronological correlation of the main coal interval in Brazilian Lower Permian: Radiometric dating of tonstein and calibration of biostratigraphic framework. J S Am Earth Sci 39: 1-15.

SOKOL E, NOVIKOV I, ZATEEVA S, VAPNIK YE, SHAGAM R AND KOZMENKO O. 2010. Combustion metamorphism in the Nabi Musa dome: for a mud volcanic origin of the Mottled Zone, Dead Sea area. Basin Res 22: 414-438.

STEELE-MACINNIS M, BODNAR RJ AND NADEN J. 2011. Numerical model to determine the composition of H_2O–NaCl–$CaCl_2$ fluid inclusions based on microthermometric and microanalytical data. Geochim Cosmochim Ac 75:21-40

VASCONCELLOS EMG, LICHT OAB, BRAGA LS AND BITTENCOURT AVL. 2001. Gabros da Bacia do Paraná: aspectos petrográficos e geoquímicos. Annals, VIII Congresso Brasileiro de Geoquímica, Curitiba, Paraná, abs., 1 p.

WALKER F. 1953. The pegmatitic differentiates of basic sheets. Am J Sci 251: 41-60.

WILDNER W, ARIOLI EE, LICHT OAB, COSTA VS, CARRILHO JC, LONGO EG, CANTARINO SC, SANDER A, PERROTA M AND FILHO CRS. 2006. Geologia e Recursos Minerais do Sudoeste do Estado do Paraná. Convênio CPRM/ MINEROPAR, Brasília, Distrito Federal, 95 p.

Figure captions

Figure 1. Geological map of the southeastern portion of South America, highlighting the Paraná Basin, Paraná volcanic province (light grey), Bauru Group sedimentary rocks (dark gray) and older sediments, igneous and metamorphic rocks (white area), with the location of the study areas of paralavas in Palmeira das Missões (RS), Francisco

Beltrão (PR) and Jardim (MS). The indicated area in the Paraná state is related to the samples initiated with WW and KN from CPRM. Modified from Peate et al. (1992).

Figure 2. Field photos of paralava outcrops in the Paraná volcanic province. A) Outcrop in the northwestern Paraná state showing the paralava sills and the host basalt. B) Schematic drawing of Figure 2A. C) Paralavas from the Dalba quarry, Francisco Beltrão, PR, showing celadonite (dark green core), the light and dark reaction rims and the host basalt. D) Schematic drawing of Figure 2C with emphasis on the relationship between the contact of the paralava (reaction rims, xenolith) and the host basalt. E) Northern portion of the Rochasul quarry in Jardim, MS, with continuous exposure of paralavas. (c) Detail of paralava highlighting the rock texture and size of the crystals of long and curved clinopyroxene. Clinopyroxene crystals highlighted in small square.

Figure 3. Photomicrographs of paralavas. A) Sample WW20b showing the texture of the host basalt. Plane polarized light. B) Sample WW20p showing the phenocrysts of clinopyroxene, plagioclase and opaque minerals in the paralava. Cross polarized light. C) Sample MS36 showing the texture of the paralava with crystals of plagioclase, clinopyroxene and magnetite-ilmenite. Plane polarized light. D) Sample MS36 showing the relashionship between phenocrysts of plagioclase, clinopyroxene and magnetite-ilmenite. Reflected light. E) Sample PD01 showing the paralava with phenocrysts of plagioclase and smaller crystals of clinopyroxene and areas with celadonite. Plane polarized light. F) Sample PD1 showing the relashionship between phenocrysts of plagioclase, clinopyroxene and magnetite-ilmenite and areas with celadonite. Reflected light.

Figure 4. Photomicrographs of paralavas with native copper. A) Sample WW20p showing the texture of the paralava with phenocrysts of plagioclase, clinopyroxene,

magnetite-ilmenite, smectite and native copper. B) The same area as Figure A in reflected light. C) Detail of the sample WW20p showing a phenocryst of magnetite-ilmenite and native copper in the paralava. D) Sample PD1 showing the texture of the paralava and areas with celadonite in plane polarized light. E) The same area shown in Figure D with reflected light highlighting the phenocrysts of magnetite-ilmenite. The dotted square shows the area with native copper. F) Detail of the dotted square of Figure E showing the relationship between crystals of clinopyroxene, native copper, celadonite and apatite in the paralava.

Figure 5. Geochemical diagrams of paralavas and host basalts; arrow indicated coexisting host and paralava (or melt) samples. A) Total alkalis-silica diagram showing the composition of studied basaltic rocks from the Paraná volcanic province, hosts and paralavas. Two basalt tephra compositions from Stromboli with corresponding laboratory melts (D'Oriano et al., 2013) and analyses from Ferreira (2011) were plotted for comparison. B) SiO_2 x MgO diagram showing the composition of the rocks of the study areas. C) P_2O_5 x TiO_2 diagram showing the two fields of host basalts and paralavas. D) Zr x Y diagram highlighting the enrichment in both elements from the host basalts to the paralavas.

Figure 6. Back-scattered electron images and classification diagrams of feldspar, clinopyroxene and magnetite-ilmenite. A) Back-scattered electron image highlighting the phenocrysts of plagioclase and the interstitial presence of KF and glass. B) Ternary Ab-An-Or diagram of feldspar. C) Back-scattered electron image highlighting the phenocrysts of clinopyroxene. D) Ternary En-Wo-Fs diagram of clinopyroxene. E) Back-scattered electron image highlighting the phenocrysts of magnetite – ilmenite. F) Binary diagram FeO x TiO_2 showing the fields of magnetite and ilmenite of paralavas. Symbology - Black dots = host basalt, red dots =

paralavas, Pl = plagioclase, Cpx = clinopyroxene, KF = potassium feldspar, Mag-Ilm = magnetite-ilmenite, Ap = apatite, Sme = smectite, Gl = glass.

Figure 7. Back-scattered electron images. A, B) Relationship between magnetite-ilmenite, smectite and native copper in the paralava. Symbology – Mag-Ilm = magnetite-ilmenite, Sme = smectite.

Figure 8. Fluid inclusions in plagioclase crystals (sample PD1). A) Thin section P51B with features of melt inclusions. Highlight for the small size of the melt inclusions. B) Thin section P6 with darkened fluid inclusions. The morphology ranging from regular (rounded) to elongated, with variable dimensions. These inclusions may be composed of a low density fluid (water vapor, CO_2 or CH_4).

Figure 9. Paralava formation model, starting with the cracking of kerogen from the Irati Formation into methane. Upward flow of methane through sedimentary formations and volcanic pile of the Paraná Basin. Autoignition of methane in the lower portion of a thick cooling flow (1,000 °C), rising temperature to approximately 1,500 °C. Host basalt melt and paralava sill and dike injection in the core of the flow.

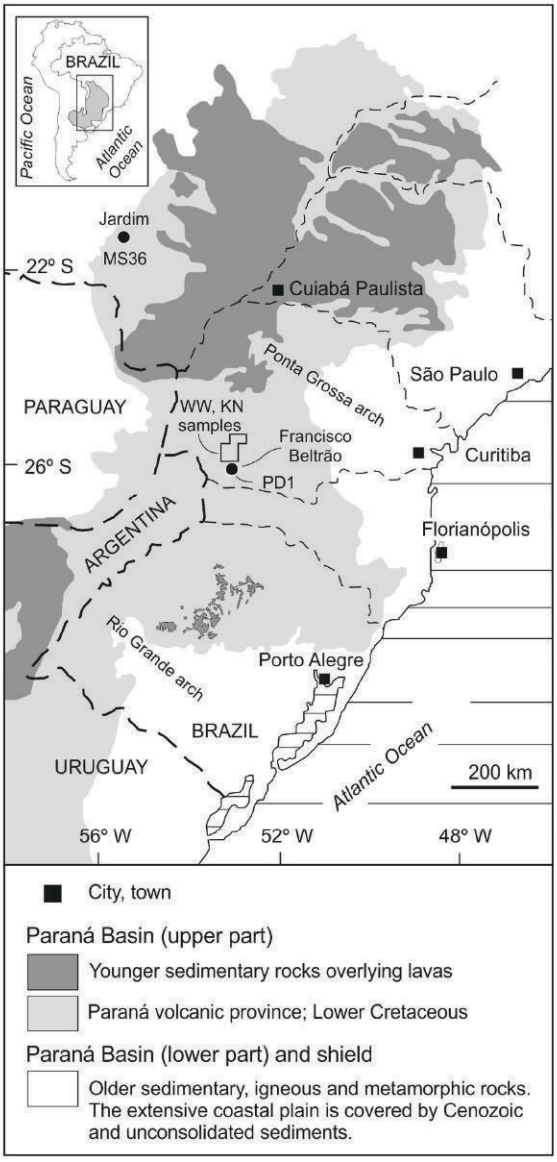

Figure 1. Geological map of the southeastern portion of South America, highlighting the Paraná Basin, Paraná volcanic province (light grey), Bauru Group sedimentary rocks (dark gray) and older sediments, igneous and metamorphic rocks (white area), with the location of the study areas of paralavas in Palmeira das Missões (RS), Francisco Beltrão (PR) and Jardim (MS). The indicated area in the Paraná state is related to the samples initiated with WW and KN from CPRM. Modified from Peate et al. (1992).
83x172mm (300 x 300 DPI)

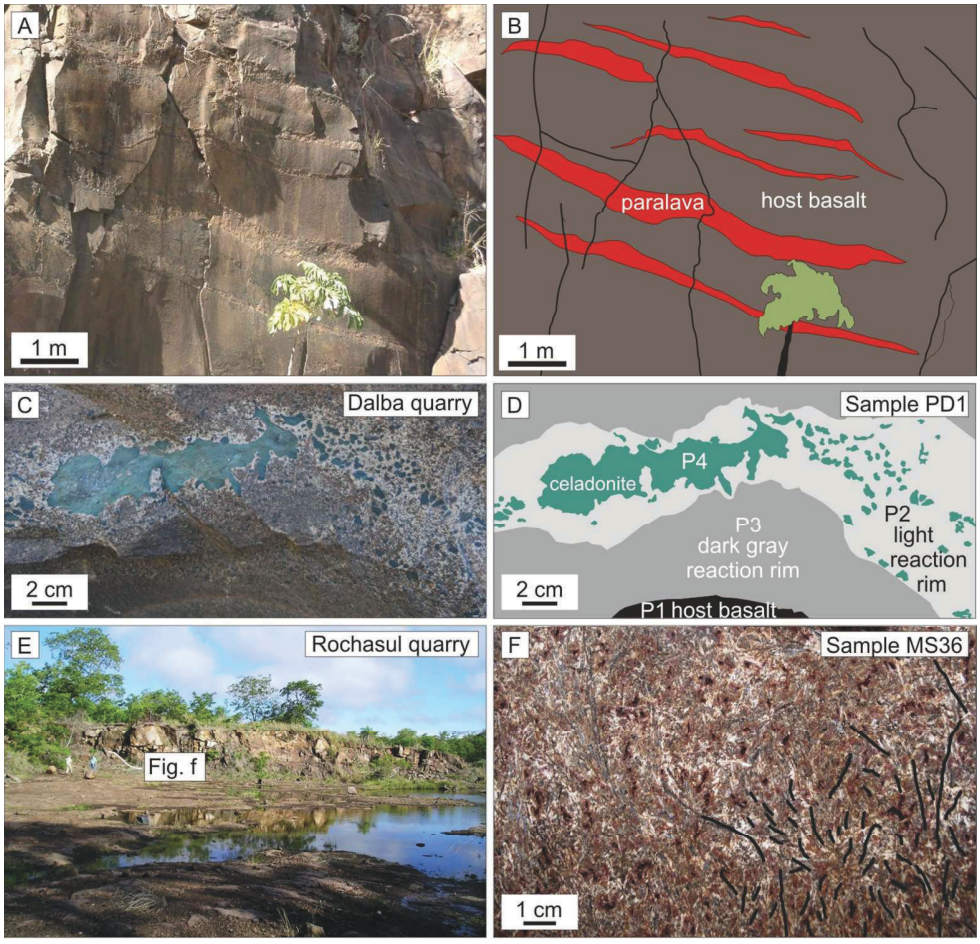

Figure 2. Field photos of paralava outcrops in the Paraná volcanic province. A) Outcrop in the northwestern Paraná state showing the paralava sills and the host basalt. B) Schematic drawing of Figure 2A. C) Paralavas from the Dalba quarry, Francisco Beltrão, PR, showing celadonite (dark green core), the light and dark reaction rims and the host basalt. D) Schematic drawing of Figure 2C with emphasis on the relationship between the contact of the paralava (reaction rims, xenolith) and the host basalt. E) Northern portion of the Rochasul quarry in Jardim, MS, with continuous exposure of paralavas. (c) Detail of paralava highlighting the rock texture and size of the crystals of long and curved clinopyroxene. Clinopyroxene crystals highlighted in small square.
126x120mm (300 x 300 DPI)

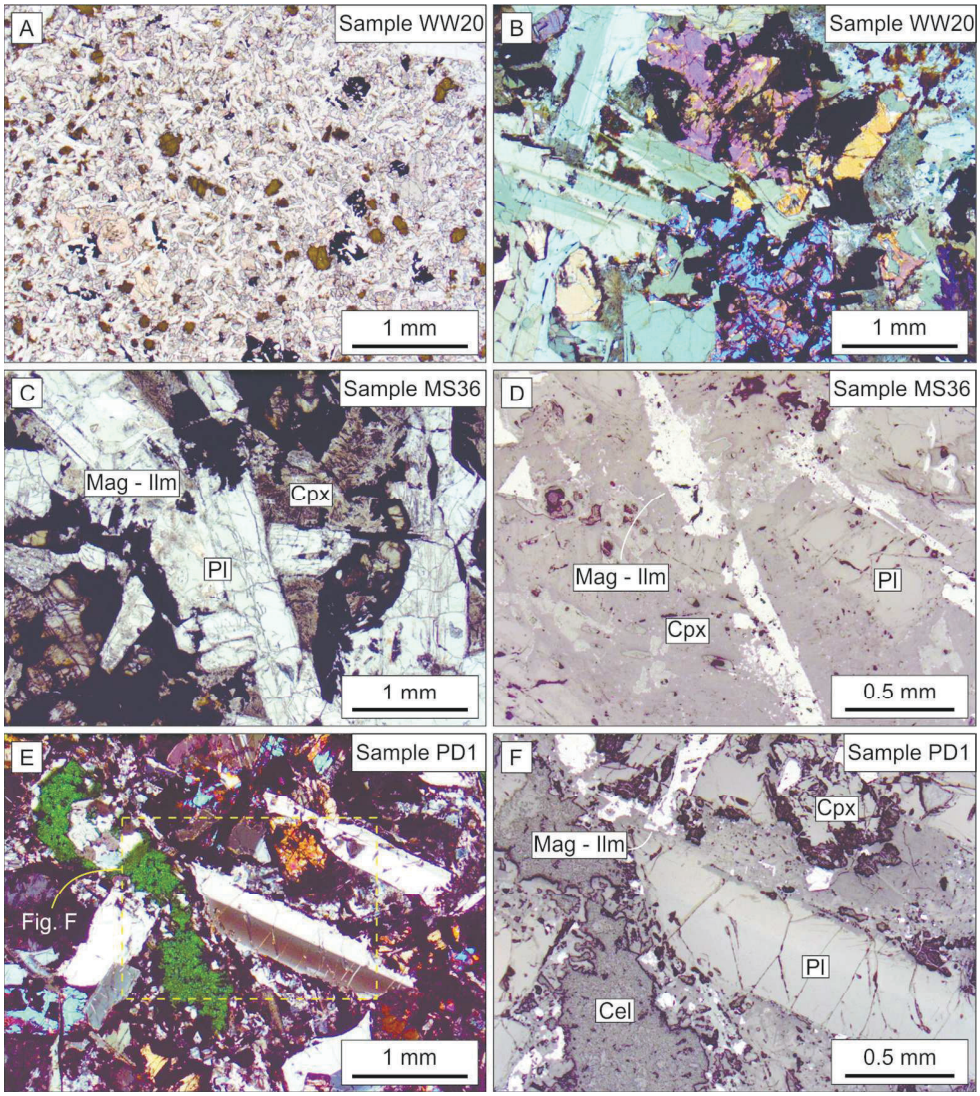

Figure 3. Photomicrographs of paralavas. A) Sample WW20b showing the texture of the host basalt. Plane polarized light. B) Sample WW20p showing the phenocrysts of clinopyroxene, plagioclase and opaque minerals in the paralava. Cross polarized light. C) Sample MS36 showing the texture of the paralava with crystals of plagioclase, clinopyroxene and magnetite-ilmenite. Plane polarized light. D) Sample MS36 showing the relashionship between phenocrysts of plagioclase, clinopyroxene and magnetite-ilmenite. Reflected light. E) Sample PD01 showing the paralava with phenocrysts of plagioclase and smaller crystals of clinopyroxene and areas with celadonite. Plane polarized light. F) Sample PD1 showing the relashionship between phenocrysts of plagioclase, clinopyroxene and magnetite-ilmenite and areas with celadonite. Reflected light.
126x141mm (300 x 300 DPI)

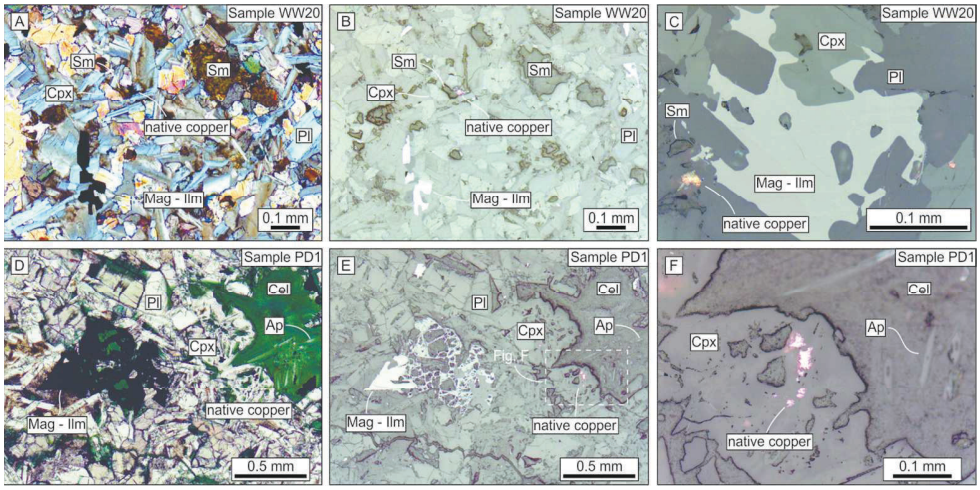

Figure 4. Photomicrographs of paralavas with native copper. A) Sample WW20p showing the texture of the paralava with phenocrysts of plagioclase, clinopyroxene, magnetite-ilmenite, smectite and native copper. B) The same area as Figure A in reflected light. C) Detail of the sample WW20p showing a phenocryst of magnetite-ilmenite and native copper in the paralava. D) Sample PD1 showing the texture of the paralava and areas with celadonite in plane polarized light. E) The same area shown in Figure D with reflected light highlighting the phenocrysts of magnetite-ilmenite. The dotted square shows the area with native copper. F) Detail of the dotted square of Figure E showing the relationship between crystals of clinopyroxene, native copper, celadonite and apatite in the paralava.
125x62mm (300 x 300 DPI)

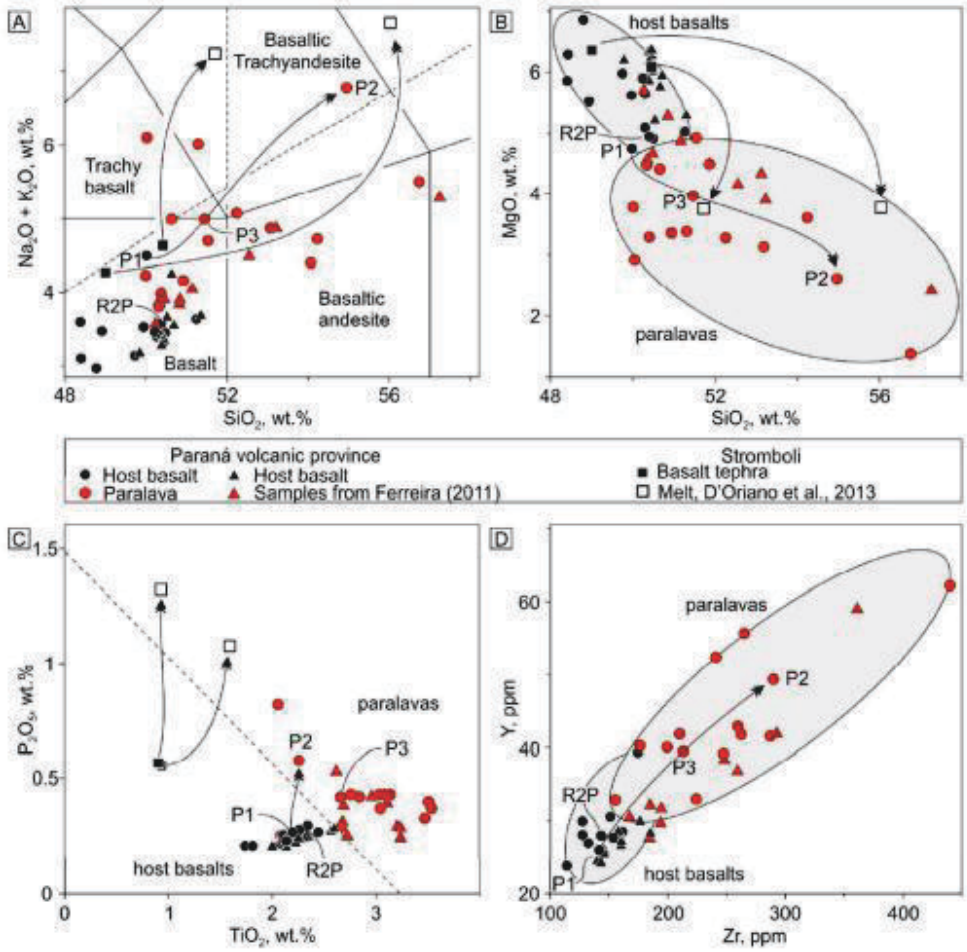

Figure 5. Geochemical diagrams of paralavas and host basalts; arrow indicated coexisting host and paralava (or melt) samples. A) Total alkalis-silica diagram showing the composition of studied basaltic rocks from the Paraná volcanic province, hosts and paralavas. Two basalt tephra compositions from Stromboli with corresponding laboratory melts (D'Oriano et al., 2013) and analyses from Ferreira (2011) were plotted for comparison. B) SiO2 x MgO diagram showing the composition of the rocks of the study areas. C) P2O5 x TiO2 diagram showing the two fields of host basalts and paralavas. D) Zr x Y diagram highlighting the enrichment in both elements from the host basalts to the paralavas.
126x124mm (300 x 300 DPI)

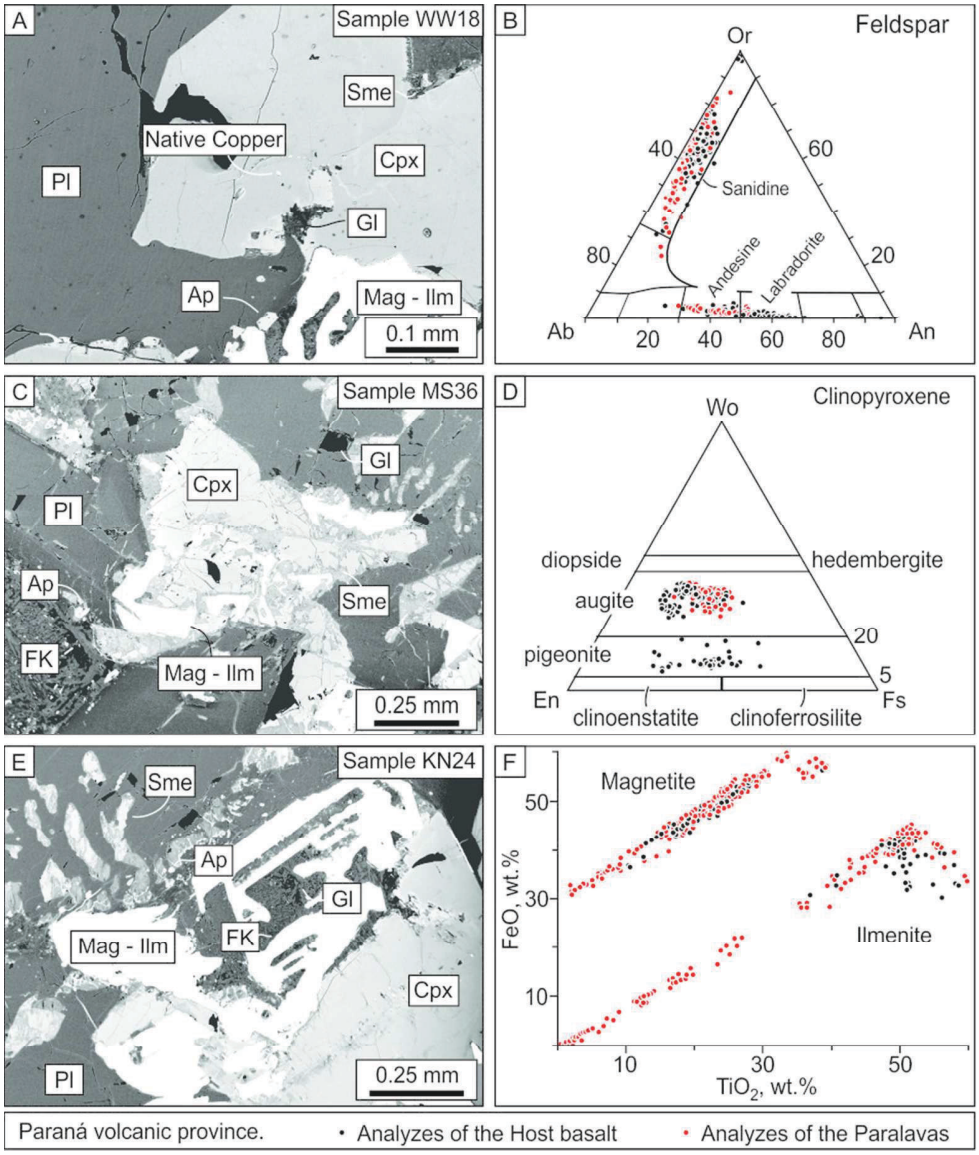

Figure 6. Back-scattered electron images and classification diagrams of feldspar, clinopyroxene and magnetite-ilmenite. A) Back-scattered electron image highlighting the phenocrysts of plagioclase and the interstitial presence of KF and glass. B) Ternary Ab-An-Or diagram of feldspar. C) Back-scattered electron image highlighting the phenocrysts of clinopyroxene. D) Ternary En-Wo-Fs diagram of clinopyroxene. E) Back-scattered electron image highlighting the phenocrysts of magnetite – ilmenite. F) Binary diagram FeO x TiO2 showing the fields of magnetite and ilmenite of paralavas. Symbology - Black dots = host basalt, red dots = paralavas, Pl = plagioclase, Cpx = clinopyroxene, KF = potassium feldspar, Mag-Ilm = magnetite-ilmenite, Ap = apatite, Sme = smectite, Gl = glass.
80x94mm (300 x 300 DPI)

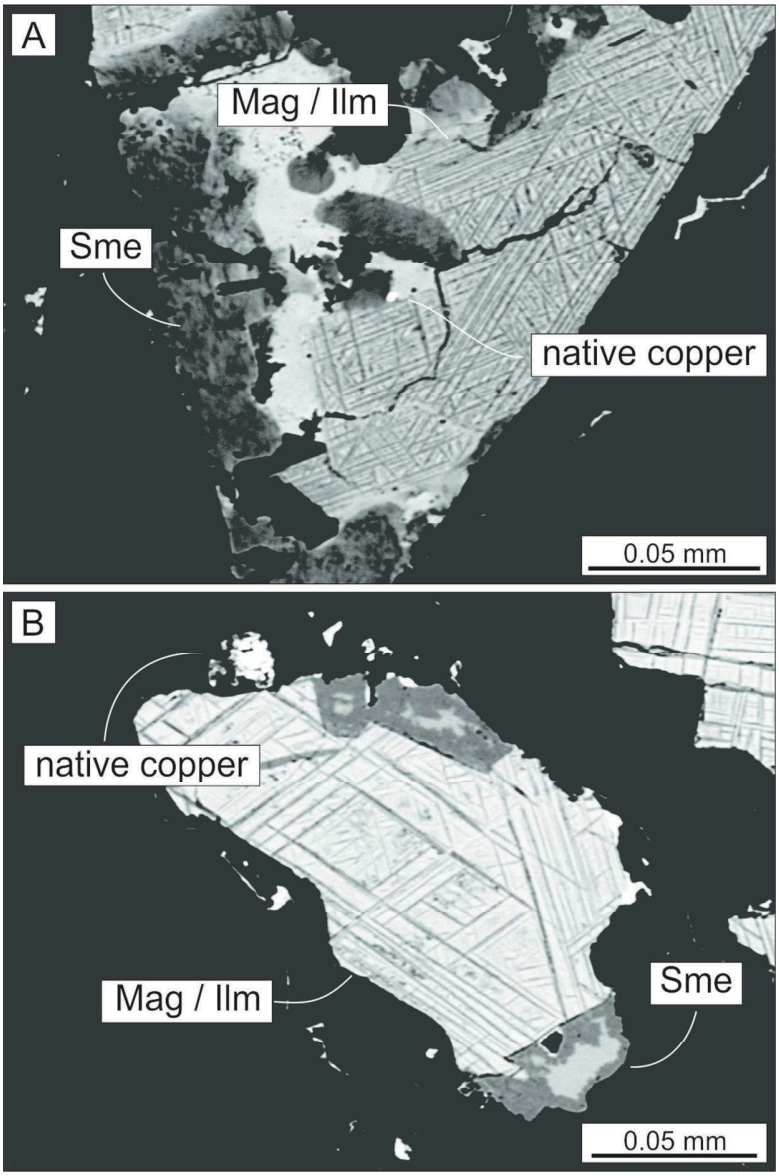

Figure 7. Back-scattered electron images. A, B) Relationship between magnetite-ilmenite, smectite and native copper in the paralava. Symbology – Mag-Ilm = magnetite-ilmenite, Sme = smectite.
92x139mm (300 x 300 DPI)

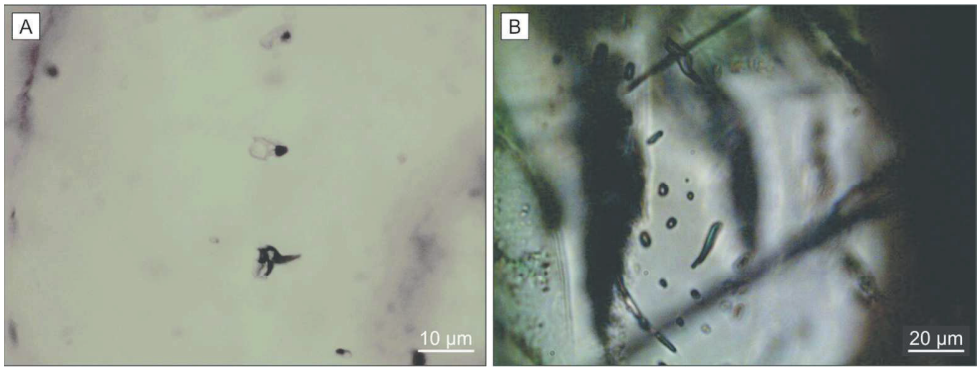

Figure 8. Fluid inclusions in plagioclase crystals (sample PD1). A) Thin section P51B with features of melt inclusions. Highlight for the small size of the melt inclusions. B) Thin section P6 with darkened fluid inclusions. The morphology ranging from regular (rounded) to elongated, with variable dimensions. These inclusions may be composed of a low density fluid (water vapor, CO2 or CH4).
126x47mm (300 x 300 DPI)

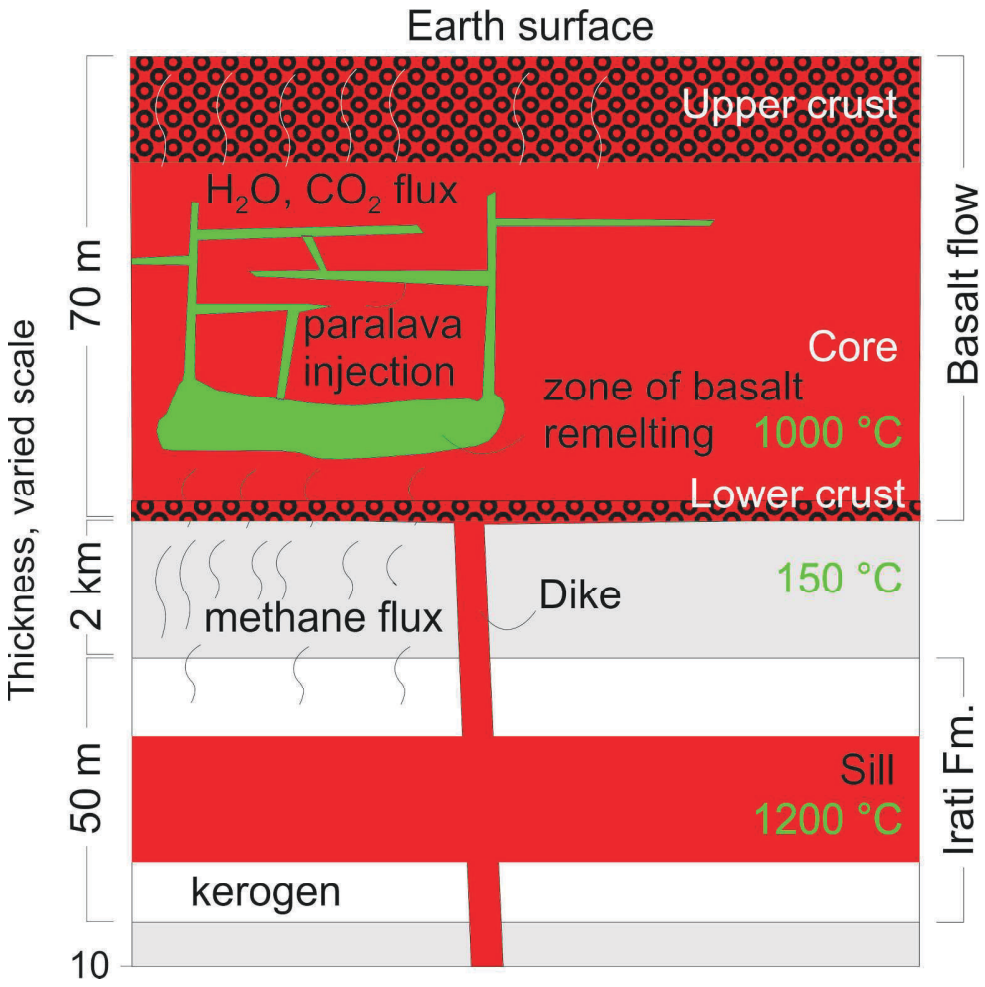

Figure 9. Paralava formation model, starting with the cracking of kerogen from the Irati Formation into methane. Upward flow of methane through sedimentary formations and volcanic pile of the Paraná Basin. Autoignition of methane in the lower portion of a thick cooling flow (1,000 °C), rising temperature to approximately 1,500 °C. Host basalt melt and paralava sill and dike injection in the core of the flow.
197x196mm (300 x 300 DPI)

Table 1. Names commonly used to classify the paralavas in continental volcanic and plutonic basaltic host rocks.

Name	Host rock	Reference
Pegmatite	North Mountain basalt, Nova Scotia Canadá	Walker (1953), Greenough e Dostal (1992b)
Pegmatitic segregation vein	Flood basalt	Puffer and Horter (1993)
Pegmatitic segregation sheet	Flood basalt flow	Philpotts et al. (1996)
Pegmatoid gabbro	Basalt, Serra Geral Group	Vasconcellos et al. (2001)
Mafic pegmatite	North Mountain basalt, Nova Scotia Canadá	Kontak et al. (2002)
Basic pegmatite	Basalt, Serra Geral Group	Arioli (2008), Silva (2011), Ferreira (2011) Gomes et al. (2013)
Pegmatitic vein	Basalt, Serra Geral Group	Gomes et al. (2013)
Paralava	Flood basalt and intrusives	This work

Table 2. Chemical composition of paralavas (samples labeled "p") and host basalts (labeled "b") from the Serra Geral Group. Oxides in wt.%, trace elements in ppm, except Au in ppb. Below detection limit: Tl (0.1), Cd (0.3), As (5), Sb (0.2), Bi (0.1), Hg (0.1), Se (0.5), TOT/S (0.01), Cr_2O_5 (0.02). (−) = below detection limit: Ag (0.1), Cs (0.1). LOI = loss on ignition.

Sample	WW 33b	WW 33p	WW 34b	WW 34p	WW 19b	WW 19p	WW 20b	WW 20p	WW 18b	WW 18p	WW 60b	WW 60p
SiO_2	50.48	50.94	50.29	50.40	48.42	50.34	48.78	53.18	48.92	50.04	48.39	50.65
Al_2O_3	12.29	11.47	12.47	11.32	13.02	10.21	13.56	11.38	12.78	11.68	12.93	11.34
Fe_2O_3	16.02	17.69	16.07	18.65	14.68	18.14	13.46	16.02	15.12	18.11	15.12	17.08
MgO	4.93	3.36	5.10	3.29	6.30	4.48	6.87	3.13	5.53	2.91	5.86	4.41
CaO	9.20	7.46	9.05	7.47	10.29	7.16	10.97	6.07	9.81	5.42	9.68	7.30
Na_2O	2.34	2.51	2.32	2.51	2.26	2.40	2.21	2.50	2.25	2.60	2.47	2.78
K_2O	1.12	1.65	1.08	1.47	0.85	1.41	0.77	2.37	1.23	3.50	1.13	2.21
TiO_2	2.28	3.14	2.34	3.09	2.09	3.47	1.74	2.76	2.44	3.54	2.08	2.66
P_2O_5	0.28	0.43	0.30	0.43	0.23	0.33	0.21	0.43	0.27	0.37	0.22	0.29
MnO	0.21	0.18	0.22	0.17	0.19	0.18	0.18	0.13	0.16	0.24	0.21	0.19
LOI	0.60	0.90	0.50	0.90	1.40	1.60	1.00	1.70	1.20	1.30	1.80	0.90
TOT/C	0.05	0.02	0.02	0.02	0.03	0.03	0.02	0.03	0.03	0.02	0.09	0.04
SUM	99.77	99.74	99.76	99.71	99.76	99.72	99.78	99.68	99.74	99.72	99.92	99.82
Ba	280	402	268	371	291	363	246	517	310	436	298	336
Be	1	2	1	1	1	2	1	2	1	1	1	1
Co	43.8	36.3	42.9	36.4	46.0	45.3	50.0	33.8	42.3	39.3	46.8	46.2
Cs	−	0.8	0.1	0.4	0.3	0.2	0.5	0.4	0.4	0.9	0.7	0.9
Ga	20.0	21.5	20.2	20.8	20.9	21.4	20.3	22.0	20.8	22.9	21.1	21.1
Hf	4.6	7.8	4.7	6.8	3.4	5.9	3.3	7.3	4.3	6.0	3.9	5.1
Nb	15.2	24.0	15.2	21.3	12.9	19.2	11.1	25.6	15.3	22.7	11.8	15.8
Rb	24.1	38.9	23.0	33.2	18.7	32.4	18.0	72.0	36.9	157.3	25.0	82.3
Sn	2	3	1	2	1	3	2	2	1	2	1	2
Sr	238	222	240	231	385	301	387	346	397	355	306	289
Ta	1.0	1.4	1.1	1.4	0.8	1.2	0.7	1.5	0.9	1.3	0.6	0.9
Th	2.4	3.9	2.0	3.7	2.7	3.6	1.9	4.7	2.5	3.5	2.5	3.4
U	0.5	0.8	0.5	0.7	0.4	0.7	0.4	0.8	0.5	0.8	0.4	0.7
V	458	424	435	420	504	800	436	336	514	520	450	599
W	0.3	0.4	0.4	0.6	0.3	0.5	0.3	0.5	0.3	0.9	0.3	0.4
Zr	174	265	174	241	131	199	114	262	150	210	127	176
Y	39.5	55.7	39.6	52.4	27.0	40.1	23.7	41.8	30.5	41.9	30.0	40.3
La	22.8	34.6	22.7	32.9	20.6	29.0	18.4	40.1	24.2	34.4	18.6	25.3
Ce	48.5	73.1	49.2	67.4	43.6	59.2	37.8	81.4	49.1	70.9	38.6	53.9
Pr	6.18	9.21	6.35	9.02	5.39	7.73	4.71	9.98	6.16	8.87	4.92	6.79
Nd	27.6	39.7	27.0	39.9	22.9	33.4	20.8	40.1	26.8	39.4	22.3	31.1
Sm	6.4	9.4	6.4	8.8	5.2	7.6	4.5	9.1	6.0	8.6	5.2	6.8
Eu	1.93	2.48	1.82	2.57	1.69	2.18	1.49	2.55	1.78	2.56	1.67	2.05
Gd	7.07	9.58	6.78	9.33	5.20	7.75	4.76	8.17	5.91	7.83	5.22	6.92
Tb	1.13	1.72	1.14	1.65	0.84	1.19	0.73	1.36	0.94	1.21	0.93	1.22
Dy	6.31	9.38	6.56	8.53	4.85	6.92	4.20	7.67	5.43	7.18	5.42	7.57
Ho	1.43	1.98	1.42	1.91	0.97	1.35	0.90	1.53	1.10	1.50	1.07	1.40
Er	4.08	5.76	4.15	5.36	2.83	3.85	2.46	4.45	3.14	4.18	3.02	3.97
Tm	0.61	0.76	0.58	0.75	0.42	0.55	0.36	0.62	0.42	0.59	0.46	0.63
Yb	3.93	5.36	3.85	5.06	2.51	3.45	2.05	4.32	2.76	3.76	2.93	4.11
Lu	0.57	0.78	0.55	0.77	0.38	0.52	0.35	0.61	0.38	0.57	0.41	0.55
Mo	1.2	1.2	0.8	0.8	1.1	1.1	1.0	1.1	0.6	1.2	0.6	0.7
Cu	205	184	235	387	215	369	201	337	268	199	42	11.34
Pb	0.9	1.1	0.9	1.2	1.0	1.4	1.0	1.1	1.0	1.4	1.0	1.2
Zn	65	63	78	65	69	104	51	84	68	141	71	98
Ni	22.0	15.4	19.6	10.8	33.8	21.3	38.3	12.5	30.5	10.4	25.9	14.9
Ag	−	0.1	−	0.1	0.1	0.2	0.1	0.1	0.1	0.1	−	0.1
Au	2.4	3.7	1.6	9.5	4.8	5.5	3.3	4.4	4.1	9.4	4.3	4.4
Sc	41	38	41	40	38	38	38	29	37	35	39	37

Table 3. Chemical composition of host basalts (labeled "b") and paralavas (labeled "p") from the Serra Geral Group. MS36 is a paralava. Oxides in wt.%, trace elements in ppm, except Au in ppb. Below detection limit: TOT/C (0.02), TOT/S (0.01), Cr_2O_3 (0.02), Be (1), W (0.5), Mo (2), As (5), Sb (0.2), Hg (0.1), Se (0.5), Ag (0.3), Bi (0.1). (–) = below detection limit: Tl (0.1), Cd (0.3), Ni (20), Pb (3), Sn (1), Au (0.5). LOI = loss on ignition.

Sample	MS 36	AS 4b	AS 4p	KN 22b	KN 22p	KN 23b	KN 23p	KN 24b	KN 24p	KN 25b	KN 25p	P1b	R2Pb	P2p	P3p
SiO_2	56.75	51.26	51.55	49.95	52.26	50.28	50.01	50.23	51.30	49.73	54.24	49.95	50.38	54.96	51.47
Al_2O_3	11.23	12.97	11.93	13.33	11.21	13.32	11.39	13.37	11.99	13.32	10.36	13.07	12.65	11.03	11.30
Fe_2O_3	15.18	14.75	14.85	13.87	17.01	14.10	17.67	14.19	15.92	13.95	15.40	14.30	14.58	15.31	16.11
MgO	1.38	5.04	4.93	5.62	3.28	5.67	3.78	5.91	3.38	5.98	3.61	4.73	4.95	2.62	3.97
CaO	5.05	9.23	7.89	10.04	5.59	9.95	7.31	10.06	5.78	10.18	6.99	8.87	9.26	4.49	6.17
Na_2O	2.72	2.55	2.90	2.49	2.66	2.52	2.63	2.49	2.77	2.34	2.73	2.26	2.45	2.41	2.27
K_2O	2.78	1.10	1.80	1.04	2.41	1.02	1.60	0.98	3.24	0.80	1.99	2.24	1.13	4.36	2.72
TiO_2	2.06	2.10	2.09	2.11	3.03	2.15	3.51	2.13	2.84	1.81	3.05	2.2	2.26	2.26	2.66
P_2O_5	0.82	0.26	0.25	0.24	0.43	0.24	0.40	0.23	0.42	0.21	0.37	0.27	0.28	0.58	0.42
MnO	0.17	0.21	0.18	0.21	0.21	0.20	0.22	0.20	0.17	0.19	0.34	0.21	0.17	0.16	0.17
LOI	1.50	0.81	1.86	1.31	2.04	1.06	1.81	0.64	1.69	1.63	1.20	1.6	1.6	1.5	2.4
SUM	99.65	100.28	100.22	100.21	100.12	100.50	100.34	100.45	99.50	100.12	100.28	99.72	99.72	99.64	99.69
Ba	727	320	312	305	556	338	453	326	488	265	446	310	298	541	433
Co	24.5	38.7	38.1	40.2	34.7	43.2	40.0	44.8	34.7	44.0	35.4	37.7	40	21.6	35.1
Cs	0.3	0.3	0.8	0.1	0.3	0.1	0.4	0.1	0.8	0.1	0.5	0.5	0.3	0.6	0.4
Ga	22.2	20.0	20.0	20.1	23.8	22.0	24.6	22.4	25.0	21.2	22	18.6	17.2	18.4	18.3
Hf	11.7	4.3	4.3	4.1	7.8	4.5	6.7	4.4	6.9	3.6	6.5	3.6	3.8	7.8	6.1
Nb	35.5	12.2	11.9	13.3	25.2	14.8	23.2	14.5	23.3	10.8	22.6	12.9	12.5	23.8	19.1
Rb	51.5	27.4	61.5	21.3	83.3	23.6	48.6	23.3	161.1	14.9	56.9	81.4	26.5	143.9	86.6
Sn	7	–	–	–	1.8	–	1.3	–	1.3	–	1.5	2	2	3	3
Sr	685	277	264	354	326	383	347	389	367	321	328	339	328	277	293
Ta	2.2	0.8	0.8	0.9	1.8	1.0	1.6	1.0	1.6	0.7	1.6	0.7	0.8	1.5	1.1
Th	6.2	2.7	2.8	2.3	4.5	2.5	3.7	2.3	3.9	2.2	3.3	2.7	2.5	5.4	4
U	1.3	0.5	0.5	0.4	0.9	0.4	0.7	0.4	0.8	0.5	0.5	0.6	0.7	1	0.8
V	49	440	492	433	298	416	497	442	397	420	556	476	459	230	363
Zr	440	155	155	143	287	160	247	153	259	127	224	144	143	290	213
Y	62.2	32.9	32.8	26.0	41.6	28.5	39.2	27.7	42.9	28.1	32.9	25.9	28	49.3	39.5
La	61.8	20.5	20.5	21.8	42.6	23.0	35.7	22.3	37.9	18.1	32.9	21.5	21.3	39.2	36.4
Ce	128.6	45.2	45.3	48.4	94.5	51.6	81.2	50.1	85.3	40.3	74.7	47.6	46	85.2	68.8
Pr	17.26	5.17	5.25	5.49	10.43	5.96	9.13	5.63	9.50	4.64	8.47	5.7	5.72	10.66	8.45
Nd	73.60	22.77	22.86	24.04	44.24	25.55	38.92	24.68	40.88	20.77	35.85	23.6	23.7	43.8	34
Sm	15.71	5.39	5.31	5.30	9.26	5.56	8.24	5.34	8.84	4.81	7.48	5.25	5.34	9.63	7.7
Eu	4.31	1.74	1.74	1.78	2.89	1.90	2.70	1.89	2.83	1.70	2.38	1.65	1.67	2.70	2.28
Gd	15.04	5.77	5.75	5.40	8.56	5.88	8.33	5.55	8.63	5.06	7.31	5.45	5.63	10.13	8.04
Tb	2.33	0.98	1.00	0.87	1.42	0.92	1.33	0.90	1.42	0.87	1.15	0.80	0.85	1.52	1.2
Dy	12.65	6.07	6.07	5.15	8.58	5.44	7.68	5.37	8.28	5.27	6.62	4.76	5.51	9.90	7.36
Ho	2.53	1.20	1.24	1.01	1.68	1.09	1.56	1.04	1.63	1.05	1.25	0.94	0.99	1.87	1.49
Er	6.60	3.55	3.60	3.06	4.83	3.27	4.36	2.95	4.62	3.13	3.61	2.71	2.88	4.88	4.08
Tm	0.87	0.55	0.54	0.43	0.74	0.46	0.63	0.43	0.67	0.46	0.51	0.41	0.45	0.77	0.61
Yb	5.52	3.42	3.26	2.37	4.28	2.61	3.63	2.59	3.71	2.45	2.79	2.51	2.58	4.77	3.61
Lu	0.84	0.50	0.50	0.33	0.60	0.37	0.52	0.34	0.56	0.37	0.43	0.38	0.40	0.72	0.54
Cu	285	211	264	234	273	239	372	226	232	227	1315	189	93	600	236
Pb	3.4	24.3	7.1	–	–	8.2	–	–	–	7.9	–	1.5	2.4	1.2	1.9
Zn	142	100	103	100	134	95	137	96	145	96	120	91	48	58	88
Ni	–	51.2	41.9	54.7	9.8	49.2	13.7	55.1	14.3	63.8	16.1	27.7	7.5	4.5	10.4
Cd	–	0.37	–	0.94	0.49	0.57	0.66	0.65	–	–	0.64	-	-	-	-
Au	1.7	5.6	4.3	5.3	12.5	4.9	10.8	6.1	9.0	6.5	7.7	2.4	-	1	7.5
Tl	–	0.11	0.19	0.14	0.21	0.14	0.41	0.11	0.34	0.12	0.33	-	-	-	-
Sc	19	40	39	38	32	38	37	38	33	39	33	35	35	25	32

Table 4
Representative electron microprobe analyses of feldspar from host basalts and paralavas (wt.%).

	Host basalts								Paralavas							
	Alkali Feldspar				Plagioclase				Alkali Feldspar				Plagioclase			
SiO_2	61.57	66.47	65.10	73.44	52.40	56.88	54.26	52.52	72.52	75.94	66.0	69.54	55.91	55.09	57.94	55.85
TiO_2	1.78	0.00	0.86	0.19	0.10	0.07	0.10	0.09	0.14	0.29	0.09	0.09	0.09	0.10	0.05	0.10
Al_2O_3	15.19	17.67	15.98	11.15	29.09	27.05	27.77	28.95	13.47	10.39	18.17	16.53	27.00	26.53	26.14	27.13
Cr_2O_3	0.00	0.00	0.00	0.00	0.00	0.00	0.00	0.00	0.00	0.00	0.00	0.00	0.00	0.00	0.00	0.00
Fe_2O_3	8.09	0.06	1.02	3.82	1.14	0.85	1.10	0.99	0.17	2.98	0.38	1.10	0.63	0.72	0.58	0.57
Mn_2O_3	0.00	0.00	0.05	0.04	0.04	0.02	0.00	0.00	0.00	0.00	0.00	0.03	0.01	0.03	0.00	0.00
MgO	3.05	0.01	0.92	1.27	0.09	0.02	0.07	0.09	0.00	0.85	0.00	0.65	0.11	0.07	0.05	0.09
CaO	0.67	0.00	0.27	0.54	12.51	9.27	11.16	12.33	0.56	0.33	0.04	1.13	9.93	10.24	8.53	9.91
Na_2O	2.27	0.05	2.65	1.83	4.36	6.03	5.07	4.52	4.23	2.01	2.24	5.25	5.65	5.45	6.18	5.87
K_2O	9.17	16.20	10.73	7.35	0.27	0.50	0.45	0.31	5.81	6.33	13.08	5.35	0.48	0.51	0.61	0.50
BaO	0.08	0.00	0.07	0.06	0.00	0.05	0.01	0.00	0.44	0.06	0.08	0.08	0.01	0.00	0.05	0.01
Total	101.86	100.47	97.64	99.69	100.01	100.75	99.98	99.81	97.35	99.19	100.07	99.75	99.83	98.74	100.12	100.04
Si	2.81	3.04	3.03	3.26	2.39	2.54	2.46	2.40	3.26	3.34	3.01	3.08	2.53	2.52	2.60	2.52
Al	0.82	0.95	0.88	0.58	1.56	1.43	1.49	1.56	0.71	0.54	0.98	0.86	1.44	1.43	1.38	1.44
Fe_3	0.28	0.00	0.04	0.13	0.04	0.03	0.04	0.03	0.01	0.10	0.01	0.04	0.02	0.02	0.02	0.02
Mn_3	0.00	0.00	0.00	0.00	0.00	0.00	0.00	0.00	0.00	0.00	0.00	0.00	0.00	0.00	0.00	0.00
Cr	0.00	0.00	0.00	0.00	0.00	0.00	0.00	0.00	0.00	0.00	0.00	0.00	0.00	0.00	0.00	0.00
Ti	0.06	0.00	0.03	0.01	0.00	0.00	0.00	0.00	0.00	0.01	0.00	0.00	0.00	0.00	0.00	0.00
su1	4.18	4.00	4.03	4.06	4.00	4.00	3.99	3.99	3.99	4.05	4.01	4.03	4.00	3.99	4.00	3.99
Ba	0.00	0.00	0.00	0.00	0.00	0.00	0.00	0.00	0.01	0.00	0.00	0.00	0.00	0.00	0.00	0.00
Ca	0.03	0.00	0.01	0.03	0.61	0.44	0.54	0.60	0.03	0.02	0.00	0.05	0.48	0.50	0.41	0.48
Na	0.20	0.00	0.24	0.16	0.39	0.52	0.45	0.40	0.37	0.17	0.20	0.45	0.50	0.48	0.54	0.51
K	0.53	0.95	0.64	0.42	0.02	0.03	0.03	0.02	0.33	0.36	0.76	0.30	0.03	0.03	0.03	0.03
su2	0.77	0.95	0.89	0.60	1.01	1.00	1.02	1.02	0.74	0.54	0.96	0.81	1.00	1.02	0.98	1.02
Components																
An	0.04	0.00	0.02	0.04	0.60	0.45	0.53	0.59	0.05	0.03	0.00	0.07	0.48	0.49	0.42	0.47
Ab	0.26	0.00	0.27	0.26	0.38	0.52	0.44	0.39	0.50	0.32	0.21	0.56	0.49	0.48	0.55	0.50
Or	0.69	1.00	0.72	0.69	0.02	0.03	0.03	0.02	0.45	0.65	0.79	0.37	0.03	0.03	0.04	0.03

Table 5
Representative microprobe analyses of clinopyroxenes from host basalts and paralavas (oxides in wt.%).

	Host basalt								Paralavas							
	Augite				*Pigeonite*				*Augite*							
SiO_2	50.42	51.02	50.19	50.87	51.25	50.32	50.80	50.78	50.57	50.05	49.88	49.59	50.23	49.68	50.25	50.15
TiO_2	0.79	1.23	0.86	0.92	0.46	0.48	0.43	0.46	0.96	1.06	0.72	1.11	0.81	0.95	1.01	0.98
Al_2O_3	1.06	1.40	1.47	1.36	0.62	0.77	0.53	0.62	1.55	1.65	0.95	2.13	1.35	1.79	1.69	1.55
Cr_2O_3	0.02	0,01	0.00	0.02	0.00	0.01	0.01	0.00	0.05	0.00	0.00	0.00	0.00	0.01	0.01	0.05
FeO	18.24	16.25	15.63	15.04	26.26	26.68	27.17	25.25	15.47	16.58	19.94	17.41	15.02	15.09	15.71	17.21
MnO	0.41	0.36	0.35	0.41	0.58	0.58	0.56	0.51	0.28	0.40	0.49	0.46	0.35	0.28	0.31	0.39
MgO	12.08	13.77	13.94	13.85	17.06	15.50	15.34	16.97	12.79	13.29	10.64	10.89	13.81	13.59	13.33	12.73
CaO	16.97	16.16	17.32	16.88	4.53	4.56	4.78	4.30	17.63	16.48	16.53	17.32	16.99	17.31	16.85	16.44
Na_2O	0.23	0.23	0.29	0.22	0.06	0.05	0.06	0.06	0.26	0.20	0.25	0.31	0.25	0.25	0.22	0.22
K_2O	0.01	0.00	0.03	0.03	0.00	0.05	0.00	0.01	0.03	0.00	0.01	0.11	0.03	0.01	0.00	0.00
Total	100.23	100.45	100.09	99.60	100.82	99.00	99.68	98.96	99.60	99.71	99.39	99.33	98.85	98.96	98.38	99.72
Atoms per formula unit calculated on the basis of 6 oxygen																
Si	2.24	2.24	2.22	2.25	2,25	2.26	2.27	2.27	1.94	1.92	1.95	1.92	1.93	1.91	1.93	1.93
Ti	0.03	0.04	0.03	0.03	0.02	0.02	0.01	0.02	0.03	0.03	0.02	0.03	0.02	0.03	0.03	0.03
Al	0.06	0.07	0.08	0.07	0.03	0.04	0.03	0.03	0.07	0.07	0.04	0.10	0.06	0.08	0.08	0.07
Cr	0.00	0.00	0.00	0.00	0.00	0.00	0.00	0.00	0.00	0.00	0.00	0.00	0.00	0.00	0.00	0.00
Fe	0.68	0.60	0.58	0.56	0.96	1.00	1.02	0.94	0.50	0.53	0.65	0.56	0.48	0.49	0.50	0.55
Mn	0.02	0.01	0.01	0.02	0.02	0.02	0.02	0.02	0.01	0.01	0.02	0.02	0.01	0.01	0.01	0.01
Mg	0.80	0.90	0.99	0.91	1.12	1.04	1.02	1.13	0.73	0.76	0.62	0.63	0.79	0.78	0.76	0.73
Ca	0.81	0.76	0.82	0.80	0.21	0.22	0.23	0.21	0.72	0.68	0.69	0.72	0.70	0.71	0.69	0.68
Na	0.02	0.02	0.02	0.02	0.02	0.00	0.01	0.01	0.02	0.01	0.02	0.02	0.02	0.02	0.02	0.02
K	0.00	0.00	0.00	0.00	0.00	0.00	0.00	0.00	0.00	0.00	0.00	0.01	0.00	0.00	0.00	0.00

Table 6
Representative microprobe analyses of magnetite and ilmenite from host basalts and paralavas (oxides in wt.%).

	Host basalt								Paralavas							
	Magnetite				*Ilmenite*				*Magnetite*				*Ilmenite*			
TiO_2	20,70	24,63	14,68	18,47	49,56	50,04	49,54	49,79	20,35	23,64	29,70	27,65	51,19	48,20	50,64	50,89
Al_2O_3	1,58	1,40	1,87	2,68	0.00	0.00	0.00	0.00	1,23	1,33	0,31	0,68	0.00	0,08	0.00	0.00
Cr_2O_3	0,20	0,15	0,45	0,24	0.00	0,03	0,05	0,01	0,03	0,23	0,05	0,03	0.00	0,01	0,01	0,01
Fe_2O_3	24,32	16,09	36,16	26,76	5,22	4,51	6,64	5,53	26,78	20,01	6,96	11,22	3,49	2,66	3,72	1,03
FeO	48,11	49,93	42,98	45,16	42,43	38,60	41,20	40,85	48,57	50,69	55,52	54,10	44,33	41,53	44,05	44,38
MnO	0,43	2,35	0,17	1,79	0,42	5,19	0,40	0,43	0,44	0,72	0,75	0,64	0,63	0,45	0,93	0,65
MgO	0,48	0,16	0,60	0,16	0,97	0,65	1,66	1,96	0,30	0,65	0,29	0,31	0,60	0,77	0,31	0,41
Total	95,81	94,72	96,91	95,26	98,59	99,02	99,49	98,58	97,70	97,28	93,59	94,63	100,25	93,70	99,66	97,36

Table 7. Two main hypotheses on the origin of paralavas (previously known as basaltic pegmatites or segregation sheets).

Origin	Main observation	References
Methane streaming forms paralava, buoyant rise	Pyrometamorphism of kerogen-rich shales at depth (Irati Formation) by intruding basalt magmas liberates CH_4. Streaming of methane through crystalline basalt at 1,000 ºC causes melting (75%) of host basalt and buoyant rise of paralava, resulting in later quench-crystallization of clinopyroxene and other minerals in a glassy matrix.	This work
Fractional crystallization, buoyant rise	In the Levering lava of the Columbia River province, "…the segregated melt is generated by fractional crystallisation from a crystal mush horizon within the basal zone of the lava flow, and rises buoyantly through the flow." "Extraction of enriched intercrystalline material." Magma structure rigid but plastic, forming lenses of residual liquid.	Hartley and Thordarson, 2009. Other references, similar origin: Cornwall, 1951; Puffer and Horter, 1993; Marsh, 1995; Philpotts et al., 1996, 1999; Dragovic and Philpotts, 2002; Philpotts and Dickson, 2002; Cheadle et al., 2004; Greenough and Dostal, 1992b; Greenough et al., 2004; Gomes et al., 2013.

Table 8. Number of drill cores containing sills and average thickness of basaltic sills in sedimentary formations from the southeastern portion of the Paraná Basin; based on compilation of 835 cores drilled in the coal basin by CPRM in 1986.

Formation	Number	Average thickness, m
Serra Alta	42	22
Irati	377	23
Palermo	31	12
Rio Bonito	109	18
Itararé	13	27

ANEXO I

Título da Dissertação/Tese:

"RELAÇÃO DO MAGMATISMO, HIDROTERMALISMO E ALTERAÇÃO SUPERGÊNICA COM A GERAÇÃO DE MINERALIZAÇÕES DE COBRE E AMETISTA NA PROVÍNCIA VULCÂNICA PARANÁ."

Área de Concentração: GEOQUÍMICA

Autor: **SÉRGIO BENJAMIN BAGGIO**

Orientador: LÉO AFRANEO HARTMANN

Examinador: LUIZ HENRIQUE RONCHI

Data: 18/05/2015

Conceito: A (EXCELENTE)

PARECER:

A TESE ESTÁ SEM ESTRUTURADA COM TEXTO INTEGRADOR INICIAL EM PORTUGUÊS, UM ARTIGO PUBLICADO EM REVISTA INTERNACIONAL DE RECONHECIDO BOM NÍVEL, DOIS ARTIGOS EM REVISTAS INTERNACIONAIS TAMBÉM BONS, PORÉM SUBMETIDOS, ALÉM DE UM QUARTO ARTIGO EM REVISTA BRASILEIRA COM CIRCULAÇÃO INTERNACIONAL, O QUE É EXCELENTE. OS OBJETIVOS SÃO BEM JUSTIFICADOS, COERENTES E ABORDAM O TEMA DE MANEIRA ORIGINAL TORNANDO O TRABALHO UMA REFERÊNCIA INCONTORNÁVEL EM ESTUDOS FUTUROS. A METODOLOGIA UTILIZADA É IMPECÁVEL E UTILIZA TÉCNICAS MODERNAS E INOVADORAS PERMITINDO ~~ANEXO~~ ATINGIR OS OBJETIVOS ALMEJADOS. APESAR DISSO É NOTÁVEL A QUANTIDADE E QUALIDADE DOS TRABALHOS DE CAMPO, CUJAS INFORMAÇÕES PERMITEM RESOLVER DÚVIDAS E QUESTÕES FUNDAMENTAIS. O MODELO GEOLÓGICO ASSIM CONSTRUÍDO É TESTADO COMO GUIA PROSPECTIVO PARA DEPÓSITOS DE GEODOS DE AMETISTA OBTENDO RESULTADOS POSITIVOS. UMA MUDANÇA SIGNIFICATIVA NOS CONCEITOS ESTABELECIDOS NA LITERATURA ESPECIALIZADA, SOBRE SUPOSTA TEXTURA PEGMATÍTICA NESSAS LAVAS, É O CONCEITO DE PARAJAVA, CUJA ORIGEM É DISCUTIDA DE MANEIRA PERTINENTE E ORIGINAL. FINALMENTE DESTACA-SE A INTEGRAÇÃO DO MODELO GENÉTICO E EVOLUTIVO ENVOLVENDO FLUIDOS HIDROTERMAIS DE ALTA E

BAIXA TEMPERATURA, CIRCULANDO DESDE AS AREIAS SOTUCATU E CRIANDO NÃO SÓ AS ARENITOS, COMO MODIFICANDO O ~~CRISTALIZANDO~~ E ALTERANDO MINERAIS DO BASALTO.

CONSIDERANDO OS ASPECTOS ANTERIORES ESSA TESE É APROVADA COM CONCEITO A.

Assinatura: [signature] Data: 18/05/2015

Ciente do Orientador:

Ciente do Aluno:

ANEXO I

Título da Dissertação/Tese:

" RELAÇÃO DO MAGMATISMO, HIDROTERMALISMO E ALTERAÇÃO SUPERGÊNICA COM A GERAÇÃO DE MINERALIZAÇÕES DE COBRE E AMETISTA NA PROVÍNCIA VULCÂNICA PARANÁ."

Área de Concentração: **GEOQUÍMICA**

Autora: **Sérgio Benjamin Baggio**

Orientador: **Prof. Dr. Léo Afraneo Hartmann**

Examinador: **Prof. Dr. Marcus Vinícius Dorneles Remus**

Data: 18 de maio de 2015

Conceito: (A) EXCELENTE c/ LOUVOR

PARECER:

A tese foi apresentada na forma de integração de artigos científicos e esta adequada as Normas do PPGeo.
O assunto abordado, mineralização de Cu e ametista, possui relevância científica e interesse econômico.
O trabalho possui boa estrutura, as ilustrações são adequadas e o texto traduz e conduz o leitor às principais conclusões de modo elegante!!
Assim, a tese está bem construída e os argumentos utilizados para tecer as conclusões principais são sólidos e baseiam-se em dados de campo e analíticos. O autor utiliza um largo espectro de técnicas analíticas para obter os dados. Destacam-se os dados de elementos traço em minerais individuais, obtidos por LA-ICPMS que demonstram com clareza a precisão a fonte do Cu.
O autor demonstra que os óxidos e os clorosilicatos são a principal fonte do Cu para as mineralizações de Cu nativo e carbonatos e silicatos de Cu.
Notam-se poucos erros de ortografia

e ausencia de preposições em algumas frases. Desta forma, incentivo pequenas revisões de texto.

A obra é um marco importante para o entendimento das humanizações de Cu e aquíferos e servirá de referência para estudos futuros.

A hipótese das paralavas é um assunto inovador e merece o reconhecimento do mérito da proposta. Entretanto, recomendo investigar o mais detalhe os IFs e esclarecer porque não ocorre subfácies nas paralavas tendo em vista que as intrusões que atravessam as camadas de sedimentos possuem subfácies (camadas reduzidas).

Pelo conjunto da obra, incluindo a discussão de assuntos inovadores e a aplicação de técnicas avançadas de micro-análise, combinado ao extenso trabalho de campo, atribuo o voto de louvor para o candidato.

Assinatura: Data: 18.05.2015

Ciente do Orientador:

Ciente do Aluno:

ANEXO I

Título da Dissertação/Tese:

"RELAÇÃO DO MAGMATISMO, HIDROTERMALISMO E ALTERAÇÃO SUPERGÊNICA COM A GERAÇÃO DE MINERALIZAÇÕES DE COBRE E AMETISTA NA PROVÍNCIA VULCÂNICA PARANÁ."

Área de Concentração: GEOQUÍMICA

Autor: **SÉRGIO BENJAMIN BAGGIO**

Orientador: LÉO AFRANEO HARTMANN

Examinador: PAULO CESAR SOARES

Data: 18/05/2015

Conceito: A (EXCELENTE)

PARECER:

A tese apresenta conteúdo inovador tanto em termos conceituais como de métodos e técnicas. Os procedimentos adotados permitiu alcançar plenamente os objetivos perseguidos. Percebe-se um trabalho intenso envolvendo diversos métodos e técnicas, desde trabalhos de campo intensivos até avançadas tecnologias.

O texto está bem elaborado, com exposição clara.

A argumentação está bem embasada na bibliografia, extensa e atualizada.

A tese e os artigos em publicação e já publicados revelam uma contribuição significativa e de referência internacional nas pesquisas de províncias basálticas continentais.

Por esta razão proponho a atribuição de "Voto de Louvor".

Paulo Soares

Assinatura: Paulo Moura Data: 19/05/2015

Ciente do Orientador:

Ciente do Aluno: